GALAXY GROUPS FROM OBSERVATIONS AND SIMULATIONS

by

ALIAKBAR DARIUSH

A thesis submitted to

The University of Birmingham

for the degree of

DOCTOR OF PHILOSOPHY (PHD)

Astrophysics and Space Research Group

School of Physics and Astronomy

The University of Birmingham

October 2008

Abstract

The cold dark matter model has become the leading theoretical paradigm for the formation of structure in the Universe. Together with the theory of cosmic inflation, this model makes a clear prediction for the initial conditions for structure formation and predicts that structures grow hierarchically through gravitational instability. As a result, small structures collapse first and eventually build large structures such as groups and cluster of galaxies. While clusters are among the most massive bound structures in the Universe, groups are more numerous and most of the galaxies reside within galaxy groups. Testing this model requires that the precise measurements delivered by galaxy surveys can be compared to robust and equally precise theoretical models.

The current project consists of two parts. In the first part, we investigate the existence and evolution of early-formed fossil galaxy groups, and the development of the luminosity gap between its brightest galaxies. We study the correlation of these properties with the group mass assembly history, by comparing observations to the Millennium simulation of dark matter particles, and the associated semi-analytic catalogues of galaxies, together with the Millennium gas simulation.

Fossil Galaxy Groups are believed to be the end result of galaxies merging within a normal galaxy group, leaving behind the X-ray halo characteristic of a group. The sample of fossils in our study are selected according to the useful definition of fossil groups. The luminosity gap statistics in the Millennium Run are compared to the theoretical models. The study of the mass

evolution of fossils shows that in comparison to normal groups, fossils are more evolved systems and have assembled their masses at higher redshifts, while normal groups are still evolving. Our work suggests the earlier formation and higher mass concentration of fossil systems. The estimated space densities from the Millennium Run are smaller (sometimes in agreement within the range of errors in the observations) than those obtained from the observations.

Furthermore, we study the development of magnitude gap from a general point of view and its correlation with the mass assembly of groups and clusters of galaxies using the same dark matter simulations. The results show that the current definition of fossils, based on the magnitude gap $\Delta m_{12} \geq 2$, does not satisfy the necessity for a group or cluster to be an early formed system. Moreover, the fossil phase (the duration in which the magnitude gap of a galaxy group remains always above a threshold value, i.e. $\Delta m_{12} \geq 2$) is a temporary phase in the life of groups, and most groups would experience such a phase in their lifetime. We revise the current optical definition of fossil groups, by studying the evolution and history of various physical parameters associated with the mass assembly of galaxy groups and clusters.

In the second part of this dissertation, we study the optical properties of a sample of 25 optically selected groups from the XMM-IMACS (XI) project. The project aims to improve our knowledge of how the dynamics and properties of group galaxies describe the global characteristics of groups, by using a combination of radio, X-ray, infrared, and optical observations together with the imaging and spectroscopy of the group galaxy population. The observations were performed during three observing run at the Las Campanas observatory. Image processing and precise astrometry was done for spectroscopic follow-up observations. Group virial radii were found by combining the spectroscopic results together with those from the Millennium simulation. Finally we determined the group luminosity functions using the overdensity radii, with the extracted colour-magnitude relation from the spectroscopic observations, and find that the luminosity function of optically selected groups are very similar to that of X-ray selected groups.

Acknowledgements

I would like to express my deep and sincere gratitude to my supervisor, Dr. Somak Raychaudhury, whose wide knowledge and support have been of great value for me. His understanding, encouragement, and personal guidance have provided a good basis for the present thesis.

I am deeply grateful to Dr. Habib Khosroshahi who expertly guided me during my first steps into the field of fossil groups of galaxies and helped me during the first two years. I owe my most sincere gratitude to Prof. Trevor Ponman, the head of the extragalctic group, from whom I learnt logical way of thinking. I thank Prof. Ponman for his constructive comments, and support throughout this work.

During my PhD times, I have collaborated with many colleagues for whom I have great regard, and I wish to extend my warmest thanks to all those who have helped during this period. I warmly thank Dr. Frazer Pearce (University of Nottingham), for his valuable advice and friendly help during the Millennium simulation's project. His extensive discussions about my work have been very helpful for this study. I wish also to express my warm and sincere gratitude to Dr. John Mulchaey and Dr. Jesper Rasmussen from the Carnegie Institution of Washington.

My special gratitude is due to my parents, my sisters and brother for their loving support as they have lost a lot due to my research abroad. Without their encouragement and support it would have been impossible for me to accomplish this work. I owe my loving thanks to my best ever friend, Ms. Kamelia Morady who always reminds me of my sister Sarvin and never made me feel alone during the last three years of my education in the UK.

My loving thanks are due to my best friends Mr. David Stops, Ms. Smriti Mahajan, Mr. Antonio Perreca, Mr. Chris Haines, Mr. Walter Del Pozzo, Mr. Hans Chou, Ms. Helena Blazkova, Mrs. Ladan Shantia, Mrs. Soodabeh Saadat-Shafiee, Mr. Will Hartley, and Mr. Saeed Soheyli.

I am especially grateful to Prof. Yousef Sobouti, the director of the Institute for Advanced Studies (Iran), for all the support before starting my PhD. The financial support of the school of Physics and Astronomy, University of Birmingham is gratefully acknowledged.

Birmingham, England, October 2008

Ali Dariush

Statement of originality

The work presented in this thesis involves the analysis of the results of the Millennium Simulation of the evolution of dark matter halos and the associated semi-analytical models of galaxies. All the data are publicly available at http://www.mpa-garching.mpg.de/millennium/.

The Millennium Gas simulations used in this work, were provided by our collaborator, Dr. F. Pearce from the University of Nottingham.

The spectroscopic information of XMM-IMACS(XI) groups, were provided by our collaborator, Dr. John Mulchaey from the Carnegie Institution of Washington.

The results of the optical observations presented in the current thesis are based on four observing runs at the ESO (La Silla) and the LCO (Las Campanas), Chile. I conducted three of these observations myself, and one session was done by our collaborator Dr. Jesper Rasmussen (Carnegie Institution of Washington).

In addition, the 2dFGRS group catalogue used in Chapter 3 was kindly provided by Dr. Frank C. van den Bosch, of the Max-Planck-Institute for Astronomy (MPIA) in Heidelberg.

Full reference is given to the original authors where derivations are presented and the origin of the work is either wholly or in part from other sources. The work has not been presented previously for any degree.

I hereby certify that the work embodied in this report, has been done entirely by myself, under the supervision of Dr. Somak Raychaudhury (University of Birmingham), and is the result of collaboration with Dr. H. Khosroshahi and Prof. T. Ponman from the University

of Birmingham, Dr. F. Pearce and Mr. W. Hartley of the University of Nottingham (for the Millennium project), as well as Dr. John Mulchaey and Dr. Jesper Rasmussen from the Carnegie Institution of Washington (for the XI-project).

All of the data analysis as well as the image processing and optical data analysis, presented in this work, have been done by myself.

Publications

Publication in Refereed Journals

1. The Mass Assembly of Fossil Groups of Galaxies in the Millennium Simulation: Dariush, A., Khosroshahi, H.G., Ponman, T.J., Pearce, F., Raychaudhury, S., Hartley, W., 2007, MNRAS, 382, 433. (This paper is integrated into Chapter 2)

Manuscript in preparation

1. The Luminosity Gap and Mass Assembly Correlation in Groups and Clusters of Galaxies: A. Dariush, S. Raychaudhury, T. Ponman, A.J. Benson, H. Khosroshahi, F. Pearce (expected date for submission: December 2008. This article is integrated in chapter 3).

2. Optical properties of the XI-groups: A. Dariush, S. Raychaudhury, J. Mulchaey, T. Ponman, J. Rasmussen (expected date for submission: January 2009. This article is integrated in chapters 4 and 5).

3. The XMM / IMACS / GMRT Study of the Role of Cold Gas in the Evolution of Galaxy Groups: Sengupta, C., Raychaudhury, S., Mulchaey, J.S., Dariush, A., Dwarakanath, K.S., Ponman, T.J. (Manuscript in preparation for publication - My contribution was to estimate the galaxy optical diameter D_{25} for group galaxies. As this is a part of XI-project, the method has been explained in Chapter 5).

Publication in Contributed Conference Proceedings

1. Formation of Fossil Groups of Galaxies in the Millennium Simulation: Dariush, A., Raychaudhury, S., Ponman, T.J., Khosroshahi, H.G., Pearce, F., The RAS National Astronomy Meeting, 31st March 4th April 2008, Queen's University, Belfast

2. Dark Haloes of Fossil Galaxy Groups and Clusters: Observations and Simulations: Khosroshahi, Habib G., Dariush, A., Ponman, T., Pearce, F., The 6th International Heidelberg conference on DARK MATTER IN ASTRO & PARTICLE PHYSICS, Sept. 24-28, 2007, Sydney, Australia

Contribution to other work

1. The Luminosity Gap Statistic and Assembly History of Massive Galaxy Clusters at z=0.2: Habib G. Khosroshahi, Graham P. Smith, , A. Dariush, J. E. Taylor, V. H. Hamilton-Morris, J. P. Stott, A. C. Edge, D. P. Stark, T. J. Ponman, J. P. Kneib (Manuscript in preparation for publication - My contribution was to study the magnitude gap in a sample of clusters from the Millennium simulation).

Contents

List of Figures

List of Tables

Chapter 1

Groups of galaxies

1.1 Introduction

Astronomical redshift surveys in the last few decades such as 2dFGRS (2dF Galaxy Redshift Survey) and SDSS (Sloan Digital Sky Survey) have revealed that the nearby universe, and indeed out to very large distances, the distribution of the galaxies is not uniform. An overwhelming majority of galaxies lie in gravitationally bound structures known as *groups* (Tucker et al. 2000; Giuricin et al. 2000; Merchán, Maia & Lambas 2000; Ramella et al. 2002; Mercha'n & Zandivarez 2002; Eke et al. 2004; Yang et al. 2005; Merchán & Zandivarez 2005) though a noticeable fraction of them reside within *clusters* and *super clusters*.

Hence, studying and identifying galaxies in groups is important as the formation and evolution of most galaxies takes place in group environment. Another important issue is that since groups are regions of intermediate density in comparison to field and cluster regions, we can also study the environmental effects on the evolutionary states of galaxies and compare them with results from observation of galaxies in field and clusters.

Groups typically contain fewer galaxies than clusters though the number of constituent galaxies does not provide a reliable definition for either groups or clusters. Obviously, such

a quantity depends on the number of galaxies found to a certain magnitude limit, within a limited volume. Therefore, though clusters are larger than groups, there is not an explicit sharp dividing line between a group and a cluster.

There are similarities between groups and clusters. For instance, early type galaxies in groups are found closer to group centres and tend to be more clustered similar to the density-morphology relation found in clusters (Dressler 1980; Binggeli, Tammann, & Sandage 1987). But in general, the physical properties of clusters such as the velocity dispersion of individual galaxies, the matter content and the total optical luminosity are different from those of groups.

While clusters contain a small fraction ($\sim 2\%$) of the total stellar mass in the Universe, groups of small size contain most of them (Eke et al. 2005). Furthermore, unlike clusters which are essentially virialized systems, different groups may represent different evolutionary stages of system of galaxies. There is a wide diversity of groups in evolutionary stage. On the other hand, there are groups like Local group which are coming together for the first time, and at the other end of the spectrum there are fossil groups which are dominated by a luminous large central elliptical galaxy and presumably are the end product of galaxy merging within groups (Ponman & Bertram 1993; Jones et al. 2003; D'Onghia et al. 2005). Galaxy groups may have been different from each other in terms of shapes, sizes, and morphologies, i.e. loose or rich groups, poor groups, or compact groups. The Local Group of which the Milky Way is a member of that, is a poor galaxy group. Our Milky Way together with M31 are the only two largest spiral galaxies in the Local Group. It is the only place that astronomers can explore various properties such as galaxy kinematics, star formation history, etc. by detailed studying of their galaxy stellar population.

1.2 Galaxy groups: an overview

A galaxy group or cluster is a concentration of galaxies, embedded in an extended dark matter halo. The galaxies are physically bound together due to their mutual gravitational attraction and the presence of dark matter halo, which is extends far beyond the radius at which one sees galaxies. There is a wide variety of galaxy groups in terms of size, richness, velocity distribution and distribution and morphology of constituent galaxies.

Groups have a typical size of a few megaparsecs (Mpc) with total masses (including dark matter halo masses) in the range $M = 10^{12.5-14} h^{-1} M_{\odot}$ (Huchra & Geller 1982). Groups can be classified as rich or poor, X-ray luminous or X-ray-dim, cool or hot, early formed (fossils) or late formed according to the properties being studied. For example, Hickson (1982) listed groups of galaxies known as Hickson Compact Groups (HCG) which are compact configurations of several galaxies that show their own peculiarities in terms of morphology, star bursts or AGN activity (Hickson 1997).

Of course not all of these groups are real physical and bound systems as they could be a result of chance superpositions of galaxies at different redshifts or galaxies within filament that are viewed edge-on. Such groups are unbound systems or pseudo-groups rather than real gravitationally bound groups (Ramella, Pisani & Geller 1997; Hernquist, Katz & Weinberg 1995).

Since galaxy groups have sufficiently high densities but low velocity dispersions, galaxy evolution processes such as transformation and merging occur more frequently in groups rather than clusters where galaxies have large velocity dispersions. This is mainly due to the larger dynamical friction force in group environment where galaxies have lower velocities. According to Chandrasekhar (1943), the dynamical friction force f_{dyn} between a galaxy of mass M and velocity v_M in a galaxy system with the surrounding matter of density ρ, has the following form

$$f_{dyn} \propto \frac{M^2 \rho}{v_M^2}. \tag{1.1}$$

In Eq. 1.1, $f_{dyn} \propto v_M^{-2}$ which means that the fractional rate of galaxy energy loss is lower at high velocities, i.e. in cluster environments dynamical friction is relatively less important than in groups. Conversely groups with low galaxy velocity dispersions provide a suitable environment where galaxies can lose energy due to dynamical friction and fall more rapidly toward the group centre, where a rapid transition of galaxy properties (star formation, morphology, etc.) may occur more efficiently. Thus group environment is very important particularly in the evolution of galaxies and their interactions with intra-group environment.

Groups do not contain many luminous galaxies, and the optical study of groups alone does not provide considerable insight into these systems. Because of this, there are uncertainties in estimated dynamical properties of groups (in comparison to galaxy clusters) from optical observations of their small number of luminous galaxies. Observations at other wavelengths, notably in the X-ray and radio part of the electromagnetic spectrum, provide valuable insight into the nature of galaxy groups.

1.2.1 Group catalogues

The identification of group members against foreground and background galaxies requires the groups to be well isolated in space in order to minimise the contamination due to non-group galaxies. Also, redshifts need to be known in order to find group in a 3D distribution of galaxies. Normally the bright group galaxies (ellipticals, lenticulars, or spirals) are identified based on their spectroscopic or line-of-sight velocity data. The spectroscopic measurements are not easily accessible for dwarf group galaxies with fainter luminosities. Therefore, in most redshift surveys only the identification of most brightest group galaxy members is possible as such surveys are limited to bright apparent magnitudes, leaving the redshift measurements of very

faint dwarf group galaxy members undetected. The number of such faint galaxies could be find statistically by comparing galaxy counts in a group with an adjacent reference field (Miles, Raychaudhury, & Russell 2006). In this method, the excess in the measured number of faint galaxies is assigned to the group population. A major problem is the diversity and nonuniform distribution of field galaxies. Besides, groups themselves have a low density contrast (in comparison to clusters) relative to the field which makes this procedure uncertain.

From the earliest redshift surveys, Geller & Huchra (1983) presented a statistically homogeneous catalogue of 176 groups, identified in the CfA redshift survey of galaxies at redshifts $z \sim 0.03$. Carlberg et al. (2001) identified ~ 200 groups at intermediate redshifts ($0.1 \leq z \leq 0.55$) within the CNOC2 intermediate-redshift galaxy survey.

However, the recent galaxy group catalogues are constructed using automated group finding algorithms based on large-scale galaxy redshift surveys which list galaxy groups in the nearby Universe. For example, using the Two-degree Field Galaxy Redshift Survey (2dFGRS) final data release, Eke et al. (2004) compiled a catalogue containing more than 3×10^4 groups extending up to redshift $z \sim 0.25$ (2PIGG). Similarly there are several other identified and published galaxy group catalogues which are constructed based on the 2dFGRS and the SDSS redshift surveys respectively (Mercha'n & Zandivarez 2002; Merchán & Zandivarez 2005; Yang et al. 2007; Tago et al. 2008).

The techniques used in such catalogues to identify groups from large-scale galaxy redshift surveys is the *friends-of-friends* (FoF) algorithm developed by Geller & Huchra (1983). Alternative methods have been used to identify groups. The 2PIGG catalogue of Eke et al. (2004) used a Percolation based algorithm. Another example is the group catalogue from DEEP2 Galaxy Redshift Survey (Gerke et al. 2005) in which groups have been identified using the Voronoi-Delaunay Method of (Marinoni et al. 2002) over a small sky area with redshifts in the range $0.7 \leq z \leq 1.4$.

1.3 Virial theorem and time scales

1.3.1 Virial theorem

According to the virial theorem, the total gravitational potential energy of a group is related to the sum of the kinetic energies of all of the individual galaxies that make up the group. Each galaxy in a group has a kinetic energy and a gravitational potential energy which is due to the gravitational interaction of that galaxy with all the other galaxies and the dark matter halo of the group. The potential energy of a system of gravitating particles (here galaxies) is negative, since work needs to be done to assemble them in a group, from a large distance away where they have negligible influence on each other. If a group is in a state of equilibrium, then the virial theorem states that the total kinetic energy and the total potential energy are related by (Binney, & Tremaine 1987)

$$2T + V = 0, \tag{1.2}$$

where T and V are the total kinetic energy and potential energy in the system (proof is given in Goldstein 1980).

Virial mass of groups and clusters

One method of identifying a group or cluster is to regard them as material lying within a sphere, centred on a local maximum density or minimum potential, whose radial extent r_Δ is defined by an enclosed isodensity condition

$$\frac{M(< r_\Delta)}{\frac{4}{3}\pi r_\Delta^3} = \rho_t(z). \tag{1.3}$$

Such spherical overdensity masses require a choice of threshold density $\rho_t(z)$ which is multiple Δ of the critical density $\rho_c(z)$, i.e. $\rho_t(z) = \Delta\rho_c(z)$. The critical density $\rho_c(z)$ is in fact

the boundary density between the case where the universe has enough mass per unit volume to cause eventual collapse of the universe, and too little mass per unit volume to stop the expansion and is defined as follow

$$\rho_c(z) = \frac{3H^2(z)}{8\pi G}, \tag{1.4}$$

where $H(z) = 100h(z)$ km s^{-1} Mpc^{-1} is the Hubble parameter at redshift z. Notice that the Hubble parameter appears in the critical density relation since it measures the expansion rate of the universe. The current critical density is approximately $\sim 1.06 \times 10^{-29}$ g cm^{-3}.

One of the useful applications of the virial theorem is that it connects the velocity dispersion σ_r and ICM (intracluster medium) or IGM (intragroup medium) temperature T, within a sphere of radius r_Δ, to the corresponding overdensity mass M_Δ via the form

$${\sigma_r}^2 \propto \frac{kT_{gas}}{\mu m_p} = \varepsilon \frac{GM_\Delta}{r_\Delta}, \tag{1.5}$$

where μ is the mean molecular weight of the IGM/ICM, m_p the proton mass, ε a dimensionless constant that depends primarily on the internal density profile of clusters, and T_{gas} is the intragalactic medium temperature. Using the definition of critical density $\rho_c(z)$ together with Eq. 1.3 one obtains

$$M_\Delta = M_{vir} = \Delta \times \frac{r_\Delta^3 H^2(z)}{2G}. \tag{1.6}$$

The density contrast Δ (at virialization) in Eq. 1.6 is an important parameter in fitting theoretical calculations to observation and depends on the density parameter Ω[1] which in turn depends on different cosmological models. In a flat universe for which $\Omega = 1$, a spherical clump of matter virializes at a density contrast of order 100 (Peacock 1999). For example Cole & Lacey (1996)

[1]The density parameter Ω is defined as the ratio of the density of the Universe ρ over critical density ρ_c at a particular epoch.

has shown that $\Delta = 178$ separate well the interior of the virialized halo from the surrounding infalling material while for $\Omega \neq 1$, Δ depends on Ω (Eke, Cole, & Frenk 1996). However, recent cosmological simulations have adopted $\Delta = 200$ in which Eq. 1.6 reduces to (Evrard et al. 2002; Croton et al. 2006)

$$M_{vir} = \frac{100 r_{vir}^3 H^2(z)}{G}, \tag{1.7}$$

where $r_{vir} = r_{200}$ is the virial radius of a group or cluster.

1.3.2 Timescales

Hubble time

According to Hubble's law, there is a linear relationship between the receding velocity v of a galaxy with the distance to that galaxy d at time t due to the expansion of the overall universe. The relation is

$$v = H(t) \times d, \tag{1.8}$$

where $H(t)$ is the constant of proportionality known as the Hubble constant (also called Hubble parameter which is a value that is time dependent) at time t, c is the speed of light in vacuum. In Eq. 1.8, the quantity $H^{-1}(t)$ is in time units (s) and is known as the *Hubble time* and is a measure of the age of the universe since it is the amount of time one predicts by projecting back assuming the universe has always been expanding at its current rate. Recent data from the Wilkinson Microwave Anisotropy Probe (WMAP) project estimates the age of the universe to be $(13.73 \pm 0.12) \times 10^9$ yr with an uncertainty of 120 million years (Hinshaw et al. 2008).

Dynamical timescale (Crossing time)

Consider a homogeneous sphere of density ρ and mass $M(r)$. A test particle within the sphere experiences a gravitational potential of

$$\phi(r) = -G\frac{M(r)}{r}. \tag{1.9}$$

If the test particle moves in a circular orbit with circular velocity v_c and period T then

$$\begin{cases} v_c(r) = \sqrt{\frac{GM(r)}{r}} = \sqrt{\frac{4\pi G\rho}{3}}r \\ T = \frac{2\pi r}{v_c} = \sqrt{3\pi}G\rho \end{cases} \tag{1.10}$$

If the test mass is released from rest at radius r in the gravitational field given by Eq. 1.9, its equation of motion is

$$\frac{d^2r}{dt^2} = -\frac{GM(r)}{r^2} = -\frac{4\pi G\rho}{3}r, \tag{1.11}$$

which is the equation of motion of a harmonic oscillator of angular frequency $2\pi/T$. Since the period T is independent of the initial value of r, the test mass will reach $r = 0$ in a quarter of a period $T/4$, or

$$t_{dyn} = \frac{T}{4} = \sqrt{\frac{3\pi}{16G\rho}}. \tag{1.12}$$

For a system of mean density ρ, the *dynamical time* is defined using Eq. 1.12 and is approximately equal to the time required for an orbiting star to travel halfway across the system of this mean density. For a non-homogeneous system, say a cluster of radius R and N galaxies with individual mass m_i, it is easy to use the virial theorem and show that

$$t_{dyn} = \frac{R}{v} \approx (\frac{8R^3}{GM})^{\frac{1}{2}}, \tag{1.13}$$

where $M = \sum_{i=1}^{N} m_i$, is the total mass of the cluster, and v is the average speed of the galaxy with respect to the centre of the cluster.

Cooling time

Cooling time is the timescale over which the gas can continue to lose energy at its current rate which is a simple estimate of the susceptibility of gas to radiative cooling. Thus defined, the cooling time (in seconds) of a parcel of gas with volume, V (in cm^3), and luminosity, L_X (in erg s^{-1}), is given by

$$t_{cool} = 1.602 \times 10^{-9} \times \frac{3kT\rho V\mu_e}{2\mu L_X}, \tag{1.14}$$

where kT is the deprojected gas temperature (in keV), ρ is the electron number density (in cm^{-3}) and the constants μ_e and μ are the mean mass per electron (1.167) and the mean molecular weight (0.593) of the gas (Sanderson, Ponman, & O'Sullivan 2006). Given typical values for physical parameters of groups and clusters (Binney, & Tremaine 1987), one can see that t_{cool} $\sim$(0.3-6)$\times H_0 h$ km s^{-1}Mpc^{-1} which means that the cooling time for most of the groups and clusters is more than one Hubble time.

Dynamical friction time

The merger times of a satellite galaxy moving on the periphery of the primary galaxy, obtained under the impulsive and adiabatic approximations, reduce to the decay time predicted by Chandrasekhar's formula for dynamical friction (Chandrasekhar 1943) if the satellite galaxy is regarded as a mass point (Binney, & Tremaine 1987). Based on these assumptions the time needed for a satellite galaxy to merge with the central galaxy of a dark halo is estimated as

$$t_{\text{friction}} = 1.17 \frac{V_c r_{sat}^2}{G m_{sat} \ln \Lambda}. \tag{1.15}$$

This formula is valid for a satellite of mass m_{sat} orbiting in an isothermal potential of circular velocity V_c at radius r_{sat}. The parameter $\ln\Lambda$ is the Coulomb logarithm equal to

$$\mathbf{\Lambda} \equiv b_{max} V_c^2 / G(M_{vir} + m_{sat}), \tag{1.16}$$

where b_{max} is the maximum impact parameter of the encounter. In numerical simulations, $\ln\Lambda$ is approximated by $(b_{max}/b_{min})^2$ where b_{min} is the minimum impact parameter, and $\ln\Lambda$ could be in the ranges of $\sim 1-4$ (Velázques & White 1999; Fellhauer et al. 2000). Given typical estimates for parameters of groups and clusters of galaxies (see Table 1-4 of Binney, & Tremaine 1987), it is easy to show that the dynamical friction time in clusters is $\sim$50 times more than that those for groups where $t_{\rm friction}$ is not more than a few gigayears,i.e. less than one Hubble time.

1.4 Formation of groups

The current model of the formation of the Universe is based on the *Big Bang* model. The model constructs a framework for the standard cosmological model, in which the Universe starts to expand from a singularity or an initial dense state. Shortly after the Big Bang, the inflation happens in which the Universe experiences an extreme rapid expansion. Such model has been proved to be useful in explaining several long-standing problems in cosmology (Guth 1981). Within the current view, the formation of structures is hierarchical in which the larger structures form by clustering of smaller structures. Smaller structures originate due to development of initial perturbations in the density field.

In the very beginning, near after the Big Bang the temperature was very high. Under such condition baryons synthesise to form deuterium, helium, light elements etc., until the temperature drops below a critical value needed for further nuclear reactions to take place. This baryon

[2] In the Millennium semi-analytic simulation of Croton et al. (2006) used in this work, Eq. 1.16 is approximated by $\ln\Lambda = \ln(1 + M_{vir}/m_{sat})$.

material later makes up the visible or observable matter, though the largest fraction of matter in the Universe is in the form of dark matter, which only interacts gravitationally.

As the temperature drops, the neutral hydrogen atoms form by combining the protons with electrons. At this stage the radiation field which was previously coupled to the baryonic matter, becomes decoupled from it (while still have little interaction with baryonic material) and the wavelength of the radiation shifts as the Universe expands. This radiation is called the *Cosmic Microwave Background Radiation* (CMBR) with a thermal black body spectrum at a temperature of ~ 2.73 K (Penzias & Wilson 1965). Once decoupled from the radiation, clouds of matter begin to collapse under gravity, as it overcomes the expansion caused by the cloud's thermal energy. This happens if the perturbations are larger than a critical value,i.e. the *Jeans' Length* [3],

$$\lambda_J = c_s \left(\frac{\pi}{G\rho} \right)^{1/2}. \tag{1.17}$$

In other words, if the oscillation wavelength of perturbations becomes larger than λ_J, then gravitational collapse will occur, otherwise the system remains in stable oscillating condition. In Eq. 1.17, G is the gravitational constant, while c_s and ρ are the sound speed and enclosed mass density respectively.

Based on the assumed properties of dark matter, cosmologists have developed two major theories of structure formation. These two theories are the Hot Dark Matter (HDM) model and the Cold Dark Matter (CDM) model. Each model assumes a different for the composition of dark matter particles. In the HDM model, dark matter are composed of relativistic subatomic particles such as the neutrino which are in thermal motion. Also in HDM, largest structures form at the beginning and later smaller structures form by fragmentation of the larger ones, i.e. the process of structure formation is a *top down* process.

In contrast the structure formation in the CDM model is hierarchical in which larger struc-

[3] An alternative form of the Jeans Length is $\lambda_J = \sqrt{\frac{15 k_B T}{4\pi G \mu \rho}}$. Here, G and k_B are the Gravitational and the Boltzmann's constants respectively, T and r are the cloud's temperature and radius, μ is the cloud's mass per particle, and ρ is the mass density of the baryonic cloud,i.e. the cloud's mass divided by its volume.

tures form by clustering of smaller objects. Hence, CDM is a *bottom up* process in which dark matter particles are composed of nonthermal, slow moving particles. The nature of such particles is still unexplored. However, $> Gev$ particles such as the gravitino or axion are among possible candidates (Okada & Seto 2005; Duffy et al. 2006).

One way to reveal whether the Universe is dominated by HDM or CDM is the way that matter such as clusters and groups are distributed throughout the Universe. The comparative studies between HDM and CDM models using the results of large scale cosmological simulations show that CDM model reproduces the observed properties of the Universe and the clustering of matter better than other models particularly with the cosmological parameters where $\Lambda \simeq 0.7$ (ΛCDM model; Springel et al. 2005).

Also according to the HDM model, galaxies should have been formed recently and groups and clusters should be early formed systems. However, deep field observations show the existence of Lyman break galaxies at very high redshift which is in conflict with the predictions of HDM which states that galaxies have formed recently (Steidel et al. 1996).

Structure formation and CDM

The collapse of matter happens when a perturbation starts to turn around while the Universe is expanding. The process of collapsing continues until the internal velocity of system's components are large enough to hold the system against more collapse. At this stage the system reaches to a state of dynamic equilibrium in which the virial theorem reduces to Eq. 1.2. Using Eq. 1.2 together with energy conservation, one finds that the size of the system while it is in the state of equilibrium is half of its size at turn around stage,i.e. just before collapsing. As the system's volume scales as inverse cube with its radius, i.e. $V \propto r^{-3}$, then the density of the collapsed system will be eight times its average density at the time when the system turns around.

Even before collapsing, the system's perturbation is noticeably denser than the mean density

of the Universe otherwise it does not turn around. Therefore the final virialized system will be overdense in comparison to the mean density of the Universe by more than a factor of eight. The spherical top-hat perturbation solution of Peebles (1980) estimates an overdensity of ~ 178 ($18\pi^2$) for the resulting collapsed system. This estimation is for a critical Universe in which the mean density of the Universe goes beyond a fixed threshold known as the critical density (Eq. 1.4) however for an open or closed Universe the overdensity can be significantly lower (Bryan & Norman 1998).

Dark matter versus baryonic matter

Unlike baryonic matter, the behaviour of dark matter does not depend on the scale of the system since dark matter only interacts gravitationally. It means that dark matter halos with different sizes and masses are scaled versions of each other. But incase of baryonic matter, this is not true and their properties are not scale free as they could undergo other physical processes rather than gravity alone. The interaction between baryonic matter and the electromagnetic field in the intragroup or intracluster medium is an example of such physical process. The mutual influence of the interactions between electromagnetic field and baryonic matter results in pressure forces that alter the energy of baryonic matter via electromagnetic radiation.

In small structures, the dominant physical process is cooling, which causes baryons to be more central concentrated than dark matter halos. Such process lead baryons to collapse while forming stars and galaxies. In contrast, in large structures, baryons experience a deeper gravitational potential and gain potential energy as they fall to the centre of halo. This process heats baryon and increases its temperature via shocks. As a result, baryon experiences pressure forces which does not let them to be as concentrated as its host dark matter. Therefore in large scale structures, the process of cooling will be important in their dense cores where the gas cools as it flows inward, resulting in a sharp tip in their observed X-ray luminosity profile.

The effect of heating on the gas dynamics is less pronounced in large structures, in compari-

son to small ones, unless the heating is very large. Observation of groups and clusters in optical and X-ray, and the study of the metal content of IGM or ICM, show that a significant fraction of gas in IGM or ICM has been processed through group or cluster galaxies (Rasmussen & Ponman 2007). Such amount of gas can carry a significant amount of energy out of galaxies, which in turn could heat the gas component of the groups and clusters and affect their dynamics.

The Press-Schechter formalism

The Press-Schechter model was first developed by Press & Schechter (1974). It provides an analytical method in explaining the structure formation in the Universe. In this model, the Universe is assumed to be well defined by low amplitude density perturbations with an isotropic random Gaussian field distribution. The field can be completely described by its power spectrum and the amplitudes of its Fourier components as fluctuations have random phases. The variations of the initial density perturbations are very small, i.e. $\delta \equiv \Delta\rho/\bar{\rho} \ll 1$ and their evolution can be described linearly. However, these variations grow with time and their evolution at some point become non-linear, i.e. $\delta \sim 1$. In such a non-linear regime, the evolution of perturbations can no longer be expressed by simple analytic methods.

To avoid such difficulty, Press-Schechter formalism postulates that the evolution of density perturbations can be followed based on linear assumptions until the clustered matter turns around while breaking away from the expansion of the Universe. Assuming a spherical top-hat perturbation, this separation happens at density contrast $\delta_c \equiv (\rho/\bar{\rho}) - 1 \sim 1.686$ where ρ is the mean density of the clump of matter and $\bar{\rho}$ is the mean background density of the Universe in the Einstein-de Sitter model (Gunn & Gott 1972). The clustered matter then collapses quickly and independently from its surroundings. It is followed then by a violent relaxation which removes the internal structure of the clustered matter (Lynden-Bell 1967). In such condition the collapsed region behaves as a single body of large mass to the rest of the Universe. Thus, one can apply the linear equation to the cloud of particles to estimate their mass distribution.

Though the above results simplify the equations defining the evolution of the density field, still it is necessary to find a solution in counting the number of nonlinear objects of a given mass. To do it, the probability distribution of the density field fluctuations averaged over a given volume V must be related to the probability that a given region is overdense enough to collapse on the same scale V. This probability can be used later to estimate the fraction of the mass of the Universe that will be retained within the clumps of mass $\bar{\rho}V$.

Finally in the framework of the Press-Schechter formalism the mass function $n(M)$ (where $n(M)$is the comoving number density of the collapsed objects in the range dM) is defined as

$$\frac{M}{\bar{\rho}}n(M) = \Big|\frac{df}{dM}\Big|\frac{\delta_c}{\sqrt{2\pi}\sigma}\frac{1}{M}\Big|\frac{d\ln\sigma}{d\ln M}\Big|\exp\Big(-\frac{1}{2}\frac{\sigma^2}{\delta_c^2}\Big), \tag{1.18}$$

where $f(>\delta_c, M)$ is the probability that collapsed structures of masses larger than M appear at a given point.

1.5 The structure of groups

Groups and clusters of galaxies range in size from small systems consisting of pairs of galaxies up to rich, massive clusters of several thousands of galaxies. But galaxies are not very important in such galaxy systems as their contribution to the total mass of the system is ~ 10 percent. Unlike galaxies, dark matter halo is the main component in groups and clusters that makes up the majority (~ 90 percent) of the mass. Baryons contribute to the rest of the mass in the form of galaxies and gas, i.e. intragroup (IGM) and intracluster (ICM) mediums respectively. The gas component is basically hot and ionised in the case of clusters but in case of groups, the nature of gas has not been yet fully explored.

1.5.1 Intra-group medium (IGM)

At the present time our view of the evolution of groups comes from the observed properties of the luminous galaxies of the groups, and the diffuse X-ray emitting group halo as well as numerical simulations (Mulchaey et al. 1993; Athanassoula, Makino, & Bosma 1997). Besides, measurements of metal abundance and radio observation of neutral hydrogen in IGM provide useful insights into the star formation history, structure, enrichment, and evolution of groups.

Results of X-ray observations indicate that a large number of groups have X-ray emission, from the hot intragalactic medium (IGM) extended beyond their optical extent, with temperature ranges from ~ 0.3 keV to 2.0 keV (Mulchaey 2000). Indeed, using the first results of the *ROSAT* X-ray observatory, Ponman & Bertram (1993) and Mulchaey et al. (1993) presented detailed studies of groups, and found that the observed X-ray emission in groups consists of a diffuse component related to the group as well as an emission component associated with individual galaxies.

They also compared the total mass of the group ($\sim 10^{13} h_{100}^{-1} M_{\odot}$), estimated from the X-ray ROSAT data, with the total mass derived from the observed optical luminosity of the constituent galaxies and concluded that the majority of mass in these groups is in the form of dark matter. The X-ray emission from hot IGM or ICM gas is characterised by thermal Bremsstrahlung for which, in the case of fully ionised hydrogen gas, the energy emitted per unit volume per unit time in frequency interval ν and $\nu + d\nu$ is given by (see for example Henriksen & Mushotzky 1986):

$$l_{\nu} d\nu = 5.44 \times 10^{-40} (4\pi n_e^2) T^{-1/2} e^{-h\nu/kT} d\nu [\mathrm{W/m^3}], \tag{1.19}$$

where T and n_e are the gas temperature and the number density of the electron respectively.

Note that X-ray observations of groups are only sensitive to the hot ionised gas component of the IGM with high temperature in a range of $10^6 \lesssim T \lesssim 10^7$ K and electron gas density

of the order of $10^{-4} - 10^{-5}$ cm^{-3} (Tripp, Lu, & Savage 1998; Pisano et al. 2004). There are groups without any signature of hot, diffuse X-ray emission from their IGM (such as Local group). Such groups are believed to be non-virialized systems in which the IGM gas has not yet been heated up to such temperatures as a result of gravitationally collapse, and therefore their temperature is still low or they are deficient in hydrogen (Rasmussen et al. 2006). Nevertheless, in the case of virialized systems, the equation of state for the IGM or ICM can be approximated by the ideal gas law

$$P = nkT, \tag{1.20}$$

where P, T, and n are the gas pressure, temperature, and number density of gas particles respectively and k is Boltzman constant.

The IGM gas is not entirely primordial though it is composed mainly of hydrogen and helium, but it is also contaminated by other heavier elements or metals (such as Iron, Silicon, etc.). The chemical enrichment of the IGM is believed to originate from the ejected material from group galaxies by supernovae, galaxy-galaxy, and galaxy-IGM interactions. Therefore, studying the metal content and its distribution within IGM provide an excellent method for investigating the physical processes and mechanisms, that, together with gravity, have shaped the thermodynamic properties of gas in IGM (Rasmussen et al. 2006; Rasmussen & Ponman 2007).

1.5.2 Dark matter halos

The first evidence of the existence of dark matter was provided by Zwicky (1933) from the observation of the dynamics of galaxies in the Coma cluster. He found that the estimated cluster's total mass based on the motions of galaxies is far more than the expected mass. Zwicky (1933) concluded that extra mass is required as the gravitational potential of the visible cluster galaxies would be too small for such fast orbits. He then inferred that there must be some sort of *dark*

matter,i.e. a non-visible or hidden form of matter which would provide enough potential due to its large mass to hold the cluster components together.

Dark matter affects galaxy groups as well. The main evidence that the dominant constituent of groups is a dark matter halo comes from the study of the *velocity dispersions* of group galaxy members about the mean group recession velocities and from the X-ray study of the IGM (i.e., Ponman & Bertram 1993 and Mulchaey et al. 1993). Though further support for the existence of dark matter halos and and the shape of their density profile comes from the studies of gravitational lensing due to the observation of galaxy clusters (e.g. Sand et al. 2004; Meneghetti, Bartelmann, & Dolagde 2005; Smith et al. 2005; Shu et al. 2008).

The radial velocity dispersion, σ_r, of a galaxy group or cluster is a statistical quantity that provides a measure of the range of speeds of galaxies along the line of sight and is calculated as

$$\sigma_r^2 = \sum_i \langle (v_{r_i} - \langle v_{r_i} \rangle)^2 \rangle. \tag{1.21}$$

The measurement of galaxy velocity dispersion yields an estimate of the group or cluster mass (e.g. Eq. 1.5).

Both IGM temperature or the velocity dispersion σ are too high for the gravitational potential produced by the observed mass of group galaxies and IGM to confine them within the group. So a large amount of mass within the groups is necessary which is believed to be in the form of dark matter to prevent the group galaxies as well as the IGM escape from the group potential. In the presence of such a mass, galaxies would have a negative binding energy that keep them together in group gravitational potential.

As is obvious from its name, dark matter can not be observed directly. In order to follow the temporal evolution of dark matter perturbations , formation of dark matter structures, and the density profiles of dark matter halos, numerical simulations are the only tools at our disposal. For example, the numerical simulations have been very useful in determining the form of dark

matter *density profile*. Navarro, Frenk, & White (1996) proposed the following form for the distribution of dark matter density from their numerical simulations of the formation of dark matter halos

$$\rho(r) = \frac{\rho_0}{x\,(1\,+\,x)^2}, \tag{1.22}$$

where $x = r/R_s$. Navarro, Frenk, & White (1996) has shown that over a wide range of mass scales, from dwarf galaxies to rich groups and clusters, Eq. 1.22 (*the NFW profile*) does describe the distribution of dark matter very well with the normalising density ρ_0 and the scale radius R_s as fitting parameters.

According to Eq. 1.22, density profile $\rho(r)$ in dark matter halos essentially scales as $\sim r^{-2}$ over the whole halo but is less steeper near the centre ($\sim r^{-1}$) and more steeper near the halo outskirt ($\sim r^{-3}$). Note that the distribution of dark matter in groups or clusters is expected to match an NFW profile in the form of Eq. 1.22 if they are in the stage of *virialization*. Thus, if a group or cluster is collapsing or shows a significant fraction of substructures then its dark matter density profile does not follow exactly the same distribution as NFW.

From the numerical simulations of the formation of dark matter halos, Moore et al. (1999) suggested a steeper asymptotic slope of -1.5, and a sharper turn-over resulting in a profile of the following form:

$$\rho(r) = \frac{\rho_0}{\left(\frac{r}{R_s}\right)^{1.5}\left(1\,+\,\frac{r}{R_s}\right)^{1.5}}. \tag{1.23}$$

The ratio of the virial radius to the scale radius of a group or cluster is called the concentration c of the galaxy system. It is a measure of the density of the dark matter halo in its inner regions and is defined as

$$c = \frac{R_{200}}{R_s}, \tag{1.24}$$

where R_{200} is the virial radius within which the average density of the system is equal to 200 times the mean density of the Universe. So at a fixed virial radius, a higher value of c implies a higher density of the halo and vice versa. The concentration also depends on group or cluster halo mass such that lower mass halos are more concentrated than higher mass halos, i.e. the halo mass is anti-correlated with the halo concentration (Navarro, Frenk, & White 1997).

This effect is normally explained in terms of the epoch of formation of groups and clusters in the hierarchical model of structure formation, in which the small structures form first. Clustering of smaller systems, leads to larger structures form later. Since the Universe has a larger mean density at higher redshifts, the structures that formed earlier should be denser. Thus at a fixed halo mass, a group or cluster with higher concentration tend to be older (have been formed earlier) than its counterpart with lower concentration (Khosroshahi, Ponman, & Jones 2007).

1.5.3 Galaxies

There are substantial differences between galaxy populations in the field and those in clusters and groups. Dressler (1980) showed that the galaxy morphology is a strong function of galaxy density, and numerous studies since then have shown the dependence of galaxy properties on local environment (e.g Lewis et al. 2002; Balogh et al. 2004). While in the field, the majority of galaxies are spirals, groups and clusters are populated mainly by lenticular and elliptical galaxies. In groups however there is more variance in the fraction of spiral to elliptical galaxies, mainly due to differences in evolutionary states of galaxy groups (Mulchaey 2000).

At the centre of the potential in the majority of the relaxed groups and clusters (such as fossils), there is a cD galaxy. A cD galaxy is defined as a galaxy with a nucleus similar to high luminous elliptical galaxies, embedded in a low surface brightness, extended halo (Morgan 1958). cD galaxies in fossil groups or clusters are believed to grow by accreting or merging with other galaxies. Numerical simulations support scenarios that suggest galaxies within groups merge eventually to form large elliptical galaxies (Athanassoula, Makino, & Bosma 1997).

Obviously dynamical friction plays an important role in the formation and growth of cD galaxies at the centre of fossil groups and clusters. Obviously dynamical friction is larger and more effective in lower mass systems due to the lower velocity dispersion of galaxy members in such systems, in comparison to clusters where galaxies have higher relative velocities.

1.6 The ages of groups

A long-standing and important issue in the field of galaxy groups and clusters is to find one or more observable properties of such systems that are correlated with their formation history, age, or mass assembly. In other words, how does one distinguish between an early-formed and late-formed system in terms of their physical and observational properties? For example, Smith & Taylor (2008) use the gravitational lensing masurements of substructure in galaxy cluster cores to investigate the connection between evidence of substructure with cluster assembly histories. Though such a technique is an efficient way to identify early formed clusters, it is not very useful in studying the formation history in galaxy groups. The reason is that groups in general do not contain a large number of galaxies and rarely have relaxed morphology and hence an identification of substructures within groups is a very difficult and challenging task.

A combination of X-ray and optical study of galaxy systems is in principle a possible way to identify early formed groups and clusters. Galaxy groups are ideal sites for galaxy-galaxy mergers. This is mainly because of the relatively high galaxy density and low velocity dispersion of groups. The merging timescales or collision time for bright group galaxies with $L \approx L^*$ is less than a Hubble time which implies that many of the bright galaxies in groups should have already merged into a single giant object (presumably an elliptical galaxy) by the present time if the systems had formed early (Zabludoff & Mulchaey 1998). In this sense, galaxy merging might be a common process in the cores of galaxy groups.

Unlike the collision time, the cooling time for the intragroup medium is longer than a Hubble

time, which is due to the lower density of the gas in the outer region of groups, in comparison to the gas density at the core. Thus while the bright galaxies in some groups have had enough time to collapse via merging, the original X-ray halos of the groups remain unchanged.

Based on this hypothesis, one can expect the extreme case to be such that most of the galaxies have merged, leaving a spatially extended X-ray source with a central bright galaxy. Numerical simulations of Barnes (1985) imply that many group members are merger remnants and that groups of galaxies evolve significantly on a dynamical time scale. Thus one expects that a good way of finding groups that have been formed early is to study the so-called "fossil groups". The extended X-ray emission of such groups together with a relative large luminosity gap between their brightest galaxies helps to distinguish them from normal galaxy groups.

1.6.1 Fossil galaxy groups

Ponman et al. (1994) used the ROSAT X-ray All-Sky-Survey to discover the first fossil group candidate. Using *Chandra* X-ray data, Khosroshahi, Ponman, & Jones (2007) have compiled a list of seven fossil groups and have presented X-ray scaling relations for them. The selection criteria of fossil groups here are based on the definition of fossils given by Jones et al. (2003); that is groups with X-ray luminosity of $L_{X,bol} \geq 10^{42} h_{50}^{-2}$ erg s^{-1} and $\Delta m_{12} \geq 2.0$ mag, where Δm_{12} is the difference between the luminosity of the first and the second ranked galaxies in the R-band within half the projected virial radius of the group centre. Though there is no upper limit on the X-ray luminosity of fossil groups, their gravitational mass and physical size cannot be arbitrarily large. An overwhelmingly large mass for a group would cause the scale time for dynamical friction, over which a galaxy sinks to the centre of the group or cluster and merges with the central galaxy, to exceed the Hubble time and hence the age of the universe (Khosroshahi et al. 2006a; Milosavljević et al. 2006).

Because of the relatively large Δm_{12}, the central galaxy of a fossil group has a large contribution to the total optical luminosity of the group. The results of Khosroshahi, Ponman,

& Jones (2007) suggest that fossils have formed earlier than normal groups and clusters and confirms the lack of recent star formation and recent major merger in fossil groups proposed by Jones, Ponman, & Forbes (2000) by studying the spectral features of the central galaxy of RXJ1340.5+4017, a group in which 70% of the optical luminosity of the group comes from its giant central elliptical galaxy and $\Delta m_{12} = 2.5$. I will address this issue in detail in the next two chapters.

1.7 Self-similar evolution

1.7.1 Introduction

Groups and clusters are believed to form as a result of the gravitationally driven process of collapsing of baryonic and dark matters together. The process eventually leads to formation of virialized structures while the gas particles are heated up to virial temperature via shocks and adiabatic compression due to gravitational potential of the system. Dark matter particles are at the same temperature as the gas particles since there is no interaction and energy transfer between the gas and dark matter in this model. The initial conditions are set by adjusting the power spectrum of the initial perturbations which is scale independent, i.e. the virialized structures following the the collapse of the perturbations are scaled versions of one another and their properties should not depend on their size.

Such assumptions which involve self-similar behaviour are useful in the study of groups and clusters though they might not be necessarily true. The investigation of any deviations in the observed properties of groups and clusters from those expected using self-similarity is a good approach in the study of galaxy systems since they reveal the important contribution to non-gravitational physical process. Such comparison with self-similar behaviour provides a baseline to explore the extra physical processes underway in the formation and evolution of groups and clusters.

Weak and strong self-similarity

There are two types of self-similarity, i.e. weak and strong self-similarity (Bower 1997). According to weak self-similarity (Kaiser 1986) different populations of virialized systems should all be self-similar, independent of their observed epochs. Contrarily strong self-similarity specifies that a given population of virialized systems will be self-similar versions of one another for a given epoch, which is stricter condition than weak self-similarity.

One weak point about strong self-similarity is that even in the case of fully gravitational collapse, it might not be necessarily true. The reason is that even within the same range of mass, groups or clusters could have very different merger histories and therefore their structures would not necessarily be similar to each other. However, comparison between strong self-similarity predictions and the observed properties of groups and clusters in the real world gives us noticeable insight into the merger histories of galaxy systems and the physical processes within such objects.

1.7.2 Scaling relations

Based upon the assumptions of self-similar model of formation and evolution of structures in the Universe, it is possible to estimate how various observed properties of galaxy groups and clusters would be expected to be interrelated. These observations are carried out at different wavelengths which enable astronomers to measure group physical properties.

In the optical band the observables include:

- the overall luminosity of the galaxies of the group, which comes from the integrated luminosity of the individual galaxies and
- the velocity dispersion of group's member galaxies.

Up to the present time, most of the X-ray studies of groups have been conducted with the help of *ROSAT*, *ASCA*, *XMM-Newton* and *CHANDRA* X-ray telescopes. Their observations

differ from each other in terms of spatial resolution and the X-ray photon energy sensitivity. The observables in the X-ray band are:

- the overall X-ray luminosity of the group, coming from the hot gas trapped in the group's gravitational potential,
- the temperature of the group inferred from the X-ray spectrum of the gas and
- the abundances of various elements (metallicity) of the intragroup medium (IGM), inferred from the emission lines in the spectrum of the hot gas.

Scaling relations between different physical parameters of groups and clusters provide a powerful method to investigate the nature of these systems in comparison with theoretical models. Bound, virialized systems of hot gas are expected to obey self-similar scaling relations.

Preheating model

In the standard hierarchical clustering model (ΛCDM), in which the Universe is filled with adiabatic gas with dark halos adopting an NFW profile (Navarro, Frenk, & White 1996), the gas temperature T of galaxy groups and clusters is expected to scales with their bolometric X-ray luminosities in a self-similar way, i.e. $L \propto T^2$ (Kaiser 1986; Kaiser 1991; Evrard & Henry 1991). However, the observed relationship is considerably steeper ($L \propto T^3$; e.g., Arnaud & Evrard 1999), especially for groups having $T \lesssim 1.0$ keV ($L \propto T^4$ or more; Helsdon & Ponman 2000).

There are also other respects in which the properties of groups and cluster are different. For example groups have a lower baryon fraction with a larger fraction of stellar mass in comparison to massive clusters (Renzini 1997; David et al. 1990; David & Blumenthal 1992). Entropy profiles evaluated for groups and clusters indicate that the gas entropy in groups exceeds the self-similar expectation by $S \sim 100$ keV cm^2 which cannot be achieved through gravitational

collapse alone (David, Jones, & Forman 1996; Ponman, Cannon, & Navarro 1999; Lloyd-Davies, Ponman, & Cannon 2000).

The minimum observed entropy in groups is called the *entropy floor*. It is not exactly clear whether such a minimum entropy exist in massive clusters or not. This is because the entropy in massive clusters is much larger than those in groups which is due to stronger shocks originating from collapse within cluster environment. So it would be difficult to detect such entropy floor in clusters. Such deviations in the entropy of groups from self-similarity are consistent with the preheating model for the hot gas in groups. In this scenario, the intragalactic gas in groups was heated by $0.5 - 1.5$ keV per particle at earlier epochs.

Such additional heating could be due to feedback from non-gravitational astrophysical sources such as supernovae, star formation, active galactic nuclei etc. These could provide such additional heating to the gas before or during its deposition into the group halos (Kaiser 1991; Evrard & Henry 1991). The preheating model explains the observed $L-T$ and $S-T$ scaling relations in groups. Such preheating leads to a more extended gas component in groups than in rich clusters, lower central gas densities (and therefore increase the entropy of the intragalactic medium) and shallower density slopes. Moreover, without preheating, groups appear to over-produce the X-ray background (Wu, Fabian, & Nulsen 2000).

$\sigma - T$, $\sigma - M$ relations

Since the velocity dispersion of the galaxies and the temperature of the intragroup medium provide a measure of the gravitational potential strength (Eq. 1.5), a correlation between these two quantities is expected. The virial theorem (Eq. 1.2) tells us that the total kinetic energy of the intragalactic medium $T \propto \sigma_r^2 \propto GM/R$, where M and R are the total mass and the radius of group or cluster. Since the density of the baryonic matter $\rho_{\rm baryonic} \propto MR^{-3}$, then using Eq. 1.5 it is obvious that

$$T_{gas} \propto \sigma_r^2 \quad , \quad M \propto \sigma_r^3. \tag{1.25}$$

Fig. 1.1 shows the observed X-ray temperature against velocity dispersion for a sample of clusters and high temperature ($T_X \sim 1$ keV) groups. The group data are taken from the literature compilation of Xue & Wu (2000), with the addition of the groups in Helsdon & Ponman (2000). The cluster data are taken from Wu, Xue, & Fang (1999). Groups appear to follow the extrapolation of the trend found for rich clusters (i.e. $T_X \propto \sigma_r^2$; Mulchaey & Zabludoff 1998; Helsdon & Ponman 2000).

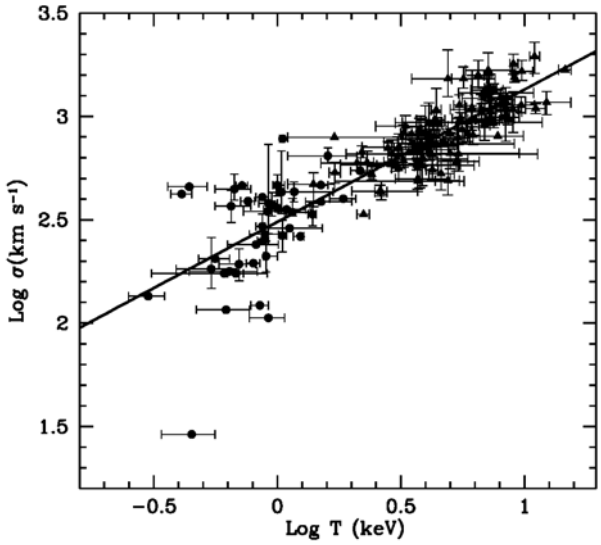

Figure 1.1: Logarithm of the X-ray temperature versus logarithm of optical velocity dispersion for a sample of groups (*circles*) and clusters (*triangles*). The solid line represents the best fit for the sample of clusters and of galaxies is consistent with the scaling relation $T_X \propto \sigma^2$. Within the large scatter, the relation for the groups is consistent with the relation for the clusters (Credit: Mulchaey 2000). The slope of the relation does not appreciably change from clusters to groups.

$L_X - T_{gas}$, $L_X - \sigma$ relations

It has been established that X-ray luminosity is strongly correlated with the intragalactic medium temperature (Mushotzky et al. 1978). Two properties that can be obtained from the observed continuum are the gas temperature T_{gas} and the emission integral $\int n_p n_e dV$ where n_p and n_e

are the proton and electron density, and V is the volume of the gas in the group or cluster respectively (Sarazin 1986). By assumption that the X-ray emission from the intragalactic medium is mainly due to thermal bremsstrahlung, then the emission integral, X-ray luminosity L_X, and gas temperature T_{gas} are related by

$$L_X \propto \int_{\rm Volume} T_{gas}^{1/2} n_p n_e dV, \tag{1.26}$$

where the integral $\int_{\rm volume} dV \propto \rho_{\rm baryonic}^{-1} M$ is over the whole volume of the group or cluster. Again equations (1.25) and (1.26) lead us to the scaling relations among the X-ray luminosity, X-ray temperature, and the velocity dispersion in the form of

$$L_X \propto \sigma_r^4 \quad , \quad L_X \propto T_{gas}^2. \tag{1.27}$$

Figures 1.2 and 1.3 represent the observed $L_X - T_{gas}$ and $L_X - \sigma$ relations in groups (Helsdon & Ponman 2000) and clusters (Xue & Wu 2000). Fig. 1.2 shows that for the most part, these relations for groups are consistent with those for clusters. Based on ROSAT studies, the slopes derived by Mulchaey & Zabludoff (1998), Ponman et al. (1996) and Helsdon & Ponman (2000) are $L_X \propto \sigma_r^{4.3}$, $\sigma_r^{4.9}$ and $\sigma_r^{4.5}$ respectively, in fair agreement with the model. However Ponman et al. (1996) and Helsdon & Ponman (2000) found that for groups the $L_X - \sigma_r$ relationship is somewhat flatter for low velocity dispersion systems. From the ROSAT All Sky Survey data, Mahdavi et al. (1997) derived a significantly flatter slope ($L_X \propto \sigma_r^{1.56}$) and suggested that for low velocity dispersion systems the X-ray emission is dominated by hot gas clumped around individual galaxies.

Also, there is considerable deviation from the self-similar $L_X - T_{gas}$ scaling relation obtained by different authors. By studying hot groups (i.e. $T \sim 1$ keV), Mulchaey & Zabludoff (1998) found that a single $L_X - T_{gas}$ relationship in the form of $L_X \propto T_{gas}^{2.8}$ could describe groups and clusters. By including much cooler systems (down to 0.3 keV), Ponman et al.

(1996) and Helsdon & Ponman (2000) found steeper relationships for groups ($L_X \propto T_{gas}^{8.2}$ and $T_{gas}^{4.9}$, respectively). Fig. 1.3 suggests the deviation of the cool groups from the cluster relationship. The fact that the $L_X - \sigma_r$ relationship for groups appears to be similar to the relation found for clusters, while the relation involving gas temperature significantly depart from the cluster trends, may be an indication that non-gravitational heating is important in groups (Ponman et al. 1996; Helsdon & Ponman 2000; Borgani et al. 2002).

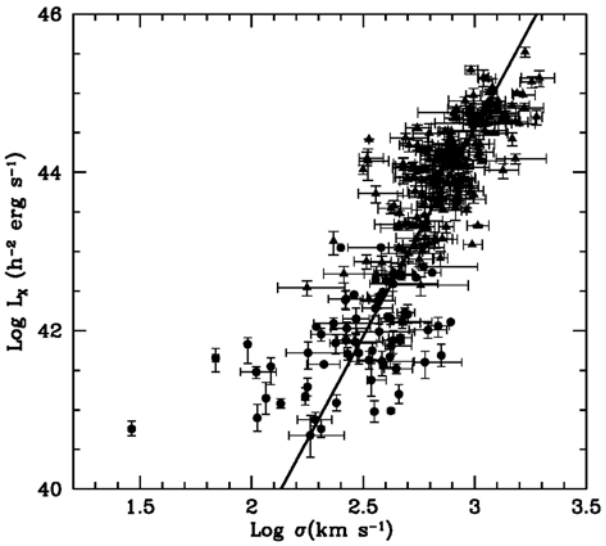

Figure 1.2: Logarithm of optical velocity dispersion versus logarithm of X-ray luminosity for a sample of groups (*circles*) and clusters (*triangles*). The solid line represents the best-fit for the sample of clusters (Credit: Mulchaey 2000).

$S - T_{gas}$ relation

The entropy is defined as

$$S = \frac{T_{gas}}{n_e^{2/3}} keV cm^2, \tag{1.28}$$

which can be determined by X-ray measurements. n_e is the electron density and T_{gas} is the intragalactic gas temperature. Since the density of the gas remains constant at a particular epoch, a self-similar relation of the following form is expected

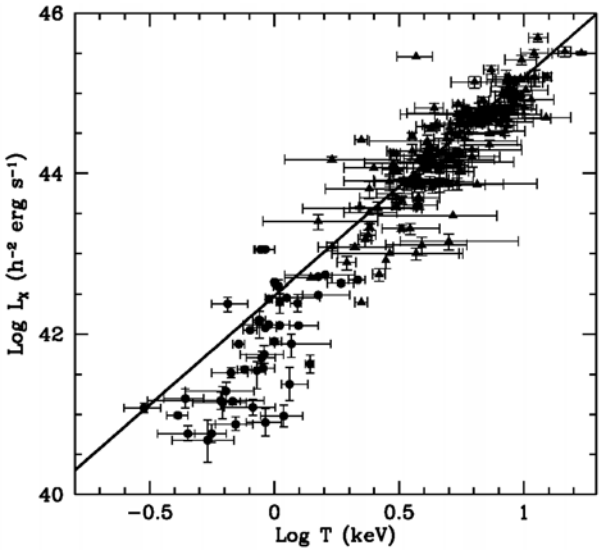

Figure 1.3: Logarithm of the X-ray temperature versus logarithm of X-ray luminosity for a sample of groups (*circles*) and clusters (*triangles*). The solid line represents the best fit for the clusters sample. The observed relationship for groups is somewhat steeper than the best-fit cluster relationship (Credit: Mulchaey 2000).

$$S \propto T_{gas}. \tag{1.29}$$

However, observations show that the $S - T_{gas}$ relation deviates from the self-similar model given in Eq. 1.29. Results from Ponman, Sanderson, & Finoguenov (2003) show the presence of excess entropy of ~ 100 keV cm^2 at a virial radius of $0.1r_{vir}$ in all temperature bands relative to the very hot systems ($T_{gas} \sim 10$ keV) which appears as flattening in S toward low T_{gas} in Fig. 1.4. Similar result was obtained by Lloyd-Davies, Ponman, & Cannon (2000) from their study of 20 galaxy clusters and groups. Though measurements close to the cluster centre provide the most sensitive probe of excess entropy, detection of additional entropy at larger radii is specially interesting. Evidence for entropy excess was found even at larger radius, r_{500} ($\sim \frac{2}{3} r_{200}$), by Finoguenov et al. (2002) and Ponman, Sanderson, & Finoguenov (2003).

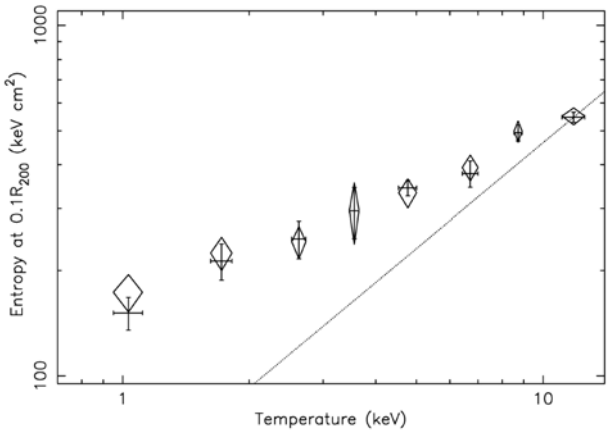

Figure 1.4: Gas entropy at $0.1r_{200}$ as a function of system temperature for 66 virialized systems, ranging in mass from single elliptical galaxies to rich clusters. The dotted line shows the self-similar slope of 1, i.e. $S \propto T_{gas}$ (Credit: Ponman, Sanderson, & Finoguenov 2003).

1.7.3 Scaling relations in fossil groups

Khosroshahi, Ponman, & Jones (2007) have provided the first detailed study of the scaling relations in seven fossil groups and have compared them to normal groups and clusters. They have also found that the mass concentration in fossils is higher than in non-fossil groups and clusters. In addition, by comparison with X-ray bright groups of Helsdon & Ponman (2003) as well as the GEMS groups of Osmond & Ponman (2004), Khosroshahi, Ponman, & Jones (2007) have shown that for a given total luminosity in the R-band (L_R), fossils are more luminous in X-rays than non-fossil groups. Also, for a given group velocity dispersion, fossil groups tend to be more X-ray luminous and hotter than non-fossil groups. However, they tend to follow galaxy clusters in the $L_X - \sigma$ and $T_X - \sigma$ planes.

1.8 Galaxy luminosity function

1.8.1 Introduction

We can learn about galactic evolutionary processes by studying the distribution of galaxy magnitudes (in any photometric passband) or the observed number of galaxies with different luminosities that exist in a given volume of space. We quantify this distribution with the galaxy luminosity function , $\Phi(L)$. The luminosity functions of galaxies belonging to different environments provide important observational ingredients for cosmology as well as studying the formation and evolution of galaxies.

The luminosity function holds basic information about the power spectrum of the primordial density fluctuations as well as the physical processes that convert mass into light such as gravitational collapse, cooling and star formation. It does help us to improve models of galaxy formation and evolution. Present semi-analytical models are being used to test such models. Also it contains information on the baryonic and luminosity densities of the universe as well as the mechanisms that evolve the morphology of galaxies such as merging, tidal interaction, and ram pressure stripping (Dressler 1984; Binggeli, Sandage & Tammann 1988).

The quantity $\Phi(L)$ is proportional to the number of galaxies that have luminosities in the range (L, L+dL). Schechter (1976) and Turner & Gott (1976b) determined the galaxy luminosity functions of small groups and rich clusters. Schechter (1976) also proposed the following form for the luminosity function according to the observed data of clusters and field galaxies

$$\Phi(L)dL = \Phi^*(L/L^*)^{\alpha}e^{(-L/L^*)}d(L/L^*), \tag{1.30}$$

or in terms of absolute magnitude

$$\Phi(M)dM = (0.4\ln 10)\Phi^* 10^{0.4(M^*-M)(1+\alpha)} \times \exp\left(-10^{0.4(M^*-M)}\right)dM, \tag{1.31}$$

with the normalisation parameter Φ^* and characteristic luminosity L^* (total magnitude M^*). Eq. 1.30 is called the *Schechter function*. At bright magnitudes, the Schechter function drops sharply. It rises at the faint-end following a power law with a slope given by α (or $-(1+\alpha)$ in case of Eq. 5.10). Thereby, the faint-end slope is decreasing, increasing, or flat for $\alpha > -1$, $\alpha < -1$, and $\alpha = -1$ respectively.

Numerous attempts have been made to determine the precise shape and parameters (α, Φ^*, and M^*) of the galaxy luminosity function, and its connection to local density and environment, spectral type, and redshift. The luminosity functions of galaxies with different morphological types for three different environments of the local field, clusters (the Virgo and Coma clusters), and groups are shown in Fig. 1.5 (Thompson & Gregory 1980; Binggeli, Sandage & Tammann 1988). According to Fig. 1.5, the overall shape of the luminosity function may be due to the varying functions of the different morphological type, however Miles, Raychaudhury, & Russell (2006) shows the above hypothesis is not true and the observed of depletion might be due a real effect, resulting from the [enhanced]merging of galaxies rather than a bright-end enhancement caused by excess star formation (see Fig. 1.6).

Though in many cases the overall Schechter function describes reasonably well the observed luminosity functions in field, clusters and groups, it is not easy to find a set of universal parameters that match to all environments. Even within the same environmental type, the determined luminosity function might not be the same. For example deep surveys of clusters of various richnesses, densities, evolutionary stages, and morphological classes have found a wide range of faint-end slopes. Also the determined luminosity function parameters for a given group or cluster are strongly correlated and significantly vary with the depth of the survey. It means that the same group or cluster population analysed to different magnitude limits will not necessarily give the same parameters for the Schechter function.

The local galaxy number density in groups is higher relative to the field. Because of that and the fact that the majority (more than 50%) of galaxies reside within galaxy groups (Eke et al.

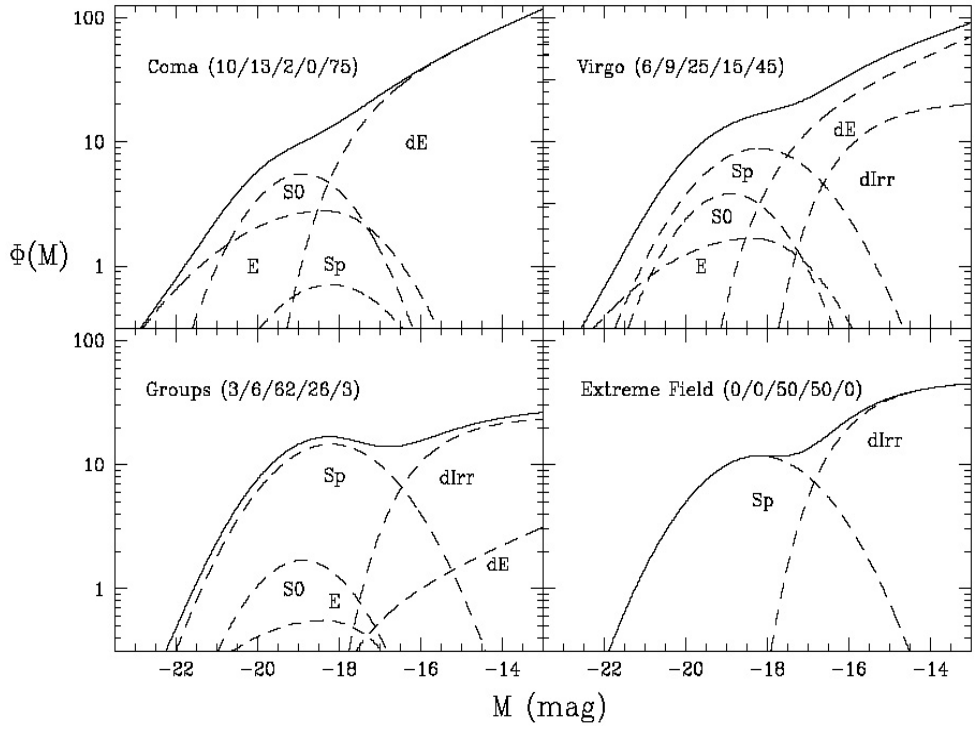

Figure 1.5: Overall luminosity functions (solid curves) for three different environments. Dashed curves show the contributions of the five main morphological galaxy types (ellipticals (E), spirals (S0, Sp), dwarf irregulars (dIrr), dwarf ellipticals (dE)) where their mixtures are indicated as percentages (Credit:Binggeli, Sandage & Tammann 1988).

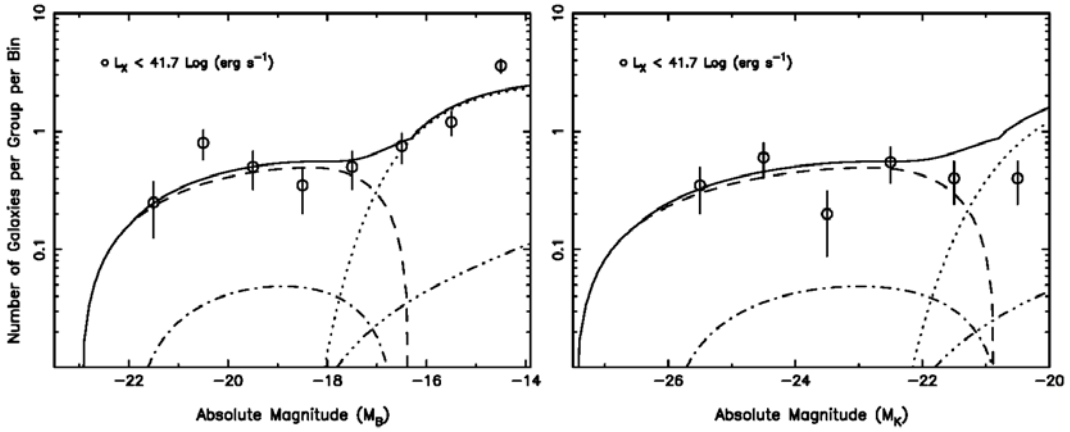

Figure 1.6: *Left panel*: the best-fitting five-component luminosity functions , one for each morphological type (ellipticals, S0s, spirals, dwarf irregulars and dwarf ellipticals), that add up to form the best model B-band LF. Also plotted are the observed data, averaged for 20 X-ray dim groups ($L_X < 10^{41.7}$ erg s^{-1}) out to 0.3 R_{500}. Here, the *dashed line*= ellipticals; *dashdoted*= S0s; *dotdashed*= dEs; *dotted line*= dIrrs and *continuous line*= sum of all components). According to these fits, spirals make a negligible contribution to the morphological makeup, contrary to observations. *Right panel*: The predicted K-band LFs of the five components, using the same line styles, together with the observed LF from the 2MASS analysis in this paper (Credit: Miles, Raychaudhury, & Russell 2006).

2004; Berlind et al. 2006), they provide an excellent site to study the formation and evolution of galaxies and their dependence on the local environment. Unlike the clusters of galaxies, galaxy groups have a small number of luminous galaxies which together with their smaller size, make them a difficult target for detection specially if they are at high redshift. Therefore, the determination of luminosity function of groups is rather difficult than clusters.

Unlike groups, cluster of galaxies show a high galaxy density contrast against the field galaxies. They contain hundreds of galaxies covering various morphological types, all located at the same distance in a small volume of space. It makes the identification of clusters easier than that of groups and make them the best place to perform luminosity function studies. Because of this, most of the studies have focused on clusters or the overall galaxy luminosity function in large redshift surveys. Studies of luminosity functions of galaxies in the group environment for large samples are relatively rare (e.g. Miles et al. 2004; Miles, Raychaudhury, & Russell 2006).

1.8.2 Is the galaxy luminosity function a universal function?

An important topic of discussion in the early studies of the luminosity function has been to determine whether the luminosity function in clusters has a universal shape or not (Oemler 1974). Schechter (1976) proposed a universal form for the cluster luminosity function in the form of Eq. 1.30 with a faint-end slope of $\alpha = -1.25$ and $M_B^* = -20.6 + 5\log h_{50}$. Several studies supported the idea for a universal luminosity function (e.g., Lugger 1986; Colless 1989; Gaidos 1997; Yagi et al. 2002; De Propris et al. 2003).

From the 2dF Galaxy Redshift Survey De Propris et al. (2003) explored the composite luminosity function of 60 catalogued clusters and found a good fit for a Schechter function with ${M_{b_J}}^* = -20.07 \pm 0.07$ and $\alpha = -1.28 \pm 0.03$. These parameters differ significantly from the field luminosity function of Madgwick et al. (2002), with a characteristic magnitude ${M_{b_J}}^*$ which is nearly 0.3 mag brighter and a faint-end slope that is almost 0.1 steeper. They found similar luminosity function for poor and rich clusters or even clusters with high or low velocity dispersions without any evidence for variations in the luminosity function across a broad range of cluster properties. Even clusters with and without substructures appeared to have the same luminosity function in their studies.

Contrarily, there are several other studies that show that the cluster luminosity function does not have a universal form (e.g. Godwin & Peach 1977; Dressler 1978; Piranomonte et al. 2001; Hansen et al. 2005; Popesso et al. 2004).

The dependence of the luminosity function on cluster-centric radius is expected as the galaxy type mixture in clusters varies with radius. That is because galaxy morphology correlates with the environmental density as inferred by Dressler (1980), which is now known as *galaxy morphology-density relation*. It means that early-type galaxies (i.e., elliptical (E), lenticular (S0), and dwarf elliptical (dE) galaxies) predominate in the high density regions whereas the field is dominated mainly by late-type (star-forming) galaxies such as spirals and and dwarf galaxies.

Type	Nb	α	$M^*_{AB}(B) - 5\log(h)$ (mag)	ϕ^* ($\times 10^{-3}\ h^3\ \mathrm{Mpc}^{-3}$)
disk	892	$-1.19^{+0.07}_{-0.07}$	$-20.22^{+0.15}_{-0.15}$	$12.39^{+2.18}_{-2.01}$
bulge	261	$-0.53^{+0.13}_{-0.13}$	$-20.20^{+0.19}_{-0.20}$	$7.48^{+1.04}_{-1.11}$
red-bulge	178	$+0.55^{+0.21}_{-0.21}$	$-19.53^{+0.14}_{-0.15}$	$7.44^{+0.56}_{-0.56}$
blue-bulge	83	-2.00	$-20.95^{+0.63}_{-0.79}$	$0.16^{+0.16}_{-0.09}$

Figure 1.7: Schechter parameters for the rest-frame B-band luminosity function in the redshift bin 0.4-0.8 and the corresponding 1σ error (Credit: Ilbert et al. 2006).

The current knowledge on the type specific luminosity functions in the field and clusters is still in early stages. As discussed by Binggeli, Sandage & Tammann (1988), different morphological types are shaped by different luminosity functions . There is some observational evidence that the cluster luminosity function does vary with cluster-centric radius (Beijersbergen et al. 2002; Hansen et al. 2005; Goto et al. 2005; Popesso et al. 2004).

By classifying the cluster galaxies into early-type, intermediate, and late-type, De Propris et al. (2003) found that the luminosity function of early-type galaxies have brighter characteristic magnitudes and shallower faint-end slopes in comparison to late-type galaxies, similar to the luminosity function in the field. But in comparison to the field, the luminosity function of early-type cluster galaxies is brighter and steeper while the luminosity function of late-type galaxies is similar in both field and cluster.

One of the most important quantities for characterising the luminosity function of a galaxy population and its correlation to different environments and morphological type is the faint-end slope α. As Fig. 1.7 shows, the value of α derived for galaxies with different morphological type seems to be different from each other (Ilbert et al. 2006).

De Propris et al. (2003) argue that the difference between the cluster and field luminosity functions for galaxies with different spectral types and morphologies can be explained qualitatively as a result of the star formation truncation in the dense environment of clusters together with galaxy mergers that produce the early type brightest cluster galaxies (BCGs).

1.8.3 The luminosity function in clusters

Unlike groups, Cluster of galaxies show a high galaxy density contrast against the field galaxies. They contain hundredes of galaxies covering various morphological types, all located at the same distance in a small volume of space. It makes the identification of clusters easier than groups and make them the best place to perform luminosity function studies.

Because of that, most of the studies have been focused on clusters (Oemler 1974; Dressler 1978; Oegerle et al. 1986; Oegerle et al. 1987; Garilli, Maccagni, & Vettolani 1991; Garilli et al. 1992; Driver, Windhorst, & Griffiths 1995; Barrientos, Schade, & Lopez-Cruz 1996; Gaidos 1997; Valotto et al. 1997; Trentham 1997; De Propris et al. 2003; Gilbank et al. 2008) or the overall galaxy luminosity function (Cole et al. 2001; Blanton et al. 2001; Norberg et al. 2002; Madgwick et al. 2002; Blanton et al. 2003; Montero-Dorta & Prada 2008).

Note that the number of references regarding the study of luminosity function in clusters is much more than what have been presented here. However, my main concern is to review the previous studies on group luminosity function . Thus I just look over a few main results from the study of luminosity function in field and clusters using large-scale galaxy surveys and then direct the discussion toward the same in galaxy groups.

An important topic of discussion in the early studies of the luminosity function has been to determine whether the luminosity function in clusters has a universal shape or not(Oemler 1974). Schechter (1976) proposed a universal form for the cluster luminosity function in the form of Eq. 1.30 with characterisation parameters of a faint-end slope of $\alpha = -1.25$ and $M_B^* = -20.6 + 5\log h_{50}$. Several studies supported the idea for a universal luminosity function (e.g.,Lugger 1986; Colless 1989; Gaidos 1997; Yagi et al. 2002; De Propris et al. 2003).

For example by using data from the 2dF Galaxy Redshift Survey De Propris et al. (2003) explored the composite luminosity function of 60 catalogued clusters and found a well fitted Schechter function with ${M_{b_J}}^* = -20.07 \pm 0.07$ and $\alpha = -1.28 \pm 0.03$. These parameters differ significantly from the field luminosity function of Madgwick et al. (2002), with a characteristic

magnitude $M_{b_J}{}^*$ which is nearly 0.3 mag brighter and a faint-end slope that is almost 0.1 steeper. They found similar luminosity function for poor and rich clusters or even clusters with high or low velocity dispersions without any evidence for variations in the luminosity function across a broad range of cluster properties. Even clusters with and without substructures appeared to have the same luminosity function in their studies.

Contrarily, there are several other studies that show that the cluster luminosity function has not a universal form such as Godwin & Peach (1977), Dressler (1978), Piranomonte et al. (2001), Hansen et al. (2005), Popesso et al. (2004).

1.8.4 Luminosity function of groups

Given the observed differences between field and cluster mean galaxy luminosity functions , several studies have attempted to investigate the luminosity function of galaxies in moderate density associations, i.e. in galaxy group environment. These studies use small group catalogues (i.e., Turner & Gott 1976b; Heiligman & Turner 1980; Ferguson & Sandage 1991; Muriel, Valotto, & Lambas 1998) or large redshift surveys of galaxies such as SDSS (Yang et al. 2005) at optical and near-infrared wavelengths. The group luminosity function may be an important indicator of evolution of group galaxy members. In particular, the luminosity function may be modified by the effect of tidal distortion, stripping, dynamical friction, and mergers, which would be expected to be quite severe in the low-velocity dispersion environment of groups (Miles et al. 2004; Miles, Raychaudhury, & Russell 2006).

The luminosity function of groups selected according to different criteria (such as normal groups, compact groups, fossil groups, or even groups selected according to their X-ray luminosities) are shown to be systematically different from each other. I summarise the main results from these studies.

Normal groups

One source of uncertainty in the determination of the group luminosity function is the small number of known members per group. Taking into account chance superpositions of galaxies along the line of sight, it would be difficult to distinguish between the bound group members and field galaxies. Statistical background subtraction on the other hand is sensitive to the large-scale structure inhomogeneities especially in the case of groups with low surface density contrast. To address such problems, it is important to study the galaxy luminosity function in a sample of groups with not only the properties of bound systems (where there is evidence that members lie in a common potential well) but also with a large number of spectroscopically confirmed group members.

Following a combined multi-object spectroscopy and wide-field CCD imaging of a sample of six nearby poor groups, Zabludoff & Mulchaey (2000) examined the form of the group galaxy luminosity function. Their sample contained five X-ray luminous groups (with more than 300 confirmed spectroscopic members) while the sixth group was marginally X-ray detected. For those five X-ray luminous groups, they found a composite group galaxy luminosity function which is well-fitted and consistent with a Schechter function with $M_R^* = -21.6 \pm 0.4 + 5 \log h$ and $\alpha = -1.3 \pm 0.1$. Results from Zabludoff & Mulchaey (2000) also show that the form of the galaxy luminosity function changes with environment, initially due to an increase in the dwarf-to-giant ratio of quiescent galaxies in higher density regions, at least up to the densities characteristic of X-ray luminous poor groups. Thus dwarf-to-giant ratios are smaller in regions outside of groups and in poorer groups than in X-ray luminous groups.

Similar results were found by Trentham & Tully (2002) and Mahdavi, Trentham, & Tully (2005) which strongly support the proposition that the faint-end slope of the luminosity function of galaxies and dwarf-to-giant ratios varies with environment. Fig. 1.8 compares the percentage of dwarf elliptical galaxies in Virgo cluster together with 6 other galaxy groups (NGC1407, Coma I, Leo, NGC 1023, and NGC 5846) and their variations with group central galaxy density

(Mahdavi, Trentham, & Tully 2005).

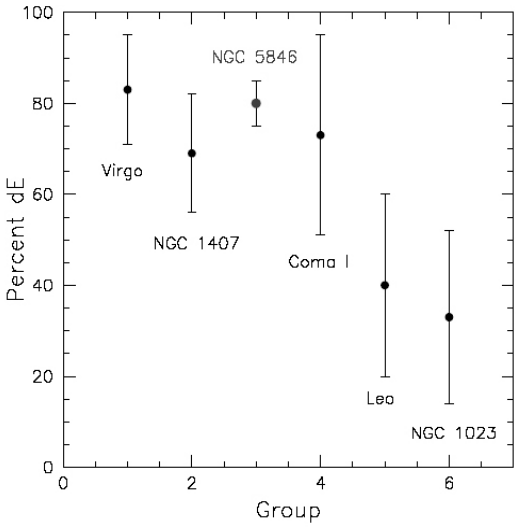

Figure 1.8: Percentage of dwarf galaxies ($-17 < M_R < -11$) classified as dE (including nucleated dE,N subtypes and transition dE/I subtypes).The x-axis shows the ranking of the groups in order of decreasing central galaxy density. (Credit: Trentham & Tully (2002), Mahdavi, Trentham, & Tully (2005)).

However, Lin, Mohr, & Stanford (2004) found a different result from what was argued by Zabludoff & Mulchaey (2000), Trentham & Tully (2002), and Mahdavi, Trentham, & Tully (2005) regarding the fraction of dwarf-to-giant galaxies in groups and clusters. Their analysis of K-band luminosity functions for a sample of 93 X-ray selected galaxy systems (with a faint-end slope $-1.1 \lesssim \alpha \lesssim -0.84$) whose virial masses range from groups ($3 \times 10^{13} h_{70}^{-1} M_{\odot}$) to clusters ($1.5 \times 10^{15} h_{70}^{-1} M_{\odot}$) show that there is a remarkable decrease in the number density of faint galaxies (fainter than M^*) as one moves from low mass groups to higher mass clusters.

Results from the large sky surveys

There have been at least two separate studies of galaxy luminosity function in groups (and in five u, g, r, i, z bands) using the SDSS data with different methods to identify groups and with

completely different results (Gonza'lez et al. 2006; Zandivarez et al. 2006).

Gonza'lez et al. (2006) computed the galaxy luminosity function in 728 spectroscopically selected nearby groups and clusters using SDSS DR3 catalogue and found a universal luminosity function in galaxy systems with only small variations of the shape of the luminosity function in the faint end, irrespective of the group integrated colour, mass, number of members, or the presence of a hot intra-cluster gas associated with X-ray emission. They argue that the galaxy luminosity function cannot be described by a single Schechter function.

Interestingly, Zandivarez et al. (2006) used the fourth release of the Sloan Digital Sky Survey to analyse the luminosity function of 14,004 samples of groups with different properties and found that the luminosity functions are well described by Schechter functions (see Fig. 1.9). Unlike the works of Gonza'lez et al. (2006), the detailed analysis carried out by Zandivarez et al. (2006) shows the dependence of the galaxy luminosity function on group masses and rule out the existence of a universal galaxy luminosity function . Their studies show a steepening of the faint-end slope α and a continuous brightening of the characteristic magnitude M^* as group mass increases.

Compact groups & bimodality in luminosity functions

Several studies have been carried out exclusively on the shape of galaxy luminosity function in Hickson Compact Groups (HCGs; Hickson 1982), which in general represent a subset of groups consist of highly concentrated bright galaxy population. There are some uncertainty in the determined luminosity function in HCGs and the population of faint galaxies in these compact systems.

Some authors believe that the standard Schechter form of the luminosity function can express the observed luminosity distribution of HCG galaxies (Heiligman & Turner 1980; Mendes de Oliveira & Hickson 1991; Zepf, de Carvalho, & Ribeiro 1997). However, more recent studies of the luminosity function of compact groups show a bimodality in the distribution of bright

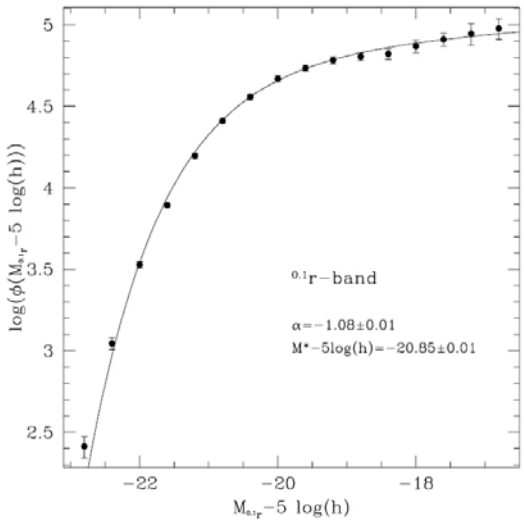

Figure 1.9: The galaxy group r-band luminosity function from the SDSS DR4. The units are arbitrary. The solid line represents the best-fitting Schechter function (Credit: Zandivarez et al. (2006)).

galaxies and dwarf galaxy population (Hunsberger, Charlton, & Zaritsky 1998; Hunsberger, Charlton, & Zaritsky 2000; Krusch et al. 2006).

From an analysis of the luminosity function and the estimated mean luminosity density of galaxies in 68 HCGs, Mendes de Oliveira & Hickson (1991) concluded that bright galaxies in compact groups merge on a relatively short time scale to form luminous elliptical galaxies. From the Schechter fitting function, Mendes de Oliveira & Hickson (1991) obtained $\alpha = -0.2$ which indicates lack of faint galaxies in compact groups in comparison to the total luminosity function of field, loose groups, and clusters in agreement with Sulentic & Rabaca (1994).

However, Ribeiro, de Carvalho, & Zepf (1994) obtained different results and found a slope of the faint end of the luminosity function of approximately $\alpha = -0.8$ which is not significantly different from that found for galaxies in other environments. Results from Ribeiro, de Carvalho, & Zepf (1994) do not support the idea that faint galaxies in compact groups are underabundance and therefore most galaxies in compact groups have not been dramatically affected by recent

galaxy-galaxy merging.

X-ray groups

Hunsberger, Charlton, & Zaritsky (1998) found a deficit (dip) of intermediate luminosity galaxies around $M_R \sim -18 + 5 \log h$ in the observed composite luminosity function of 39 HCGs observed (Fig. 1.11). They suggested that galaxy mergers and dynamical friction cause intermediate luminous galaxies to acquire mass and to move toward the bright end of the galaxy luminosity function in some poor HCGs. They found a substantial population of dwarf galaxies in X-ray HCG groups as well as groups with a dominant lenticular or elliptical galaxy. This result together with the observed bimodal luminosity function, led them to conclude that the initial dwarf galaxy population in compact groups belong to a subsequent generations which have been formed in the tidal debris remnants from interaction of giant galaxies.

Miles et al. (2004) used a sample of galaxy groups, selected from the GEMS catalogue (Galaxy Evolution Multi-wavelength Study; Osmond & Ponman 2004), with measured X-ray fluxes from ROSAT PSPC pointed observations and found that the luminosity function of galaxy groups with X-ray luminosity $L_X < 10^{41.7}$ erg s^{-1} is bimodal in comparison to X-ray luminous groups with $L_X > 10^{41.7}$ erg s^{-1}, which are not (Fig. 1.10). They interpreted this bimodality in the observed luminosity function as a result of enhanced region, aided by dynamical friction between galaxies in X-ray dim groups rather than due to the existence of galaxies with different morphological types.

The above idea is further supported by studying the near-infrared $J-$ and K-band luminosity functions of 60 GEMS group (Miles, Raychaudhury, & Russell 2006) which show a depletion of intermediate luminous galaxies around $M_K = -23$ in X-ray dim groups ($L_X < 10^{41.7}$ erg s^{-1}). They suggest that the low velocity dispersion in dim X-ray groups, resulting in rapid major mergers in agreement with their previous findings. This causes galaxies with intermediate luminosity to merge with each other and the brightest group galaxies, and is seen preferentially

in the dynamically less active poorer groups. Such a deficit of intermediate luminosity galaxies was found also by Krusch et al. (2006) from the luminosity function analysis of a sample of five HCGs.

1.9 Numerical simulations

1.9.1 Introduction

Numerical methods and statistical tools have developed significantly in the last two decades for simulating cosmic structure in the present of dark matter. In science and engineering, it is often important to simulate a physical process because the ability to analytically describe the process is limited.

The simplest form of a cosmological simulation is a gravitational N-body simulation, which calculates the trajectories of massive particles moving under mutual gravitation. Simulations of specific models of dark matter allow us to make predictions for these models and compare with observations. Simulations allow us to carry out numerical experiments with initial conditions that have little to do with the real universe. The purpose of such experiments is to understand the physics of gravitational collapse in an expanding universe. Simulations are also used for testing approximate solutions for the growth of density perturbations.

Comparisons with N-body simulations allow us to validate these approximations and understand when these approximations are useful. Finally since in observations we have limited information, we can calibrate methods for analysing observations on artificial catalogues made from N-body simulations.

A great advantage is that in N-body simulations, the details of the model, used to generate the simulation, are known, whereas the same is not true of the real universe. For example all the components of the velocity of a galaxy in a cluster, with respect to the centre of the cluster, are known, where in real observations, only the radial component can be measured from the redshift

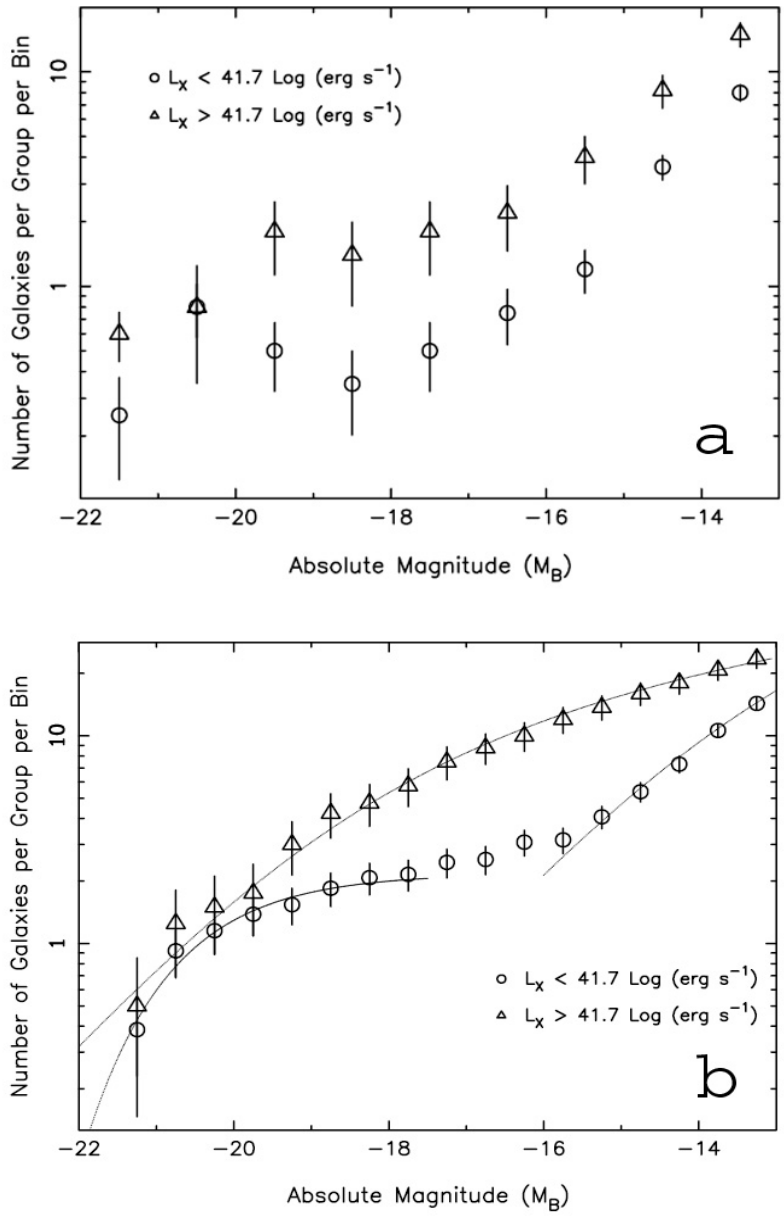

Figure 1.10: (a) Differential B-band luminosity functions of 25 GEMS groups of galaxies shows that the X-ray dim groups ($L_X < 10^{41.7}$ erg s^{-1} , *circles*) have a 'dip' in their luminosity function in the range of $-19 < M_B < -17$ in comparison to the X-ray luminous groups ($L_X > 10^{41.7}$ erg s^{-1} , *triangles*) (b) Cumulative luminosity function for the same sample as in (a). The luminosity function of the X-ray luminous groups is fitted with a single Schechter function whereas the luminosity function of X-ray dim groups represents two Schechter functions (Credit: Miles et al. (2004)).

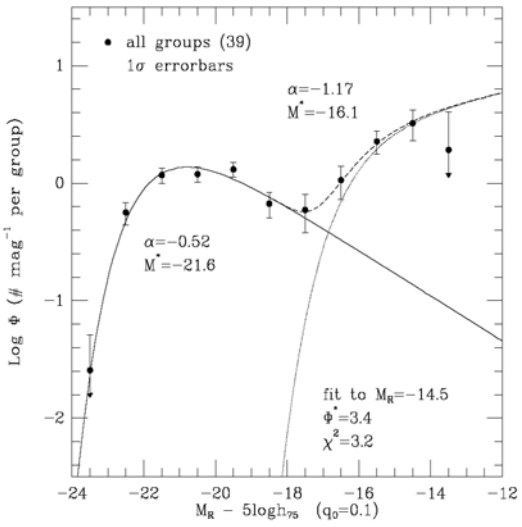

Figure 1.11: Galaxy luminosity function of 39 Hickson compact groups. *Filled circles* represent the average number of galaxies per group in each magnitude bin. The bright and faint populations are fit separately using two Schechter functions. The *Solid line* is the best fit to the bright end while the *dotted line* is the best fit to the faint end. The *dashed line* is the composite fit (Credit: Hunsberger, Charlton, & Zaritsky (1998)).

of the galaxy. Furthermore, the evolution of the same galaxy or cluster can not be observed at different redshifts.

The above algorithms of cosmological N-body simulations take only Newtonian gravitational interaction into account. Gravitational force in the Newtonian limit falls as $\sim r^{-2}$, hence it is a long range force and we cannot ignore force due to distant particles. This makes calculation of force the most time-consuming task in N-Body simulations. As a result, various algorithms and optimising schemes have been developed to achieve this, within realistic bounds of computer resources. Evaluation of force and solving the equation of motion are two key components of N-body simulations. Setting up relevant initial conditions for cosmological simulations is another important aspect.

In all N-body simulations, a value for the mass must be assigned to the particles. For

example, if we wish to study the distribution of galaxies in detail, then the mass of each particle in the simulation should be much smaller than the mass of a typical galaxy. It increases the resolution of the simulation but has a high computational cost.

Large scale cosmological simulations of structures in the Universe attempt to incorporate physical processes (adiabatic gas dynamics, radiative cooling, photoionization and recombination, radiative and heat transfer), in addition to gravitational effects, to trace back the structure of the universe from the present day to a few billion years ago, according to the cosmological models such as cold dark matter (CDM), or the ΛCDM model, in which the dark energy is included as well. Different numerical methods and computer algorithms have been developed to perform simulations with a large number of particles, dynamic range and resolution such as *Particle-Particle (PP) method*, *Tree Method*, *Fast Multipole Method*, *Particle-Mesh Method (PM)*, *Adaptive Mesh Refinement (AMR)*, *P^3M Method (Particle-Particle + Particle-Mesh)* and *Tree + PM (TMP, TreePM) Method* (for a review see Bertschinger 1998).

1.9.2 Semi-analytic modelling of galaxy formation

The Semi-analytic model (SAM) of galaxy formation has been developed by Kauffmann, White, & Guiderdoni (1993).

In most semi-analytic models of galaxy formation (e.g. Kauffmann, White, & Guiderdoni 1993) the merger trees (merging histories) of dark matter halos are identified by implementing numerical methods based on extended Press-Schechter models (Peacock & Heavens 1990b; Bower 1991; Somerville et al. 2008) which is a modified version of the Press-Schechter formalism of mass functions of dark halos (Press & Schechter 1974). The extended Press-Schechter models are basically obtained from the power spectrum of initial density fluctuations together with a spherical collapse model to specify non-linear evolution of density fluctuations (Gunn & Gott 1972). The mass functions of the progenitors of later collapsed halos, at higher redshifts, are obtained by considering density fluctuations within overdense regions correspond to those

halos at lower redshifts which will collapse later.

Several physical processes have been implemented into Semi-analytic models to enable them to reproduce the observed properties of galaxies, galaxy groups and clusters (Bower et al. 2006; Croton et al. 2006). These processes include gas cooling, star formation, heating by supernova explosions (SN feedback) and active galactic nuclei outflows (AGN feedback), cooling suppression, reionisation, and galaxy mergers which all take place within dark matter halos. To compare results from Semi-analytic runs with those from observations, a technique is used based on stellar population synthesis.

One advantage that make Semi-analytic models a good approach in understanding the physics of galaxy evolution and formation is that it is much faster than hydrodynamical simulations. The reason is that unlike hydrodynamical simulations, in numerical simulations based on Semi-analytic models, the dynamics related with physical processes among particles are not included, which enable semi-analytic model to investigate a much larger range of parameters characterising physical processes affecting the evolution and interaction of galaxies in different environments.

1.10 Aim of this thesis

In the following chapters, the mass assembly and evolution of galaxy groups are studied, using numerical simulations as well as observations. In Sec. 1.6.1, we mentioned that the selection of groups based on the definition of fossil groups is expected to identify early formed systems. To test this hypothesis, the mass assembly history and formation of fossil galaxy groups are investigated in Chapter 2 and Chapter 3, using a large scale cosmological simulation of the Universe. Our aim is to investigate whether this class of groups represent early formed systems in comparison to normal groups, and to what extent their mass function and space density are in agreement with observations. Furthermore, we would like to find how the magnitude gap

between the brightest galaxies within groups is related to their halo mass assembly history, and test whether the magnitude gap can be used as a diagnostic of the age of the group, as it often used in the literature.

The properties of galaxy groups are explored then by compiling a set of 25 galaxy groups (with different merging histories). So in Chapters 4 and 5, the sample selection, observation, data reduction, and preliminary results are given. These results include group memberships, group galaxy luminosity function , as well as colour-magnitude relation. A brief on our future work is discussed in Chapter 6.

Bibliography

Abell, G.O., 1958, ApJS, 3, 211

Arnaud, M. & Evrard, A.E., 1999, MNRAS, 305, 631

Aschenbach, B., 1988, ApOpt, 27, 1404

Athanassoula, E., Makino, J., Bosma, A., 1997, MNRAS, 286, 825

Bahcall, N.A., 1979, ApJ, 232, 689

Balogh et al., 2004, MNRAS, 348, 1355

Barnes, J.E., 1985, MNRAS, 215, 517

Barnes, J.E., 1989, Nature, 338, 123

Barrientos, L.F., Schade, D., Lopez-Cruz, O.,1996, ApJ, 460 , 89

Beijersbergen, M., Hoekstra, H., van Dokkum, P.G., van der Hulst, T., 2002, MNRAS, 329, 385

Berlind, A. A., et al. 2006, ApJS, 167, 1

Bertschinger, E., 1998, ARA&A, 36, 599

Binggeli, B., Sandage, A., Tammann, G.A., 1988, ARA&A, 26, 509

Binggeli, B., Tammann, G.A., Sandage, A., 1987, AJ, 94, 251

Binney, J. & Tremaine, S., *Galactic Dynamics.*, 1987, Princeton, NJ: Princeton University Press., USA

Blanton, M.R., Dalcanton, J., Eisenstein, D., Loveday, J., Strauss, M.A. et al., 2001, AJ, 121, 2358

Blanton, M.R., Hogg, D.W., Bahcall, N.A., Brinkmann, J., Britton, M. et al., 2003, ApJ, 592, 819

Borgani, S., Governato, F., Wadsley, J., Menci, N., Tozzi, P., Quinn, T., Stadel, J., Lake, G., 2002, MNRAS, 336, 409

Bower, R.G., 1991, MNRAS, 248, 332

Bower, R.G., 1997, MNRAS, 288, 355

Bower, R.G., Benson, A.J., Malbon, R., Helly, J.C., Frenk, C.S., Baugh, C.M., Cole, S., Lacey, C.G., 2006, MNRAS, 370, 645

Bryan, G.L. & Norman, M.L., 1998, ApJ, 495, 80

Carlberg, R.G., Yee, H.K.C., Morris, S.L., Lin, H., Hall, P.B., Patton, D.R., Sawicki, M., Shepherd, C.W., 2001, ApJ, 552, 427

Chandrasekhar, S., 1943, ApJ, 97, 255

Cole, Sh., Norberg, P.; Baugh, C.M.; Frenk, C.S.; Bland-Hawthorn, J. et al., 2001, MNRAS, 326, 255

Cole, S. & Lacey, C., 1996, MNRAS, 281, 716

Colless, M., 1989, MNRAS, 237, 799

Croton, D.J., Springel, V., White, S.D.M., De Lucia, G., Frenk, C.S., Gao, L., Jenkins, A., Kauffmann, G., Navarro, J.F., Yoshida, N., 2006, MNRAS, 365, 11

David, L.P., Arnaud, K.A., Forman, W., Jones, C. , 1990, ApJ, 356, 32

David, L.P., Blumenthal, G.R. , 1992, ApJ, 389, 510

David, L.P., Jones, C., Forman, W., 1996, ApJ, 473, 692

De Propris, R., Colless, M., Driver, S.P., Couch, W., Peacock, J.A. et al., 2003, MNRAS, 342, 725

D'Onghia, E., Sommer-Larsen, J., Romeo, A.D., Burkert, A., Pedersen, K., Portinari, L. & Rasmussen, J., 2005, ApJ, 630, L109

Dressler, A., 1978, ApJ, 223, 765

Dressler, A., 1980, ApJ, 236, 351

Dressler, A., 1984, ARA&A, 22, 185

Driver, S.P., Couch, W.J., Phillipps, S., 1998, MNRAS, 301, 369

Driver, S.P., Windhorst, R.A., Griffiths, R.E., 1995, ApJ, 453, 48

Duffy, L.D., Sikivie, P., Tanner, D.B., Asztalos, S.J., Hagmann, C., Kinion, D., Rosenberg, L.J., van Bibber, K., Yu, D.B., Bradley, R.F., 2006, PhRvD, 74a2006D

Eke, V.R., Cole, S., Frenk, C.S., 1996, MNRAS, 282, 263

Eke, V.R., Baugh, C.M., Cole, S., Frenk, C.S., King, H.M., Peacock, J.A., 2005, MNRAS, 362, 1233

Eke, V.R., Baugh, C.M., Cole, S., Frenk, C.S., Norberg, P. et al., 2004, MNRAS, 348, 866

Eke, V.R., Cole, S., Frenk, C.S., 1996, MNRAS, 282, 263

Evrard, A.E. & Henry, J.P., 1991, ApJ, 383, 95

Evrard, A.E., MacFarland, T.J., Couchman, H.M.P., Colberg, J.M., Yoshida, N., White, S.D.M., Jenkins, A., Frenk, C.S., Pearce, F.R., Peacock, J.A., Thomas, P.A., 2002, ApJ, 573, 7

Fellhauer, M., Kroupa, P., Baumgardt, H., Bien, R., Boily, C.M.,Spurzem, R., & Wassmer, N., 2000, NewA, 5, 305

Ferguson, H.C. & Sandage, A., 1991, AJ, 101, 765

Finoguenov, A., Reiprich, T.H., Bhringer, H., 2001, A&A, 368, 749

Finoguenov, A.; Jones, C.; Bhringer, H.; Ponman, T.J., 2002, ApJ, 578, 74

Gaidos, E.J., 1997, AJ, 113, 117

Garcia, A.M., 1993, A&AS, 100, 47

Garilli, B., Maccagni, D., Vettolani, G., 1991, AJ, 101, 795

Garilli, B., Bottini, D., Maccagni, D., Vettolani, G., Maccacaro, T., 1992, AJ, 104, 1290

Geller, M.J., Huchra, J.P., 1983, ApJS, 52, 61

Gerke, B.F., Newman, J.A., Davis, M., Marinoni, Ch., Yan, R. et al., 2005, ApJ, 625, 6

Gilbank, David G., Yee, H.K.C., Ellingson, E., Gladders, M.D., Loh, Y.S. et al., 2008, ApJ, 673, 742

Girardi, M., Manzato, P., Mezzetti, M., Giuricin, G., Limboz, F., 2002, ApJ, 569, 720

Giuricin, G., Marinoni, Ch., Ceriani, L., Pisani, A., 2000, ApJ, 543, 178

Godwin, J.G. & Peach, J.V., 1977, MNRAS, 181, 323

Goldstein, H., *Classical Mechanics* (2^{nd} Edition.), 1980, Addison-Wesley series in physics, USA

Gonza'lez, R.E., Lares, M., Lambas, D.G., Valotto, C. , 2006, A&A, 445, 51

Gonza'lez, R.E., Padilla, N.D., Galaz, G., Infante, L., 2005, MNRAS, 363, 1008

Goto, T., Postman, M., Cross, N.J.G., Illingworth, G.D., Tran, K. et al., 2005, ApJ, 621, 188

Gourgoulhon, E., Chamaraux, P., Fouque, P., 1992, A&A, 255, 69

Gunn, J.E. & Gott, J.R., 1972, ApJ, 176, 1

Guth, A.H., 1981, PhRvD, 23, 347

Hansen, S.M., McKay, T.A., Wechsler, R.H., Annis, J., Sheldon, E.S., Kimball, A., 2005, ApJ, 633, 122

Heiligman, G.M. & Turner, E.L., 1980, ApJ, 236, 745

Helsdon, S.F. & Ponman, T.J., 2000, MNRAS, 315, 356

Helsdon, S.F. & Ponman, T.J., 2003, MNRAS, 340, 485

Henriksen, M.J. & Mushotzky, R.F., 1986, ApJ, 302, 287

Hernquist, L., Katz, N., Weinberg, D.H., 1995, ApJ, 442, 57

Hickson, P., 1997, ARA&A, 35, 357

Hickson, P., 1982, ApJ, 255

Hinshaw, G. et al., arXive[astro-ph] 08030732v1

Huchra, J.P. & Geller, M.J., 1982, ApJ, 257, 423

Humason, M.L., Mayall, N.U. & Sandage, A.R., 1956, AJ, 61, 97

Hunsberger, S.D., Charlton, J.C., Zaritsky, D., 1998, ApJ, 505, 536

Hunsberger, S.D., Charlton, J.C., Zaritsky, D., 2000, ASPC, 209, 81

Ilbert, O. et al., 2006, A&A, 453, 809

Jones, L.R, Ponman, T.J. & Forbes, D.A., 2000, MNRAS, 312, 139

Jones, L.R, Ponman, T.J., Horton, A., Babul, A., Ebeling, H., Burke, D.J., and Forbes, D.A., 2003, MNRAS, 343, 627

Kaiser, N., 1986, MNRAS, 222, 323

Kaiser, N., 1991, ApJ, 383, 104

Kauffmann, G., White, S.D.M., Guiderdoni, B., 1993, MNRAS, 264, 201

Khosroshahi, H.G., Jones, L.R. & Ponman, T.J., 2004, MNRAS,349, 1240

Khosroshahi, H.G., Maughan, B.J., Ponman, T.J. & Jones, L.R., 2006, MNRAS, 369, 1211

Khosroshahi, H.G., Ponman, T.J., Jones, L.R., 2007, MNRAS, 377, 595

Krusch, E., Rosenbaum, D., Dettmar, R.-J., Bomans, D.J., Taylor, C.L., Aronica, G., Elwert, T., 2006, A&A, 459, 759

Lewis, I. et al., 2002, MNRAS, 334, 673

Lin, H., Kirshner, R.P., Shectman, S.A., Landy, S.D., Oemler, A., Tucker, D.L., Schechter, P.L., 1996, ApJ, 464, 60

Lin, Y-T, Mohr, J.J., Stanford, S.A., 2004, ApJ, 610, 745

Lloyd-Davies, E.J., Ponman, T.J., Cannon, D.B., 2000, MNRAS, 315, 689

Lopez-Cruz, O., Yee, H.K.C., Brown, J.P., Jones, C., Forman, W., 1997, ApJ, 475L, 97

Lugger, P.M., 1986, ApJ, 303, 535

Lynden-Bell, D., 1967, MNRAS, 136, 101

Madgwick, D.S., Lahav, O., Baldry, I.K., Baugh, C.M., Bland-Hawthorn, J. et al., 2002, MNRAS, 333, 133

Mahdavi, Andisheh; Boehringer, Hans; Geller, Margaret J.; Ramella, Massimo , 1997, ApJ, 483, 68

Mahdavi, A., Trentham, N., Tully, R.B., 2005, AJ, 130, 1502

Maia, M.A.G., da Costa, L.N. & Latham, D.W., 1989, ApJS, 69, 809M

Marinoni, C., Davis, M., Newman, J.A., Coil, A.L., 2002, ApJ, 580, 122

Markevitch, M., 1998, ApJ, 504, 27

Materne, J., 1979, A&A, 74, 235

Mendes de Oliveira, C.L., Cypriano, E.S., Sodr, L.Jr., 2006, AJ, 131, 158

Mendes de Oliveira, C.L. & Hickson, P., 1991, ApJ, 380, 30

Meneghetti, M., Jain, B., Bartelmann, M., Dolag, K., 2005, MNRAS, 362, 1301

Shu, C., Zhou, B., Bartelmann, M., Comerford, J.M., Huang, J.-S., Mellier, Y., 2008, ApJ, 685, 70

Smith, G.P., Kneib, J-P., Smail, I., Mazzotta, P., Ebeling, H., Czoske, O., 2005, MNRAS, 359, 417

Mercha'n, M.E., Maia, M.A.G., Lambas, D.G., 2000, ApJ, 545, 26

Mercha'n, M. & Zandivarez, A., 2002, MNRAS, 335, 216

Mercha'n, M.E. & Zandivarez, A., 2005, ApJ, 630, 759

Miles, T.A., Raychaudhury, S., Forbes, D.A., Goudfrooij, P., Ponman, T.J., Kozhurina-Platais, V. et al., 2004, MNRAS, 355, 785

Miles, T.A., Raychaudhury, S., Russell, P.A., 2006, MNRAS, 373, 1461

Milosavljević, M., Miller, C.J., Furlanetto, S.R. & Cooray, A., 2006, ApJ, 637, L9

Montero-Dorta, A.D. & Prada, F., 2008, arXiv0806.4930

Moore, B., Quinn, T., Governato, F., Stadel, J., Lake, G., 1999, MNRAS, 310, 1147

Morgan, W.W., 1958, PASP, 70, 364

Mulchaey, J.S., 2000, ARA&A, 38, 289

Mulchaey, J.S., Davis, D.S., Mushotzky, R.F. and Burstein, D., 1993, ApJ, 404, L9

Mulchaey, J.S. & Zabludoff, A.I., 1998, ApJ, 496, 73

Muriel, H., Valotto, C.A., Lambas, D.G., 1998, ApJ, 506, 540

Mushotzky, R.F., Serlemitsos, P.J., Boldt, E.A., Holt, S.S., Smith, B.W., 1978, ApJ, 225, 21

J.V. Narlikar, J.V., *AN INTRODUCTION TO COSMOLOGY (3^{rd} Edition)*, 2002, Cambridge University Press, Cambridge, UK

Navarro, J.F., Frenk, C.S., White, S.D.M., 1996, ApJ, 462, 563

Navarro, J.F., Frenk, C.S., White, S.D.M., 1997, ApJ, 490, 493

Nolthenius, R. & White, S.D.M., 1987, MNRAS, 225, 505

Norberg, P., Cole, Sh., Baugh, C.M., Frenk, C.S., Baldry, I. et al., 2002, MNRAS, 336, 907

Oegerle, W.R., Ernst, R.M.; Hoessel, J.G., 1986, AJ, 91, 697

Oegerle, William R., Jewison, M.S., Hoessel, J.G., 1987, AJ, 93, 519

Oemler, A.Jr., 1974, ApJ, 194, 1

Okada, N. & Seto, O., 2005, PhRvD, 71b3517O

Osmond, J.P.F. & Ponman, T.J., 2004, MNRAS, 350, 1511

Peacock, J.A., *Cosmological physics*, 1999, Cambridge University Press, UK

Peacock, J.A. & Heavens, A.F., 1990b, MNRAS, 243, 133

Peebles, P.J.E., *The large-scale structure of the universe*, 1980, Princeton, NJ: Princeton University Press., USA

Penzias, A.A. & Wilson, R.W., 1965, ApJ, 142, 419

Piranomonte, S., Longo, G., Andreon, S., Puddu, E., Paolillo, M., Scaramella, R., Gal, R., Djorgovski, S.G., 2001, ASPC, 225, 73

Pisano, D. J., Wakker, B.P., Wilcots, E.M., Fabian, D., 2004, AJ, 127, 199

Ponman, T.J., Allan, D.J., Jones, L.R., Merrifield, M. & MacHardy, I.M., 1994 Nature, 369, 462

Ponman, T.J. & Bertram, D., 1993, Nature, 365, 51

Ponman, T.J., Bourner, P.D.J., Ebeling, H., Bhringer, H., 1996, MNRAS, 283, 690

Ponman, T.J., Cannon, D.B., Navarro, J.F., 1999, Natur, 397, 135

Ponman, T.J., Sanderson, A.J.R., Finoguenov, A., 2003, MNRAS, 343, 331

Popesso, P., Biviano, A., B*ö*hringer, H., Romaniello, M., 2006, A&A, 445, 29

Press, W.H. & Schechter, P., 1974, ApJ, 187, 425

Ramella, M., Geller, M.J., Huchra, J.P., 1989, ApJ, 344, 57

Ramella, M., Pisani, A. & Geller, M.J., 1997, AJ, 113, 483

Ramella, M., Zamorani, G., Zucca, E., Stirpe, G.M., Vettolani, G. et al., 1999 , A&A, 342, 1R

Ramella, M., Geller, M.J., Pisani, A., da Costa, L.N., 2002, AJ, 123, 2976

Rasmussen, J., Ponman, T.J, 2007, MNRAS, 380, 1554

Rasmussen, J., Ponman, T.J., Mulchaey, J.S., 2006(a), MNRAS, 370,

Rasmussen, J., Ponman, T.J., Mulchaey, J.S., Miles, T.A., Raychaudhury, S., 2006(b), MNRAS, 373, 653

Renzini, A., 1997, ApJ, 488, 35

Ribeiro, A.L.B., de Carvalho, R.R., Zepf, S.E., 1994, MNRAS, 267L, 13

Sand, D.J., Treu, T., Smith, G.P., Ellis, R.S., 2004, ApJ, 604, 88

Sanderson, A.J.R., Ponman, T.J., O'Sullivan, E., 2006, MNRAS, 372, 1496

Sarazin, C.L., 1986, RvMP, 58, 1

Schechter, P.L., 1976, ApJ, 203, 297

Silk, J. & White, S.D., 1978, ApJ, 223L, 59

Smith, G.P. & Taylor, J.E., 2008, ApJ, 682, 73

Somerville R.S., Hopkins, P.H., Cox, T.J., Robertson, B.E., Hernquist L., *arXiv:0808.1227v1* [astro-ph]

Springel, V., White, S.D.M., Jenkins, A., Frenk, C.S. et al., 2005, Natur, 435, 629

Steidel, C.C., Giavalisco, M., Pettini, M., Dickinson, M., Adelberger, K.L, 1996, ApJ, 462, 17

Sulentic, J.W. & Rabaca, C.R., 1994, ApJ, 429, 531

Tago, E., Einasto, J., Saar, E., Tempel, E., Einasto, M., et al., 2008, A&A, 479, 927

Thompson, L.A. & Gregory, S.A., 1980, ApJ, 242, 1

Trentham, N., 1997, MNRAS, 286, 133

Trentham, N. & Tully, R.B., 2002, MNRAS, 335, 712

Tripp, T.M., Lu, L., Savage, B.D., 1998, ApJ, 508, 200

Tucker, D.L., Oemler, A.Jr., Hashimoto, Y., Shectman, S.A., Kirshner, R.P. et al., 2000, ApJS, 130, 237

Tully, R.B., 1987, ApJ, 321, 280

Turner, E.L. & Gott, J.R., 1976, ApJS, 32, 409

Turner, E.L. & Gott, J.R., 1976, ApJ, 209, 6

Valotto, C.A., Nicotra, M.A., Muriel, H., Lambas, D.G., 1997, ApJ, 479, 90

van den Bergh, S., 1992, A&A, 264, 75

Vel*á*zques, H., & White, S.D.M, 1999, MNRAS, 304, 257

Wells, A., Abbey, A.F., Barstow, M.A., Cole, R.E., Pye, J.P., Sims, M.R., Spragg, J.E., Watson, D.J., Willingale, R., Courtier, G.M., 1990, SPIE, 1344, 230

Wu, K.K.S., Fabian, A.C., Nulsen, P.E.J., 2000, MNRAS, 318, 889

Wu, X-P., Xue, Y-J., & Fang, L-Z., 1999, ApJ, 524, 22

Xue, Y-J. & Wu, X-P., 2000, ApJ, 538, 65

Yagi, M., Kashikawa, N., Sekiguchi, M., Doi, M., Yasuda, N., Shimasaku, K., Okamura, S., 2002, AJ, 123, 87

Yang, X., Mo, H.J., van den Bosch, F.C., Jing, Y.P., 2005, MNRAS, 356, 1293

Yang, X., Mo, H.J., van den Bosch, F.C., Pasquali, A., Li, Ch., Barden, M., 2007, ApJ, 671, 153

Zabludoff, A.I. & Mulchaey, J.S., 1998, ApJ, 496, 39

Zabludoff, A.I. & Mulchaey, J.S., 2000, ApJ, 539, 136

Zandivarez, A., Marti’nez, H.J., Mercha’n, M.E., 2006, ApJ, 650, 137

Zepf, S.E., de Carvalho, R.R., Ribeiro, A.L.B., 1997, ApJ, 488L, 11

Zwicky, F., 1933, AcHPh, 6, 110

Chapter 2

The Mass Assembly of Fossil Groups of Galaxies in the Millennium Simulation

2.1 Introduction

Galaxy groups are believed to play a key role in the formation and evolution of structure in the universe as, within a hierarchical framework, they span the regime between individual galaxies and massive clusters. They are also more varied in their properties than galaxy clusters, as seen when various scaling relations are compared with those of galaxy clusters (Kaiser 1991; Ponman et al. 1996; White et al. 1997; Allen & Fabian 1998; Mulchaey & Zabludoff 1998; Arnaud & Evrard 1999; Xue & Wu 2000; Helsdon & Ponman 2000; Xue et al. 2001; Helsdon & Ponman 2003). For instance, the relation between the luminosity and temperature of the X-ray emitting hot intergalactic medium (the $L-T$ relation) has a larger scatter and a different slope for groups, when compared to similar properties of clusters. Various feedback mechanisms are often invoked to explain these differences. In addition, due to their lower velocity dispersion, groups are rapidly evolving systems, and galaxy mergers within groups can have a more significant effect on these relations than in clusters. In principle, the presence of cool

cores and active galactic nuclei (AGN), as well as the star formation history, are all affected by major interactions in the heart of a group or cluster. It would therefore be useful to find a class of groups or clusters with no major mergers in their recent history, to provide a baseline for the evolution of a passive system, with no major disruption.

Fossil groups are good candidates for such a class of objects. They are distinguished by a large gap between the brightest galaxy and the fainter members, with an under-abundance of L_* galaxies. Zabludoff & Mulchaey (1998) suggest that, for an X-ray detected group, the merging timescale for the most luminous group members ($L \approx L_*$) is of order of a few tenths of an Hubble time, in agreement with the numerical simulations. A single giant elliptical galaxy can form as a result of multiple mergers within a few Gyr (Barnes 1989). Thus, it is likely that one can find merged groups in the form of an isolated giant elliptical galaxy with an extended halo of hot gas, since the timescale for gas infall is longer than that on which galaxies merge (Ponman & Bertram 1993). In such systems, the brighter galaxies, which have a relatively shorter merging timescale, are expected to merge earlier leaving the fainter end of the luminosity function intact (Dubinski ; Miles et al. 2004).

Following the discovery of a fossil group having the above characteristics from ROSAT observations (Ponman et al. 1994), more fossil systems have been identified (Mulchaey & Zabludoff 1999; Vikhlinin et al. 1999; Jones et al. 2000; Romer 2000; Matsushita 2001; Jones et al. 2003). They are generally based on the definition of fossil groups from Jones et al. (2003), i.e. groups with a minimum X-ray luminosity of $L_{\rm X,bol} \approx 0.25 \times 10^{42} h^{-2}$erg s^{-1}, as well as minimum magnitude difference of two between the first and second ranked galaxies, within half the projected radius that encloses an overdensity of 200 times the mean density of the universe (R_{200}). For an NFW profile (Navarro, Frenk & White 1996), this is roughly equivalent to R_{500}, the radius enclosing an overdensity of 500 times the mean (for NFW halos of the appropriate concentration, $R_{500} \sim 0.59 \times R_{200}$). A few of these fossil groups have been the subject of detailed investigations (Khosroshahi, Jones & Ponman 2004; Yoshioka et al. 2004; Sun et al.

2004; Ulmer et al. 2005; Cypriano, Mendes de Oliveira & Sodré 2006; Mendes de Oliveira, Cypriano & Sodré 2006; Khosroshahi et al. 2006).

While most previous studies have focused on X-ray properties of fossils, there is also emerging evidence that the galaxy properties in fossils are different from those in non-fossils (Khosroshahi, Ponman & Jones 2006). For instance the isophotal shapes of the central fossil galaxies appear to be non-boxy, suggesting that they may have formed in gas rich mergers. Various observational and theoretical studies have suggested a significant fraction of galaxy groups to be fossils (Vikhlinin et al. 1999; Jones et al. 2003; D'Onghia et al. 2005; Milosavljević et al. 2006; Sommer-Larsen 2006), though often the criteria used to define fossils in theoretical work are not easy to relate to observational studies.

Fossils may represent extreme examples of a continuum of group properties – they are consistently found to be outliers in the usual scaling relations involving optical, X-ray and dynamical properties (Khosroshahi, Ponman & Jones 2007). While fossils fall on the L-T relation of non-fossil groups and clusters, they appear to be both hotter and more X-ray luminous than non-fossils of the same mass. Cooler fossil groups also show lower entropy than their non-fossil counterparts. According to Khosroshahi, Ponman & Jones (2007), the halos of fossil groups appear to be more concentrated than those of non-fossil systems, for a given mass, which suggests that fossils have an early formation epoch.

As such, we have much to learn from them, and the investigation of objects with similar properties in cosmological simulations can provide important insights into the physical processes that underly the scaling relations. It can also reveal limitations in the numerical simulations, related to the treatment of physical effects like pre-heating, feedback and merging, which are difficult to model. It is thus important to study the formation and evolution of these systems in the cosmological N-Body simulations which have become essential tools for studying formation of large scale structure in the Universe.

In this paper we use the Millennium simulation (Springel et al. 2005) together with the

semi-analytic models (Croton et al. 2006) of galaxy formation within dark matter halos and the Millennium gas simulation (Pearce et al. 2007), to identify fossil groups, study their properties in the simulations and make a comparison to the observations. We begin with a brief discussion in §2 of the Millennium Simulation, and the implemented semi-analytic galaxy catalogues and gas simulations. In §3 we discuss our method of identifying *optical* and *X-ray* fossil groups from these catalogues. In §4, we discuss the various properties of these fossil groups, their abundance in the local Universe and the evolution of simulated X-ray fossils with time. Finally, in §5, we summarise the implications of our results in terms of the evolution of fossil groups in the context of multiwavelength observations. Throughout the paper we adopt $H_0 = 100\,h$ km s^{-1} Mpc^{-1} for the Hubble constant.

2.2 Description of the Simulations

In order to extract fossil groups in the Millennium simulation, using observational selection criteria, we require a simulation suite that includes the baryonic physics of hot gas and galaxies, as well as a high resolution dark matter framework and a sufficient spatial volume to limit the effects of cosmic variance. For this study we use the dark matter Millennium Simulation (Springel et al. 2005), a 10-billion particle model of a comoving volume of side $500h^{-1}$ Mpc, on top of which a publicly available semi-analytic galaxy model (Croton et al. 2006) has been constructed. For the hot gas we have repeated the Millennium simulation with a lower resolution simulation including gas physics utilising the same volume, phases and amplitudes as the original dark-matter-only model. This run accurately reproduces the structural framework of the Millennium Simulation (Pearce et al. 2007). Below we summarise the main characteristics of the above simulations.

2.2.1 The Millennium Simulation

The Millennium Simulation is based on a Cold Dark Matter cosmological model of structure formation, with a Dark Energy field Λ. The basic assumptions are those of an inflationary universe, dominated by dark matter particles, leading to a bottom-up hierarchy of structure formation, via collapsing and merging of small dense halos at high redshifts, into the large virialised systems such as groups and clusters that contain the galaxies that we observe today. The simulation was performed using the publicly available parallel TreePM code Gadget2 (Springel et al. 2001), achieving a 3D dynamic range of 10^5 by evolving 2160^3 particles of individual mass $8.6 \times 10^8 h^{-1}$ $M_\odot$, within a co-moving periodic box of side $500h^{-1}$ Mpc, and employing a gravitational softening of $5h^{-1}$ kpc, from redshift $z = 127$ to the present day. The cosmological parameters for the Millennium Simulation were: $\Omega_\Lambda = 0.75, \Omega_M = 0.25, \Omega_b = 0.045, h = 0.73, n = 1$, and $\sigma_8 = 0.9$, where the Hubble constant is characterised as $100\,h\,\mathrm{kms}^{-1}\mathrm{Mpc}^{-1}$. These cosmological parameters are consistent with recent combined analysis from *WMAP* data (Spergel et al. 2003) and the 2dF galaxy redshift survey (Colless et al. 2001), although the value for σ_8 is a little higher than would perhaps have been desirable in retrospect.

The derived dark matter halo catalogues include halos down to a resolution limit of 20 particles, which yields a minimum halo mass of $1.72 \times 10^{10} h^{-1}$ $M_\odot$. halos in the simulation are found using a friends-of-friends (FOF) group finder, tuned to extract halos with overdensities of at least 200 relative to the critical density. Within a FOF halo, substructures or subhalos are identified using the SUBFIND algorithm developed by Springel et al. (2001), and the treatment of the orbital decay of satellites is described in the next section.

During the Millennium Simulation, 64 time-slices of the locations and velocities of all the particles were stored, spread approximately logarithmically in time between $z = 127$ and $z = 0$. From these time-slices, merger trees are built by combining the tables of all halos found at any given output time, a process which enables us to trace the growth of halos and their subhalos through time within the simulation.

2.2.2 The Semi Analytic model

Using the dark matter halos of the Springel et al. (2005) simulation, Croton et al. (2006) have simulated the growth of galaxies, and their central supermassive black holes, by self-consistently implementing semi-analytic models of galaxies on the outputs of the Millennium Simulation. The semi-analytic catalogue contains 9 million galaxies at $z = 0$ down to a limiting absolute magnitude of $M_R - 5 \log\, h\, =\, -16.6$, observed in B, V, R, I and K filters. The models focus on the growth of black holes and AGNs as feedback sources. The inclusion of AGN feedback in the semi-analytic model (which allows the cooling flow to be suppressed in massive halos that undergo quasi-static cooling) and its good agreement with the observed galaxy luminosity function, colour distribution and the clustering properties of galaxies, make this catalogue well-matched and suitable for our study of fossil systems.

In the semi-analytic formulation, galaxies initially form within small dark matter halos. As the simulation evolves, such a halo may fall into a larger halo. The semi-analytic galaxy within this halo then becomes a satellite galaxy within the main halo and follows the track of its original dark matter halo (now a subhalo) until the mass of the subhalo drops below $1.72 \times 10^{10} h^{-1}$ $\mathrm{M}_{\odot}$, which corresponds to a 20-particle limit in the Millennium Simulation. At this point the galaxy is assumed to spiral into the centre, on some fraction of the dynamical friction timescale, where it merges with the central galaxy of the larger halo (Croton et al. 2006).

2.2.3 The Millennium Gas Simulation

The Millennium Gas Simulations are a suite of hydrodynamical models, utilising the same volume, and values of initial perturbation amplitudes and phases as the parent dark-matter-only Millennium Simulation. Each of the three models completed to date contains additional baryonic physics: The first does not follow the effects of radiative cooling and so overpredicts the luminosities of group-scale objects significantly. The second includes a simple preheating

scheme that is tuned to match the observed X-ray properties of clusters at the present day and the third includes a simple feedback model that matches the observed properties of clusters today, as well as having some chance of following the time evolution. We have used the second of these models in this work, as we only utilise the hydrodynamical properties of the groups at $z = 0$, where the observational and simulation results are well matched.

Each of the Millennium Gas Simulations consists of 5×10^8 particles of each species, resulting in a dark matter mass of $1.422 \times 10^{10} h^{-1}$ $M_\odot$ per particle and a gas mass of $3.12 \times 10^9 h^{-1}$ $M_\odot$ per particle. The Millennium Simulation has roughly 20 times better mass resolution than this and so some perturbation of the dark matter halo locations is to be expected. In practice the position and mass of dark matter halos above $10^{13} h^{-1}$ $M_\odot$ are recovered to within $50\, h^{-1}$kpc between the two volumes, allowing straightforward halo-halo matching in the large majority of cases.

The Millennium gas simulations used exactly the same cosmological parameters as those stated above. With the inclusion of a gaseous component, additional care needs to be taken in choosing the gravitational softening length in order to avoid spurious heating (Steinmetz & White). We use a comoving value of $25(1 + z)h^{-1}$ kpc, roughly 4% of the mean interparticle separation (Borgani et al. 2006) until $z = 3$, above which a maximum comoving value of $100h^{-1}$ kpc pertains. We have adopted a different output strategy for the Millennium Gas Simulations, preferring to output uniformly in time with an interval roughly corresponding to the dynamical time of objects of interest. This strategy results in 160 rather than 64 outputs and places particular emphasis on the late stages of the simulation.

2.3 Sample Selection

2.3.1 Definition of fossils

Fossil groups are selected according to a combination of X-ray and optical criteria, based on the observational definition given by Jones et al. (2003), which is widely followed in the literature. Their X-ray luminosity must satisfy $L_{\rm X,bol} \geq 0.25 \times 10^{42} h^{-2}$erg s^{-1}, and the difference between the R-band magnitudes of the first and second ranked galaxies, within half the projected radius enclosing 200 times the mean density (R_{200}), must be $\Delta m_{12} \geq 2$ magnitudes. A limit of $0.5R_{200}$ is used because L_* galaxies within this radius should spiral into the centre of the group due to orbital decay by dynamical friction within a Hubble time (Jones et al. 2003). The limit on the bolometric X-ray luminosity $L_{\rm X,bol}$ helps to exclude poor groups and individual galaxies with a few small satellites. Such groups are often not in dynamical equilibrium, and in addition there might be a gap in their galaxy luminosity function simply as a result of the small numbers of galaxies involved. We address this issue in § 2.3.3.

2.3.2 Selection of Fossil galaxies

For this investigation, we first selected dark matter halos from the Millennium Gas Simulation with masses $M(R_{200}) \geq 10^{13}\, h^{-1}\, {\rm M}_{\odot}$. As Fig. 2.1 demonstrates, all halos for which $L_{X,bol} \geq 0.25 \times 10^{42}\, h^{-2}$erg s^{-1} are expected to be included in this sample and thus our fossil sample will be complete. A bolometric X-ray luminosity of $0.25 \times 10^{42}\, h^{-2}$ erg s^{-1} corresponds to a temperature of $T \approx 0.5$ keV. This constraint on the halo masses results in an initial sample of 51538 dark matter halos, within which we search for fossil groups.

In order to extract information about dark matter and galaxy properties, for each of these 51538 halos found in the Millennium Gas Simulation, the counterpart in the Millennium Simulation needs to be found. This is a straightforward procedure because the simulated volume and the amplitudes and phases of the initial power spectrum were matched. However, the dark-

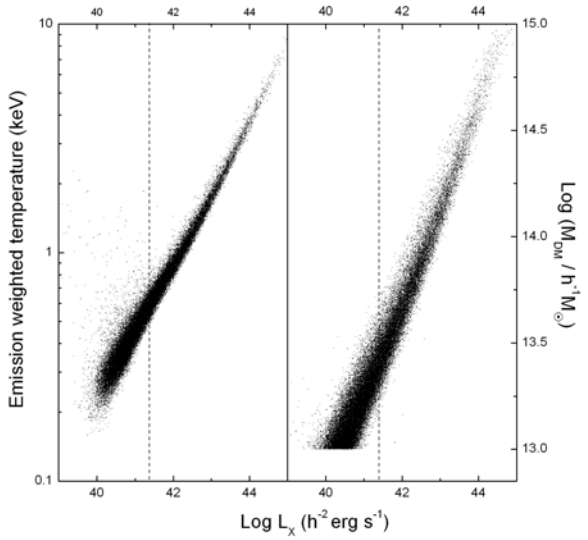

Figure 2.1: The bolometric X-ray luminosity versus dark matter halo temperature (*left panel*) and mass within R_{200} (*right panel*) for all halos in the Millennium gas simulation. The vertical dashed lines correspond to the X-ray luminosity threshold $L_{\rm X,bol} = 0.25 \times 10^{42}\, h^{-2}$erg s^{-1} adopted in this paper for defining fossil groups. The cutoff $M(R_{200}) \geq 10^{13}\, h^{-1}\, {\rm M}_{\odot}$ is adopted in § 2.3.2.

matter-only Millennium Simulation has 20 times the mass resolution of the corresponding Millennium Gas Simulation and so contains some additional small scale power. This leads to small offsets (typically around twice the gravitational softening length) in the final co-ordinates of equivalent halos, and even smaller mass differences (typically less than 5%). Of the 51538 halos, 48774 ($\sim$95%) have corresponding halos identified in the Millennium Simulation. For each of these matched halos we extracted the coordinates and $BVRIK$ magnitudes for each galaxy contained within R_{200}, from the publicly available catalogue of Croton et al. (2006).

The simulated properties of the galaxies occupying each dark matter halo were then used to calculate Δm_{12}, i.e. the difference in R-band magnitude of the first and second ranked galaxies within $0.5R_{200}$ of the centre of the halo. Out of the 48774 matched halos, 6502 are found to be *optical fossil groups*, i.e. halos with $\Delta m_{12} \geq 2$ mag, among which 1300 are *X-ray fossil groups*, i.e. optical fossil groups with $L_{X,bol} \geq 0.25 \times 10^{42}\, h^{-2}$ erg s^{-1}. As can be seen from Fig. 2.2, X-ray fossil groups do not form a separate population but are rather extreme examples of a smooth

distribution. It is also clear that the spread in Δm_{12} increases dramatically with decreasing in the X-ray luminosity and hence the enclosed mass, in agreement with the conditional luminosity function (CLF) formalism of van den Bosch et al. (2007).

Control groups are necessary for our study in order to allow us to compare the properties of X-ray fossil and non-fossil groups. We define two control group samples, based on the magnitude difference of the two brightest members of the group (within $0.5R_{200}$ of the centre of the dark matter halo): (i) $0.8 \leq \Delta m_{12} \leq 1.0$, and (ii) $0.1 \leq \Delta m_{12} \leq 0.3$. While members of the former are examples of intermediate groups, the latter could be regarded as a class of extreme non-fossil groups in that they contain at least two galaxies of very similar magnitude. The bolometric X-ray luminosity limit for each of the control samples is the same as that of the X-ray fossil group sample (see Fig. 2.2).

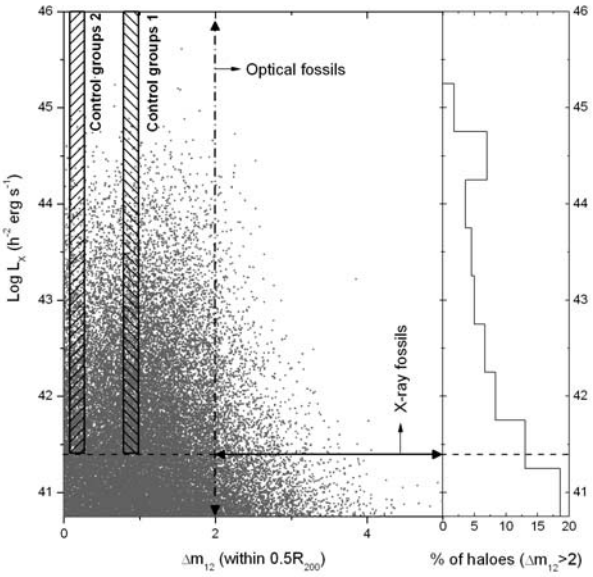

Figure 2.2: X-ray luminosity versus the R-band luminosity gap Δm_{12} within $0.5R_{200}$ for each of the dark matter halos with gas properties. The horizontal dashed-line intersects the vertical axis at $L_{X,bol} = 0.25 \times 10^{42} h^{-2}$erg s^{-1}. The top-right part of the graph shows the region for which $\Delta m_{12} \geq 2$ mag and $L_{X,bol} \geq 0.25 \times 10^{42} h^{-2}$erg s^{-1}, the optical and X-ray criteria that jointly define fossil groups. The two shaded regions show the location of our control samples (see § 2.3.2 for details). The histogram shows the fraction of optical fossils in each bin of $L_{X,bol}$.

2.3.3 The likelihood of finding groups with $\Delta m_{12} \geq 2$ at random

One of the central criteria used to define fossils is the absence of galaxies within a range of two magnitudes of the brightest galaxy ($\Delta m_{12} \geq 2$). However, for groups with only a small number of members, there is a significant probability of obtaining such a luminosity gap as a natural consequence of the high-end tail of the galaxy luminosity distribution. To quantify the likelihood of obtaining a value of $\Delta m_{12} \geq 2$ by chance, Jones et al. (2003) performed 10^4 Monte Carlo simulations for groups and clusters with absolute magnitudes selected at random from a Schechter function (Schechter 1976). Using the parameters of the composite luminosity function of MKW/AWM clusters (Yamagata & Maehara 1986), they found that for the systems of $\sim$40 galaxies, 0.4$\pm$0.06% of the generated luminosity functions had $\Delta m_{12} \geq 2$.

We performed a similar analysis for groups spanning a range in richness, and using parameters appropriate to our data from the Millennium simulation. For twenty classes of groups, containing 10, 15, 20, 25,... galaxies respectively, we randomly generated galaxies according to a Schechter luminosity function. (None of our X-ray fossil groups from the Millennium simulation contain fewer than 10 galaxies.) The characteristic magnitude $M_* \sim -22.1$ and faint-end exponent $\alpha \sim -1.19$, were adopted from a fit of the Schechter function to the R-band luminosity function of the semi-analytic catalogue. A magnitude cut off of -17.4 was then applied to the magnitude of generated galaxies as this is the R-band magnitude completeness limit of the semi-analytic catalogue. 10^6 simulations were carried out for each richness class of group.

Fig. 2.3 compares the percentage of optical and X-ray fossil groups from the Millennium simulation as a function of number of galaxies within $0.5R_{200}$ for each dark matter halo, with those populated using a Schechter luminosity function as detailed above. The lower panel shows the result when the expected number of randomly generated groups with $\Delta m_{12} \geq 2$, is subtracted from the optical fossils. For poor systems, the incidence of 'statistical fossils' is significant. It can be seen that approximately one third of the fossil systems with fewer than 25 galaxies seen in the Millennium data can be attributed to statistical chance (as opposed to

the result of physical processes generating a non-statistical luminosity gap). However, even after these random fossils are removed, the fraction of optical fossils increases as the number of galaxies within dark matter halos decreases. In contrast, for X-ray fossils, many of the poor halos which qualify as 'statistical fossils' fail to pass the X-ray luminosity threshold criterion, so the chance fraction is never much larger than 20%. We return to this issue in Sec. 2.4.1. For groups with more than 30 galaxies, the fraction of fossils meeting the $\Delta m_{12} \geq 2$ criterion by chance drops below 1.0%, and soon becomes negligible.

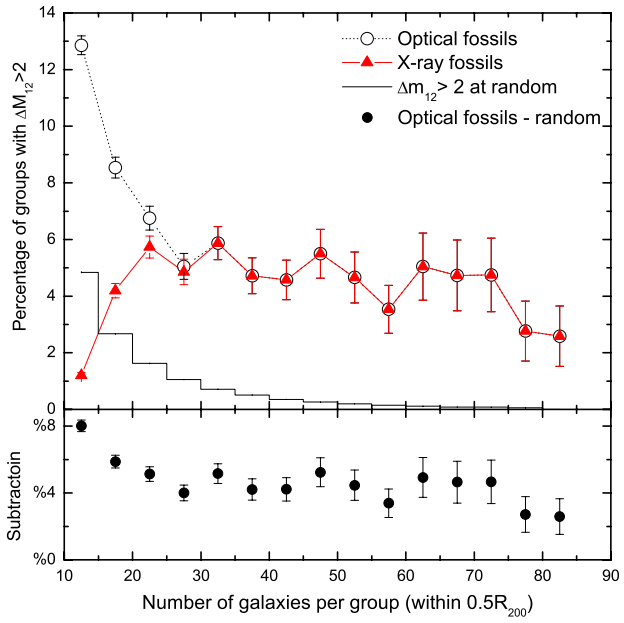

Figure 2.3: The histogram shows the incidence rate of $\Delta m_{12} \geq 2$ occurring by chance from a random population of galaxies selected from a Schechter luminosity function in comparison to fraction of optical fossils (*open circles*) and X-ray fossils (*solid triangles*) in the Millennium simulation, as a function of number of galaxies per halo within $0.5R_{200}$. The lower panel plot (*filled circles*) shows the result of subtracting random groups from the optical fossil groups.

2.4 Results

2.4.1 The Luminosity Gap Statistic

If galaxies in groups and clusters merge with the central galaxy over a finite time to produce a progressively greater massive central galaxy, then one way to quantify the dynamical age of a galaxy system is to measure the luminosity gap between the two most luminous galaxies remaining in the group, provided that there is no infall of bright galaxies from other nearby systems. A relaxed X-ray morphology in observed fossils is an indication of the absence of such a process. Within such a merging scenario for the formation of the brightest group galaxy, the luminosity gap distribution depends on the halo merger rates. This has previously only been examined in analytical studies (Bond et al. 1991), or in large-scale cosmological simulations without a hot baryonic component. Thus, while an important observational criterion for defining fossils relies on the X-ray properties of the group, this has not previously been implemented within the models.

The R-band magnitude gap distribution

Here we compare the luminosity gap distribution between the luminous galaxies found at the centre of dark matter halos extracted from the Millennium simulation with expectations from the analytical model of Milosavljević et al. (2006), and with observational properties from SDSS clusters.

Milosavljević et al. (2006) compared the distribution of the predicted luminosity gaps from their analytical model within R_{200}, as a function of halo mass, with the observed luminosity gaps in the SDSS (DR4) clusters (Miller et al. 2005), ranging in mass and redshift from $M = 0.5-10 \times 10^{14}\, h^{-1}\, \mathrm{M}_{\odot}$ and z=0.02 to 0.17, respectively, within a projected physical radius of 500 h^{-1}kpc. Halo merger rates in their model have been analytically estimated according to the excursion-set theory of Bond et al. (1991), which is also known as the extended Press-Schechter

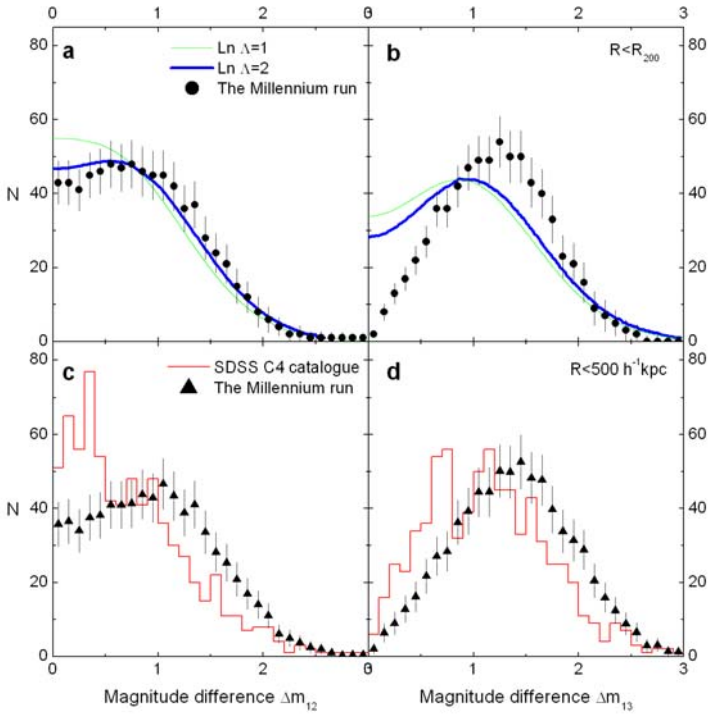

Figure 2.4: The R-band luminosity gap distribution for halos from the Millennium semi-analytic model within the mass range $M = 0.5-10 \times 10^{14}\, h^{-1}\, \mathrm{M}_{\odot}$, evaluated relative to the first and second most luminous galaxies and the first and the third most luminous galaxies, superposed on the theoretical model of Milosavljević et al. (2006) and the SDSS data for the same mass range but different searching radius (R_{200} for the model and projected radius of $500h^{-1}$kpc for the SDSS data). The Millennium data are plotted within R_{200} (*closed circles*) as well as the projected radius of $500h^{-1}$kpc (*triangles*). (a), (b): The luminosity gap statistic predictions of the theoretical model of Milosavljević et al. (2006) with $\ln \Lambda = 1$ (*thin green line*) and $\ln \Lambda = 2$ (*thick blue line*). (c), (d): The r-band luminosity gap distribution from 730 clusters (*red histogram*) in the SDSS C4 Catalogue of Miller et al. (2005).

formalism. Assuming a halo density profile of the form of Navarro, Frenk & White (1996), a subhalo of mass m merges into a primary halo of mass M ($m \geq \frac{1}{2}M$) and makes a composite halo. As the centre of the subhalo crosses the virial radius of the new composite halo, a merger happens. Then the subhalo spirals toward the centre of the composite halo in a near circular orbit, experiencing dynamical friction.

For comparison with the above study, we evaluate the R-band luminosity difference between the first and second most luminous (Δm_{12}) and the first and the third most luminous (Δm_{13})

galaxies in our Millennium data within R_{200} and within 500 h^{-1}kpc. In Fig. 2.4, we plot the R-band luminosity gap distribution of the Millennium simulation for the same mass range as the models, together with the luminosity gap distribution of 730 SDSS C4 clusters (Miller et al. 2005). Figs. 2.4a and 2.4b compare the predicted gap statistics from Milosavljević et al. (2006) for two values of the Coulomb logarithm, $\ln\Lambda = 1$ and $\ln\Lambda = 2$, within R_{200}. Since the parameter $\ln\Lambda$ is proportional to the force of dynamical friction between the centres of subhalo and primary halo during the process of merging, a higher value of $\ln\Lambda$ corresponds to a faster effective halo merger rate. In numerical simulations, $\ln\Lambda$ is approximated by b_{max}/b_{min}, where b_{max} and b_{min} are the maximum and minimum impact parameters respectively, and $\ln\Lambda$ is expected to be $\sim 1-4$ (Velázquez & White 1999; Fellhauer et al. 2000; D'Onghia et al. 2005). However, in the semi-analytic galaxy catalogues (Croton et al. 2006), based on the Millennium simulation, used in this work, the above relation is approximated by $\ln\Lambda = \ln(1 + M_{200}/m_{\rm sat})$, where m_{sat} is the halo mass of the satellite galaxy.

Within the mass range of the SDSS data there are 8842 halos in the Millennium simulation catalogue. Accordingly, in Fig. 2.4, our data have been normalised to be comparable with the SDSS data and the theoretical model of Milosavljević et al. (2006). However, the simulation data is, unlike the observations, complete and uncontaminated by spurious groups or foreground and background galaxies. All these effects are likely to be heavily dependent on the number of galaxies residing in the halo. As such, the comparison with the SDSS data shown in Fig. 2.4 should be treated with caution.

Given this caveat, our analysis based on the Millennium simulation catalogues agrees remarkably well with the models of Milosavljević et al. (2006) based on the SDSS survey for the luminosity gap distribution of the two brightest galaxies in each of the dark matter halos, particularly for $\ln\Lambda = 2$ (Fig. 2.4a). However, for the R-band luminosity gap between the brightest and third brightest galaxies in each system (Fig. 2.4b), the simulations significantly depart from the model. When comparing with the SDSS data (Figs. 2.4c and 2.4d), the sim-

ulations overpredict the frequency of groups. The simulations and the SDSS data have similar shaped distributions for the luminosity gap Δm_{13}, but with a shift of $\sim$0.5 mag toward higher Δm_{13} in the simulated halos.

We emphasise that the Millennium predictions for the luminosity gap statistic are sensitive to the assumed mass range and search radius of dark matter halos within which brightest halo members are identified. SDSS cluster masses have been estimated from total r-band luminosities, so any inaccuracies in this procedure would affect the comparison with the Millennium data.

Observationally there is an excess population of groups with a small luminosity gap between the first and second ranked galaxies, above what is predicted by the theoretical models or the simulations. This excess population is likely to result from contamination of observed group samples by local structure alignments, and renormalising to a sample without these groups scales down the "Millennium" distribution in Fig. 2.4c, bringing the simulation results and the observational measurements into better agreement. Results are similar in the K-band.

The abundance of fossil groups

The probability of finding fossil systems is expected to increase with decreasing halo mass, as shown in previous studies based on theoretical models or hydrodynamical simulations (D'Onghia et al. 2005; Milosavljević et al. 2006; Sommer-Larsen 2006; van den Bosch et al. 2007). Unfortunately, it is difficult to compare the results from different studies (both theoretical and observational), since they have used a range of search radii (from R_{180} to R_{337} – see Table. 1) within which the $\Delta m_{12} \geq 2$ mag criterion is imposed. Clearly, the larger the search radius, the more demanding is the requirement on the galaxy contents of the system, and the smaller the fraction of groups which will qualify as fossils.

In Fig. 2.5, the rates of incidence, $P_f(M)$, of optical fossils and X-ray fossils (using our preferred search radius of $0.5R_{200}$, following Jones et al. (2003)) are plotted, as a function of

the mass M of the halo, together with the predicted values from the models of Milosavljević et al. (2006) for two values of Λ. The shape of our curve for optical fossils is quite similar to the theoretical models (which included no X-ray luminosity criterion), but the latter actually employed a search radius of R_{200}. To see the effect of this, we also show our Millennium results for this larger search radius. The fraction of fossil systems falls by approximately a factor of 2, when this more demanding requirement is imposed, and so lies significantly below that predicted by Milosavljević et al. (2006).

On scales of $M \sim 10^{13} - 10^{14} h^{-1}\mathrm{M}_{\odot}$, ∼5%–18% of groups are optical fossils. This probability falls to ∼3%–5% for more massive ($M \geq 10^{14} h^{-1}\mathrm{M}_{\odot}$) fossil systems. For halo masses $> 5 \times 10^{13} h^{-1}\mathrm{M}_{\odot}$ all optical fossils in the simulation are also X-ray fossils. However, at the lowest halo masses the fraction of X-ray fossils drops steeply, since many low mass halos do not satisfy the L_X threshold criterion.

In Table. 1, we summarise the incidence rates of fossil systems from present study as well as those found in the literature. Comparison between these different estimates is difficult, since both the search radius and the halo mass range varies considerably from study to study. However, a direct comparison with the only *observational* estimate (from Jones et al. (2003)) is possible, since we have used the same definitions of fossil groups as these authors. Based on a comparison with the integrated local X-ray luminosity function of Ebeling et al. (2001), Jones et al. (2003) estimated that X-ray fossil systems constitute 8-20% of all systems of the same X-ray luminosity ($L_{X,bol} \geq 0.25 \times 10^{42} h^{-2}$erg s^{-1}). The right panel histogram of Fig. 2.2 represents the fraction of optical fossil systems in each bin of $L_{X,bol}$. Integrating this over all X-ray luminosities above the threshold value for fossils, we find that $\sim 7.2 \pm 0.2\%$ of halos with $L_{X,bol} \geq 0.25 \times 10^{42} h^{-2}$erg s^{-1} are X-ray fossils, which is reasonably consistent with the lower limit of $\sim 8\%$, derived by Jones et al. (2003).

In comparison, detailed hydrodynamical simulations by D'Onghia et al. (2005) and Sommer-Larsen (2006) of 12 galaxy groups, predict a larger fraction of 33%±16% for fossil systems of

Table 2.1: The incidence rates of fossil systems.

Mass range ($h^{-1}\mathrm{M}_{\odot}$)	L_X ($10^{42}h^{-2}$ erg s^{-1})	Fossil [a] type	Search radius	Fossil fraction (%)	Reference[b]
$\sim 10^{13}-10^{14}$	-	O	R_{200}	$\sim 5-40$	M06
$\sim 10^{13}-10^{14}$	-	O	R_{180}	$\sim 3.6 \pm 0.1$	vdB07[c]
$\geq 10^{14}$	-	O	R_{200}	$\sim 1-3$	M06
$\sim 10^{14}-10^{15}$	-	O	R_{180}	$\sim 6.5 \pm 0.1$	vdB07
$\sim 10^{14}$	-	O	R_{337}	$\sim 33 \pm 16$	SL06, DO05[d]
$\sim 10^{13}-10^{15}$	-	O	1 h^{-1}Mpc	$\sim 8-10$	S07[e]
-	≥ 0.25	X	$0.5R_{200}$	$\sim 8-20$	J03
-	≥ 0.25	X	$0.5R_{200}$	$\sim 7.2 \pm 0.2$	Present study[f]
$\sim 10^{13}-10^{15}$	-	O	$0.5R_{200}$	$\sim 13.3 \pm 0.2$	Present study

[a] O: Optical fossils , X: X-ray fossils.

[b] S07: Sales et al. (2007); M06: Milosavljević et al. (2006); vdB07: van den Bosch et al. (2007); SL06: Sommer-Larsen (2006); DO05: D'Onghia et al. (2005); J03: Jones et al. (2003).

[c] Based on the conditional luminosity function (CLF) formalism of van den Bosch et al. (2007).

[d] From hydrodynamical simulations of 12 galaxy groups.

[e] Based on the Millennium simulation. The first brightest galaxies of fossils in their sample are always brighter than $M_R = -20.5$.

[f] Histogram on the right panel of Fig. 2.2, gives the fraction of X-ray and optical fossils in each bin of L_X.

mass $10^{14}h^{-1}\mathrm{M}_{\odot}$ or larger. This may be because it is easy to overestimate the local viscosity in hydrodynamic simulations (Tittley et al. 2001), a process that would lead to central overmerging in the models.

2.4.2 The Space Density of X-ray Fossil Groups

So far, the integrated space density of X-ray fossil groups has been studied for small samples, each of three to five X-ray fossil systems, at different limiting luminosities (Vikhlinin et al. 1999; Romer 2000; Jones et al. 2003). Here, we estimate the space density by systematically counting the fossil groups in the whole 500 h^{-1} Mpc survey volume of the Millennium Simulation at $z=0$. For comparison with previous studies, we select and count X-ray fossil groups for three limiting X-ray luminosities ranging from 0.25–5$\times 10^{42}$ h^{-2}erg s^{-1}. The space densities calculated at different limiting luminosities as well as those from previous studies are given in

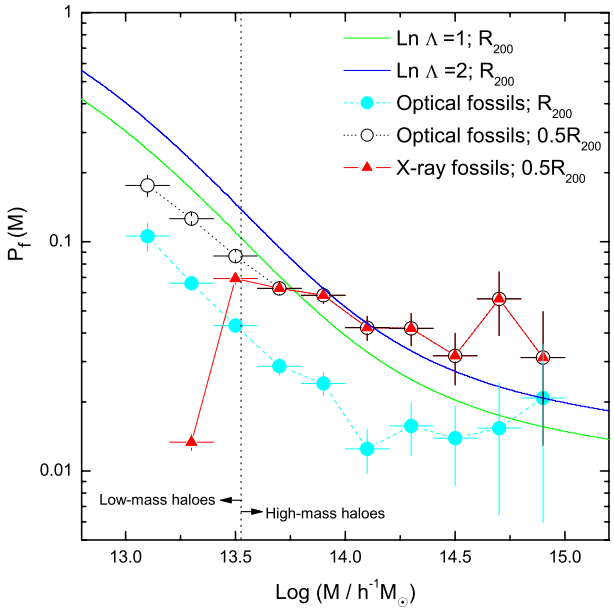

Figure 2.5: The probability, $P_f(M)$, that a dark matter halo of mass M contains an X-ray fossil group (*closed triangles*), optical fossil group within $0.5R_{200}$ (*open circles*), or optical fossil group within R_{200} (*closed circles*) from the Millennium simulation. The fossil incidence rate from the analytical study of Milosavljević et al. (2006) for two values of $\mathrm{Ln}\Lambda = 1$ (*green line*) and $\mathrm{Ln}\Lambda = 2$ (*blue line*) is also plotted. The vertical dotted-line corresponds to halo mass $\sim 3.34 \times 10^{13}\, h^{-1}\, \mathrm{M}_{\odot}$ (see Sec. 2.4.3).

Table 2. The value from Romer (2000) is a very rough estimate, since no redshifts for galaxies surrounding the central object were available in this study.

Our values show that for X-ray luminosities exceeding 2.5-5$\times 10^{42}$ h^{-2}erg s^{-1}, the space density of fossils in the Millennium simulation agrees within the errors with those estimated by Vikhlinin et al. (1999) and Jones et al. (2003). At the lowest X-ray luminosities, the density from the Millennium simulations appear to be lower than observed, though the observational values given in Table 2 have large uncertainties due to the small number of X-ray fossil groups and the effects of cosmic variance. Recent studies of Khosroshahi, Ponman & Jones (2007) and Jeltema et al. (2006) show that one of the fossils in the sample of Jones et al. (2003) does not satisfy the fossil criterion of $\Delta m_{12} \geq 2$, which reduces the observational space density. Cer-

Table 2.2: Space densities of fossil galaxy groups.

L_X[a]	N_f[b]	Density[c]	Reference[d]	Present study[c]
> 0.25	5	320^{+216}_{-144}	J03	104 ± 3
> 2.5	3	$16^{+15.2}_{-8.8}$	J03	22.4 ± 1.3
> 2.5	4	$36.8^{+47.2}_{-18.4}$	V99	22.4 ± 1.3
> 2.5	3	~ 160	R00	22.4 ± 1.3
> 5.0	4	$19.2^{+24.8}_{-9.6}$	V99	12.8 ± 1.0

[a] In units of $10^{42} h^{-2}$ erg s^{-1}
[b] Number of fossils
[c] In units of $10^{-7} h^3$ Mpc^{-3}
[d] V99:Vikhlinin et al. (1999), R00:Romer (2000), J03:Jones et al. (2003)

tainly the number of X-ray fossils found is heavily dependent on the X-ray luminosity threshold chosen and may be influenced by the scatter in X-ray group properties near this lower limit.

2.4.3 Evolution of Fossil Groups

Strong interactions and mergers between galaxies occur more efficiently in the low velocity dispersion environment of galaxy groups (Miles et al. 2004). Therefore in old, relatively isolated groups, most massive galaxies have sufficient time to merge via dynamical friction. If X-ray fossil groups are indeed systems that formed at an earlier epoch, we should be able to verify this from the merger histories of present-day fossils in the Millennium simulation: an exercise that is not directly possible to perform with observational surveys. In Fig. 2.6 we trace the mass evolution of present-day X-ray fossil systems backwards from $z = 0$, to $z = 0.82$ when the scale factor, a, of the Universe was 0.55 times its current size.

At any given redshift in Fig. 2.6 the average ratio of the mass of a halo to its final mass (at $z = 0$) is calculated for all eligible halos. The error is represented by the standard error on the mean, i.e. $\sigma/\sqrt{N}$, where σ is the standard deviation of the original distribution and N is the sample size. The same was done for both sets of control groups. The original sample of fossils was divided into two subsamples, of low mass and high mass groups (see Fig. 2.6b and Fig. 2.6c), such that both subsamples have equal numbers of groups. The boundary between the

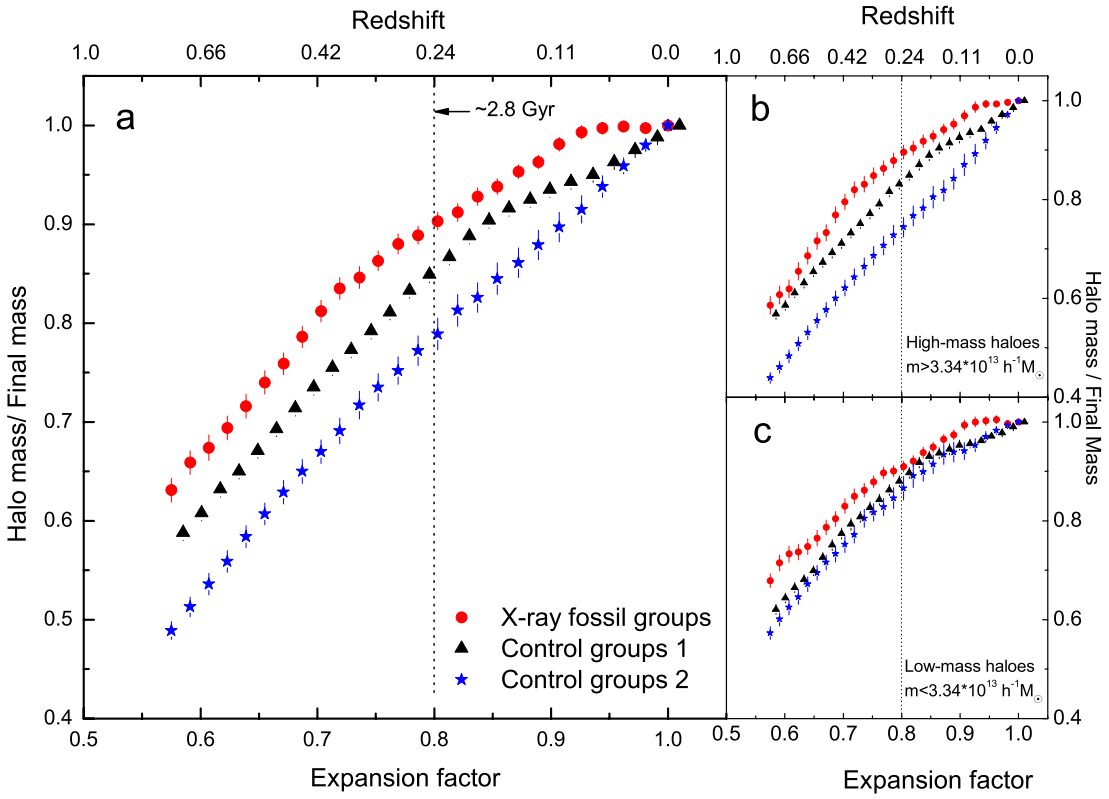

Figure 2.6: Tracing back the mass build-up of the dark matter halos as a function of expansion factor and redshift for both the X-ray fossils and the control groups 1 and 2. (a) For all halos. (b) High mass halos ($m_{\rm halo} \gtrsim 3.34 \times 10^{13}\, h^{-1}$ M$_\odot$). Both plots indicate the earlier formation of X-ray fossil groups in comparison to control groups. (c) Low mass halos ($m_{\rm halo} \lesssim 3.34 \times 10^{13}\, h^{-1}$ M$_\odot$). Here the difference in evolution between the X-ray fossil and control groups is not as pronounced as in those seen in high mass X-ray fossils. All the masses are normalised to the mass at z=0.

two subsamples corresponds to the median present-day mass $\sim 3.34 \times 10^{13}\, h^{-1}\, \mathrm{M}_{\odot}$.

Fig. 2.6a shows that at a scale factor of 0.8 ($z \sim 0.24$), the fossil groups have already attained ∼90% of their final mass while, at the same redshift, the fraction of assembled mass of the extreme non-fossil groups is about ∼77% of their final mass. The intermediate control group gives intermediate values. The fossil groups have almost all their mass in place by a redshift of $z \sim 0.1$, and show no evidence of recent major mergers, while the non-fossils seem to be assembling mass even at the present day. These results suggest an early formation and consequent higher mass concentration in fossil groups, in comparison to normal groups, particularly for the more massive fossils.

As Figs. 2.6b and 2.6c show, the difference in mass assembly is larger in more massive halos than halos with lower mass. The decreased distinction in the assembly history for our lower mass fossil systems probably results from the fact there is a large fraction of "statistical fossils" in this category: groups which achieve $\Delta m_{12} \geq 2$ due to random chance, because of the small number of members. As can be seen in Fig. 2.3, ∼50% of optical fossil groups with masses less than $\sim 3.3 \times 10^{13}\, h^{-1}\, \mathrm{M}_{\odot}$ are expected to fall into this "statistical fossil" category.

Various observational properties (Ponman et al. 1994; Jones et al. 2003; Khosroshahi, Jones & Ponman 2004; Ulmer et al. 2005; Khosroshahi et al. 2006; Khosroshahi, Ponman & Jones 2007) have suggested an early formation epoch for fossils. D'Onghia et al. (2005) and Sommer-Larsen (2006) used a set of twelve high-resolution numerical simulations in the ΛCDM cosmology to study the formation of fossil groups, and found a correlation for the magnitude gap between the brightest and second-brightest galaxies and the halo formation epoch, with fossils accreting half of their final dark matter mass at $z \geq 1$. Such an early assembly of fossil halos leaves enough time for L_{*} galaxies to merge into the central one by dynamical friction, resulting in the observed magnitude gap at $z = 0$.

Fig. 2.7 shows the history of mass assembly of a typical example of a massive fossil group (right panel) and a control group (left panel) from the Millennium Gas Simulation from redshift

$z = 1.0$ to $z = 0$. The dimension of each image is 10×10 Mpc, centred around the central halo. It can be seen that at $z = 0.3$, the X-ray fossil group has already largely been assembled, while the control group has considerable substructure even at a later epoch.

2.5 Discussion

We studied the history of the mass assembly of fossil groups, selected using the usual observational criteria at $z = 0$, from a redshift $z = 0.8$ to the present day, within the Millennium simulation. A sample of X-ray fossil groups was defined from the Millennium simulations and associated gas and galaxy catalogues, according to the usual criteria: (a) the difference between the R-band magnitudes of the first and second ranked galaxies, within half the projected radius enclosing 200 times the mean density of material (R_{200}), is $\Delta m_{12} \geq 2$ magnitudes, and (b) The bolometric X-ray luminosity of the group is $L_{\rm X,bol} \geq 0.25 \times 10^{42} h^{-2}$erg s^{-1}. While optical fossil groups fulfil just the first condition, X-ray fossils satisfy both criteria. Our main results are as follows:

- The space density of X-ray fossil groups is in close agreement with the observed space density of fossils with $L_X > 2.5 \times 10^{42}\ h^{-2}$erg s^{-1}. Although for low luminosity fossils we find roughly 1/3 of the observed fossil space density, there are several potential factors that could lead to this difference. As well as significant uncertainties in the observational studies, the X-ray properties of halos in the real Universe show far greater scatter than those seen in the preheating simulation used here (Hartley et al. 2007). Given the X-ray luminosity threshold in the definition of an X-ray fossil, scatter in L_X will alter the X-ray fossil number density, since the number density of halos is a steep function of mass.

- By selecting optical fossils from groups randomly generated from a Schechter luminosity function, we demonstrate that for small numbers of galaxies per group, a significant fraction of optical fossil groups are expected to be purely statistical, requiring no special

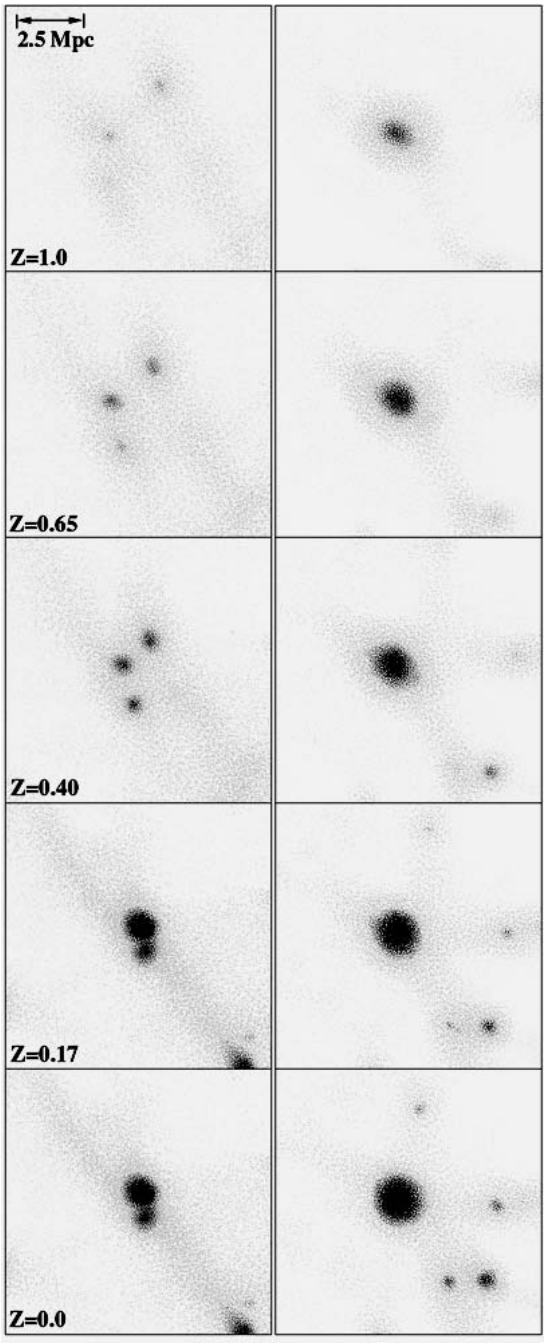

Figure 2.7: Evolution of a typical of massive X-ray fossil group (*right*) in comparison to a typical massive normal group (*left*) from redshift z=1.0 to 0. The dimension of each panel is 10×10 Mpc. The points represent individual gas particles from the Millennium Gas simulation (Pearce et al. 2007).

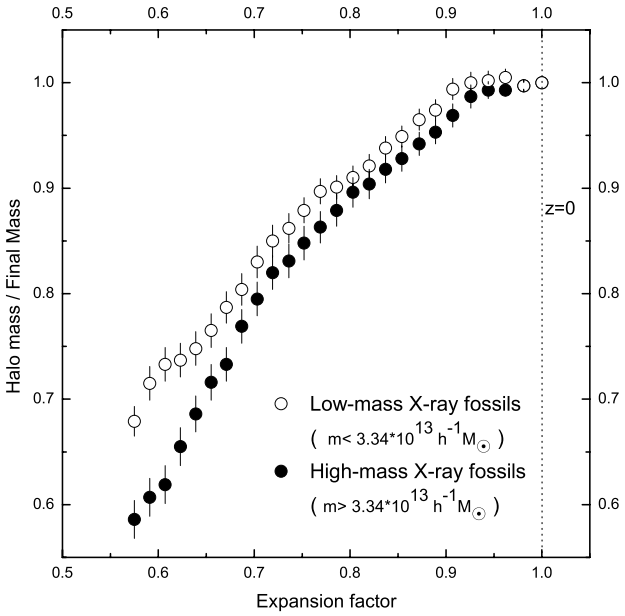

Figure 2.8: Comparison between the mass growth of high and low-mass X-ray fossils plotted in Figs. 2.6b and 2.6c.

physical mechanism to generate the 2 magnitude luminosity gap. For groups with more than 40 members, this effect largely disappears, with very few fossil groups expected at random.

- The probability of finding optical fossils with mass M, i.e, $P_f(M;\text{optical})$ is a decreasing function of: (a) group dark matter halo mass and, (b) the fraction of the virial radius within which the first and second brightest galaxies are being found. Conversely, as dark matter halo mass become small, the probability $P_f(M;\text{X-ray})$ for X-ray fossils decreases.

- Both high-mass and low-mass X-ray fossil groups are found to have assembled $\sim 90\%$ of their final masses by a redshift of $z = 0.24$. The corresponding mass fraction is about $\approx 70 - 80\%$ for two different sets of high-mass control samples, and $\approx 85\%$ for low-mass control samples, where groups fulfil the same X-ray luminosity criterion ($\gtrsim 3.34 \times 10^{14}\, h^{-1}\mathrm{M}_{\odot}$) but have the optical luminosity gaps corresponding $0.1 \leq \Delta m_{12} \leq 0.3$ and

$0.8 \leq \Delta m_{12} \leq 1.0$ magnitudes.

This study shows that fossils indeed are formed early, with more than $\sim$80% of their mass accumulated as early as 4 Gyr ago. They are also relatively isolated compared to non-fossils. The strongest X-ray fossil candidates are those with the highest X-ray luminosity as these systems are not expected to have a large luminosity gap between their first and second ranked galaxies entirely by chance. As always, systems with more than a handful of galaxies are to be preferred.

In principle, comparison of the observed space density of fossils as a function of X-ray luminosity with that of fossils from simulations can provide valuable constraints on the treatment of physical processes included in the simulations. The tentative evidence for a discrepancy, whereby the observed space density of low X-ray luminosity fossil groups may exceed that predicted from the simulations, will be worth revisiting in the future, when better observational estimates are available.

It is interesting that while the amount of recent mass assembly in control groups increases with halo mass, as is expected in the hierarchical growth paradigm, there is almost no difference between the mass assembly of high-mass and low-mass X-ray fossils after redshift $z = 0.6$ (see Fig. 2.8). It seems that both low-mass and high-mass fossil systems are undisturbed at low redshift.

Since we expect faster orbital decay and more efficient galaxy merging in lower mass systems, due to the lower velocity dispersion of individual galaxies within the group, we would expect to find a higher incidence rate of fossils amongst poor groups. Fig.2.3 shows that this is indeed the case, but the effect is not very strong, once the influence of statistical fossils is removed, and in X-ray fossils any rising trend at low richness is overwhelmed by the fact that many of the optical fossils fail to exceed the X-ray luminosity threshold. A word of caution about the treatment of orbital decay is in order here. As discussed in Sec. 2.2.2, the orbital evolution of subhalos in the Millennium simulation is well treated until these subhalos are reduced

by stripping to 20 dark matter particles, but thereafter is calculated semi-analytically, using an approximate formula. In practice, a significant fraction of the second ranked galaxies in the fossil systems we have extracted from the simulation have been stripped below this 20 particle limit. For example, in fossils with masses of only $10^{13}\,h^{-1}\,\mathrm{M}_{\odot}$, approximately 35% of second ranked galaxies have been stripped below the limit, though this fraction drops to $\sim$10% for systems with mass $> 10^{14}\,h^{-1}\,\mathrm{M}_{\odot}$. For such galaxies the timescale for their subsequent decay and merger with the central galaxy is not very reliable. However, this is not a major issue for massive halos, and it is interesting and surprising that the incidence of fossils in rich systems is fairly flat at 3-4%. Observational studies should, in due course, show whether this is reflected in the real Universe. One example of a fairly rich fossil cluster has already been reported by Khosroshahi et al. (2006).

The magnitude gap distribution of halos at different X-ray luminosities and the mass evolution of fossil groups discussed above both support the idea that X-ray fossil groups are not a distinct class of objects but rather that they are extreme examples of groups which collapse early and experience little recent growth, so that their galaxies have time to undergo orbital decay and merging. The X-ray and optical scaling properties of such extreme groups can be expected to differ from those of groups with more typical evolutionary histories, and such differences have already been observed (Khosroshahi, Ponman & Jones 2007). A comparison of such observed differences with the properties seen in the Millennium simulation groups is underway, and should provide a valuable check on the adequacy with which feedback processes and other baryon physics is handled in the simulations.

The final caveat is the fact that our results presented in this chapter depend upon the semi-analytic model used to study fossil groups. We will see in the next chapter that parameters such as space density, distribution of magnitude gap, etc. change remarkably if one uses another semi-analytic model of galaxy formation. We will discuss more about this issue in Chapter 3.

Bibliography

Allen, S.W., & Fabian, A.C., 1998 MNRAS, 297, L57

Arnaud, M,. & Evrard, A.E., 1999, MNRAS, 305, 631

Balogh, M.L., Babul, A, Voit, G.M., McCarthy, I.G., Jones, L.R., Lewis, G.F., & Ebeling, H., 2006, MNRAS, 366, 624

Barnes, J.E., 1989, Nature, 338, 123

Bond, J. R.,Cole, S., Efstathiou, G. & Kaiser, N., 1991, ApJ, 379, 440

Borgani S., et al., 2006, MNRAS, 367, 1641

Colless, M. et al., 2001, MNRAS, 328 ,1039

Croton, D.J., Springel, V., White, S.D.M., De Lucia, G.; Frenk, C. S.; Gao, L.; Jenkins, A., Kauffmann, G., Navarro, J. F. & Yoshida, N., 2006, MNRAS, 365, 11

Cypriano, E.S., Mendes de Oliveira, C.L. & Sodré, L.Jr., 2006, AJ, 132, 514

D'Onghia, E., Sommer-Larsen, J., Romeo, A.D., Burkert, A., Pedersen, K., Portinari, L. & Rasmussen, J., 2005, ApJ, 630, L109

Dubinski, J., 1998, ApJ, 502, 141

Ebeling, H., Jones, L.R., Fairley, B.W., Perlman, E., Scharf, C., & Horner, D., 2001, ApJ, 548L, 23

Fellhauer, M., Kroupa, P., Baumgardt, H., Bien, R., Boily, C. M., Spurzem, R., & Wassmer, N., 2000, NewA, 5, 305

Hartley, W. et al., 2007, submitted MNRAS

Helsdon, S.F. & Ponman, T.J., 2000, MNRAS, 315, 356

Helsdon, S.F. & Ponman, T.J., 2003, MNRAS, 340, 485

Jeltema, T.E., Mulchaey, J.S., Lubin, L.M., Rosati, P., & Böhringer H., 2006, ApJ, 649, 649

Jones, L.R, Ponman, T.J., Horton, A., Babul, A., Ebeling, H. & Burke, D.J., & Forbes, D.A., 2003, MNRAS, 343, 627

Jones, L.R, Ponman, T.J. & Forbes, D.A., 2000, MNRAS, 312, 139

Khosroshahi, H.G., Jones, L.R. & Ponman, T.J., 2004, MNRAS,349, 1240

Khosroshahi, H.G., Maughan, B.J., Ponman, T.J. & Jones, L.R., 2006, MNRAS, 369, 1211

Khosroshahi, H.G., Ponman, T.J. & Jones, L.R., 2006, MNRAS, 372, L68

Khosroshahi, H.G., Ponman, T.J. & Jones, L.R., 2007, MNRAS, 377, 595

Kaiser, N., 1991, ApJ, 383, 104

Matsushita, K., 2001, ApJ, 547, 693

Mendes de Oliveira, C.L., Cypriano, E.S. & Sodré, L.Jr., 2006, AJ, 131, 158

Miles, T.A., Raychaudhury, S., Forbes, D.A., Goudfrooij, P., Ponman, T.J. & Kozhurina-Platais, V., 2004, MNRAS, 355, 785

Miller, C.J. et al., 2005, AJ, 130, 968

Milosavljević, M., Miller, C.J., Furlanetto, S.R. & Cooray, A., 2006, ApJ, 637, L9

Mulchaey, J.S. & Zabludoff, A.I., 1999, ApJ, 514, 133

Mulchaey, J.S. & Zabludoff, A.I., 1998, ApJ, 496, 73

Navarro, J.F., Frenk, C.S., & White, S.D.M., 1996, ApJ, 462, 563

Pearce, F. et al., 2007, submitted MNRAS

Ponman, T.J., Allan, D.J., Jones, L.R., Merrifield, M. & MacHardy, I.M., 1994 Nature, 369, 462

Ponman, T.J. & Bertram, D., 1993, Nature, 365, 51

Ponman, T.J., Bourner, P.D.J., Ebeling, H., & Bohringer, H., 1996, MNRAS, 283, 690

Romer A.K. et al., 2000, ApJS, 126, 209

Sales, et al., 2007, astro-ph:0706.2009v3

Schechter, P.L., 1976, ApJ, 203, 297

Spergel, D. N. et al., 2003, ApJS, 148, 175

Sommer-Larsen, J., 2006, MNRAS, 369, 958

Springel, V., White, S.D.M., Tormen, G. & Kauffmann, G., 2001, MNRAS, 328, 726

Springel, V. et al., 2005, Natur, 435, 629

Steinmetz, M., & White, S.D.M., 1997, MNRAS, 288, 545

Sun, M., Forman, W., Vikhlinin, A., Hornstrup, A., Jones, C. & Murray, S.S., 2004, ApJ, 612, 805

Tittley, E.R., Pearce, F.R., & Couchman, H.M.P., 2001, ApJ, 561, 69

Ulmer, M.P. et al., 2005, ApJ, 624, 124

Vikhlinin, A., McNamara, B.R., Hornstrup, A., Quintana, H., Forman, W., Jones, C. & Way, M., 1999, ApJ, 520L

White, D.A., Jones, C., & Forman, W., 1997, MNRAS, 292, 419

Xu, G., 1995, ApJS, 98, 355

Xue, H., Jim, G., & Wu, X.P, 2001, ApJ, 553, 78

Xue, Y.J, & Wu, X.P, 2000, ApJ, 538, 65

Yamagata T. & Maehara H., 1986, PASJ, 38, 661

Yoshioka, T., Furuzawa, A., Takahashi, S., Tawara, Y., Sato, S., Yamashita, K. & Kumai, Y., 2004, AdSpR, 34, 2525

van den Bosch, F.C., Yang, X., Mo, H.J., et al., 2007, MNRAS, tmp..139V

Vel*á*zquez, H., & White, S.D.M., 1999, MNRAS, 304, 254

Zabludoff, A.I. & Mulchaey, J.S., 1998, ApJ, 496, 39

Eke, V.R., Baugh, C.M., Cole, S., Frenk, C.S., Norberg, P. et al., 2004, MNRAS, 348, 866

Chapter 3

The mass assembly of galaxy groups in the Millennium Simulation and the evolution of the luminosity gap

3.1 Introduction

Existing observations of large scale structures overwhelmingly favor cold dark matter (CDM) cosmologies, although the paradigm faces challenges both from the luminous passive galaxies at high redshift, and small galaxy over-densities in the local universe (Balogh et al. 2008). Galaxies dominate the visible universe and any cosmological model is expected to reproduce the observed global properties of galaxies, at least statistically, in the first instance. Based on CDM hierarchy, small systems such as groups are the primary environments for galaxies where processes such as galaxy mergers occur with higher efficiency than in massive halos such as galaxy clusters.

Even though the Millennium Dark Matter simulation (Springel et al. 2005), is the largest cosmological simulation available, it has very few cluster scale halos and better serves the

studies of group scale over-densities. In the previous chapter, we studied the formation of fossil groups (Dariush et al. 2007) in the Millennium Simulations. Fossils are known to be archetypal relaxed systems, optically dominated by a giant elliptical galaxy (Ponman et al. 1994) and can be used to test halo evolution models owing to their clear definition (Jones et al. 2003) and homogeneity (Khosroshahi, Ponman, & Jones 2007).

The results of these and similar studies depend heavily on modelling of galaxy models, e.g. semi-analytic modelling, which describe galaxy formation and evolution in the hierarchical merging of dark matter halos in the CDM model. Once the the merging hierarchy is computed, from N-body simulations, galaxy formation is then modelled by considering the rate at which gas can cool within these halos, the rate of galaxy merging (driven by dynamical friction) and the rate and efficiency of star formation and the associated feedback in individual galaxies (Croton et al. 2006; Bower et al. 2006). There are two sets of observations which are used to constrain the semi-analytic models, the local galaxy luminosity function and the colour-magnitude relation (Bower et al. 2006). However, the number of tunable parameters and the physical processes implemented in the models are well above those two constraints. Other observations often used to make the semi-analytic models self-consistent are primarily based on the observation of IGM and hot gas properties within the halos which itself is at the center of extensive investigations, and requires more detailed observations and addressing of observational biases. In addition the IGM models still employ simple prescriptions for cooling and heating. Thus, more observations are needed, preferentially involving galaxy properties, to test the models.

Our aim is to analyze the Millennium simulation data in order to study early-formed galaxy systems. So far early-formed groups are identified mainly based on their observed luminosity gap between the first two brightest group galaxies. In this chapter we investigate whether such a criterion is a valid method, using the best current cosmological simulations. If this method is found to be less than adequate, we wish to discover what conditions one needs to apply to

identify early-formed systems in an optimised way. In other words, is there any connection between the magnitude gaps between galaxies within groups and their halo mass assembly history? If so, then how are they related to each other, and what is the physical basis of this relations?

In an earlier study of the Millennium Simulations, we showed that the conventional definition of fossils, namely a large luminosity gap between the two brightest galaxies within half a virial radius and the group X-ray luminosity $\geq 10^{42}$ erg/s, results in halos which are significantly (15%-30%) more massive than the rest of the population of galaxy groups with the same halo mass, when the Universe was half of its current age. This suggests an early formation epoch for fossils. The conventional fossil selection criteria, specially the requirement of high X-ray luminosity, filter out "statistical" fossils, and therefore there is a very small probability for a large luminosity gap in a halo to occur at random. The fraction of fossils with non-statistical origin is $\approx 8\%$, almost independent of halo mass (Dariush et al 2007, Khosroshahi et al 2008). Another important finding of the study was consistency between the space density of fossils in the simulations and in the observational estimates.

In this chapter we use an alternative semi-analytic model (Bower et al. 2006) on the basis that it provides galaxy properties at different epochs. We select a new class of early formed galaxy groups, purely on the basis of their halo mass evolution, and study the luminosity gap between their brightest galaxies. We compare fossil groups selected based on conventional selection, with this new model based selected groups.

3.2 Data

We start with a catalogue of groups extracted by a friends-of-friends (FoF) algorithm from the Millennium DM runs (see Chapter 2). Hereafter a "group" or "group halo" would refer to a group taken from this catalogue.

In order to follow the evolution of groups from $z \sim$1.0 to present epoch, we require various combinations of the Millennium FoF group and the semi-analytic catalogues. We select groups of $M(R_{200}) \geq 10^{13}\, h^{-1}\, \mathrm{M}_{\odot}$ from the FoF group catalogue at $z = 0.998$. The mass cut-off is intended to ensure that the progenitors of the present day galaxy groups are indeed groups at $z \sim$1 with at least four or five members (galaxies), above the magnitude cut of the catalogue.

The evolution of each group was followed from $z = 0.998$ to $z = 0$ (at 23 discrete values, equally spaced in $\log z$) by matching the position of each halo to its descendants at later redshifts.

The position of the central galaxy of each galaxy group, and the corresponding dark matter halo, were used to identify the member galaxies of each group. At each redshift and for each group halo, optical properties were extracted for its corresponding galaxies from the semi-analytic galaxy catalogue. The model galaxies become incomplete below a magnitude limit of $\mathrm{M}_K - 5\log(h) \sim -19.7$, due to the limited mass resolution of the Millennium simulation. We applied a K-band absolute magnitude cut-off of $\mathrm{M}_K \lesssim -19$ on galaxies at all redshifts.

During the matching process, for more than 99% of the groups at each redshift, corresponding galaxies were found in the semi-analytic galaxy catalogue. The remaining groups were excluded from our final compiled list.

In order to find the gas properties of all groups at z=0, further cross-correlation was carried out using the Millennium gas catalogue, which enables us to select galaxy groups at z=0 according to their bolometric X-ray luminosity. The gas halos were well matched to all dark matter group halos at redshift $z = 0$.

Out of 19066 dark matter group halos with $M(R_{200}) \geq 10^{13}\, h^{-1}\, \mathrm{M}_{\odot}$ selected at $z = 0.998$, optical properties from the semi-analytic catalogue (as well as gas properties from the gas simulations at z=0) and the entire history of evolution at all redshifts up to z=0, were found for 17866 ($\sim$94% of the initial sample at $z \sim 1$) of group halos. Fig. 3.1 shows the bolometric X-ray luminosity from the Millennium gas simulation, plotted against the the corresponding

dark matter halo mass of each group, at redshift z=0 for all of the matched 17866 groups. The vertical dashed line in Fig. 3.1 corresponds to the conventional X-ray luminosity threshold ($L_{\rm X,bol} = 0.25 \times 10^{42}\, h^{-2}$erg s^{-1}) for fossil groups (Jones et al. 2003), as adopted in Sec. 3.3.2 to define X-ray bright groups. There are 14628 groups above this threshold, out of 17866 groups. With the exclusion of Sec. 3.3.1 and Sec. 3.3.2, where the whole range of halo mass has been explored to study the luminosity gap statistics and the local environment of groups, X-ray bright groups constitute the main data set for the rest of our analysis.

3.3 Results

3.3.1 The R-band Magnitude Gap Statistic

The distribution of the magnitude gap between the brightest galaxy, and the second and third brightest galaxies, in each group, provide useful statistics to probe the reliability of physical processes (e.g. prescriptions for feedback) implemented in semi-analytic models to predict the interaction and merging of galaxies in a system. The magnitude gap statistics therefore is an essential key parameter in studying fossil groups of galaxies as it quantifies the dynamical age of galaxy groups (Milosavljević et al. 2006; van den Bosch et al. 2007; Dariush et al. 2007; von Benda-Beckmann et al. 2008). This is because dynamical friction $f_{\rm dyn}$ will cause multiple luminous group galaxies to merge on a time scale which depends upon the velocity dispersion of galaxies within groups as $f_{\rm dyn} \propto v^{-2}$.

We determine the magnitude gaps from the Millennium semi-analytic models of Bower et al. (2006) and Croton et al. (2006), and compare them with observational results from the Sloan Digital Sky Survey (SDSS) C4 cluster catalogue data of Miller et al. (2005) and the 2-degree Field Galaxy Redshift Survey (2dFGRS) group catalogue of van den Bosch et al. (2007).

The 2dFGRS group catalogue is constructed based on a halo-based group finder algorithm of Yang et al. (2005) and contains ~ 6300 groups within the mass range $\log(M/h^{-1}\,{\rm M}_{\odot}) \geq$

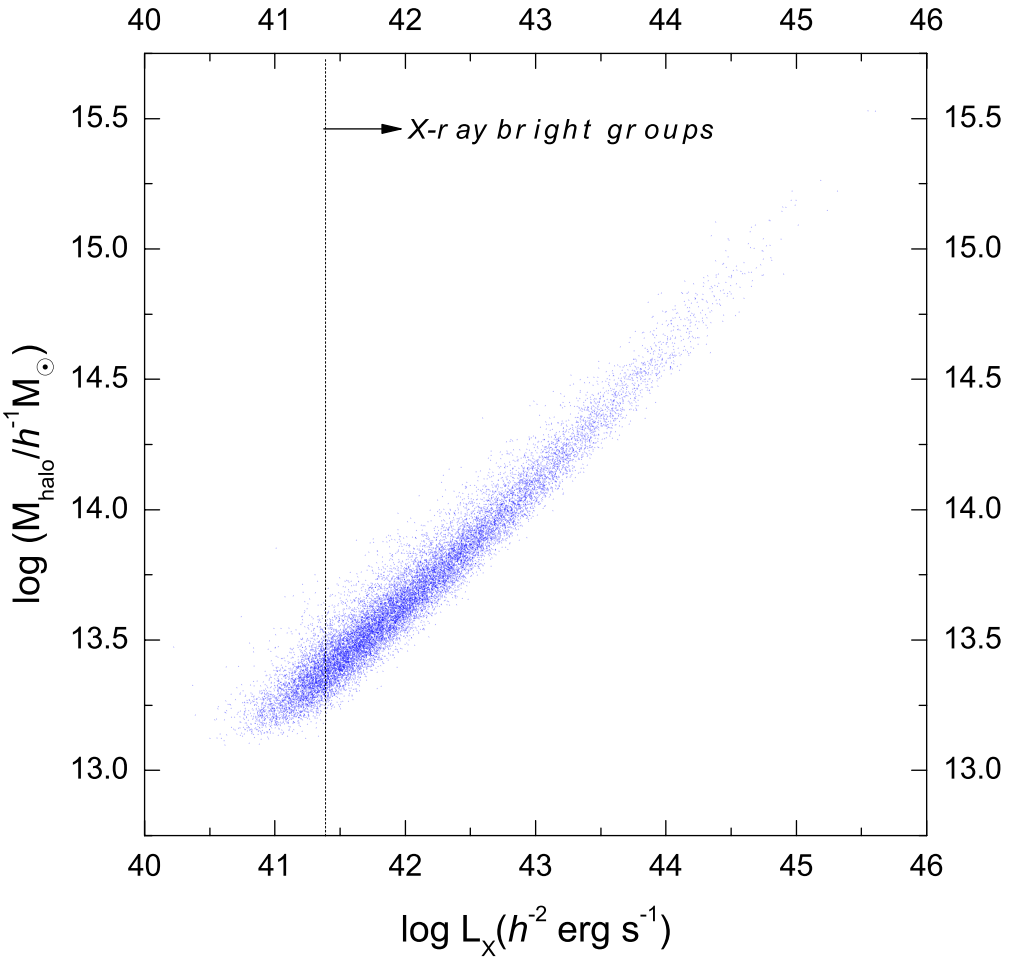

Figure 3.1: The relation between the mass of group halos (within R_{200}) at $z = 0$ from the Millennium DM simulation, and the bolometric X-ray luminosity of the corresponding halos in the Millennium gas simulation. All groups have $M(R_{200}) \geq 10^{13}\,h^{-1}\,\mathrm{M}_{\odot}$ at $z \sim 1.0$. The *vertical dashed-line* corresponds to the X-ray luminosity threshold $L_{\mathrm{X,bol}} = 0.25 \times 10^{42}\,h^{-2}$erg s^{-1} adopted in this paper for defining X-ray bright groups (see Sec. 3.3.2). Of the 17866 groups matched in the two catalogues, 14628 groups lie above this threshold.

13.0 where the mass of each group has been determined from the total luminosity of all group members brighter than $M_{b_j} - 5\log h = -18$.

Contrarily the C4 catalogue Miller et al. (2005) consists of ~ 730 clusters identified in the spectroscopic sample of the Second Data Release (DR2) of the SDSS inside the mass range $13.69 \leq \log(M/h^{-1}\,\mathrm{M}_{\odot}) \leq 15.0$, estimated from the total r-band optical luminosity of cluster galaxies. The results are shown in Fig. 3.2 where the *blue histogram* displays the observational data together with estimated R-band magnitude gaps from semi-analytic models of Bower et al. (2006) as well as Croton et al. (2006).

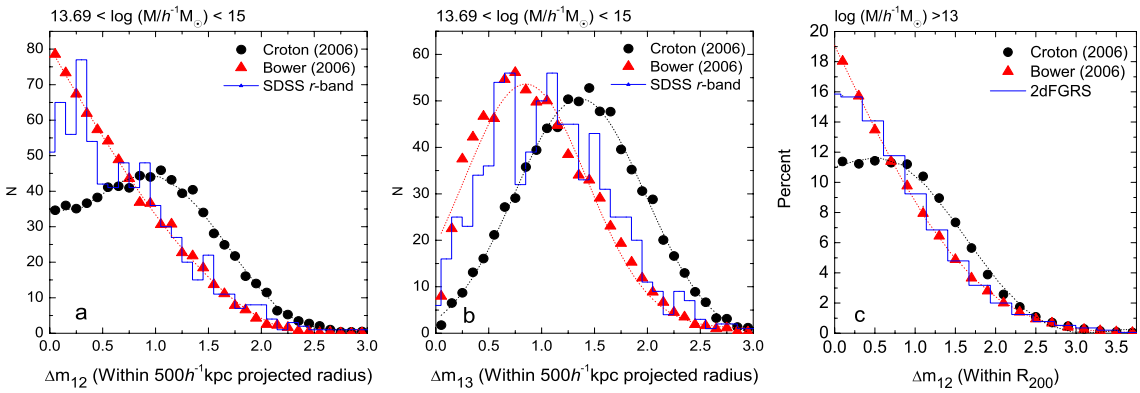

Figure 3.2: The R-band luminosity gap distribution for halos from the Millennium semi-analytic models of Bower et al. (2006) (*red triangles*) and Croton et al. (2006) (*black circles*) superposed on the data from 2dFGRS group catalogue of van den Bosch et al. (2007) as well as SDSS C4 cluster catalogue of Miller et al. (2005) (*blue histograms*). (a) The magnitude gap Δm_{12} between the the first and second most luminous galaxies, compared with galaxies from the SDSS C4 catalogue of clusters computed within projected radius of $500h^{-1}$ kpc. (b) The same as in (a) but for the magnitude gap Δm_{13} between the first and the third most luminous galaxies. (c) The magnitude gap Δm_{12} estimated within R_{200}, compared with galaxies from the 2dFGRS group catalogue. The ~ 6300 2dFGRS groups are within the mass range $\log(M(R_{200})/h^{-1}\,\mathrm{M}_{\odot}) \geq 13.0$, and those from SDSS C4 catalogue consist of ~ 730 clusters within mass range $13.69 \leq \log(M(R_{200})/h^{-1}\,\mathrm{M}_{\odot}) \leq 15.0$.

Fig. 3.2 shows that the luminosity gap statistics Δm_{12} and Δm_{13} from Bower et al. (2006)

are in excellent agreement with those obtained from 2dFGRS group catalogue and SDSS C4 catalogue of clusters. However, the semi-analytic galaxy catalogue of Croton et al. (2006) predicts a larger fraction of groups with $\Delta m_{12} \geq 2.0$ for both the SDSS and 2dFGRS samples. This is in particular of great importance to the determination of the space density of fossil galaxy groups, which use the magnitude gap as a key discriminant, and comparison of fossil samples drawn from simulated and observed catalogues (e.g., see Table 2.1 or Table 1 of Dariush et al. (2007)).

3.3.2 Evolution of galaxy groups

In cosmological simulations, the age of galaxy groups can be expressed in terms of the rate of the mass assembly of the groups. This means that for a given group halo mass, groups that formed early, assemble most of their masses at an earlier epoch in comparison to younger groups. Thus the *assembly time* of a dark matter halo, defined as the look-back time at which its main progenitor reaches a mass that is half of the halo's present day mass, is larger in "older" systems than in "younger" ones. Of course, in cosmological simulations such as the Millennium runs, where the structures in Universe from hierarchically, massive systems which form later turn out to have shorter assembly time than low mass groups. Therefore one should take into account the mass of systems when comparing the mass assembly of various types of groups and clusters.

Fossil groups of galaxies

How does the history of mass assembly of a group or cluster is related to its present observable parameters? For example, it is expected that groups which have formed earlier tend to have a hotter IGM/ICM (intra group/cluster medium) and therefore be more dynamically relaxed and X-ray luminous, while groups with the same mass that have formed late, and are still in a state of collapse, would not show X-ray emission associated to their IGM/ICM gas (Rasmussen et al.

2006).

Hitherto the so-called *fossil galaxy groups*, which are supposed to be canonical examples of groups that have formed early, have been identified by requiring that they X-ray luminosities exceed $L_{\rm X,bol} \geq 0.25 \times 10^{42} h^{-2}$erg s^{-1} (e.g. Khosroshahi, Ponman, & Jones 2007; Jones et al. 2003). In addition, a fossil group needs to have, within half a virial radius of the group's centre, the second brightest galaxy to be at least 2-mag fainter than the brightest galaxy, i.e. $\Delta m_{12} \geq 2.0$ [1] So far these two observational criteria have been jointly used to explore fossil groups and clusters of galaxies. Therefore, Fig. 3.3, which displays all the *X-ray bright groups* fulfilling the X-ray criterion in Fig. 3.1, and the optical criterion $\Delta m_{12} \geq 2.0$ (dotted horizontal line) should separate groups which have been formed earlier in comparison to their counterparts with $\Delta m_{12} < 2.0$.

Note that in numerical simulations fossils are identified as groups with $\Delta m_{12} \geq 2.0$ within R_{200} or $0.5R_{200}$. Our results from this study as well as those represented in Dariush et al. (2007) show that the fraction of fossils (and therefore their space densities) depend on the search radius within which Δm_{12} is estimated, whereas the history or mass assembly does not change that much.

The mass assembly of X-ray fossil groups

Let us introduce the parameter α_z which for an individual group is the ratio of its mass at redshift z to its final mass at $z = 0$, i.e. $\alpha_z \equiv M_z/M_{z=0}$. Thus at a given redshift z, groups with larger α_z have assembled a larger fraction of their final mass by z=0 than groups with smaller values of α_z.

In Fig. 3.3, we plot the magnitude gap Δm_{12} (within $0.5R_{200}$), estimated for all 14628 X-ray bright groups (i.e. groups with $L_{\rm X,bol} \geq 0.25 \times 10^{42} h^{-2}$erg s^{-1}) at $z = 0$ as a function of their mass fraction $\alpha_{1.0}$ at $z = 1$. Groups are colour-coded according to their dark matter halo

[1] This condition can be replaced by $\log(L_2/L_1) \leq -0.8$ where L_1 and L_2 are the luminosities of the first two brightest galaxies.

mass. The horizontal dashed line separates groups into fossils ($\Delta m_{12} \geq 2.0$) and non-fossils ($\Delta m_{12} < 2.0$). All data points on the right side of the *vertical dashed-line* have assembled more than 50% of their mass by z ∼1.0 and hence have a minimum assembly time of about ∼7.7 Gyr. The contour lines represent the number of data points (groups) in each of 25×25 cells of an overlaid grid which is equally spaced along both the horizontal and vertical axes.

Two results emerge from this plot: (i) As is expected, on average the rate of mass growth in massive systems is higher than in low mass groups as the majority of massive groups and clusters have assembled less than 50% of their final mass at z ∼1.0. (ii) Less massive groups (and therefore early-formed ones) tend to develop larger magnitude gaps in comparison to massive groups and clusters. Consequently the fraction of massive fossils, identified in this way, is less than low mass fossil groups. However, at the same time, for a given $\alpha_{1.0}$, groups with smaller values of $\Delta m_{12} < 2$ exceeds the number of fossil groups, as it is evident from the density of the contours.

Unlike the first result, the second conclusion is not in agreement with our current view that groups with relatively large Δm_{12} are older systems. Clearly, a majority of groups with similar high values of $\alpha_{1.0}$ have smaller magnitude gaps. Without doubt, the parameter Δm_{12} is influenced by infall and merging of galaxies and sub-groups within galaxy groups. This could end up with an increase (in case of merging) or decrease (in case of infalling of new galaxies) in Δm_{12}. Indeed, in the work of von Benda-Beckmann et al. (2008), one finds that the "fossil" phase of any fossil group is transient, since the magnitude gap criterion will sooner or later be violated by a galaxy comparable to the brightest galaxy falling into the core of the group.

To quantify the above results, we study the evolution with redshift of various physical parameters for two different sample of groups, drawn from the distribution of galaxy groups in Fig. 3.3. In the first sample, halos are divided into **old**($\alpha_{1.0} \geq 0.5$, b+c in Fig. 3.3) and **young** ($\alpha_{1.0} \leq 0.5$, a+d in Fig. 3.3) groups respectively. In the second population, halos are classified as **X-ray fossil** ($\Delta m_{12} \geq 2.0$, a+b in Fig. 3.3) and **control** ($\Delta m_{12} \leq 0.5$, d+c in Fig. 3.3)

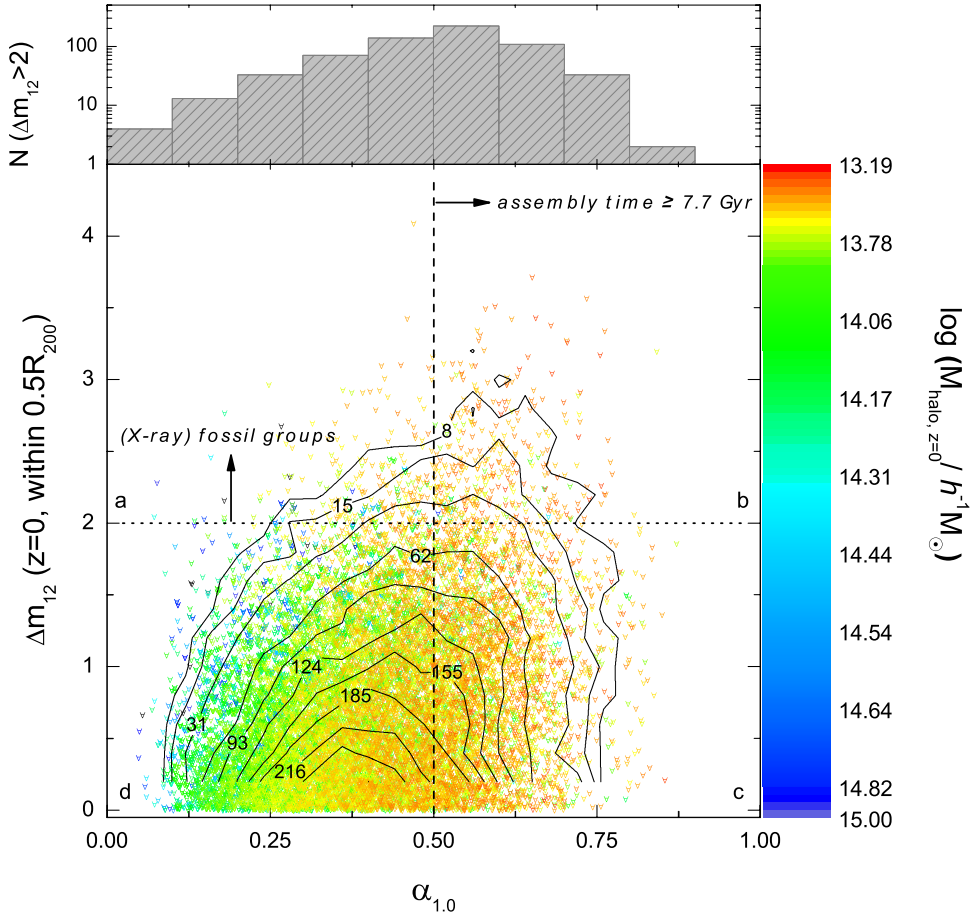

Figure 3.3: The magnitude gap Δm_{12} within $0.5\,R_{200}$, estimated for all 14628 X-ray bright groups in Fig. 3.1 (i.e. groups with $L_{\rm X,bol} \geq 0.25 \times 10^{42} h^{-2}$erg s^{-1}) at $z = 0$ versus the ratio of the group halo mass at redshift $z = 1$ to its mass at $z = 0$ ($\alpha_{1.0}$). The *horizontal dashed-line* separates groups into fossils ($\Delta m_{12} \geq 2.0$) and non-fossils ($\Delta m_{12} < 2.0$). The *vertical dashed-line* corresponds to $\alpha_{1.0} = 0.5$. Groups with $\alpha_{1.0} \geq 0.5$ have formed more than half of their mass by $z \sim 1.0$ and hence have a minimum assembly time of about ~ 7.7 Gyr. Data points are colour-coded according to FoF group halo mass M_{R200} at the present epoch. The density of data points is represented by *black contour lines* which is the number of groups in each of 25×25 cells of an overlaid grid, equally spaced horizontally and vertically. The *upper panel* represents the histogram of X-ray fossil groups, i.e. all groups with $\Delta m_{12} \geq 2.0$.

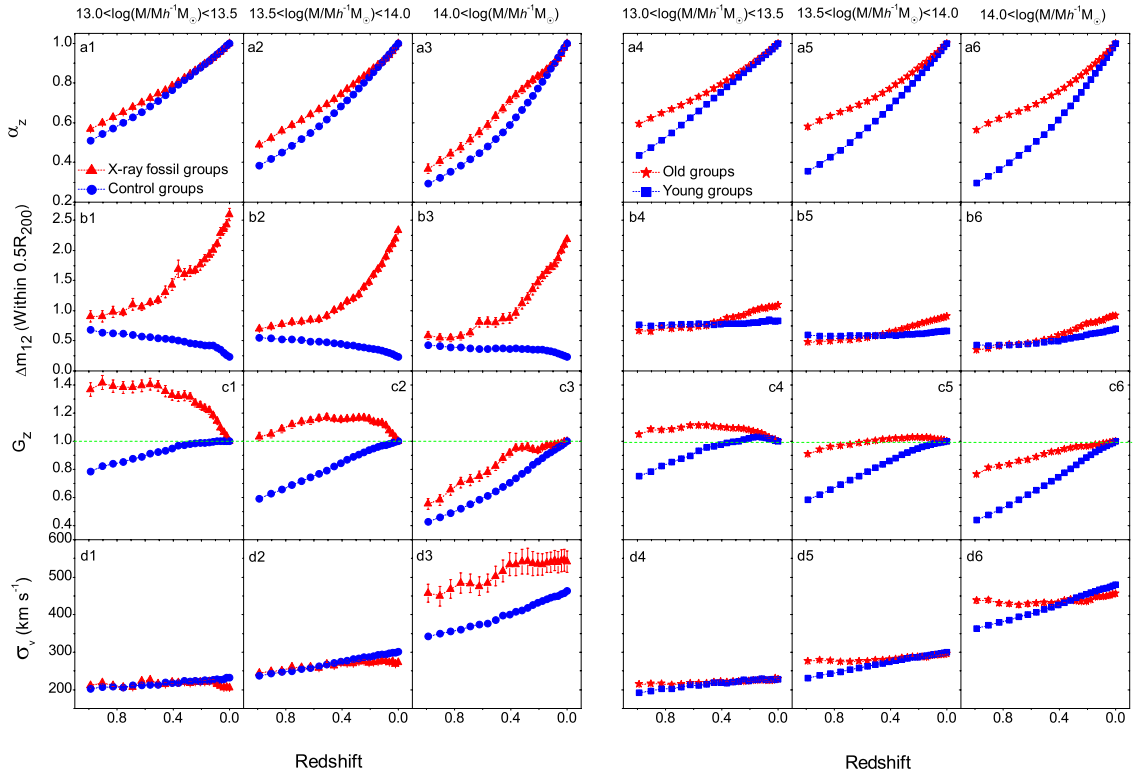

Figure 3.4: Evolution of various physical parameters of X-ray bright groups versus redshift in different group mass bins. *Left panel:* Haloes are classified as **X-ray fossil** ($\Delta m_{12} \geq 2.0$, *red triangles*) and **control** ($\Delta m_{12} \leq 0.5$, *blue circles*) groups based on the magnitude gap between the first and the second brightest galaxies within $0.5R_{200}$. *Right panel:* Groups are divided into **old**($\alpha_{1.0} \geq 0.5$, *red stars*) and **young** ($\alpha_{1.0} \leq 0.5$, *blue squares*) population respectively. The horizontal *green dashed-lines* intersect y-axis at $G_z = 1$. Each row represents the evolution of one parameter belonging to galaxy groups. From top to bottom these parameters are: α_z ($a1, ..., a6$); the magnitude gap Δm_{12} within $0.5R_{200}$ ($b1, ..., b6$); ratio of the number of galaxies within $0.5R_{200}$ at redshift z of a given galaxy group to the number of galaxies within $0.5R_{200}$ at redshift $z = 0$ of the same group, i.e. G_z ($c1, ..., c6$); and group velocity dispersion σ_V in km s^{-1} ($d1, ..., d6$).

groups based on the magnitude gap between the first and the second brightest galaxies within half a virial radius of the centre of the group.

For each sample, the evolution of various parameters are shown in two panels of Fig. 3.4. From top to bottom these parameters are:

- α_z, i.e. the ratio of the group halo mass at redshift z to its mass at $z = 0$,
- Δm_{12} within $0.5R_{200}$,
- Ratio of the number of galaxies within $0.5R_{200}$ at redshift z of a given galaxy group to the number of galaxies within $0.5R_{200}$ at redshift $z = 0$ of the same group, i.e. G_z,
- Group velocity dispersion σ_V in km s^{-1}.

In each panel of Fig. 3.4, the left, middle, and right columns correspond to different group mass bins, as indicated. The left panel in Fig. 3.4 illustrates X-ray fossil (*red triangles*) and control (*blue circles*) groups respectively while the right panel shows old (*red stars*) and young (*blue squares*) groups. The horizontal *green dashed-lines* intersect y-axes at $G_z = 1$. Errors on data points are the standard error on the mean, i.e. $\sigma/\sqrt{N}$, where σ is the standard deviation of the original distribution and N is the sample size.

A comparison between Figs. 3.4$a1, a2, a3$ and Figs. 3.4$a4, a5, a6$ shows that old groups which have been picked up according to their lower rate of mass growth (i.e. larger $\alpha_{1.0}$), represent a *perfect class* of fossils, though they develop a magnitude gap Δm_{12} which is not as large as those seen in X-ray fossils (see also Figs. 3.4$b1, ..., b6$).

On the other hand, unlike old groups, X-ray fossils develop large magnitude gaps, which do not necessarily correspond to their rapid mass growth, specially in massive groups with $\log(M(R_{200})/h^{-1}\,\mathrm{M}_{\odot}) \geq 14.0$. It reflects the fact that the majority of real passive groups have a small magnitude gap between their two brightest galaxies. Thus the expression $\Delta m_{12} \geq 2$ only partially separates genuine old/passive groups from young/forming groups, as there are a larger fraction of genuine old groups but with small Δm_{12}.

From Figs. 3.4$c4, c5, c6$, it is obvious that old groups are essentially more relaxed systems without recent major merger, as the rate of infall of galaxies is equal or even less than the rate at which galaxies merge with the central group galaxy. Therefore in old groups the parameter G_z is more or less constant in time in comparison to young groups within the same group mass bin. The situation is a bit different in X-ray fossils with $\log(M(R_{200})/h^{-1}\,\mathrm{M}_{\odot}) \leq 14.0$ (Figs. 3.4$d1, d2$) since the rate of galaxy merging is noticeably larger than infall of galaxies. As a result, very large magnitude gaps are being developed in X-ray fossil groups. However, both massive X-ray fossils and control groups with $\log(M(R_{200})/h^{-1}\,\mathrm{M}_{\odot}) \geq 14.0$ (Fig. 3.4$d3$) are in a state of rapid mass growth. As a consequence, massive X-ray groups are not dynamically relaxed systems as they are influenced by infall of galaxies and substructures.

Finally, it is worth considering how the velocity dispersion, plotted in Figs. 3.4$d1, ..., d6$ changes in different type of groups. As Figs. 3.4$d4, d5, d6$ show, as long as the rate of infall of substructures of groups, is close to 1.0 (*green dashed-line*) the velocity dispersion does not change significantly in time which in turn is a sign that these groups are certainly relaxed systems.

BCG R-band magnitudes

Since the central galaxy in fossil groups has been subjected to numerous mergers in such a way that $\mathrm{L}_{\star}$ galaxies have merged with the central galaxy, more X-ray fossils are expected to be dominated by luminous (R-band) BCGs than their non-fossil counterparts. Thus one may pick up genuine old systems by selecting galaxy groups with large magnitude gaps, and brighter central galaxies. Therefore it worth checking the correlation between the luminosity of the central galaxies of groups, with large magnitude gaps, as well as their mass assembly history.

The four panels in Fig. 3.5 demonstrate the relation between the absolute R-band magnitude of BCGs for all X-ray bright groups and the magnitude gap Δm_{12} within $0.5\mathrm{R}_{200}$ in four different mass bins. In each panel of Fig. 3.5, an overlaid grid of 45×55 cells has been used where

each cell is colour-coded according to the median of $\alpha_{1.0}$ in that cell. Accordingly contour lines in each panel represent the regions with the same $\alpha_{1.0}$ values.

Fig. 3.5 shows clearly that both $\alpha_{1.0}$ and BCG R-band magnitudes increase with decrease in group halo masses. But it does not show a tight correlation between the R-band luminosity of BCGs and group magnitude gaps Δm_{12}, though the correlation is more pronounced in clusters with $M(R_{200}) \geq 10^{14}\, h^{-1}\, \mathrm{M}_{\odot}$ (Fig. 3.5d). Therefore, putting any magnitude cut in BCG of groups, end up in loosing many real genuine groups which are not X-ray fossil systems according to the optical condition on Δm_{12}.

The Fossil phase in the life of groups

The existence of large magnitude gaps in X-ray fossils in Figs. 3.4$b1, b2, b3$ is expected as these groups were initially selected according to their Δm_{12} at z=0. It would be interesting if they could be shown to have maintained such large magnitude gaps for a longer time, in comparison to control groups, which would be the case if X-ray fossils were relaxed groups without recent major mergers. Also if fossil groups in general are the end results of galaxy merging, then we do expect the majority of fossils selected at higher redshifts to still be detected as fossils at the present epoch. To put it another way, the *fossil phase* in the life of a galaxy group should be a long-lasting phase and not a temporary one, in which the group may change its status from fossil to non-fossil frequently.

We carry out a further investigation by selecting three sets of fossil groups with $\Delta m_{12} \geq 2.0$ at three different redshifts. Then by tracing the magnitude gap of each set from z=1.0 to z=0, we examine the fossil phase of each set in time. In Fig. 3.6, fossils (*black shaded histogram*) and control (*red dotted-line histogram*) groups are selected at z=0 (*left column*), z=0.5 (*middle column*), and z=1.0 (*right column*). Fractions of fossil and control groups in each column of Fig. 3.6 have been estimated separately by normalising the number of fossil and control groups at other redshifts to their total numbers at the redshift at which they were initially selected.

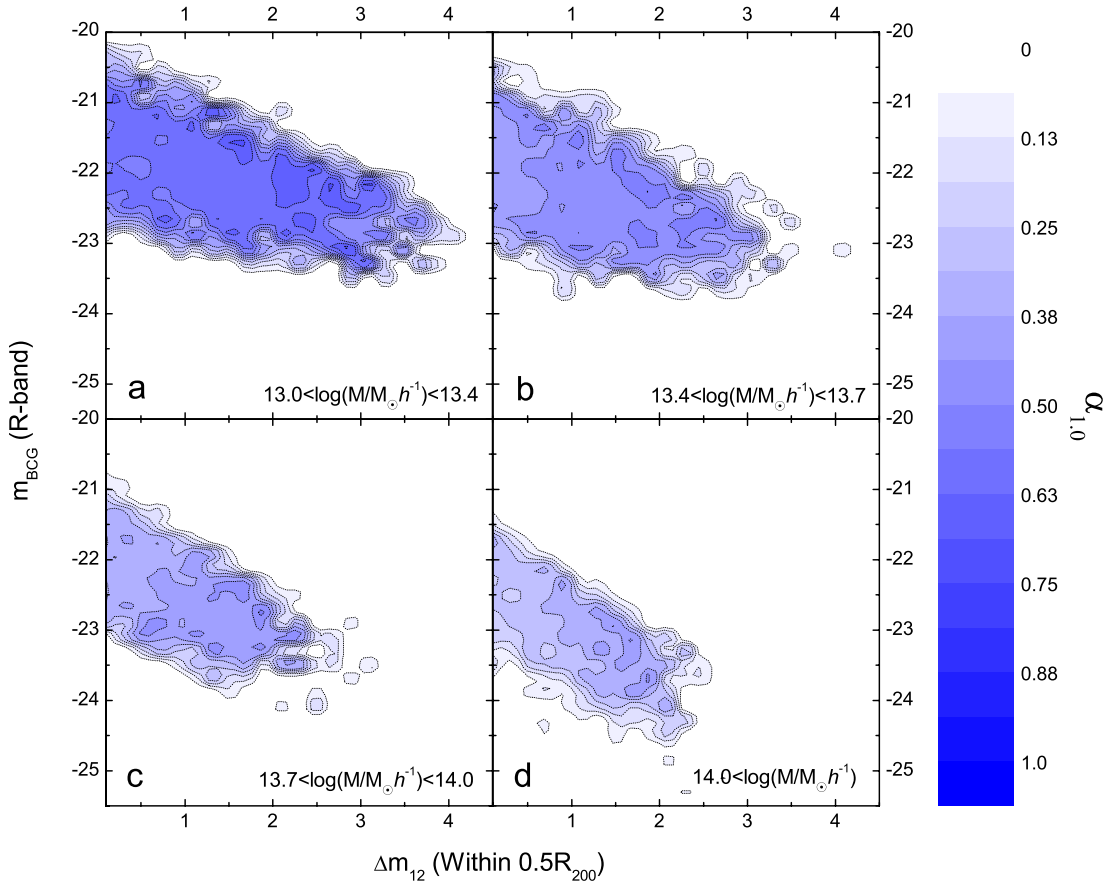

Figure 3.5: The absolute R-band magnitude of BCGs for all X-ray bright groups versus the magnitude gap Δm_{12} within $0.5R_{200}$ in four different mass bins. Groups are weighted according to $\alpha_{1.0}$. An overlaid grid of 45×55 cells has been used in each panel to estimate the median of $\alpha_{1.0}$ in that cell according to which the cell is colour-coded. Contour lines in each panel represent the regions with the same $\alpha_{1.0}$ values. All panels in Fig. 3.5 have the same scale.

This plot shows that, contrary to expectation, no matter at what redshift the fossils are selected, after ∼4 Gyr, more than ∼80% of them change their status and become non-fossils. It means that the fossil-phase is a temporary phase in the life of fossil groups, rather than a long-lasting phase (also see von Benda-Beckmann et al. 2008). Therefore, there is no guarantee that an observed fossil group, at a relatively high redshift, remains a fossil until the present time, if fossils are selected according to their magnitude gap $\Delta m_{12} \geq 2.0$, as many groups seem to go through a transient phase.

The environment of X-ray fossils

If the merging mechanism is responsible for the absence of L_* galaxies in fossil groups, then most of the mass infall into these systems would have happened at a relatively earlier epoch. Therefore at the present time, X-ray fossil groups should be more isolated than non-fossil groups. Fig. 3.7 shows the fraction of environmental density Δ_4 of halos, which is the number of halos within a distance of 4 h^{-1}Mpc from the centre of each group in the X-ray fossil and control categories. The local densities are calculated at $z = 0$ according to the following equation:

$$\Delta_4 = \frac{\rho_4}{\rho_{bg}} - 1. \tag{3.1}$$

In Eq. 3.1, ρ_4 is the number density of halos within a spherical volume of of 4 h^{-1}Mpc in radius and ρ_{bg} is the background density of halos within the whole Millennium volume. Since the mass assembly of groups is mostly influenced by the infalling of substructures, which individually have masses typically below ∼10% (and often substantially smaller) of the parent halo mass, it is important to take into account all halos with $M(R_{200}) \geq 10^{11}\, h^{-1}\, \mathrm{M}_\odot$ from the FoF group catalogue in order to estimate Δ_4.

Fig. 3.7 also shows that X-ray fossils are slightly more likely to lie in lower density regions than control groups. The polynomial fit to control groups (Fig. 3.7, *red dotted line*), peaks

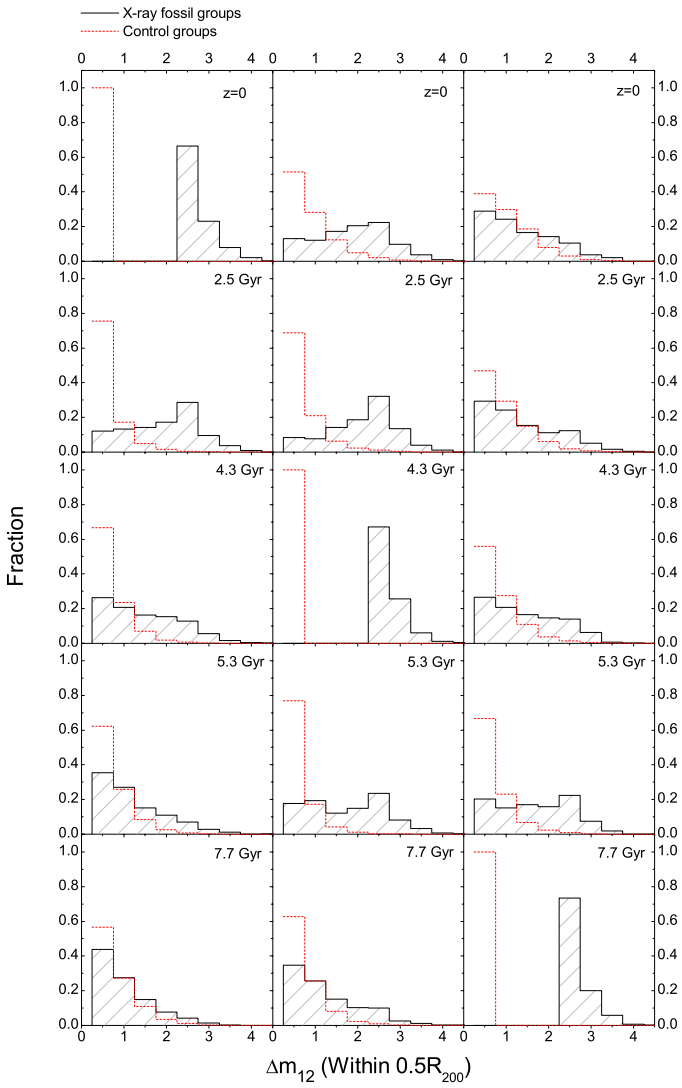

Figure 3.6: The fraction of fossil and control groups at different redshifts. Fossil groups (*black shaded histogram*) and control groups (*red dotted-line histogram*) are selected at z=0 (*left column*), z=0.5 (*middle column*), and z=1.0 (*right column*). Fractions of fossil and control groups in each column have been calculated by normalising the number of fossil and control groups at other redshifts to their corresponding total numbers at the redshift at which they were initially selected.

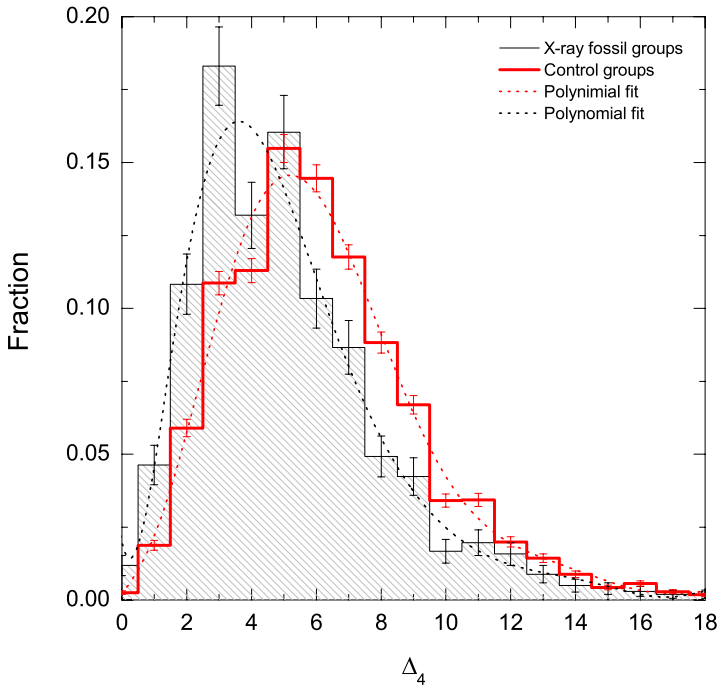

Figure 3.7: Histograms of the environmental density Δ_4 of halos within a distance of 4 h^{-1}Mpc (see Eq. 3.1). from the centre of X-ray fossil groups (*black shaded histogram*) and the control groups (*red thick histogram*) estimated using all halos with $M(R_{200}) \geq 10^{11}\, h^{-1}\, \mathrm{M}_{\odot}$ from the FoF group catalogue. The *black dotted line* and *red dotted line* are polynomial fits to fossil and control groups respectively.

around $\sim$5.1 while the same for X-ray fossils (Fig. 3.7, *black dotted line*) peaks about $\sim$3.7. Thus the difference is not large enough, from what one expects to see for X-ray fossils in comparison to control groups.

A similar trend is seen for Δ_5 and Δ_6 but as the sampling volume increases ($> \Delta_6$), the above trend disappears, showing that the trend is related to the immediate environment of groups.

3.3.3 Revising the Optical Criterion for finding fossil groups

Based on these results, using the Millennium simulation DM runs as well as the gas and semi-analytic galaxy catalogues based on them, it seems that the conventional optical condition $\Delta m_{12} \geq 2$, used to classify groups as fossils, does not support fully the idea that these systems represent an old class of galaxy groups, in which the central galaxy has grown through the merging of other comparable group galaxy members. Having said that, it is true that the magnitude gap in a galaxy group is related to the mass assembly history of the group, for we saw that in groups such a gap develops gradually in time. However, the difference in luminosities between the first two brightest galaxies in groups is not very reliable for our purpose, as it could be altered by the infall of satellite galaxies. We therefore look for a more optimal way of defining the magnitude gap among the brightest galaxies in a group, which would help in better identifying systems where most of the mass has assembled at an early epoch.

A general criterion for the magnitude gap

Assume a general optical condition in defining fossils according to the magnitude gap between the brightest group galaxy and other group galaxies in the following form:

$$\Delta m_{1i} \geq j, \tag{3.2}$$

where Δm_{1i} is the difference in R-band magnitude between the first brightest group galaxy and the i^{th} brightest group galaxy within R_{200} of the group centre. The current definition of fossils is based on $i = 2$ and $j = 2$. Obviously the group should contain at least $i + 1$ galaxies. We do not consider $i > 10$ since then we have to exclude most groups in our sample, and it would turn out not be be very useful for observers as well. The i^{th} galaxies are being found within R_{200} instead of $0.5R_{200}$, which improve our statistics noticeably.

As we consider the magnitude gap between the brightest to the $i = 1, 2, ...10^{\rm th}$ brightest

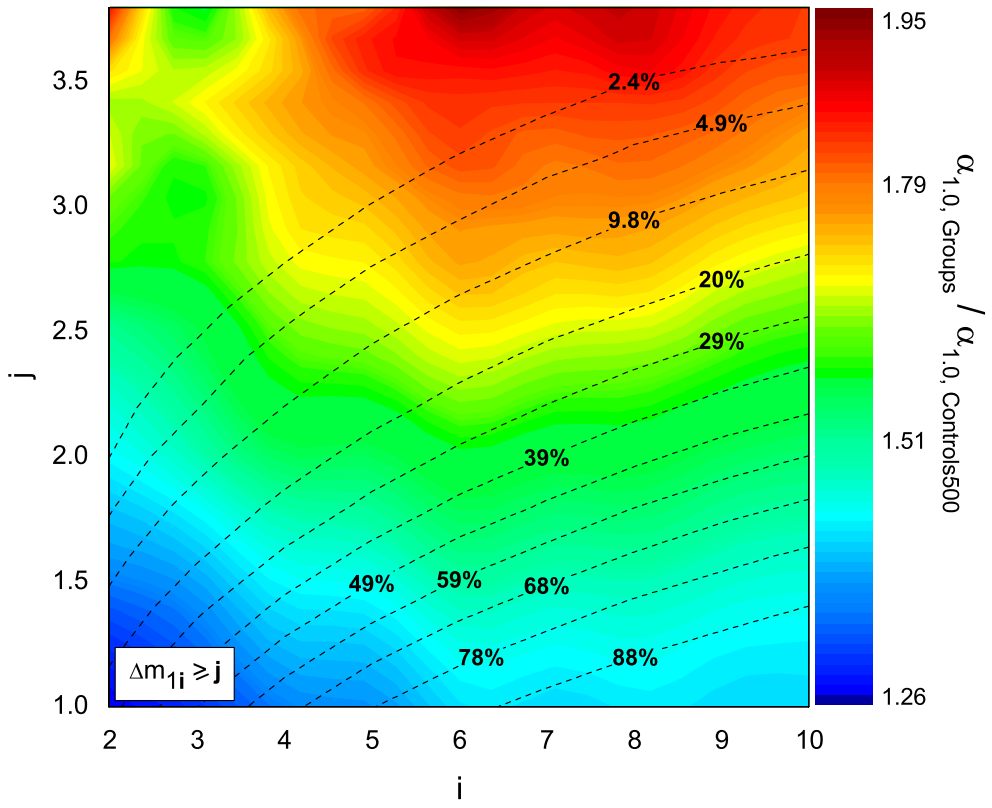

Figure 3.8: Colour-coded ratio of the mass assembly parameter $\alpha_{1.0}$ for groups that satisfy $\Delta m_{1i} \geq j$, to the value $\alpha_{1.0}$ of control$_{500}$ groups. In each bin of i and for all values of j in that bin, the first 500 groups with minimum magnitude gaps and at least i galaxies serve as control$_{500}$ groups in that bin. *Dashed contours* represent the equality lines where the fraction of groups is the same in the two samples.

galaxy, the value of the magnitude gap varies from $j \gtrsim$0 to $j \lesssim$5. Our aim is to find the pair (i, j) in (Eq. 3.2) which yields the best selection of genuinely old groups with a history of early mass assembly. A suitable choice of i and j not only should select more isolated groups, but also should pick up those systems which have been in the fossil phase for a longer time.

The colour-coded plot in Fig. 3.8 shows the ratio of the mass assembly fraction $\alpha_{1.0,\mathrm{Groups}}$ for groups to $\alpha_{1.0,\mathrm{Control500}}$ of control groups, for pairs of (i, j) satisfying Eq. 3.2. In each bin of i in Fig. 3.8 and for all values of j in that bin, the first 500 groups with at least i galaxies and lowest magnitude gaps serve as the control groups in that bin. Hereafter to avoid any confusion between these recent controls and those we selected earlier, we denote the new sets as control$_{500}$ groups. The outlines (*black dashed-line*) of Fig. 3.8 represent the equality lines, i.e. the locations where the fraction of groups are the same.

Fig. 3.8 suggests that systems with i=8 and j=3.5, i.e. $\Delta m_{18} \geq 3.5$ led to the largest difference in mass assembly between selected groups and their counterparts in control$_{500}$ samples. In addition, the fraction of groups picked out by applying $\Delta m_{18} \geq 3.5$ is identical to those selected according to i=j=2 and is equal to $\sim$2.4$\%$. But it limits our new groups to those with at least i=8 galaxies.

A more appropriate pair (i, j) can be selected in such a way that it would be applicable to groups with fewer members, while retaining the ability to identify a larger fraction of genuine old groups. By choosing i=6 and j=3, the fraction of groups with $\Delta m_{16} \geq 3$ would be doubled in comparison to i=j=2. Therefore, it is more practical as one can apply it to groups with at least i=6 galaxies. However, the difference in the rate of mass assembly of groups and controls$_{500}$ is slightly less (~ 2.5 percent) if one adopts i=6 and j=3.0 rather than i=8 and j=3.5.

The optical criterion $\Delta m_{16} \geq 3.0$ within R$_{200}$

Our aim in this section is to show that a better way to find genuine fossil groups (i.e. groups that form early) is by applying the optical criterion $\Delta m_{16} \geq 3$ in the R-band, rather than

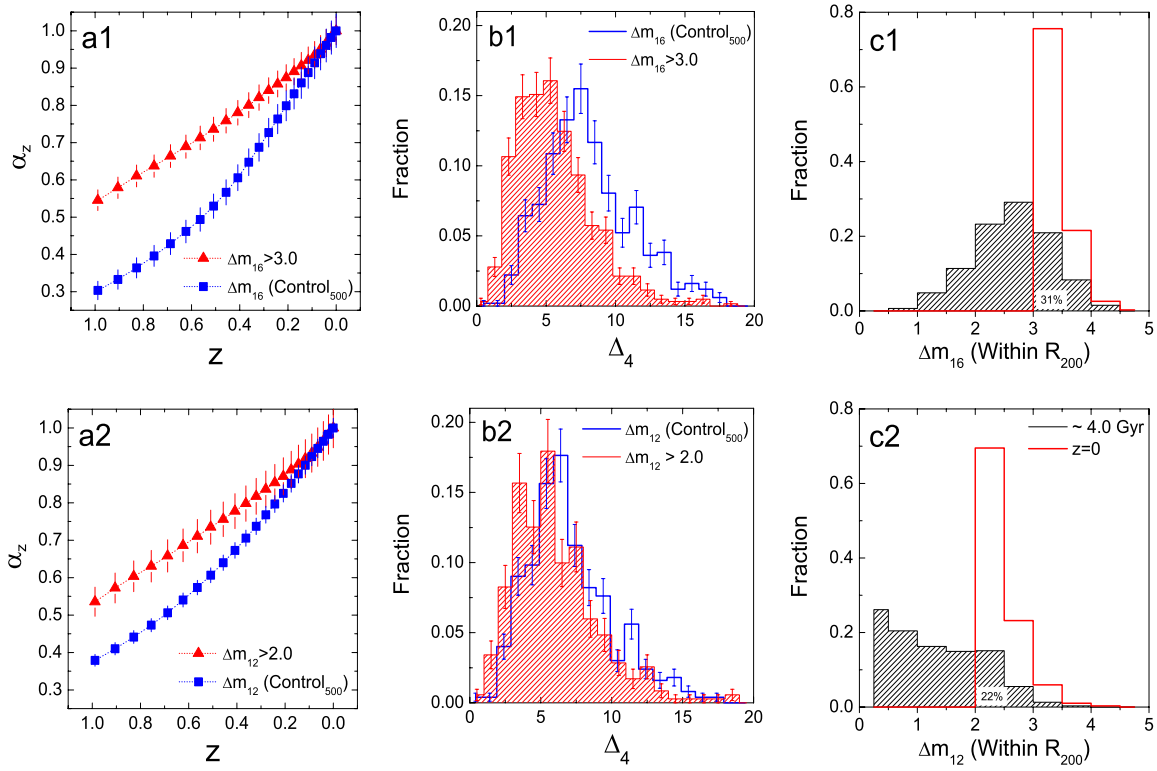

Figure 3.9: a1,a2: Mass growth history of groups$_{16}$ and groups$_{12}$ (*red triangles*) versus their counterpart control$_{500}$ groups (*blue squares*). b1,b2: Histogram of the environmental density Δ_4 of the same groups as in a1 and a2. Groups$_{16}$ and groups$_{12}$ are shown in *red-shaded histogram* while *blue histograms* represent control$_{500}$ groups. c1,c2: Phase of groups$_{16}$ and groups$_{12}$ at redshifts $z = 0$ (*red histogram*) and $z = 0.36$ (look-back time ~ 4 Gyr, *black shaded histogram*) respectively.

using $\Delta m_{12} \geq 2$ in the same band. The new expression improves the efficiency of separating fossil groups from normal groups, compared to the current definition. To test the validity of this statement we compare the mass assembly of groups selected according to $\Delta m_{16} \geq 3.0$ (hereafter *groups*$_{16}$) with those groups selected according to $\Delta m_{12} \geq 2.0$ (hereafter *groups*$_{12}$). Note that the mass assembly of X-ray fossils presented in Fig. 3.4 is for groups, where their Δm_{12} values have been estimated within 0.5R$_{200}$ whereas the same is R$_{200}$ for groups$_{12}$.

The comparison between the mass assembly, and environment, of groups$_{16}$ and groups$_{12}$ as well as their counterpart controls$_{500}$ for all X-ray bright groups are presented in Fig. 3.9. As before, all groups are selected from the X-ray bright population displayed in Fig. 3.1. It is worth recalling that for a given i, the control$_{500}$ groups are the first 500 groups with minimum magnitude gaps Δm_{1i} within R$_{200}$. Fig. 3.9(a1) clearly shows that in comparison to control$_{500}$ groups at z=1.0, groups$_{16}$ have assembled $\sim$10% more mass than groups$_{12}$ [shown in Fig. 3.9(a2)]. Note that $\alpha_{1.0}$ of groups$_{16}$ is greater than $\alpha_{1.0}$ of groups$_{12}$ by only $\sim$1.0% however the fraction of groups$_{16}$ is twice as the fraction of groups$_{12}$ which means that by using $\Delta m_{16} \geq 3.0$, we can not only select a population of groups which are older than their corresponding control$_{500}$ groups but also it picks almost twice as many groups than when they are selected according to $\Delta m_{12} \geq 2.0$.

The difference in the environment (Δ_4) of groups$_{16}$ and groups$_{12}$ is rather interesting to examine. As Figs. 3.9b1 and b2 show (groups$_{16}$) groups with $\Delta m_{16} \geq 3.0$ are essentially more isolated and tend to have lower Δ_4 relative to control$_{500}$ groups, whereas in groups$_{12}$ the difference in Δ_4 is not very pronounced. This is in agreement with our expectation of early formed groups as they are assumed to be in low-density environments.

Moreover, Fig. 3.9(c1) shows that out of all groups$_{16}$ selected at z=0 (*thick red line*), $\sim$31% of of them maintain their magnitude gap Δm_{16} to be more than 3.0 till z $\sim$0.36 (look-back time $\sim$4 Gyr, *black shaded area*) whereas in contrast in Fig. 3.9(c2) the same is $\sim$22% in groups$_{12}$.

The abundance of groups

Various studies have shown that the fraction of early-formed groups increases as the group halo mass decreases (e.g. Milosavljević et al. 2006; Dariush et al. 2007). This phenomenon reflects the fact that structures form hierarchically, where, unlike small virialised groups, most massive clusters are late-forming systems. As the merging of galaxies in clusters is less efficient than in groups, due to the high velocity dispersion of cluster galaxies, clusters are less likely to develop large magnitude gaps. At the same time, dynamical friction is more effective in ensuring galaxies fall to the core of the system, in low-mass groups due to the smaller relative velocities involved. As a result the existence of large magnitude gaps should be more frequent in groups rather than in clusters. Thus, to find an old population of groups according to some criterion, and to study the way the criterion depends on group halo mass, would be a good test on the validity of the condition.

Fig. 3.10 displays the abundance of groups$_{12}$(*red triangles*) and groups$_{16}$(*black squares*) versus group halo mass for group mass range $\log M(R_{200}) \gtrsim 13.4$ in units of $h^{-1}\,\mathrm{M}_{\odot}$. Below this mass range the number of groups abruptly decrease, since all groups here have been chosen to be X-ray bright groups (see Fig. 3.1). The *red dashed line* and *black dotted line* are polynomial fits to the groups$_{12}$ and groups$_{16}$ data points respectively. The result is encouraging as most of the groups$_{16}$ consist of less massive halos. Beside, there are almost no groups$_{16}$ with halo mass $M(R_{200}) \geq 10^{14}\,h^{-1}\,\mathrm{M}_{\odot}$ (just two groups out of 703 groups$_{16}$) while ∼4.5% of groups$_{12}$ have massive halos with $M(R_{200}) \geq 10^{14}\,h^{-1}\,\mathrm{M}_{\odot}$. It should be noted that the estimated abundance of groups shown in Fig. 3.10 is a function of radius where the brightest galaxies are selecting. It means that we may find massive halos with Δm_{16} more than 3.0 if Δm_{16} is estimated within $0.5R_{200}$, but the fraction of groups with $\Delta m_{12} \geq 2.0$ increases in a way that the ratio of their abundances remain almost intact.

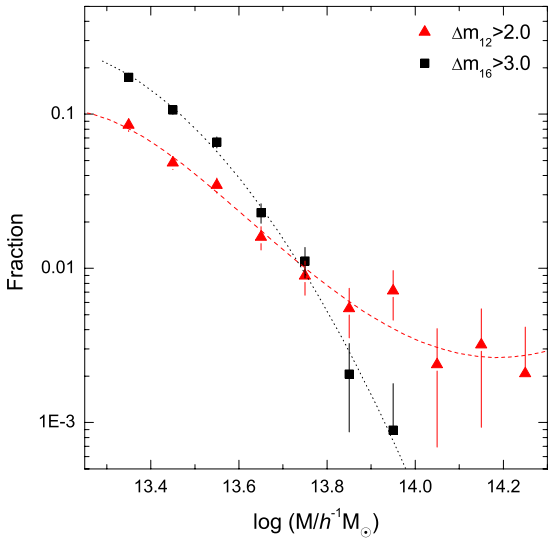

Figure 3.10: The abundance of groups$_{12}$(*red triangles*) and groups$_{16}$(*black squares*) versus group halo mass. The *red dashed line* and *black dotted line* are polynomial fits to groups$_{12}$ and groups$_{16}$ data points respectively.

3.4 Discussion

Several studies show that early formed systems of galaxies develop a larger magnitude gap between their first two brightest galaxies in comparison to normal or late formed systems. The idea is supported observationally (e.g. Ponman et al. 1994; Khosroshahi, Ponman, & Jones 2007) and theoretically (e.g. Milosavljević et al. 2006; van den Bosch et al. 2007) or from N-body numerical simulations (Barnes 1989; Dariush et al. 2007). These studies also predict that such early formed galaxy groups or clusters should be relaxed and relatively more isolated systems in comparison to their late formed counterparts. As such, Jones et al. (2003) define such early formed systems to have a minimum X-ray luminosity of $L_{\rm X,bol} \geq 0.25 \times 10^{42} h^{-2}$erg s^{-1} in addition to their large magnitude gap in the R-band between their first two brightest galaxies, i.e. $\Delta M_{12} \geq 2.0$ to separate them from non-virialised, late formed groups and clusters, some of the latter systems are in the stage of collapsing rather than being virialised systems and possibly

are not luminous in X-ray but could have large magnitude gaps. von Benda-Beckmann et al. (2008) found that ΔM_{12} is not a good indicator for identifying early formed groups, as it does change with infall of satellite galaxies into group. However their simulation and the derived galaxy properties are based only on the evolution of dark matter particles and it is not still very clear that the optical parameter ΔM_{12} used so far in identifying early formed groups, and its link with group halo mass assembly, is the optimal one to discriminate between early and late formed systems.

Here, we studied the evolution of the luminosity gap in galaxy groups and its correlation with the group mass assembly history, using the results from cosmological N-body simulations. By comparing the estimated magnitude gaps in galaxy groups from two different semi-analytic models of Bower et al. (2006) and Croton et al. (2006) with the measured magnitude gaps from SDSS and 2dFGRS sky survey group catalogues, we found the semi-analytical model of Bower et al. (2006) to be more suitable for our intention of studying the evolution of magnitude gaps in galaxy groups. A group catalogue was then compiled, consisting of group dark matter halo and galaxy properties (from $z \simeq 1.0$ to $z = 0$) as well as group gas properties at $z = 0$ by combining the Millennium dark matter simulation of Springel et al. (2005) together with the semi-analytic model of Bower et al. (2006) and the Millennium gas simulation. Our major conclusions can be summarised as follow:

1. The parameter ΔM_{1i} defined for a galaxy system as the magnitude gap between the first and i^{th} brightest galaxies is not necessarily linked to the halo mass assembly of that galaxy system. Though in a given galaxy group, the merging of the i^{th} galaxy with the group central galaxy results in an increase of ΔM_{1i}, such a gap could be filled later by the infalling of satellite galaxies into that group. Therefore such a phase in which the group could maintain its large magnitude gap is essentially a temporary phase, and all groups more or less spend a part of their life in such a phase. Therefore groups with small magnitude gaps are not necessarily late formed systems. This result is in agreement with

von Benda-Beckmann et al. (2008) who investigated the *fossil phase*, i.e., the time period in which a group could maintain its magnitude gap ΔM_{12} to be always above 2.0, in their subset of simulated groups.

2. Statistically the optical criterion $\Delta M_{16} \gtrsim 3.0$ in the R-band does better in identifying early formed groups in comparison to $\Delta M_{12} \geq 2.0$ [in the same filter] which is generally used in classifying galaxy systems into *fossil groups*. In this sense the new optical condition has the following advantages:

   (i) The maximum difference in halo mass assembly between galaxy groups with large magnitude gaps and their control counterparts with small magnitude gap is ~ 10 percent more if early formed groups are selected based on $\Delta M_{16} \gtrsim 3.0$ rather than $\Delta M_{12} \geq 2.0$ (see Fig. 3.9a1 and Fig. 3.9a2),

   (ii) In comparison to systems selected based on $\Delta M_{12} \geq 2.0$, the identified groups according to $\Delta M_{16} \gtrsim 3.0$ are more isolated than their corresponding control groups (see Fig. 3.9b1 and Fig. 3.9b2),

   (iii) Moreover, after ~ 4.0 Gyr, only $\sim$22% of groups selected according to $\Delta M_{12} \geq 2.0$ maintain their magnitude gap while the same is $\sim$31% if groups are selected using the condition $\Delta M_{16} \gtrsim 3.0$ (see Fig. 3.9c1 and Fig. 3.9c2).

3. Finally a study of the abundance of groups, as illustrated in Fig. 3.10, show that identified groups based on $\Delta M_{16} \gtrsim 3.0$ are mostly populated by the low-mass halos. This is to be expected from the hierarchical formation of dark matter halos. At the same time, systems selected based on their $\Delta M_{12} \geq 2.0$ contain massive groups and clusters.

Note that these results depend to some extent on the employed semi-analytic model in our current analysis and the statistics may change if one uses different analytical model of galaxy formation. Physical prescriptions such as galaxy merging, supernova and AGN feedback used in

such models are somewhat different from one another. Though merging is the most important process that affects galaxies in groups, there are still other physical processes such as ram pressure stripping, interactions and harassment, group tidal field, and gas loss, that are not fully characterised by current semi-analytic models. In addition, superfluous mergers that are artifacts of the standard Friends-Of-Friends (FOF) halo identification algorithm, do exist within the Millennium dark matter simulation. By removing such effects, one may find a lower merger rate compared to the one used in our study (Genel et al. 2008).

In this work, we used the Bower et al. (2006) model since we showed it to be better compatible with the observed surveys than the Croton et al. (2006) model. The number of observed fossil galaxy groups is small which makes it difficult to have a direct comparison between the observation and simulation. For example, according to Sales et al. (2007) who derived the magnitude gap from the published results of the luminosity functions of three fossil groups (e.g. Jones, Ponman, & Forbes 2000; Cypriano, Mendes de Oliveira, and Sodre 2006; Mendes de Oliveira , Cypriano, & Sodre 2006), the value of ΔM_{10} (magnitude gap between the first and 10^{th} brightest galaxies) in fossil groups span the range from ~ 3 to ~ 5. Sales et al. (2007) found the observed range of ΔM_{10} in agreement with their results from the analysis of the Millennium data together with the semi-analytic catalogue of Croton et al. (2006).

Bibliography

Balogh, M.L., McCarthy, I.G., Bower, R.G., Eke, V.R., 2008, MNRAS, 385, 1003

Barnes, J.E., 1989, Nature, 338, 123

Borgani S., et al., 2006, MNRAS, 367, 1641

Bower, R.G. et al., 2006, MNRAS, 370, 645

Colless, M. et al., 2001, MNRAS, 328 ,1039

Croton, D.J., Springel, V., White, S.D.M., De Lucia, G.; Frenk, C. S.; Gao, L.; Jenkins, A., Kauffmann, G., Navarro, J. F. & Yoshida, N., 2006, MNRAS, 365, 11

Cypriano E. S., Mendes de Oliveira C. L., Sodre L. J., 2006, AJ, 132, 514

Dariush, A., Khosroshahi, H.G., Ponman, T.J., Pearce, F., Raychaudhury, S., Hartley, W., 2007, MNRAS, 382, 433

GENEL, S., GENZEL, R., BOUCHE, N., NAAB, T., & STERNBERG, T., arXive: astro-ph: 0812.3154

Jones L. R., Ponman T. J., Forbes D. A., 2000, MNRAS, 312, 139

Jones, L.R. et al., 2003, MNRAS, 343, 627

Khosroshahi, H.G., Ponman, T.J., Jones, L.R., 2007, MNRAS, 377, 595

Mendes de Oliveira C. L., Cypriano E. S., Sodre L. J., 2006, AJ, 131, 158

Miller, C.J. et al., 2005, AJ, 130, 968

Milosavljević, M., Miller, C.J., Furlanetto, S.R. & Cooray, A., 2006, ApJ, 637, L9

Ponman, T.J., Allan, D.J., Jones, L.R., Merrifield, M. & MacHardy, I.M., 1994 Nature, 369, 462

Rasmussen, J., Ponman, T.J., Mulchaey, J.S., Miles, T.A., Raychaudhury, S., 2006, MNRAS, 373, 653

Sales, L.V., Navarro, J.F., Lambas, D.G., White, S.D.M., Croton, D.J., 2007, MNRAS, 382, 1901

Spergel, D.N. et al., 2003, ApJS, 148, 175

Springel, V., White, S.D.M., Tormen, G. & Kauffmann, G., 2001, MNRAS, 328, 726

Springel, V. et al., 2005, Nature, 435, 629

Steinmetz, M., & White, S.D.M., 1997, MNRAS, 288, 545

van den Bosch, F.C. et al., 2007, MNRAS, 376, 841

von Benda-Beckmann A.M., D'Onghia E., Gottlöber S., Hoeft M., Khalatyan A., Klypin A., Müller V., 2008, MNRAS, 386, 2345

Yang X. H., Mo H. J., van den Bosch F. C., Jing Y. P., 2005, MNRAS, 356, 1293

Chapter 4

An optically selected sample of poor groups of galaxies- The XMM-Imacs (XI) sample

4.1 Introduction

In hierarchical models of structure formation of the Universe, structures grow progressively as they detach from the Hubble expansion, collapse, and eventually form virialized systems. In this scenario, larger structures such as galaxy groups and clusters form later, i.e. at the present epoch. As a result, the bulk of the matter in the Universe at lower redshifts is believed to be dominated by systems of galaxies such as galaxy groups (Fukugita, Hogan, & Peebles 1998). Hence, understanding groups and the physical processes that lead to their formation and evolution is essential in understanding the Universe. The velocity of galaxies in groups is not more than a few hundred km s^{-1} which is similar to those of individual galaxies. Such low galaxy velocities together with a shallower potential wells in galaxy groups (in comparison to galaxy clusters) make them an ideal site for the interaction of galaxies with each other, and

galaxies with the group potential (Sersic 1974; Menon 1992; Mendes de Oliveira et al. 2003; Miles at al. 2004). Therefore, the group environment does affect the properties of its galaxy members while the group itself evolves through mergers or via collapsing or virialization.

In comparison to clusters, less attention has been paid to groups though they have an important role in formation and evolution of structure of the Universe. One reason is that in general groups do not contain a large number of bright galaxies. As such, the dynamical studies of groups is more difficult in comparison to larger clusters. On the other hand, observations of groups in optical wavelengths suffer from the fact that some catalogued groups do not represent real physical system of galaxies (Hernquist, Katz, & Weinberg 1995; Frederic 1995; Ramella, Pisani, & Geller 1997) as they can be large-scale structure filaments viewed edge-on (in case of compact groups, Mamon 1986) or but rather chance superpositions of galaxies which do not belong to galaxy groups. In this sense, X-ray observation offers a more reliable method of detecting real galaxy groups. Such X-ray emission results from the existence of hot gas in intragroup medium (IGM) of virialized systems. Several attempts have been made so far using pointed ROSAT X-ray observations to investigate various properties of galaxy groups (Mulchaey et al. 1996; Mulchaey & Zabludoff 1998; Zabludoff & Mulchaey 1998; Zabludoff & Mulchaey 2000; Helsdon & Ponman 2000; Helsdon & Ponman 2003; Osmond & Ponman 2004). Although galaxy groups in these studies cover a wide range of properties, they are still biased since all of them are selected based on their X-ray emission.

Meanwhile there are various studies of galaxy systems based on data from the ROSAT All-Sky Survey (RASS) in which an unbiased sample of galaxy groups (or even poor clusters) are optically or redshift selected (Ebeling, Voges, & Bohringer 1994; Burns et al. 1996; Mahdavi et al. 1997; Mahdavi et al. 2000). Unlike Mahdavi et al. (1997) and Mahdavi et al. (2000) whose their studies do not cover the dynamics of groups, work done by Burns et al. (1996) contains detailed information on the galaxy dynamics. However, group selection in Burns et al. (1996) is based on photometric enhancements and not on velocity information. Also due to the low

RASS exposures ($\sim$ a few hundred seconds), groups with $L_X \lesssim 10^{42}$ erg^{-1} can not be studied properly as in many cases just the hot intragroup gas could be detected which does not allow a detailed investigation of gas properties in groups.

Recent observations of groups with XMM-Newton and Chandra have usually focused on systems which have been studied before as a part of pointed ROSAT X-ray observations, or those which have been detected in X-ray using RASS data. Hence, most of these groups are X-ray selected and therefore do not necessarily represent the overall population of galaxy groups at lower redshifts. Indeed, observations and studies of galaxy clusters show that selection of galaxy systems based on their X-ray could incorporate some bias effects. As such, optically selected and X-ray selected systems show dissimilar X-ray properties and in some cases the samples are entirely different (Donahue et al. 2008). For example Gilbank et al. (2004) showed that a large fraction of optically selected galaxy clusters do not exhibit clear X-ray emission in ROSAT data though their spectroscopic follow-up observation shows that even faint systems in their sample are real physical system of galaxies.

Based on multicolour imaging in optical wavelengths, Barkhouse et al. (2006) found such similar result using Chandra X-ray data. In addition, from the X-ray study of a high-redshift, optically-selected sample of galaxy clusters, Lubin, Mulchaey, & Postman (2004) found that for a given velocity dispersion σ_v, galaxy clusters in their sample are X-ray underluminous and the $L_X - \sigma_v$ scaling relation from their measurements deviate from those estimated for nearby, rich X-ray clusters. Both Hicks et al. (2004) and Popesso et al. (2004) reached to similar results where the latter worked out on a subset of Abell clusters and found that their sample were X-ray underluminous with respect to the virial mass of their clusters.

These results indicate that the selection of large galaxy systems based on their X-ray properties provides a biased picture of clusters. The effect should be the same in galaxy groups and since groups are naturally less luminous in X-rays than their cluster counterparts, such an effect is expected to be even more stronger in groups than in clusters. Most X-ray studies on

small galaxy systems have employed X-ray selected groups or those groups which already have been observed to have X-ray emission in RASS data. Therefore, at the present time there is no unbiased statistics of hot gas properties and their correlation to the dynamics of galaxies within groups of galaxies.

The initial goal of the XI Project is to understand and study the nature and evolution of an unbiased subset of optically (redshift) selected galaxy groups, and to investigate the way in which the properties of such a group population are connected to those of their member galaxies. Besides, an important outcome of the project is to find an estimate of the fraction of optically selected groups which actually hold a hot IGM and the way that such hot IGM is correlated to the dynamical state of galaxy groups. Such studies can be done by taking advantage of using large redshift surveys, together with the spectral capability, spatial resolution, and high sensitivity of Chandra and XMM-Newton X-ray telescopes. While the properties of any hot intragroup gas can be studied using deep X-ray data from XMM-Newton, the group dynamical state can be found spectroscopically using the 6.5-m Baade/Magellan telescope at Las Campanas equipped with the IMACS multi-object camera and spectrogram (Bigelow & Dressler 2003).

4.2 Group sample selection

The XI-groups consists of a redshift-selected subset of galaxy groups. X-ray selection may introduce some bias since it fails in detecting galaxy groups which have been collapsed but still are not virialized. Groups are selected from the 2dF Galaxy Redshift Survey (2dFGRS) catalogue of 2209 groups extracted by Mercha'n & Zandivarez (2002)(hereafter, MZ02) who used a friends-of-friends (FOF) algorithm in constructing the catalogue. From this catalogue, 25 groups have been selected with the following additional conditions:

- (i) Groups are within the same redshift, i.e. $z = 0.060 - 0.063$. This condition chose all groups at the same luminosity distance where the overdensity radius R_{200} corresponds

to angular size of ~ 13 arcmin for groups with typical characteristic radii of ~ 1Mpc. Such angular size is well matched to both the IMACS and XMM fields of view. Another advantage is that limiting groups to a narrow slice of z removes any bias due to the growth of the friends-of-friends linking length with redshift. Otherwise group properties may vary systematically with z.

- (ii) All groups have relatively low velocity dispersion, i.e. $\sigma_v \lesssim 500$ km s^{-1}. This condition limits the selected systems to poor groups in which the dynamical friction is more efficient and galaxy-galaxy interactions are stronger. Thus, groups are subject to rapid dynamical evolution. Besides, the majority of galaxies in the Universe are within such poor groups (Eke et al. 2004).

- (iii) The number of spectroscopically confirmed 2dFGRS members of each groups should not be less than five, i.e. $N_{gal} \geq 5$. Such condition guarantees that the selected groups are all real physical galaxy systems. Results from numerical N-body simulation show that in general FOF groups with $N_{gal} \geq 5$ could hardly be an unbound density fluctuation and generally all of them are real gravitationally bound structures (Ramella, Pisani, & Geller 1997).

- (iv) To avoid an incompleteness in redshift, groups with poor completeness or those that are too close to the edges of the 2DFGRS area have not been selected.

Within the above constraints, 25 groups have been selected randomly which spanning a wide range of group properties (see Table 4.1).

4.3 Preliminary results

In this section, to show what kind of groups the XI sample represents, I summarise the preliminary results given by Rasmussen et al. (2006) (hereafter, RJ06) from optical and X-ray data of

four XI-groups (MZ 4577, MZ 5383, MZ 9014, MZ 9307).

Comparison to X-ray selected groups

According to RJ06 there is no detectable diffuse emission in two groups MZ 5383 and MZ 9307 whereas group MZ 4577 shows evidence of very low IGM emission which is not significant at the 3σ level. However, in galaxy group MZ 9014, some X-ray emission has been detected at a 3σ significance, though the X-ray luminosity of this system is among the lowest found for X-ray detected galaxy groups (see Table.3 of RJ06). In addition, all of these four groups are X-ray underluminous in comparison to X-ray detected groups with similar velocity dispersions.

Fig. 4.1 represents the observed $L_X - \sigma_v$ scaling relation in four XI-groups together with those from the GEMS groups of Osmond & Ponman (2004), along with observationally measured $L_X - \sigma_v$relations from Mahdavi et al. (1997) and Helsdon & Ponman (2000). The derived slopes of the $L_X - \sigma_v$ relation illustrated in Fig. 4.1, spans a large range of gradients from $L_X \propto \sigma_v^{1.56}$ to $L_X \propto \sigma_v^{4.5}$. Though a combination of these measurements results in a highly scattered relation in $L_X - \sigma_v$, still the four XI groups are noticeably underluminous for their velocity dispersions.

This result strongly suggests that unlike the present optically selected groups, previous X-ray detected sample of galaxy groups represent a biased picture of the group population.

Physical state of the IGM

Following the results shown in Fig. 4.1, the main question is how to explain the lack of significant X-ray emission in these observed four groups and whether such deficiency in L_X is linked to their dynamical state. It is most improbable that the two X-ray undetected groups are not gravitationally bound systems, as only galaxy groups with number density contrasts $\delta\rho/\bar{\rho} \geq 80$ have been included in the MZ02 group catalogue where $\bar{\rho}$ is the mean galaxy number density used in MZ02 FOF algorithm to distinguish groups from field galaxies. This leaves the follow-

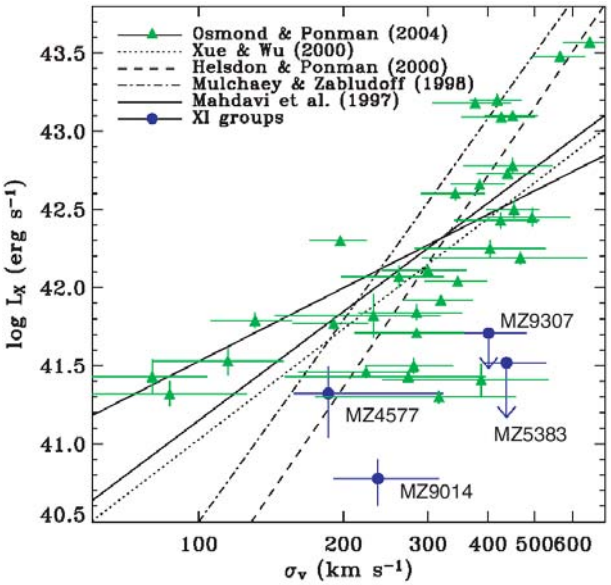

Figure 4.1: $L_X - \sigma_v$ relations for X-ray bright groups. Downward arrows represent 3σ upper limits. Overplotted for comparison are the data points of Osmond & Ponman (2004) for GEMS groups. (Credit: Rasmussen et al. 2006)

ing three possible interpretations for the lack of significant IGM emission in these four groups.

- (i) These four groups are in the stage of collapsing for the first time. If this is true, then the velocity dispersion σ_v may not be a good representative of the depth of the group gravitational potential well or its gas temperature. Thus, a large amount of IGM gas may not have been shock-heated to the virial temperature of the final group in which case one might expect an evidence of dynamical substructure in the distribution of group galaxy members. Results from studying group galaxy velocities suggest that the velocity dispersion in these groups are bimodal. The stacked histogram of the normalised galaxy velocities derived for all four groups are shown in Fig. 4.2. The histograms show that there is a deficiency in the velocity distribution of group galaxies. Such bimodality suggests these groups are still in the process of dynamical relaxation.

- (ii) Another explanation for the lack of remarkable amount of X-ray emission in these groups is that the gravitational potentials of these groups are too shallow so they can

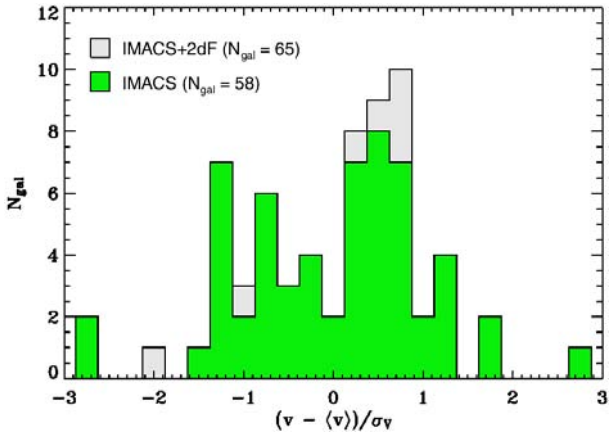

Figure 4.2: Stacked histogram of all galaxy velocities belong to four groups MZ 4577, MZ 5383, MZ 9014, MZ 9307 measured relative to the mean velocity for each group and normalised to the velocity dispersion of that group. Green shaded area outlines the histogram for the three groups with IMACS velocities, while the lighter gray shaded area also includes MZ 9307. (Credit: Rasmussen et al. 2006)

not heat the intragroup gas to X-ray temperatures. In other words, there could be plenty of groups with very low temperature ($\sim 10^6$ K) intragroup gas which make the gas undetectable in these observations. But given the high velocity dispersions measured for these group, which are unlikely to be substantially overestimated, such an argument is unattractive and not very strong.

- (iii) Finally the groups could be X-ray dim because many of them could have simply very little intragroup gas. As such, the unbiased selection of XI-groups possibly is picking up such systems since they are more populated than X-ray bright groups. Physical processes like strong galactic feedback can eject a remarkable fraction of the initial intragroup gas from the group potential. But if such a mechanism is responsible for the lack of the significant amount of IGM gas, then it is not understood why this process is more effective in some groups, such that it reduces the detectable X-ray hot gas mass by a few order of magnitude, in comparison to other groups with similar depth of potential well. Besides, such feedback should be linked to some extent with the formation of elliptical galaxies (Arnaud et al. 1992). As a result, groups with large amount of feedback should have a

lower fraction of spiral galaxies. This is not the case in XI-groups as the spiral fraction of this sub-sample of four groups is $\sim$65 percent. Such that a large fraction of spiral galaxies may not be easily correlated with the idea that galactic feedback has expelled much of the IGM from the groups.

Finally RJ06 conclude that the lack of significant X-ray emission in the four XI-groups, is most likely related to the fact that these systems are collapsing for the first time, i.e. they belong to scenario (i). However they do not exclude completely the other two scenarios which state that such observed low diffuse X-ray luminosity of four groups is because of the absence of IGM or its very low temperature. To have a better understanding of the status of IGM within XI-groups, our collaborators have started a programme to observe and monitor the H I content of XI-groups using the Giant Metrewave Radio Telescope (GMRT). Using H I imaging of the groups, it is easier to test the validity of either scenarios (ii) or (iii) as mentioned above.

4.4 Group size

A major goal in optical studies of galaxy groups and clusters is to investigate the luminosity function of these systems. In this sense, the group size (radius) would be a key parameter in determining group luminosity function . There are different ways in determining the radius for a given group. Here I just want to make a comparison between the virial radii estimated for XI-groups using different methods.

4.4.1 The original catalogue of MZ02

The original group *virial radius* (see Table 4.1) estimated by MZ02 is based on the following formula:

$$R_{\rm vir} = \frac{\pi}{2} N_g(N_g-1)\left(\sum_{i>j}^{N} R_{ij}^{-1}\right)^{-1}, \tag{4.1}$$

where N_g is the number of group galaxy members and R_{ij} is the projected distances between the i^{th} and j^{th} group galaxy members. In fact, Eq. 4.1 represents group's *mean harmonic radius* r_H given by Huchra & Geller (1982) as follows:

$$r_{\rm H} = \frac{\pi}{2} D_L \sin\left[N_g(N_g-1)\left(\sum_{i>j}^{N} \frac{1}{\theta_{ij}^{-1}}\right)^{-1}\right], \tag{4.2}$$

where θ_{ij} is the angular separation between galaxy members and D_L is the group luminosity distance. However Huchra & Geller (1982) consider the *mean pairwise separation* as a measure of the size of the group given by:

$$r_{\rm P} = \frac{8}{\pi} D_L \sin\left[\frac{1}{N_g(N_g-1)}\sum_{i>j}^{N}\theta_{ij}\right]. \tag{4.3}$$

Note that the mean harmonic radius r_H is purely geometrical. From a sample of 60 galaxy groups (GEMS catalogue) Osmond & Ponman (2004) estimates the R_{500} of a group as a function of group velocity dispersion σ_v in the following form:

$$R_{500}(\text{Mpc}) = \frac{0.96\sigma_v}{H_0}, \tag{4.4}$$

where σ_v is the group one-dimensional velocity dispersion. Assuming $R_{500} \approx 0.66 R_{200}$ (Voit 2005), Eq. 4.4 can be rewritten in logarithmic form as follow:

$$\log R_{200}(\text{Mpc}) = \log \sigma_v(\text{km/s}) - 2.682. \tag{4.5}$$

The calculated R_{200} based on Eqs. 4.5 is expected to be more reliable (for groups with large velocity dispersion) as it is a function of group's physical properties.

4.5 Estimating the radii of groups from the Millennium simulation

Results from cosmological simulations provide an alternative way to determine group size. In this section I use the Millennium simulation (Springel et al. 2005) together with the semi-analytic catalogue of Bower et al. (2006) to examine how does group size scales with velocity dispersion in galaxy groups. To find a description of the Millennium dark matter and semi-analytic catalogue, see Chapter 2.

To compile a catalogue of groups with galaxy properties, I start with a catalogue of groups extracted by a FOF algorithm from the Millennium dark matter runs. Groups of $M(R_{200}) \geq 10^{13}\, h^{-1}\, \mathrm{M}_{\odot}$ are selected from the FOF group catalogue at $z = 0$. The mass cut-off is intended to select halos in group or cluster mass range. The xyz position of the central galaxy of each galaxy group, and the corresponding group dark matter halo, were used to identify all group members. Galaxy magnitudes become incomplete below a magnitude limit of $\mathrm{M}_K - 5\log(h) \sim -19.7$, due to the limited mass resolution of the Millennium simulation. Therefore in our analysis we apply a K-band absolute magnitude cut-off of $\mathrm{M}_K \lesssim -19$ on all galaxy members. Then for each group halo, optical properties were extracted for its corresponding galaxies from the semi-analytic galaxy catalogue. These include the magnitude of galaxies as well as their velocity dispersion components. The group one-dimensional velocity dispersion in x direction then was estimated using the following formula:

$$\sigma_v = \left\langle (v_x - \langle v_x \rangle)^2 \right\rangle^{\frac{1}{2}}, \tag{4.6}$$

where v_x is the galaxy velocity relative to its host group halo. During the the process of matching galaxies with their associated halos, for 51547 groups at present epoch, corresponding galaxies were found in the semi-analytic galaxy catalogue with the exclusion of remaining groups from

our final compiled list.

4.5.1 Results

Each data point in Fig. 4.3 represents a group with mass $\log M \geq 10^{13} h^{-1} M_{\odot}$ at redshift $z = 0$ (total number of groups is 51547). For each group, R_{200}, the radius enclosing a mean density of 200 times the critical density of the Universe, has been estimated using the Millennium dark matter simulation (Springel et al. 2005).

Within the Millennium simulation $M \propto R_{200}$, so a cut-off in group halo mass selects groups with corresponding R_{200} above the threshold value ~ 0.55Mpc. The corresponding one-dimension velocity dispersion σ_v for each group has been adopted using Eq. 4.6.

The linear fit to the Millennium group data points suggests an empirical relation for R_{200} as a function of group one-dimensional velocity dispersion σ_v in the following form:

$$\log R_{200}(\text{Mpc}) = 0.89 \times \log \sigma_v(\text{km/s}) - 2.19. \tag{4.7}$$

In Fig. 4.3, the value of R_{200} is plotted against the one-dimension velocity dispersion σ_v for groups from the Millennium simulation. In the same plot *Red circles* represent the sample of 59 GEMS groups from Osmond & Ponman (2004). The *Blue line* has been plotted using Eq. 4.5 while the *black dashed-line* shows a linear fit to the Millennium group data points (i.e. Eq. 4.7).

Though the distribution of GEMS groups in Fig. 4.3 is in agreement with distribution of the Millennium data but, still there is a clear offset between the determined R_{200} using Eq. 4.5 and the linear fit to the Millennium data points. In fact Osmond & Ponman (2004) use Eq. 4.5 to estimate group size where the information on group temperature is not available and not for all 60 groups in their GEMS sample.

In Fig. 4.4, the median of the velocity dispersion $\sigma_{v_{\rm median}}$ in each bin of R_{200} is represented by *red circles*. The $\pm 1\sigma$ limits in each bin of R_{200} were then found by finding the minimum and

maximum values of σ_v (e.g. σ_{v-} and σ_{v+}) centred around the median value such that the terms N(σ_{v+})-N($\sigma_{v_{\rm median}}$) and N($\sigma_{v_{\rm median}}$)-N(σ_{v-}) each contain $\sim 34.2\%$ of the total number of groups in that bin, where N(σ_v) is assumed to be the number of groups with velocity dispersion $\leq \sigma_v$. A linear fit on the median has the following form:

$$\log R_{200}(\text{Mpc}) = 1.13 \times \log \sigma_v(\text{km/s}) - 2.48. \tag{4.8}$$

It is clear from Fig. 4.4 that there is a large scatter in the estimated velocity dispersion of small size groups. So the fit to the median data points shows a small deviation from a linear correlation (i.e. a linear fit with slope=1.0). This is partly due to statistical effect since to take the average in Eq. 4.6, the term inside $\langle\rangle$ was divided by N_{gal} rather than $N_{gal}-1$ where N_{gal} is the number of group galaxies within each simulated dark halo. This does not affect the derived σ_v for groups with large number of galaxies (for example $N_{gal} \gtrsim 10$) but in groups with a few galaxies the effect becomes important. Generally the first few bins of R_{200} in Fig. 4.4 is populated by such groups. In addition the estimated slope in Eq. 4.8 is not very different from 1.0. Therefore, we can consider simply a linear fit to the median data points with fixed slope (=1.0) and rewrite Eq. 4.8 as:

$$\log R_{200}(\text{Mpc}) = \log \sigma_v(\text{km/s}) - 2.50. \tag{4.9}$$

The *black dashed-line* in Fig. 4.4 shows a linear fit to the velocity dispersion median values using Eq. 4.9. The *blue lines* are the corresponding ± 1 σ confidence levels which have been estimated at each bin of R_{200} separately. Table 4.1 summarise the determined R_{200} for XI-groups. The virial radius $R_{\rm vir}$ given in Table 4.1 is from the group catalogue of MZ02 has been calculated by means of Eq. 4.1. The last column shows R_{200} for XI-groups using Eq. 4.9.

In Fig. 4.5 a comparison has been made among different measured virial radii for all 25 XI-groups using data given in Table 4.1. The *dashed line* shows the equality line. The circle

size of each data point illustrated in Fig. 4.5 scales with its corresponding observed line-of-sight group velocity dispersion.

Though we do not expect that group R_{200} derived from the Millennium simulation be exactly the same as the estimated R_{vir} given by MZ02, however, a closer look at Fig. 4.5 shows that the majority of groups with large offsets from the equality line are among those with low σ_v. In fact the estimated error in the observed line-of-sight velocity dispersion range from $\sim 20-40$ km/s. Such an error is important in estimating R_{200} for low velocity dispersion groups if one uses Eq. 4.9 to estimate group σ_v.

A visual test on the relative positions of group galaxy members shows that Eq. 4.9 underestimates the size of groups with small values of σ_v since a significant fraction of galaxies belong to these groups fall outside of group R_{200}. For the time being that spectroscopic observations of these groups are underway, I consider a minimum fixed value of R_{200}, estimated at the median velocity dispersion of the whole sample of 25 groups, using Eq. 4.9. The median velocity dispersion of the current sample is ~ 250 km s^{-1}. As such for every group with $\sigma_v \lesssim 250$ km s^{-1}, a value of $R_{200} \simeq 0.75$ Mpc has been adopted.

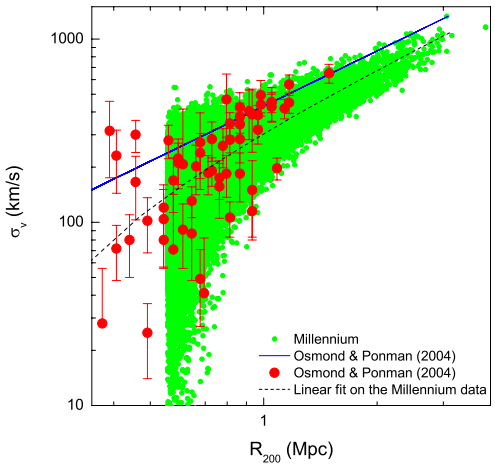

Figure 4.3: Plot of R_{200} versus one-dimension velocity dispersion σ_v for 51547 galaxy groups from the Millennium simulation. *Red circles* represent the sample of 59 GEMS groups from Osmond & Ponman (2004). The *Blue line* has been plotted using Eq. 4.5 of Osmond & Ponman (2004), while the *black dashed-line* shows a linear fit to the Millennium group data points (Eq. 4.7).

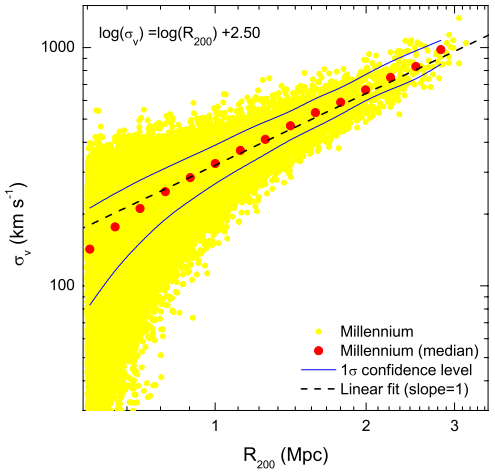

Figure 4.4: Plot of R_{200} versus one-dimension velocity dispersion σ_v for 51547 galaxy groups from the Millennium simulation. *Red circles* represent the median of σ_v in each bin of R_{200} while the *black dashed-line* shows a linear fit with fixed slope (Eq. 4.9) to the velocity dispersion median values. The *blue lines* are the corresponding ± 1 σ confidence levels.

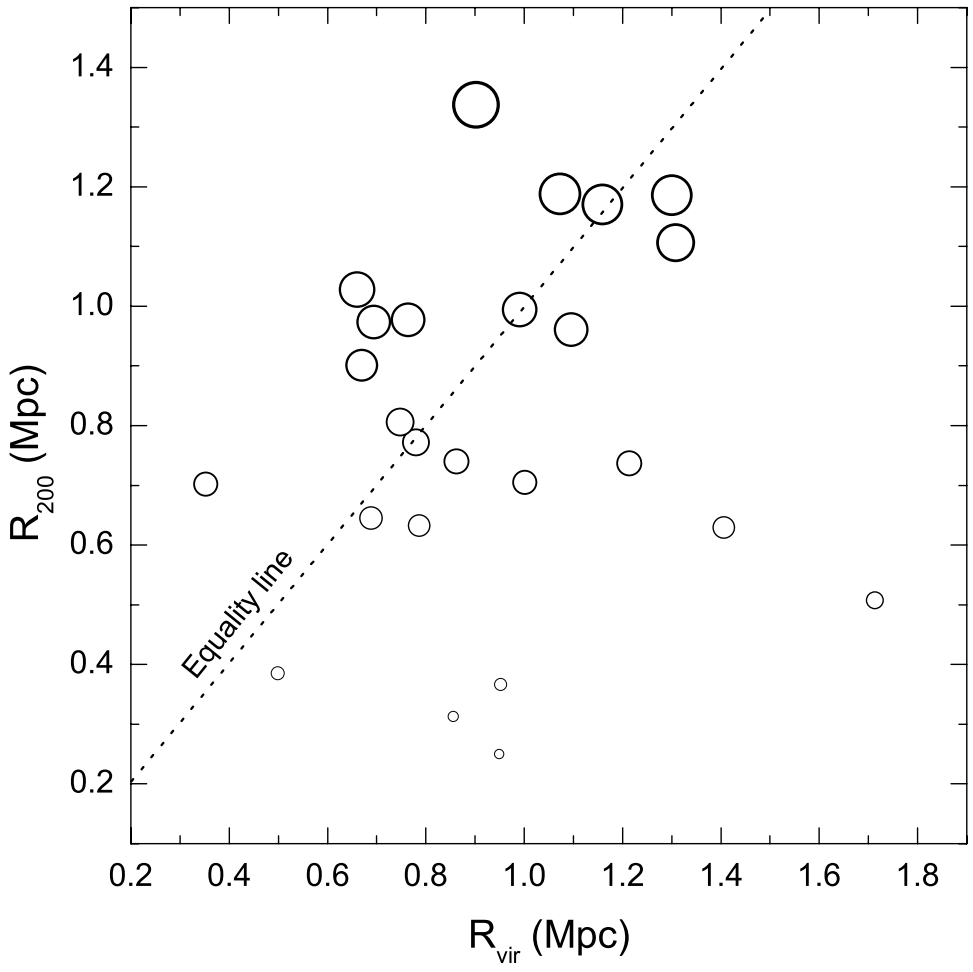

Figure 4.5: The estimated R_{vir} from the original catalogue of MZ02 (i.e. Eq. 4.1) in comparison to the current analysis of the Millennium data using Eq. 4.9. The *dashed line* shows the equality line where $R_{vir} = R_{200}$. The circle size of each data point scales with its corresponding observed line-of-sight group velocity dispersion as tabulated in Table 4.1.

Group Name	RA J2000.0	DEC J2000.0	N	σ_v km s^{-1}	R_{vir} (Mpc) MZ02	R_{200} (Mpc) Millennium sim.
MZ 770	22:16:09.27	-27:58:09.8	10	79	0.669	0.250
MZ 1766	00:38:32.01	-27:11:17.6	12	99	0.779	0.313
MZ 3067	22:16:16.42	-25:42:26.4	7	116	0.951	0.367
MZ 3182	22:19:17.34	-27:01:21.8	8	122	0.786	0.386
MZ 3541	10:03:41.03	-04:09:48.8	12	161	0.498	0.509
MZ 3698	09:59:27.30	-05:43:58.8	9	199	0.990	0.629
MZ 3849	10:27:35.61	-03:21:30.5	13	200	1.094	0.632
MZ 4001	10:16:23.25	-03:15:17.1	23	204	1.001	0.645
MZ 4548	10:53:52.88	-05:59:43.7	4	222	1.713	0.702
MZ 4577	11:32:30.79	-04:00:00.8	16	223	0.352	0.705
MZ 4592	11:30:52.15	-03:47:27.4	24	233	1.405	0.737
MZ 4881	11:39:50.67	-03:30:29.5	15	234	1.308	0.740
MZ 4940	11:36:04.74	-03:39:56.6	9	244	0.948	0.772
MZ 5293	12:16:19.85	-03:23:37.7	6	255	0.855	0.806
MZ 5383	12:34:52.83	-03:35:54.3	25	285	1.158	0.901
MZ 5388	12:34:04.54	-03:22:21.2	20	304	0.693	0.961
MZ 8816	00:06:43.24	-27:47:33.4	22	308	1.213	0.974
MZ 9014	00:37:48.12	-27:30:29.1	25	309	0.862	0.977
MZ 9069	00:28:25.31	-27:28:57.0	24	315	0.659	0.996
MZ 9137	00:18:53.59	-27:54:58.9	13	325	1.300	1.028
MZ 9307	00:40:48.64	-27:27:06.1	14	350	0.763	1.107
MZ 9994	02:01:58.99	-29:14:43.3	14	370	1.072	1.170
MZ 10167	01:51:12.40	-27:44:09.7	19	375	0.688	1.186
MZ 10300	02:24:27.21	-28:19:20.1	31	376	0.747	1.189
MZ 10451	02:29:30.40	-29:37:44.1	36	423	0.901	1.338

Table 4.1: List of all 25 XI-groups and their estimated overdensity radii. The assumed richness of each group N represents the number of spectroscopic confirmed group galaxy members.

Bibliography

Arnaud M., Rothenflug R., Boulade O., Vigroux L., Vangioni-Flam E., 1992, A&A, 254, 49

Barkhouse W. A. et al., 2006, ApJ, 645, 955

Bertin, E. & Arnouts, S., 1996, A&AS, 117, 393

Bigelow B.C., Dressler A.M., 2003, Proc. SPIE, 4841, 1727

Bower, R.G., Benson, A.J., Malbon, R., Helly, J.C., Frenk, C.S., Baugh, C.M., Cole, S., Lacey, C.G., 2006, MNRAS, 370, 645

Burns J. O., Ledlow M. J., Loken C., Klypin A., Voges W., Bryan G. L., Norman M. L., White R. A., 1996, ApJ, 467, L49

Chandreyee, S. et al., 2008, in preparation

Donahue, M., Scharf, C.A., Mack, J., Lee, Y.P., Postman, M., et al.,2002, ApJ, 569, 689

Ebeling H., Voges W., Bohringer H., 1994, ApJ, 436, 44

Eke, V.R., Baugh, C.M., Cole, S., Frenk, C.S., Norberg, P. et al., 2004, MNRAS, 348, 866

Frederic J.J., 1995, ApJS, 97, 259

Fukugita M., Hogan C. J., Peebles P. J. E., 1998, ApJ, 503, 518

Gilbank D. G., Bower R. G., Castander F. J., Ziegler B. L., 2004, MNRAS, 348, 551

Haynes, M.P. & Giovanelli, R., 1984, AJ, 89, 758

Helsdon, S.F. & Ponman, T.J., 2000, MNRAS, 315, 356

Helsdon, S.F. & Ponman, T.J., 2003, MNRAS, 340, 485

Hernquist L., Katz N., Weinberg D.H., 1995, ApJ, 442, 57

Hicks A., Ellingson E., Bautz M., Yee H., Gladders M., Garmire G., 2004, 35th COSPAR Scientific Assembly, 1624

Huchra, J.P. & Geller, M.J., 1982, ApJ, 257, 423

Lubin L. M., Mulchaey J. S., Postman M., 2004, ApJ, 601, L9

Lupton, R. & Ivezic, Z., ASPC, 338, 151

Mamon, G.A., 1986, ApJ, 307, 426

Mateo, M., 1998, ARA&A, 36, 435

Mahdavi A., Bohringer H., Geller M. J., Ramella M., 1997, ApJ, 483, 68

Mahdavi A., Bohringer H., Geller M. J., Ramella M., 2000, ApJ, 534, 114

Mendes de Oliveira C., Amram P., Plana H., Balkowski C., 2003, AJ, 126, 2635

Menon T. K., 1992, MNRAS, 255, 41

Mercha'n, M. & Zandivarez, A., 2002, MNRAS, 335, 216

Miles T. A., Raychaudhury S., Forbes D. A., Goudfrooij P., Ponman T. J., Kozhurina-Platais V., 2004, MNRAS, 355, 785

Mulchaey, J.S. & Zabludoff, A.I., 1998, ApJ, 496, 73

Mulchaey J. S., Davis D. S., Mushotzky R. F., Burstein D., 1996, ApJ, 456, 80

Osmond, J.P.F. & Ponman, T.J., 2004, MNRAS, 350, 1511

Popesso, P., Biviano, A., Bohringer, H., Romaniello, M., 2006, A&A, 445, 29

Ramella M., Pisani A., Geller M.J., 1997, AJ, 113, 483

Rasmussen, J., Ponman, T.J., Mulchaey, J.S., Miles, T.A., Raychaudhury, S., 2006, MNRAS, 373, 653

Roberts, M.S. & Haynes, M.P., 1994, ARA&A, 32, 115

Seljak U. et al., 2005, Phys. Rev. D, 71, 103515

Sersic J. L., 1974, Ap&SS, 28, 365

Spergel D. N. et al., 2003, ApJS, 148..175

Springel, V., White, S.D.M., Jenkins, A., Frenk, C.S. et al., 2005, Natur, 435, 629

Stetson, P.B., 2000, PASP, 112, 925

Sung, H., Bessell, M. S., 2000, PASA, 17, 244

Voit, G.M., 2005, Rev.Mod.Phys., 77, 207

Zabludoff, A.I. & Mulchaey, J.S., 1998, ApJ, 496, 39

Zabludoff, A.I. & Mulchaey, J.S., 2000, ApJ, 539, 136

Chapter 5

XI groups: Optical observations and Data analysis

5.1 Observation

Optical observations of XI groups used in the present study were performed during three observing runs in August/September 2006, December 2007, and April/May 2008 using the 2.5-meter (100-inch) Irénée du Pont telescope, operating at Las Campanas Observatory[1]. The telescope was calibrated with the wide field reimaging CCD (WFCCD) camera which reimages a 25 arcminute diameter field onto the TEK5 CCD camera, with a scale of 0.77 arcsec pixel^{-1}. The characteristic redshift of XI groups is $z \sim 0.06$ which corresponds to a luminosity distance $D \sim 265$ Mpc, using a flat concordance cosmology with $H_0 = 71$ km s^{-1} Mpc^{-1}, $\Omega_m = 0.27$, and $\Omega_\Lambda = 0.73$. At this distance the comoving radial distance (which is used in the Hubble law) is ~ 250 Mpc. The angular scale at this distance is 1.144 kpc arcsec^{-1}. At this scale, 1 Mpc is ~ 14.57 arcmin. Therefore, the field of view of WFCCD camera is slightly smaller than the actual FOV necessary for imaging our groups. Thus for each group four different pointings

[1]The August/September 2006 was done by Jesper Rasmussen, our collaborator from the Carnegie Institution of Washington

were used. Each pointing has an offset of 6 arcminute in both RA and DEC from group centre which covers the whole group FOV.

For each galaxy group a total exposure time of 3600s and 1440s were applied in B-band and R-band respectively. Since each group image is a mosaic frame consisting of four individual pointings, the actual exposure time used for each group is one fourth of those values, i.e. 900s in B-band and 360s in R-band. The exposure times in B and R was not applied continuously as there is a risk that group images being saturated by bright stars in the field of view. So the exposure times were split and each pointing was taken as three separate images, each with 300s and 120s in B-band and R-band. Splitting images would help us also in removing of cosmic rays during data reduction. Another advantage in taking several low-exposure images rather than a long continuous one is to prevent the bright stars in the FOV from being saturated. A dithering was applied between individual exposures by moving the telescope in either RA or DEC by $\sim$10 arcsec which should be taken into account during image processing.

The observed magnitudes of galaxies are instrumental magnitudes which are different from standard magnitudes. Thus in order to calibrate the observed galaxy magnitudes, images of standard stars are necessary. These images of standard stars should be taken two or three times per night as the weather condition might not be stable during the whole night in which case the calibration of magnitudes based upon one standard field is not reliable. During the observation of XI groups, the Stetson Photometric Standard Fields were used [2] with exposure times range from 10-16 sec in B-band and 4-8 sec in R-band.

5.2 Preliminary data reduction

The images of XI-groups were analysed using IRAF [3](Image Reduction and Analysis Facility). IRAF is an astronomical data analysis package which is a collection of different computer

[2]http://www3.cadc-ccda.hia-iha.nrc-cnrc.gc.ca/community/STETSON/standards/
[3]http://iraf.noao.edu/ - also http://iraf.noao.edu/docs/docmain.html

algorithms in order to analyse images. There are several parameters in each algorithm or IRAF task, to be set by the user. Usually the default settings are the optimised ones but a few of them such as `CCD GAIN` depend on CCD type, used during the observation. To reduce and calibrate the CCD images in IRAF, the following steps were followed.

5.2.1 Making bad pixel map file

A common problem with CCD images is the presence of poorly performing pixels in the CCD array, which produce unsatisfactory images. The process of detecting and correcting these bad pixels is easy. We need two sets of bias subtracted flat field images, taken with different exposure times. We call these two sets of images as *short* (short exposure time) and *long* (long exposure time) flats, i.e. `FlatS.fits` and `FlatL.fits`. The steps involved in constructing a bad pixel map (also called bad pixel mask) are as follow

```
imarith FlatS / FlatL Flatdiv   !create the new flat filed image
                                 'Flatdiv.fits'

ccdmask Flatdiv mask=badmap.pl  !create a pixel mask from the
                                 CCD image 'Flatdiv.fits'

fixpix ImageName.fits badmap.pl !fix pixels identified by the
                                 bad pixel file 'badmap.pl'
```

5.2.2 Aligning images

As galaxies are usually faint objects and we want to achieve some limiting signal-to-noise or limiting surface brightness, long exposure time is needed for CCD imaging. This could be

done either by taking a continuous, single long exposure image of the object, or taking several shorter exposures and combine them (using IRAF task `imcombine`). One advantage is that by stacking a series of images, pixels which have very deviant values from the others in the series (due to the arrival of cosmic rays on the CCD chip for example) can be rejected. Also between each exposure, an offset of ~ 10 arcsec is needed either in RA or DEC so that on none of the series of images the object is exactly at the same location on the CCD chip. So in case that an object's image falls on bad pixels, it is less probable that it happens again in the next image as the telescope has dithered for a few arcseconds. Note that image alignment should be carried out only on fully reduced images.

For example, to align three images of the same object, i.e. `ccd01`, `ccd02`, and `ccd03`, each shifted a bit from the others, the image names were first listed in the file `images.list`. One image (for example `ccd01`) was selected to be the reference image. A coordinate file was then created, using the IRAF task `imexamine` program from the measurement of the centroids of 4 or 5 stars in the field on the reference image. These centroids (1 per line) were recorded in a file called `images.coord`. To estimate the shifts for the other frames[with respect to the reference frame], one of the stars in the `images.coord` file was selected, and its coordinate was measured on the other images in the sequence. The shift in RA or DEC was estimated by subtracting the location of that star on the reference frame from the other images, i.e. $x_{ref} - x_{obj}$, $y_{ref} - y_{obj}$. The list looks like this:

```
images.list     images.coord     images.shift
 ccd01            374  557           0  0
 ccd02            597  533          64  0
 ccd03            602  501         -64  0
                  655  453
```

Note that the first line of the `images.shift` file indicates no shift on the reference image relative to itself. Finally, `imalign` aligns all three images:

```
 cl > lpar  imalign
input   =         ccd01,cd02,ccd03     Input images
referenc=         ccd01                Reference image
coords  =         images.coord         Reference coordinates file
output  =         sccd01,sccd02,sccd03 Output images
(shifts =         images.shift)        Initial shifts file
........
```

Now these images are combined into a single frame, say `result.fits`, using `imcombine`.

5.3 Astrometry

The spectroscopic observations of group galaxies have been performed using the Inamori-Magellan Areal Camera and Spectrograph (IMACS) multi-slit spectrograph. In general for studying galaxy population in groups, the selected slit width is not more than a few arcsec. This makes the determined positions of group galaxies very crucial as the construction of slit masks are based on the extracted coordinates. Fig. 5.1 illustrates a typical IMACS spectrum using a mask with 240 slits.

The raw CCD images obtained at the observatory do not contain any information on the right ascension (RA) and declination (DEC) of objects in the CCD field of view. In order to calibrate our images to celestial coordinate systems in which the coordinate of each object is expressed in RA and DEC, we need to compute plate solutions using the IRAF task `ccmap`. For each CCD image to be calibrated, `ccmap` asks for an input text file (`input.txt`) containing the pixel and celestial coordinates of points in the input image. It is worth identifying six or more reference stars as input for plate solution. To find the celestial coordinates, corresponding

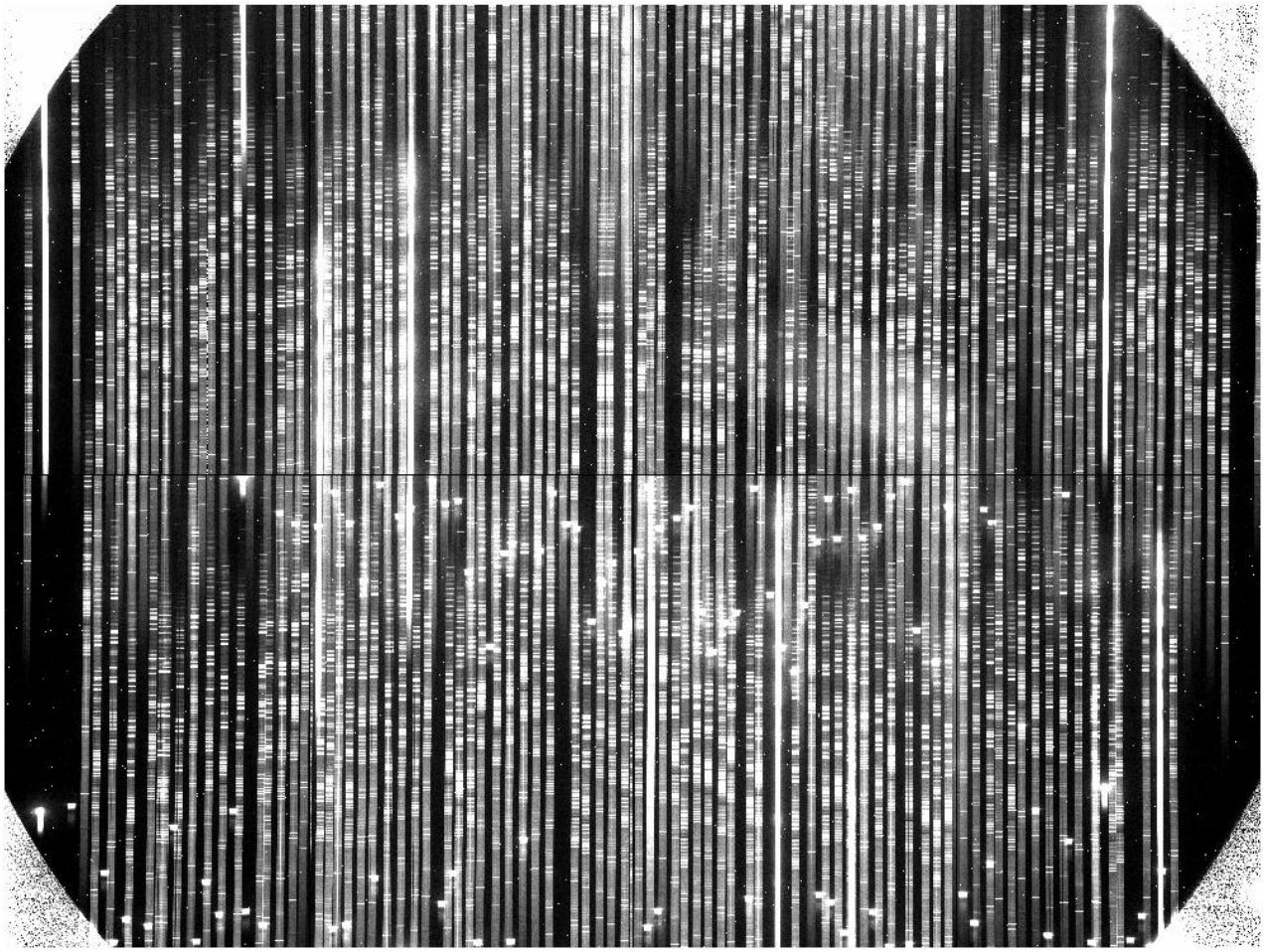

spectrum (240 slits)

Figure 5.1: A typical IMACS slit mask with 240 slits. (Credit: Robert W. O'Connell, University of Virginia).

to selected stars, I used USNO-A2.0 catalogue of astrometric standards[4], available from the NED (NASA extragalactic Database) database[5]. The coordinates are listed one per line with `x`, `y`, `RA`, and `DEC` in the columns specified by the `xcolumn`, `ycolumn`, `lngcolumn`, and `latcolumn` parameters respectively. The input file `input.txt` looks like this:

```
x       y       RA           DEC
------- ------- ----------- -----------
1245.03 1049.89 11:35:55.98 -03:45:34.2
1034.67  881.87 11:35:44.84 -03:47:47.8
 806.07  865.68 11:35:32.97 -03:47:59.4
1061.79 1324.94 11:35:46.33 -03:42:03.4
1318.06 1300.99 11:35:59.64 -03:42:23.2
 730.65 1226.03 11:35:29.11 -03:43:19.1
```

As `ccmap` uses different fitting functions to estimate a new world coordinate system (wcs) for CCD frames and to minimise the residuals between the image wcs and the model fitting functions in either `x` or `y` directions, we selected stars with small point spread functions (PSFs) and with symmetric surface and accurate radial profiles. After running `ccmap` in non-interactively mode, a list of the fitted values of the `ra` and `dec` and their residuals appear on the screen. One must try to select sufficient number of proper reference stars to end up with residuals around ~ 0.2 or less in both `ra` and `dec`.

5.4 Photometry

The imaging and photometry of XI groups is important for the following reasons: (i) To find the exact position of each group galaxy for IMACS followup spectroscopy. This is necessary

[4]http://tdc-www.harvard.edu/software/catalogues/ua2.html
[5]http://nedwww.ipac.caltech.edu/

to find the redshift and spectrum of group galaxies and from that the group memberships, metal abundance, and also to identify AGN and star forming galaxies, (ii) To study the dynamical state of XI groups from colour-magnitude relation among group galaxy members as well as group luminosity functions , and (iii) To study the morphology of group galaxies and its correlation with group's environment.

5.4.1 Magnitude Zero Point

The first step in doing photometry is to find the zero point magnitude m_{zp}. It is basically an offset between the observed instrumental magnitude of a standard star and its actual apparent magnitude m. The apparent magnitude in turn is related to the flux (F) of photons emitted by the standard star in each second via the following relation

$$m = -2.5 \times \log F + m_{zp}. \tag{5.1}$$

Eq. 5.1 still does not take into account the effect of the Earth's atmosphere at different wavelengths. In fact the column density of air along the line of sight is minimum if stars are being observed at the zenith rather than toward the horizon. Defining the *air mass* as the ratio of air column density at an arbitrary angle to its value at zenith, one can find a simple correlation for the air mass at zenith angle z in form of

$$\mathrm{airmass} = \sec z. \tag{5.2}$$

This formula is valid for plane-parallel atmosphere, but it does not change noticeably if one take that into account the curvature of the atmosphere. Also the response of atmosphere is not the same at all wavelengths and the atmospheric extinction (k) produces the dimming of starlight which depends on the filter's bandpass. I adopted $k_R \approx 0.1$ and $k_B \approx 0.3$ as extinction coefficients in B-band and R-band respectively (Sung & Bessell 2000). Considering all of these

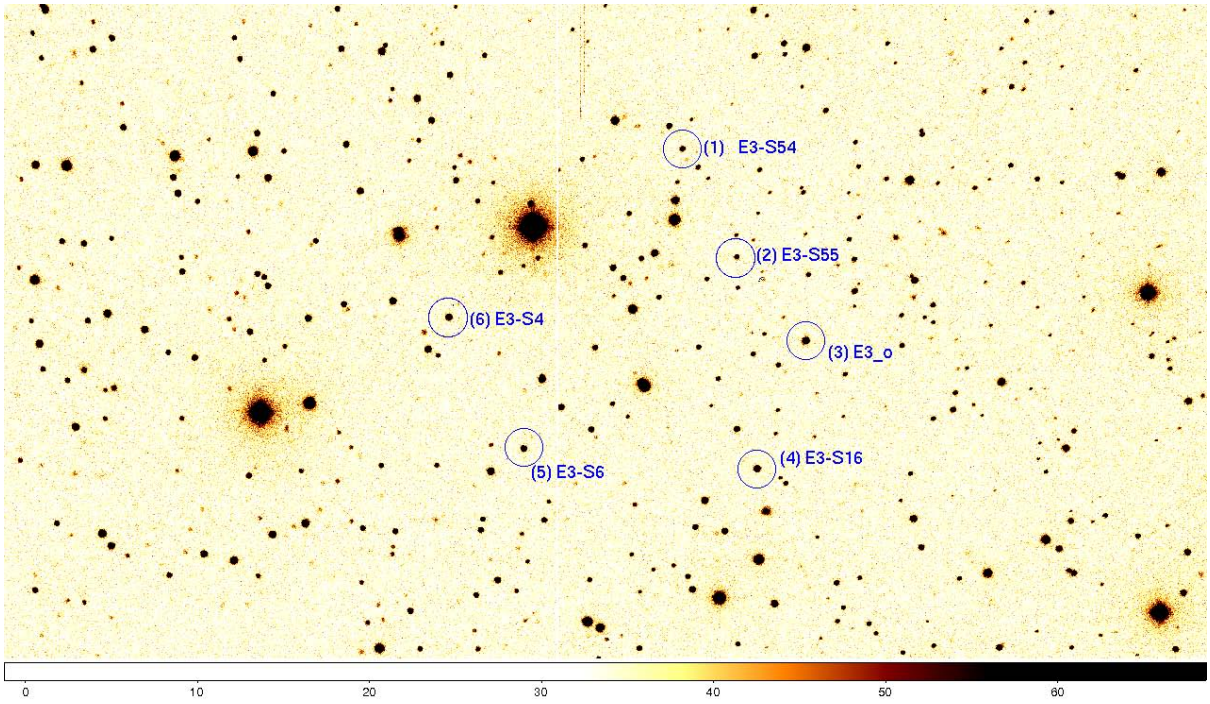

Figure 5.2: A sample of standard field from Stetson E3 field (RA=06:42:22.9-DEC=-45:12:30) used for calibrating the observed magnitude of galaxies.

effects, we can rewrite Eq. 5.1 as

$$m_I = -2.5 \times \log(\frac{F}{t_{exp}}) - k \times \sec(z) + m_{zp}, \tag{5.3}$$

where m_I is the airmass corrected instrumental magnitude and t_{exp} is the image exposure time in second. Note that flux given in Eq. 5.3 is the *net flux* and is estimated by subtracting the *sky flux* from the *total flux*, i.e $F = F_{net} = F_{tot} - F_{sky}$. To estimate F in Eq. 5.3, we use a sample of standard stars from images of Stetson standard star fields taken several times during each night of observation. Fig. 5.2 is a sample of such standard field from Stetson E3 field (RA=06:42:22.9-DEC=-45:12:30). In comparison to science images of galaxy groups, the exposure times used for standard stars is much smaller. The reason is that stars are much brighter than galaxies. In each image a set of five or six stars should be selected where their standard apparent magnitudes are given in the catalogue of standard stars.

There are several tasks in IRAF to perform aperture photometry on selected stars. Here I use the IRAF task `daophot/phot` which is suitable for single aperture photometry.

After running `phot` the command asks for input parameters `aperture radii`, `annulus`, and `dannulus`. These parameters are better displayed in Fig. 5.3 where `annulus` and `dannulus` correspond to *inner radius of sky* and *width of sky* respectively. The parameter `aperture radii` defines a circle which encloses the starlight flux. It must not be very small so that it does not include the star light itself or should not be so large as some other extra light from other faint sources may enter into our calculation. Normally `aperture radii` should be 4 or 5 times the size of star's FWHM (full width at half maximum) to ensure that all light are being measured. The IRAF task `imexamine` can be used to find the FWHM of a star. The task also allows us to do a variety of analysis on images. I run `imexamine` and put the cursor on the star I wish to measure its flux. Then by hitting `r` the radial profile of the star would be displayed as is shown in Fig. 5.4. Three values of FWHM (in unit of pixel) are printed at the end of status line on the bottom of the plot according to different algorithms such as Gaussian and Moffat fitting functions. The procedure can be repeated for all the standard stars in the field, but it is better to use the same `aperture radii` for all standard stars.

A good test to see whether a suitable value of `aperture radii` has been selected is to use a series of apertures including the one which has been estimated from the star's FWHM and see how the measured fluxes are changing. Those radii are acceptable for which the measured fluxes do not depend on small changes in radii. For example after running `phot`, the command asks for a list of aperture radius which can be entered as `r1:r2:step` (`5:25:2`). Note that all parameters in `phot` are in scale units of pixel.

As mentioned before several short exposure times were used for imaging of standard stars. In the R-band for example these include 4.0, 6.0, 8.0, 10.0, and 12.0 sec. The idea behind this is to check the CCD linearity before doing further image processing. In fact the most advantage of CCDs over photographic plates is that the CCD picture elements response in a linear way

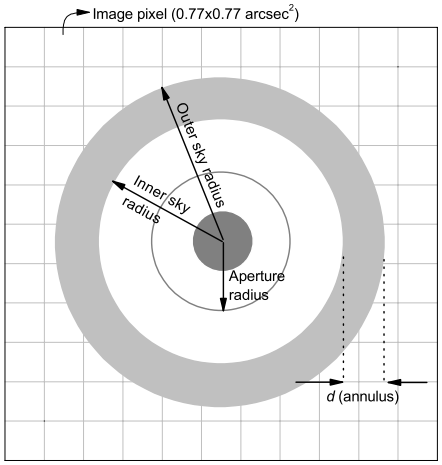

Figure 5.3: A cartoon of the various IRAF command `phot` input parameters used for doing aperture photometry (see Sec. 5.4.1 for more details).

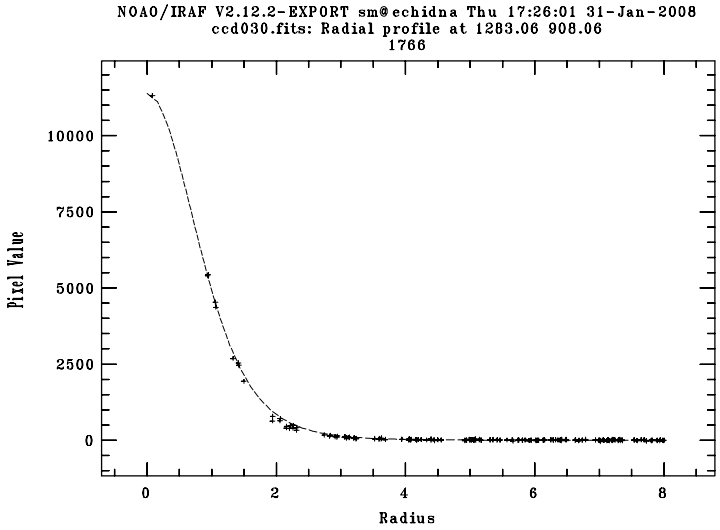

Figure 5.4: The radial profile of a sample star using the IRAF command `imexamine`.

to light photons, i.e the CCD counts or the number of electrons generated in each CCD pixel is a linear function of time. For a set of observed standard stars, the fluxes are estimated from images taken with 6.0, 8.0, and 10.0 sec of exposure times and are shown in Fig. 5.5 versus their corresponding standard apparent magnitudes. Note that the estimated fluxes from which the instrumental magnitudes in Fig. 5.5 have been measured are normalised to 1.0 sec. That is why we find the same instrumental magnitudes correspond to different exposure times.

The final step in finding the magnitude zero point is to plot the instrumental magnitudes estimated for the standard stars versus their correspondent standard apparent magnitudes given in the standard star catalogue of Stetson (2000). This has been done in Fig. 5.6 where the dotted line represents a linear regression in the form of

$$m_I = b \times m_S + ZP, \tag{5.4}$$

where b is the slope of the linear fit and ZP is Y-intercept or the *magnitude zero point*. m_I and m_S are the instrumental and apparent standard magnitudes respectively. The slope b in Eq. 5.4 is fixed to one ($b = 1.0$) as both magnitudes (instrumental or standard) have been measured using CCDs. Hence any sort of discrepancy should be accounted in ZP. The instrumental magnitude or the determined zero point magnitude depends on weather condition at the night of observation as both parameters are directly affected by airmass as well as atmospheric extinction. Therefore at each night of observation and in each filter (B-band, R-band, or V-band), one needs to estimate a separate value of zero point magnitude. Table. 5.4.1 is an example of the determined zero point magnitudes during the observing run of XI-groups in December 2007.

5.4.2 Astronomical Source Extractor (SExtractor)

The magnitude of galaxies in different bands is a key parameter in investigating various physical properties of these objects such as galaxy luminosity function, colour-magnitude relation, star

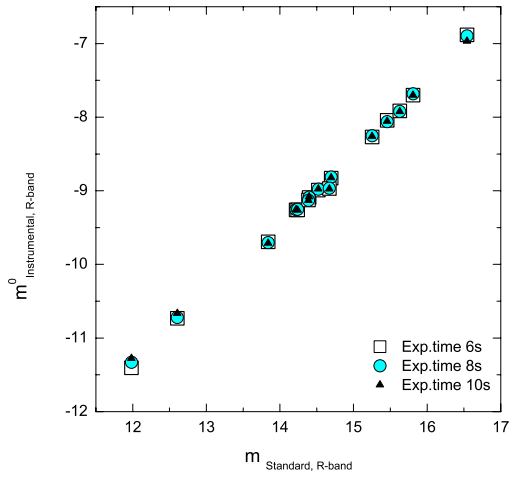

Figure 5.5: The estimated instrumental R-band magnitudes m_I for a typical sample of standard stars using different exposure times of 6.0s, 8.0s, and 10.0s versus their corresponding standard magnitudes m_S. Instrumental fluxes are normalised to 1.0sec. This demonstrates the linearity of the CCD images.

Table 5.1: Determined zero point magnitudes estimated from observational run of XI-groups in December 2007.

Date (December 2007)	ZP(R)	ZP(B)	ZP(V)
10-11	22.92	23.06	-
11-12	23.14	23.23	-
12-13	23.23	23.24	-
13-14	23.18	23.28	23.14
14-15	23.19	23.23	23.08
15-16	23.20	23.24	23.12
16-17	23.24	-	-

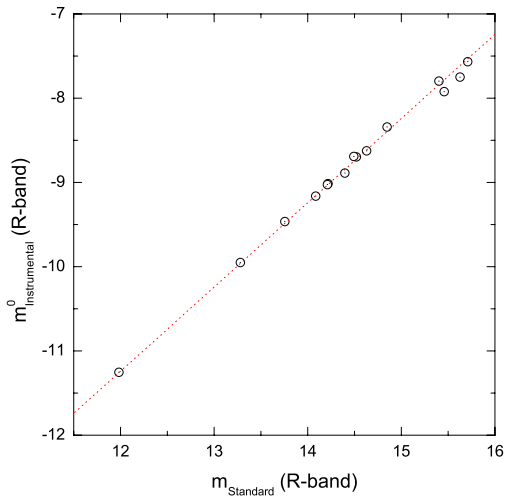

Figure 5.6: The same as in Fig. 5.5 but for a single exposure time. The *dotted line* is a linear fit (with fixed slope=1.0) to the observed data points in R-band. The y-intercept of the linear fit is an estimation of the zero point magnitude.

formation activity etc. There are several methods to determine and estimate the magnitude of a galaxy. Since for a given type of galaxy, its projected image and physical appearance on the sky is not circular, we can not use the same IRAF packages, tasks or algorithms used to measure the flux of stars, i.e. `qphot, apphot, phot`, which use circular apertures.

Fig. 5.7 shows that such circular aperture may contains extra photons due to contamination from other astronomical sources such as stars or faint galaxies which are close or in vicinity of the target galaxy. So one needs to measure fluxes from non-spherical objects with non-circular projected images using elliptical apertures. There are different methods to measure the object's flux for non-circular sources. For example it can be done using the IRAF task `ellipse` within `stsdas` package (`stsdas/analysis/isophote/ellipse`). The `STSDAS` is an IRAF external package, i.e. it runs under IRAF but is distributed separately from the core IRAF system. The package is very useful in determining photometric parameters such as galaxy *optical diameter D25* (see Sec. 5.6), however it is not oriented towards reduction of large scale

galaxy-survey data similar to ours.

An alternative way is to use the *astronomical source extractor* program or the *SExtractor* (Bertin & Arnouts 1996) which is a code that builds a catalogue of objects with information on their fluxes, magnitudes, and physical shapes from astronomical images. SExtractor is particularly suitable for reduction of large astronomical data files. Though various useful documents on using SExtractor are available via the world wide web however, I discuss a few major points on running the code [6].

After installation of the programme, one can run the code simply by typing `./sex image.fits`. The image file must be in *fits* format and should be in the same directory as SExtractor. The output files consist of an analysed image file in FITS format (`check.fits`) from which various parameters have been estimated by SExtractor and stored in another plain TXT `image.cat` file (image catalogue file).

Setting up SExtractor is the most important step in using the program. Each time before running SExtractor on a specific image, two major files must be modified. These two files are `default.sex` and `default.param`. The first file (`default.sex`) acts as SExtractor *input* file and the user should adjust a couple of initial parameters according to his/her image characteristics and scientific purpose. The second file serves as the *output* parameter file and the user can control the number of exported parameters by editing the content of `default.param`. Each line in `default.param` corresponds to one parameter. Whether that parameter appears in the output file or not can be controlled by adding # symbol at the beginning of each line. For example out of following four parameters

```
#A-IMAGE
#B-IMAGE
 A-WORLD
 B-WORLD,
```

[6]To download the latest version of SExtractor as well as its documentation see: http://terapix.iap.fr/soft/sextractor/

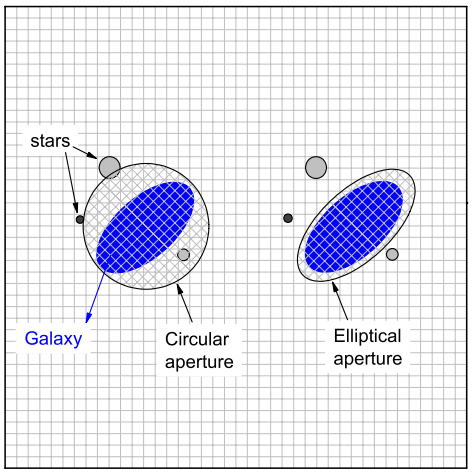

Figure 5.7: The effect of aperture's shape in determining the object's flux. There is a less chance for the measured flux to be over estimated due to the existence of stars in the vicinity of galaxy if the aperture is elliptical rather than circular.

only the last two parameters (`A-WORLD,B-WORLD`) would appear in the output `image.cat` file.

5.4.3 Setting up SExtractor input parameter file `default.sex`

Modification of SExtractor input parameter file `default.sex` is essential in getting right values of output parameters. Similar to the output parameter file `default.param`, each line in the input file `default.sex` that starts with # symbol, represents a comment and would not be read by the computer. A default value has been assigned to each parameter in the input configuration file. A few of these parameters are related to the instrument which have been used during observation such as `PIXEL-SCALE` and `GAIN` which describe the size of CCD pixels in arcsec and detector gain in electron/ADU respectively. During the observation with du Pont telescope the *ccd* command window allows for the selection of 3 possible CCD gain settings. For direct imaging, it is suggested that gain 3 be used, which gives approximately

3.0 electrons/ADU and a read out noise of ≈ 7 electrons. Thus in our case `GAIN=3.0` with `PIXEL-SCALE=0.77`.

There are other parameters which are essential in calibration of the output values estimated by SExtractor from astronomical sources in the input image like `MAG-ZEROPOINT` and `SEEING-FWHM`. These two parameters which are respectively the magnitude zero point and the stellar *full width at half maximum* (FWHM) in arcsec and the way they have been measured are discussed in Sec. 5.4.1. As a final caveat it should be noted that if the input image which has been taken with an exposure time of t sec is not normalised to 1.0 sec, then `MAG-ZEROPOINT`=$ZP + 2.5 \times \log(t)$ rather than `MAG-ZEROPOINT`=ZP otherwise SExtractor overestimates the measured fluxes of individual sources by a factor of t, i.e. the final measured magnitudes would have an offset of $-2.5 \times \log(t)$ from their real values.

The last parameter which I think is important in terms of the scientific goal is the `DETECT-MINAREA` parameter or minimum number of pixels above threshold. The parameter forces the code to fix the minimum object size to be detected by SExtractor. For example, the luminosity function of galaxy groups in our study is one of the major quantities that direct us upon the population of galaxies at different bins of absolute magnitudes. In such case even very faint dwarf galaxies are important and have to be detected. However, our detection threshold is limited by two factors: (i) CCD pixel size and (ii) observed limiting apparent magnitudes in B and R filters which depend on the given exposure times.

A typical dwarf galaxy with a diameter of ~ 5kpc appears in observed images as an object with an optical diameter of ~ 4 arcsec. Given that each CCD pixel is 0.77 arcsec/pixel, we find that such a dwarf galaxy does appear as a source with a maximum diameter of ~ 5 pixels. Though studies of local dwarf galaxies show that dwarf galaxies could have smaller size (Mateo 1998), but we can not detect or classify smaller objects in our images given current CCD pixel size and exposure times. Hence in all of our analysis a value of 10 pixels was assigned to the parameter `DETECT-MINAREA` within the input parameter file `default.sex`.

5.5 Reliability of magnitudes

Measuring galaxy magnitudes in different bands is of great importance in studying galaxy groups, since they are used in estimating galaxy colours, luminosity functions etc. Therefore it is very important to know the reliability of our measured magnitudes. This could be done by comparing the observed magnitudes of galaxies in different bands with large sky surveys such as the well known Sloan Digital Sky Survey (SDSS)[7]. Fortunately SDSS has some overlap with the field of view of XI galaxy groups. Of course we do not need to check individual group fields with their SDSS counterparts as we have used the same method to reduce all of our galaxy group images.

For a given source (whether star or galaxy) in an image, SExtractor estimates several magnitudes, each according to a different algorithm where detailed description of each of these magnitudes are given in SExtractor manuals. In brief, these magnitudes are `MAG-ISO`, `MAG-ISOCOR`, `MAG-APER`, `MAG-AUTO`, and `MAG-BEST`. For example either `MAG-AUTO` or `MAG-BEST` magnitudes give the object's total magnitude, estimated from its total flux within an aperture which depends on the shape of the source. Such magnitudes are useful in determining the luminosity function of galaxies. Yet if one needs to find the colour of galaxies, the aperture magnitude `MAG-APER` must be used rather than `MAG-BEST` or `MAG-AUTO`. In fact unlike two other magnitudes, `MAG-APER` is the magnitude of an object estimated from its flux within a fixed circular aperture. The size of the aperture has to be set via the `aperture-size` parameter within the SExtractor input parameter file `default.sex`.

In our study of XI-groups, `MAG-BEST` has been adopted to estimate galaxy apparent magnitudes in either R-band or B-band. To compare our observed magnitudes with those from SDSS, we need to know the transformations between the SDSS $ugriz$ and $UBVR$ magnitudes. There have been several efforts in calculating transformation equations between ugriz (or u'g'r'i'z') and UBVRI. Here, we focus on Lupton & Ivezi (2005) who derived transformation equations

[7] http://www.sdss.org/

for stars. These equations are derived by matching SDSS DR4 (Data Release 4) photometry to Peter Stetson's published photometry for stars (Stetson 2000) and are as follow:

$$\begin{cases} B = u - 0.8116 \times (u - g) + 0.1313 & \text{sigma} = 0.0095 \\ B = g + 0.3130 \times (g - r) + 0.2271 & \text{sigma} = 0.0107 \\ \\ R = r - 0.1837 \times (g - r) - 0.0971 & \text{sigma} = 0.0106 \\ R = r - 0.2936 \times (r - i) - 0.1439 & \text{sigma} = 0.0072 \end{cases} \tag{5.5}$$

Fortunately there are overlaps between the observed field of view of seven groups in our sample (MZ 3849, MZ 4001, MZ 4881, MZ 4940, MZ 5293, MZ 5383 , MZ 5388) and those from the SDSS. For a set of 2032 objects (representing both galaxies and stars) in field of view of the observed group images, Eq. 5.5 has been used to transform SDSS magnitudes to B and R band magnitudes. The results of such comparison are shown in Fig. 5.8.

The *left panel* in Fig. 5.8 suggests an excellent agreement between our observed R-band magnitudes and those from the SDSS for objects fainter than $m_R \gtrsim 14$. However, in B-band our observed magnitudes are systematically fainter than those from the SDSS by $\lesssim 0.2$ mag as is shown in the *right panel* of Fig. 5.8. Such an offset is unlikely to be due to an error in our analysis or pixel saturation of our observed B-band images, and is possibly due to the conversion formula used for comparison between our B-band data and those from the SDSS. The current conversion formula as given in Eq. 5.5 are transformation equations for stars. At the moment, there are no transformation equations explicitly for galaxies. Furthermore, all of our luminosity functions presented in this chapter (e.g. Figs. 5.21, 5.22, and 5.23) are estimated in the R-band magnitude bins of 1.0 which is not affected by the observed offset of $\lesssim 0.2$ mag in the B-band.

There are two additional features in distribution of data points shown in Fig. 5.8. First one

is the large scatter of a few data points about the line of equality. These objects are those with large FLAG values in the output of Sextractor. FLAGs are produced by the various detection and measurement processes within SExtractor; they tell for instance if an object has been truncated at the edge of the image or the object contains bad or noisy pixels. Therefore, such data points can be removed easily by selecting objects with FLAG=0 as is shown in the right panel of Fig. 5.9.

In addition, Fig. 5.8 indicates that for bright objects ($m_R \lesssim 14$ or $m_B \lesssim 16$) our estimated fluxes are underestimated in comparison to those from SDSS as our data points deviate from lines of equality. The reason is that since our exposure times are longer than the one used by the SDSS survey, bright objects (mainly stars) in our images are partially saturated. This is clear from the left panel of Fig. 5.9 where the objects are colour-coded according to their STELLARICITY index. A visual inspection of the images of these deviant objects in DS9, shows that they are stars which are partially saturated but have not been detected by Sextractor. However, it does not affect our results on the estimated galaxy colour or their luminosity functions as magnitudes of the brightest group galaxies in our sample are fainter than 14. Furthermore, galaxies are extended objects in comparison to stars with sharp central light profiles. So while a star starts to get saturated for a given magnitude m, a galaxy with the same magnitude does not necessarily get saturated.

5.6 Galaxy Optical Diameter

Galaxies within groups lose their gas (mostly composed of neutral hydrogen HI) via gravitational interaction with other group galaxies. Also the gas can be stripped away due to the interaction of galaxies with intragroup medium. In both cases galaxies would be deficient in gas in comparison to their field counterparts of the same size and similar morphological type. Such interactions take place in galaxy clusters as well however it should be more efficient in group

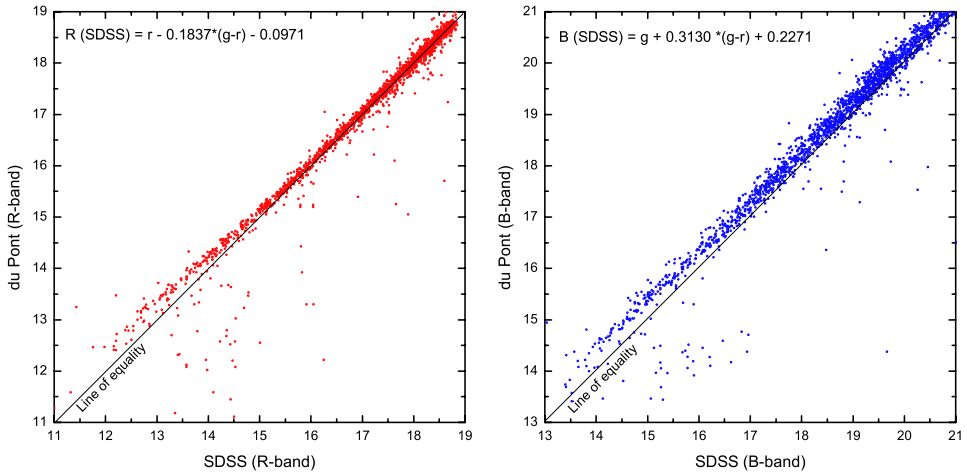

Figure 5.8: Comparison between the observed R-band MAG-BEST (*left panel*) and B-band MAG-BEST magnitudes (*right panel*) of 2032 objects selected from the field of view of seven XI-groups (MZ 3849, MZ 4001, MZ 4881, MZ 4940, MZ 5293, MZ 5383 , and MZ 5388) with their corresponding magnitudes from the SDSS using Eq. 5.5. The points in these figures represent images of both stars and galaxies.

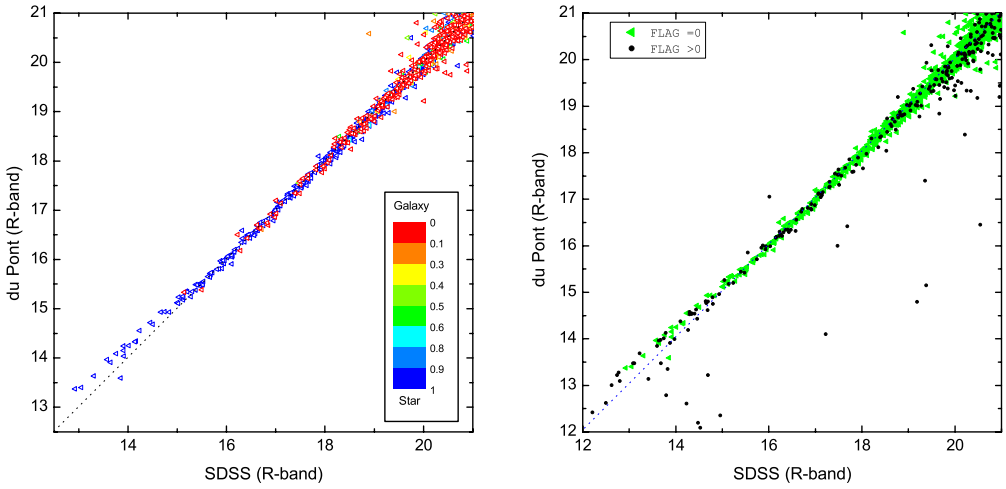

Figure 5.9: Comparison between the observed R-band MAG-BEST magnitudes with their corresponding magnitudes from the SDSS (using Eq. 5.5). The dashed lines in both panels represent the line of equality. *Left panel*: Objects are colour-coded according to their STELLARICITY index. *Right panel*: Data points are colour-coded according to their FLAG index.

environments due to low velocity dispersion of galaxies in groups. The parameter that quantifies neutral hydrogen deficiencies for individual galaxies is known as H_I *deficiency* (*DEF*) and is expressed as (Haynes & Giovanelli 1984):

$$DEF = \log(\frac{M_{H_I}}{D_l^2})|_{field} - \log(\frac{M_{H_I}}{D_l^2})|_{obs}. \quad (5.6)$$

In Eq. 5.6, H_I is the galaxy neutral hydrogen mass and D_l is the galaxy optical major isophotal diameter measured at or reduced to the surface brightness level m=25.0 mag arcsec^{-2} in the B-band (hereafter I call this parameter as D_{25}, See Fig. 5.11).

If the H_I content of a galaxy scales with its apparent diameter in B-band, then for a given galaxy morphological type the value of *DEF* estimated according to Eq. 5.6 should be positive for galaxies within groups. The reason for using B-band images in determining D_{25} is that B-band images can better represent the young population of stars within galaxies. Since the formation of young stars is correlated to the amount of interstellar cold gas resources, mostly in the form of hydrogen, B-band images are better represent the area of the galaxies where star formation is occurring. The study of H_I deficiencies in galaxy groups is beyond the scope of this thesis. I measured the parameter D_{25} for all galaxy members of three XI-groups for the radio 21cm line radio follow up observations. These groups are MZ4577,MZ5383, and MZ9014 where their hydrogen contents have been measured from the H_I 21 cm line observations using the Giant Metrewave Radio Telescope (GMRT) near Pune in India (Sengupta et al. 2009). In the rest of this section, I discuss the way I measured D_{25} for galaxy members for these three XI-groups.

5.6.1 Measuring D_{25} in IRAF

Finding D_{25} of a galaxy is not as simple as finding galaxy total apparent magnitude. The external IRAF package `STS` and its implemented tasks were found to be quite useful in finding

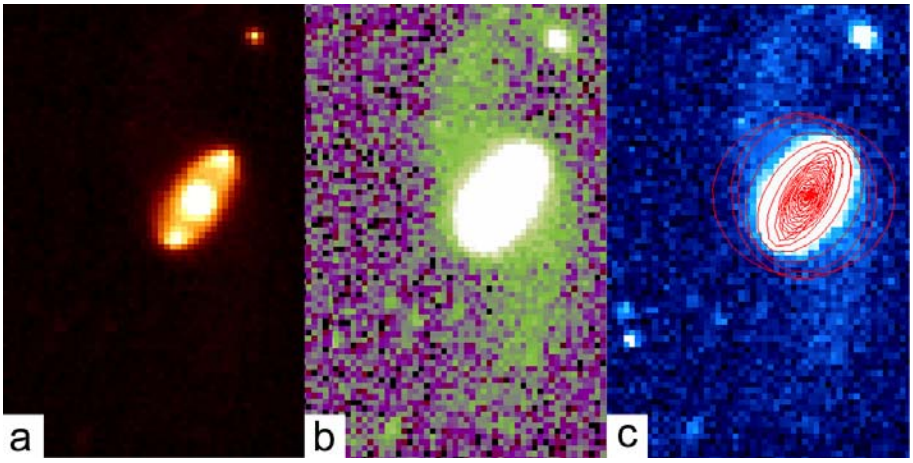

Figure 5.10: The B-band image of the galaxy LCRS B123236.4-032105 in galaxy group MZ5383. **(a),(b)**: show the same galaxy but the image contrast and brightness are different. As a result, the galaxy's spiral arms appears in image (b). **(c)**: By using the IRAF package `STS`, successive isophotes are plotted and overlaid on the image of galaxy.

D_{25}. For example, the galaxy in Fig. 5.10a is similar to a ring galaxy while its spiral arms appears in Fig. 5.10b. Using `STS`, successive isophotes are plotted and overlaid on galaxy image as appears in Fig. 5.10c. Note how the direction of outward successive isophotes in Fig. 5.10c start to change when they are plotted in the regions where spiral arms emerge from the bulge of the galaxy. Such isophotes are an output example of the `STS` package which can be used to estimate D_l for individual galaxies. Here I go through the steps, I adopted to measure the optical diameter D_{25} for XI-group galaxies.

As Fig. 5.11 shows, various isophotes can be fitted to a two dimensional image of a galaxy. In galaxies, light intensity decline radially from galaxy centres. Hence, the net flux in outer isophotes is always less than the total flux within inner isophotes. The objective is to find the length of the semimajor axis or diameter of a galaxy isophote such that the net flux within that isophote would be equal to 25 magnitude per square arcsec (in B-band). To do this, I use the task `ellipse` (`stsdas.analysis.isophote`) which fits successive elliptical isophotes to images of galaxies by reading image sections in FITS format. Then it produces a table as an output which contains many parameters for each fitted isophote, one table row for each isophote.

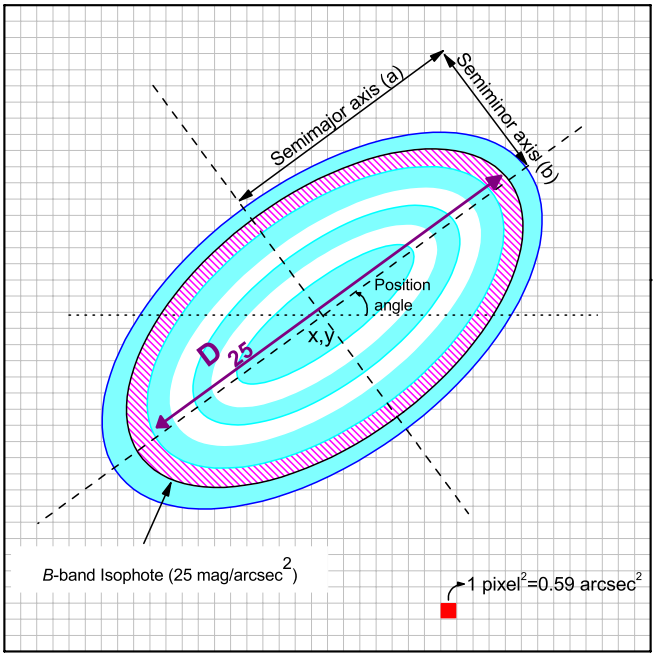

Figure 5.11: The galaxy optical major isophotal diameter D_{25} measured at or reduced to the surface brightness level m=25.0 mag/arcsec^2 in B-band.

In order to measure D_{25} I followed the following procedure:

- Normalising the image exposure time to 1.0 second (`imarith image.fits / exposure.time new-image.fits`).

- While the image is open in ds9, I select the `X, Y` coordinates of up to 5 or 6 regions of the background where at least within a radius of 20 or 30 pixels of a circle centred on `X, Y`, there would be no bright sources such as stars or galaxies and save those coordinates in a separate file, i.e. `sky.coord`.

- Run `noao.digiphot.daophot.phot` on the image while setting the `input name` (`epar phot`) as `sky.coord` and the `output name` as `sky.mag`. The task `phot` then generates `sky.mag` file which contains the information on the sky fluxes of those selected background regions (`MSKY` in `sky.mag`).

  Taking an average of all of these gives an estimation of the overall background flux of the image. If you have done the preliminary reduction properly, then the level of background counts should be around ~ 1.0. Note that the `MSKY` of each region should not be very different from the other regions. For example in my case, all of these five or six background fluxes are within ± 0.05 counts of each other. If the galaxy is close to a bright source such as a bright star then for that galaxy, a local background flux must be estimated separately.

- Once the average background sky level of an image was found it can be either subtracted from the image itself (which has been already normalised to 1.0 second exposure time) or it can be used later as the sky level input before running `ellipse`. I subtracted the sky level from my image of each galaxy group.

- Load the `isophote` package in `stsdas.analysis`. Before running `ellipse` a few parameters should be set. These parameters are the `x, y` coordinate of the target galaxy

for which we are to find the isophotal magnitudes and image zero point magnitude m_{zp}. These two parameters have to be set by editing `geompar@` and `magpar@` respectively.

- The last step in estimating the isophotal magnitudes is to run `ellipse`. It could be done in either `interactive` or `non-interactive` mode. After running `ellipse`, the command starts fitting several isophotes using an initial guess for the centre of isophotes `x,y` as well as their *position angles* (see Fig. 5.11. The output parameters estimated from each isophote would be saved in a `stsdas` table file format, i.e. `*.tab`. This format is different from `ASCII` format and is readable by `stsdas` tasks such as `isoexam` which plots ellipses on the image display.

- After finishing running `ellipse` on all galaxy images, we have as many as `*.tab` files equal to the number of our galaxies. To finalise the procedure, it is worth checking these output files to see whether `ellipse` has done a good job on our galaxy images or not. The `stsdas.isoexam` task is an ideal algorithm to do it. The task reads simultaneously the galaxy image file in ds9 while overlaying its isophotes using the `ellipse` output table file already generated for that galaxy. I checked all images one by one by eye for the two following reasons:

  (i) There are cases in which the `ellipse` makes a wrong guess for the initial isophotal position angle and the task follows to adopt the same *incorrect* position angle for successive isophotes. It happens normally when the galaxy image is very small or due to the lack of sufficient resolution. Fig. 5.12 shows such an example for one of MZ5383 group galaxy members. It is obvious from this figure that the initial guess made by `ellipse` for the position angle (*red dashed line*) is very different from the correct angle (*blue dashed line*).

  (ii) It is not unusual to find stars or even other galaxies in close vicinity of a target galaxy. In such a case `ellipse` takes them into account when measuring isophotal

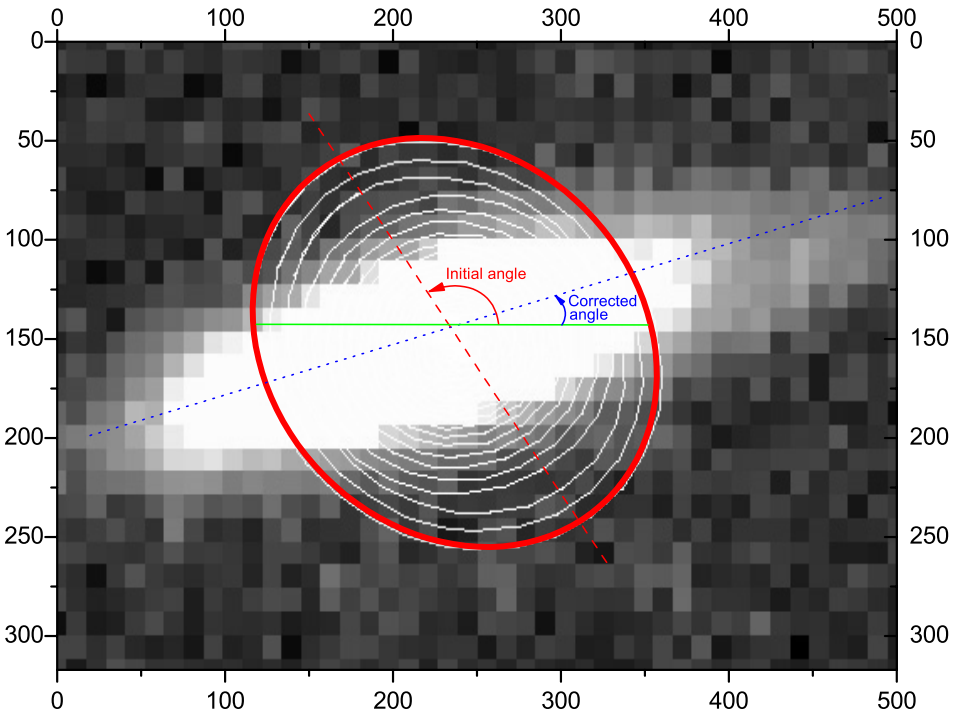

Figure 5.12: An example of a galaxy in which the initial guess made by `ellipse` for the position angle (*red dashed line*) is very different from the correct angle (*blue dashed line*).

magnitudes which results in overestimating of isophotal magnitudes and hence underestimating galaxy optical diameter. The *left panel* of Fig. 5.13 represents such an example for a member group galaxy. Basically such objects should be blocked or masked to prevent them being involved in estimating galaxy isophotes.

Using `ellipse` in interactive mode one may get rid of such problems. If the `ellipse` task starts with the `interactive` parameter set to `yes`, several cursor commands become available in a way that the user can, at any time, list and modify parameters and the current ellipse geometry. It is possible to mask or unmask regions in the image, discarding them from subsequent galaxy image. These regions may be specified by a single keystroke which will mask a square region of specified size centred on the cursor position (see *right panel* of Fig. 5.13).

It is also possible to specify a completely new semi-major axis, centre and orientation or position angle. The cursor returns after each isophote fit, until you select non-interactive mode (by hitting `'d'` key). I found the keystroke commands `'a','c','d'`, and `'f'` very useful. A help file regarding running `ellipse` in non-interactive mode is available via `elcursor` help file in `stsdas.analysis.isophote`.

The final `ellipse` output table file contains information on total and isophotal galaxy flux and magnitude. Since these output parameters depend upon pre-set parameters such as those in `magpar@`, then if any one of those pre-set parameters are wrong, the estimated isophotal magnitudes would be wrong as well. Apart from checking geometrical shape of isophotes that already has been discussed, we can check the total magnitude and see whether is it equal to the one measured by SExtractor or not. This is a good test to ensure that are presetting have been adjusted properly.

Both `isopall` and `isoplot` can be used to check the total magnitude of the target galaxy. The main table generated by `ellipse` is used as input for these two tasks. The difference between `isopall` and `isoplot` is that unlike the second one, the first one plots all results of

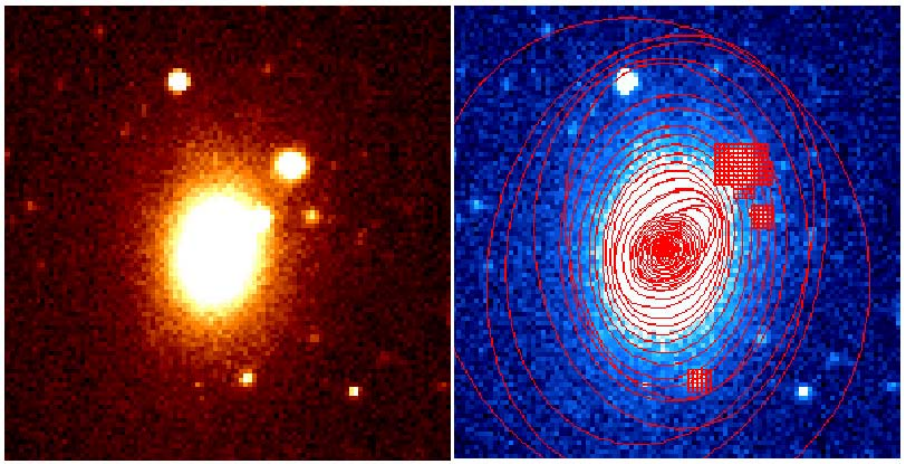

Figure 5.13: *Left panel*: an example of a galaxy with bright stars in its vicinity. Such stars are sources of bias in measuring the galaxy optical diameter D_{25}. *Right panel* Such stars can be blocked using the IRAF command `ellipse` in interactive mode.

the isophotal analysis. To estimate the galaxy total magnitude, after running `isoplot`, I plot `SMA` (semi-major axis length in pixel) versus either `TMAG-E` (total flux enclosed by ellipse) or `TMAG-C` (total flux enclosed by circle). However as the comparison is being made with SExtractor and the object is a galaxy with elliptical shape, it is better to use `TMAG-E`.

The output table generated by `ellipse` is not in `ASCII` format. To convert the table from `stsdas` format to `ASCII` format, the task `stsdas.ttools.tdump` must be used. Here is an example:

```
tdump INPUT.tab cdfile=STDOUT datafile=STDOUT > OUTPUT.txt.
```

All fluxes and from that the magnitudes as well as other parameters such as the length of semi-major axis (`SMA`) estimated by `ellipse` are in units of image pixel while in our definition of D_{25}, the isophotal magnitudes must be expressed in *mag/arcsec*^{2}. Therefore the correct conversion formula should be applied to the `ellipse` output data to find D_{25}. An example of such a conversion is shown in Fig. 5.14 where D_{25} has been estimated for the galaxy shown in Fig. 5.13.

Fig. 5.14 is in fact a conversion of the profile shown in the inset (*red plus signs*). The

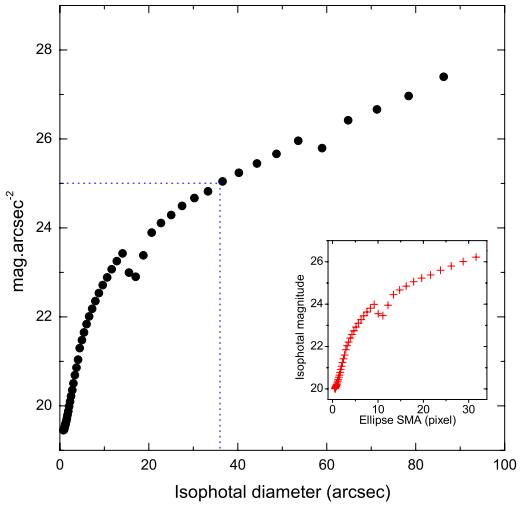

Figure 5.14: A plot of the isophotal diameter versus flux surface density for a given galaxy. The inset shows basically the same plot but before converting the axes into proper units for measuring the galaxy optical diameter D_{25}.

inset has been plotted directly from the measured isophotal data while the main plot takes into account the fact that plate scale of our images is 0.77 arcsec.pixel^{-1} which should be considered to find the right conversion from mag/pixel^2 to mag/arcsec^2.

5.7 Results

5.7.1 Galaxy spatial distribution within groups

As was outlined in Chapter 4, for high velocity dispersion groups with $\sigma_v \gtrsim 250$ km s^{-1}, the virial radius is adopted using the following equation (see Chapter 4 for more details):

$$\log R_{200}(\mathrm{Mpc}) = \log \sigma_v(\mathrm{km/s}) - 2.50, \tag{5.7}$$

while for groups with $\sigma_v \lesssim 250$ km s^{-1} the group R_{200} is estimated (using Eq. 5.7) at the median velocity dispersion of groups which is 250 km s^{-1}. However, initial estimates show that the derived R_{200} (based on Eq. 5.7) for high velocity dispersion groups with $\sigma_v \gtrsim 250$ km s^{-1} in our sample is larger than the observed field of view. This will introduce some bias in finding the group luminosity function. Hence, I decided to measure the group luminosity function within $0.7 \times R_{200}$.

Since the interstellar medium does affect the observed galaxy fluxes, the estimated magnitude of galaxies should be corrected for the interstellar or galactic extinction. Such extinction not only varies with galactic latitude but also it varies with wavelength such that the shorter the wavelength the stronger the extinction. To correct the galaxy magnitudes for galactic extinction in a given filter either in B-band or R-band, I use the galactic extinction presented as total absorption A_λ in magnitudes, as calculated by Schlegel, Finkbeiner & Davis (1998). Hence, for each galaxy in the field of view of a given galaxy group, the value of A_λ was extracted from the NED and subtracted from the estimated magnitude of galaxies.

Each panel in Fig. 5.16 shows the spatial distribution of galaxies in one of the XI-groups. Galaxies are shown with *blue circles* while their sizes are in proportion to their R-band luminosities. In the same plot, the overlaid circles correspond to different group radii. The *black dotted circle* and the *black cross sign* correspond to group virial radius R_{vir} and group centre as measured by Mercha'n & Zandivarez (2002). The group $0.7 \times R_{200}$ is shown with a *red circle*. Note that group $0.7 \times R_{200}$ is centred around the new estimated group centre (*red plus sign*) which is the luminosity-weighted mean position estimated according to the following equations:

$$\begin{cases} \mathrm{RA}_{new} = \dfrac{\sum_{i=1}^{N} L_{R_i} \times RA_i}{\sum_{i=1}^{n} L_{R_i}} \\ \mathrm{DEC}_{new} = \dfrac{\sum_{i=1}^{N} L_{R_i} \times DEC_i}{\sum_{i=1}^{n} L_{R_i}} \end{cases} \tag{5.8}$$

where N is the number of galaxies in each group and L_R is the galaxy R-band luminosity. We need to revise the positions of groups as our current group sample contains more spectroscopic confirmed member galaxies than what was found initially by Mercha'n & Zandivarez (2002). However, these new galaxies could belong to other groups and not necessarily a member of the current group. Group MZ 3541 is a good example of such a case. In this sense the estimated group centre from X-ray data analysis should be more reliable. Otherwise it is better to rely on the original group centres rather than the new ones.

For example our new determined group position for MZ 9014 (RA=9°.41;DEC=-27°.507) is in agreement with the one found from the analysis of diffuse X-ray emission in the XMM-Newton observationss (RA=9°.42;DEC=-27°.508, Rasmussen et al. 2006) while according to Mercha'n & Zandivarez (2002), the position of MZ 9014 is RA=9°.45;DEC=-27°.508. The estimated offsets in RA and DEC between new R-band Luminosity-weighted mean positions (e.g. Eq. 5.8) and those from group catalogue of Mercha'n & Zandivarez (2002) is shown in Fig. 5.15. Each data point represents a group where its size corresponds to the deviation of its position from ΔRA=ΔDEC=0.

Finally the *green rectangles* in each panel present the observed field of view which is the same for all groups and is equal to $\approx 30 \times 30$ arcmin^2.

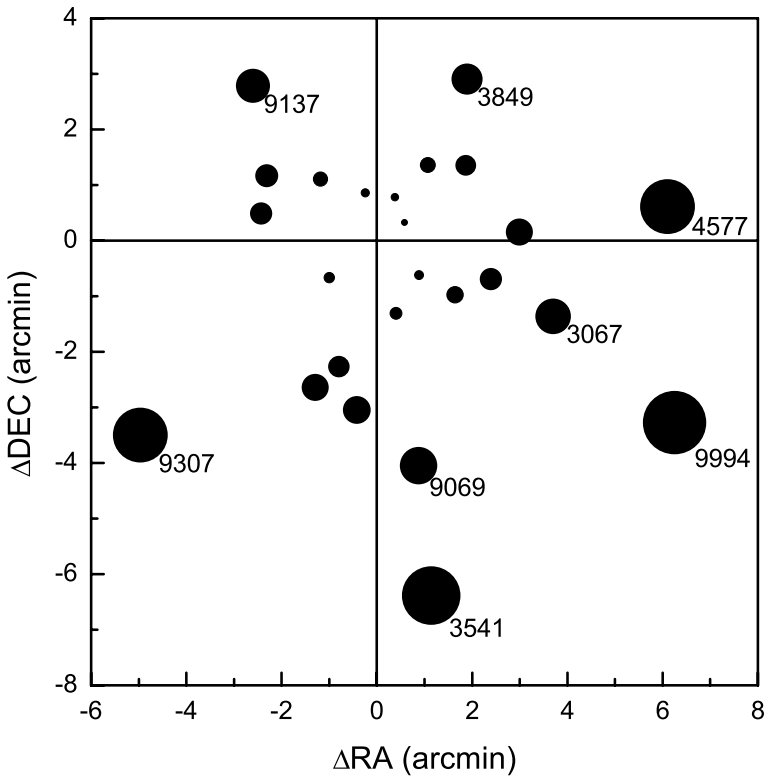

Figure 5.15: The estimated offsets in RA and DEC between the new R-band Luminosity-weighted mean positions and those from group catalogue of Mercha'n & Zandivarez (2002). Each data point represents a group where its size corresponds to the deviation of its position from ΔRA=ΔDEC=0.

5.7.2 Group member luminosity function

In this section I examine the luminosity function of groups just from their spectroscopically confirmed members. The results are illustrated in Fig. 5.17 where each histogram represents the luminosity function of individual groups based on the number of group members within the estimated $0.7 \times R_{200}$. Groups are ordered by their ascending velocity dispersions σ_v from left to right and top to bottom in the same way as in Fig. 5.16. The plot shows that the distribution of members at faint end declines at $-20 \lesssim M_R \lesssim -18$. This is mainly due to fact that the current spectroscopic sample of group galaxies is incomplete at $M_R \gtrsim -20.0$.

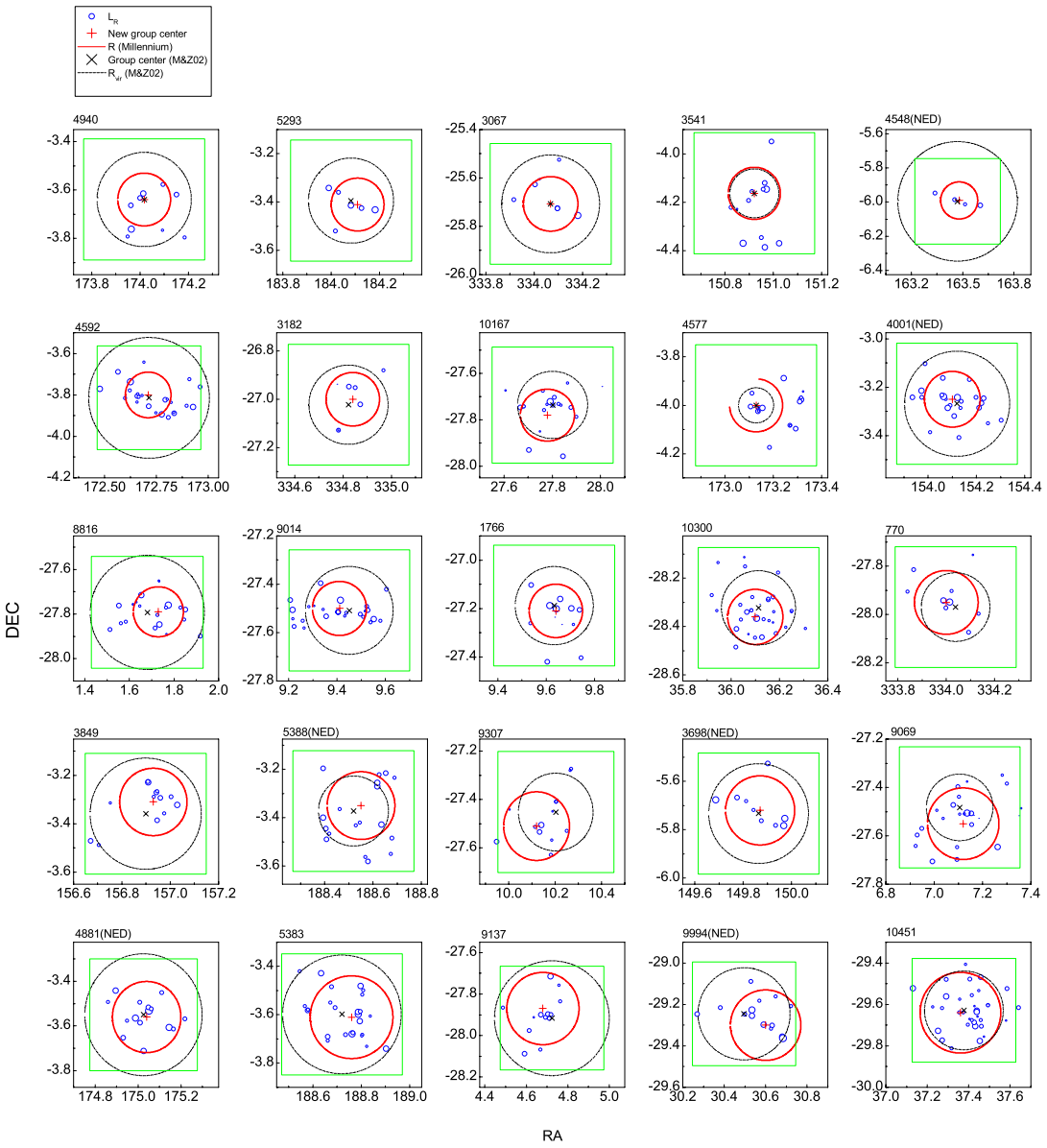

Figure 5.16: Spatial distribution of galaxy members in XI-groups, ordered by ascending group velocity dispersion σ_v from left to right and top to bottom. The *green rectangular* in each panel presents the observed field of view which is the same for all groups and is equal to $\approx 30 \times 30$ arcmin^2. Galaxies are shown with *blue circles* while the circle size is in proportion to galaxy R-band luminosity. The *black-dotted circle* and the *black-cross sign* correspond to group virial radius and group centre measured by Mercha'n & Zandivarez (2002). The *red circle* in each panel shows the group $0.7 \times R_{200}$ (from the Millennium data using Eq. 5.7). Group $0.7 \times R_{200}$ is centred on the new estimated group centre (*red plus sign*) which is the luminosity-weighted mean position estimated according to Eq. 5.8.

This is more clear in Fig. 5.18 where the individual group luminosity functions are stacked together using all group galaxy members, i.e. including all members inside and outside $0.7 \times R_{200}$. The left panel in Fig. 5.18 shows the stacked luminosity function for all 25 groups while on the right (the two small panels), groups are divided into two sub-groups, i.e. low-velocity dispersion ($\sigma_v \lesssim 250$ km s^{-1}) and high-velocity dispersion groups ($\sigma_v \gtrsim 250$ km s^{-1}). The *black line* shows the differential luminosity function while the *red dashed-line* represents the cumulative luminosity function . The plot shows clearly that in either low or high velocity dispersion groups, the spectroscopic sample becomes incomplete at $M_R \gtrsim -20.0$. Therefore, the observed galaxy luminosity function based on the spectroscopic members is not reliable as our imaging data is complete up to $M_R \simeq -16$. In the following sections, I use a different method to study the luminosity function in XI-groups.

5.7.3 Colour-magnitude diagram

Following the aperture photometry in both R and B filters, the $B-R$ colour for all objects as well as group galaxy members is measured as presented in Fig. 5.19. The size of the aperture within which the aperture magnitudes have been estimated in either B or R was selected to be ~ 5 arcsec in diameter. To check the variations in the estimated colour with the selected aperture size, two other different apertures of ~ 4 arcsec and ~ 3.5 arcsec were also examined but results remain the same. So an aperture of ~ 5 arcsec was adopted to find $B-R$ colours.

The *yellow data points* in Fig. 5.19 represent the objects in the observed fields of view. Overlaid are the colour-magnitude diagram for spectroscopically confirmed group members. Galaxy members outside group $0.7R_{200}$ are shown with *green triangles* while *red circles* represent those members which are within group $0.7R_{200}$. The *red line* is a linear fit to all group galaxy members while the *blue dotted lines* are 99% confidence levels. The inset shows the normalised histograms of the $B-R$ colour distribution of group galaxy members inside (*red histogram*) and outside (*green shaded histogram*) group $0.7R_{200}$. A few results emerge from

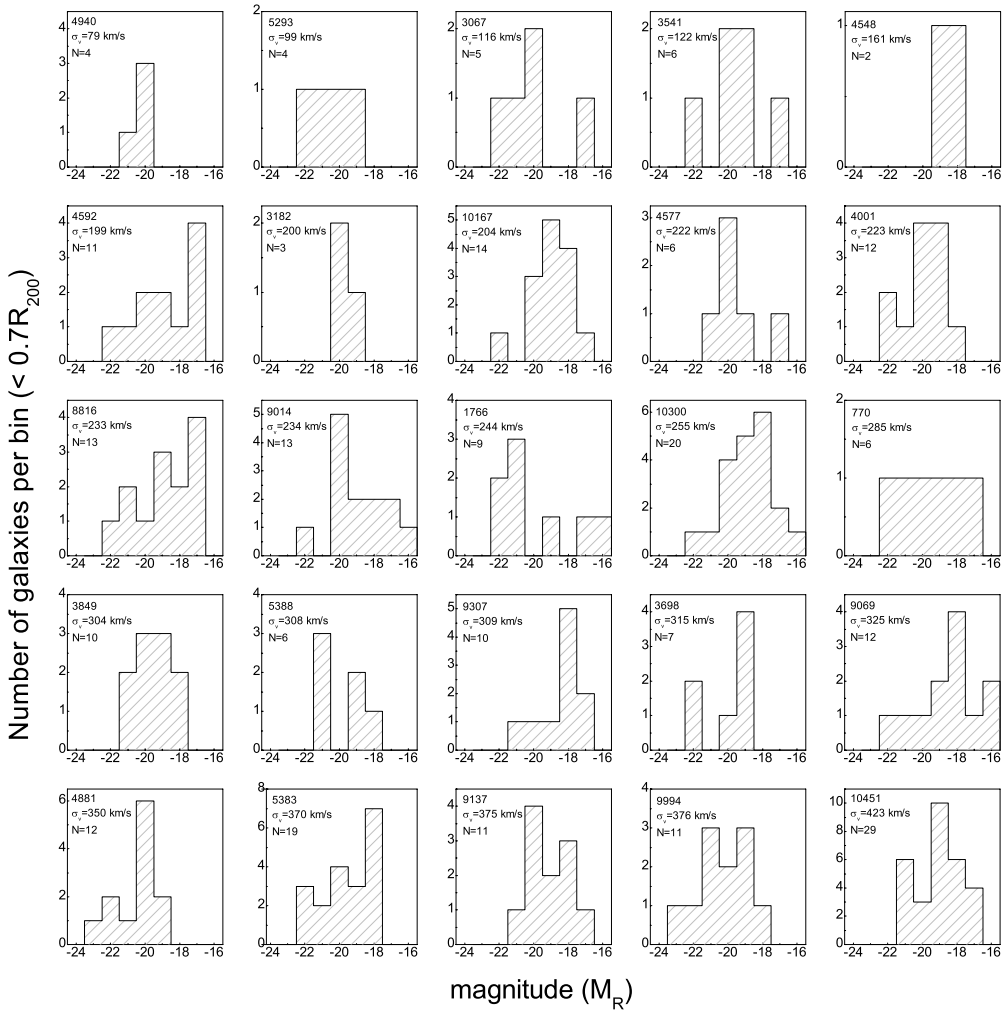

Figure 5.17: Individual group luminosity function calculated within $0.7 \times R_{200}$ from spectroscopically confirmed members, ordered by ascending group velocity dispersion σ_v from left to right and top to bottom.

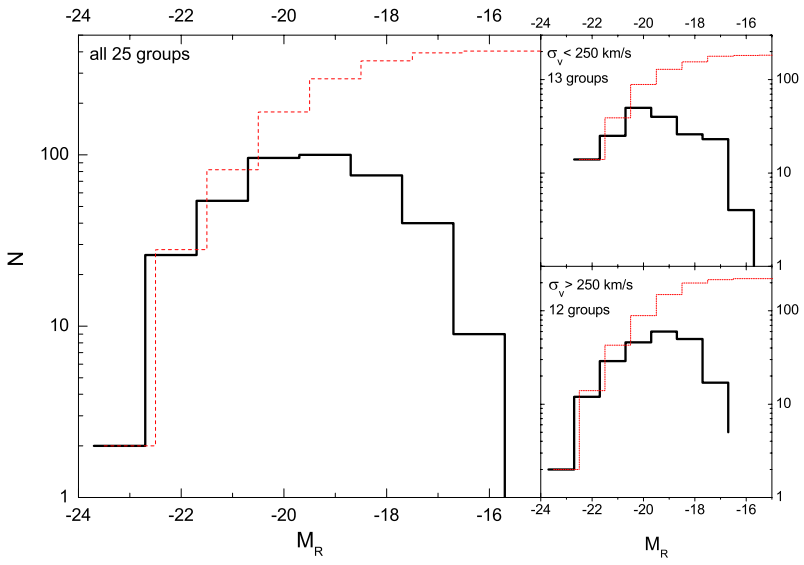

Figure 5.18: Group luminosity function using all spectroscopically confirmed members. The *left panel* shows the stacked luminosity function for all groups while on the *right panels* groups are divided into two sub-groups, i.e. low-velocity dispersion ($\sigma_v \lesssim 250$ km s^{-1}) and high-velocity dispersion groups ($\sigma_v \gtrsim 250$ km s^{-1}). The *black line* shows the differential luminosity function while the *red dashed line* represents the cumulative luminosity function .

Fig. 5.19:

- (i) The R-band photometry is complete up to $m_R \simeq 19$ as the number of objects in the observed fields of view decline at fainter magnitudes.

- (ii) The overall observed $B - R$ colour distribution of group galaxy members does not span a wide range as at all range of apparent magnitude m_R, $1.0 \lesssim B - R \lesssim 2.5$. This is very useful in determining group luminosity functions since one can put an upper limit on the observed colour of galaxies to increase the chance of identifying group galaxy members.

- (iii) The inset shows that those galaxy members inside group $0.7R_{200}$ are in general redder than those outside group $0.7R_{200}$. This suggests that galaxies in the inner regions of group

potential, are brighter, and are more evolved systems in comparison to those which are further away from group central regions. A KS-test on the colour distribution of the two galaxy populations, i.e. those inside and outside group $0.7R_{200}$ shows that the probability that these two distributions are drawn from the same population is just $P \sim 0.03$.

The results from this section will be used in Sec. 5.7.4 in determining group luminosity functions .

5.7.4 The luminosity function of XI Groups

Since in Sec. 5.7.2, we found that the spectroscopically confirmed members in the current status of the survey are incomplete fainter than $M_R = -20$, venture now to examine the luminosity function of a colour-selected sample solely based on the photometric data.

Following the extraction of fluxes and other optical properties for all identified objects using the package SEXTRACTOR (Bertin & Arnouts 1996) objects with stellaricity ≥ 0.95 were removed from the final compiled sample as they are assumed to be definitely stellar objects. Galaxies were selected as being likely group members on the basis of the estimated upper 99% confidence level found in Sec. 5.7.3 from a linear fit to $B - R$ colour of group members. Therefore for all groups, a $B - R$ colour cut-off was applied at

$$B - R = -0.13 \times m_R + 4.6, \tag{5.9}$$

where m_R is the apparent R-band magnitude of any object in the field. Though such a cut in colour removes the majority of background galaxies, there are still contamination from foreground-background objects. To take into account the effect of such objects, a statistical method of background subtraction is applied. To do so, four regions each ~ 5 arcmin in diameter are selected at the corners of each group [mosaic] image (see Fig. 5.20). The average background luminosity function (LF_{BG}) is then found by taking the average over all four re-

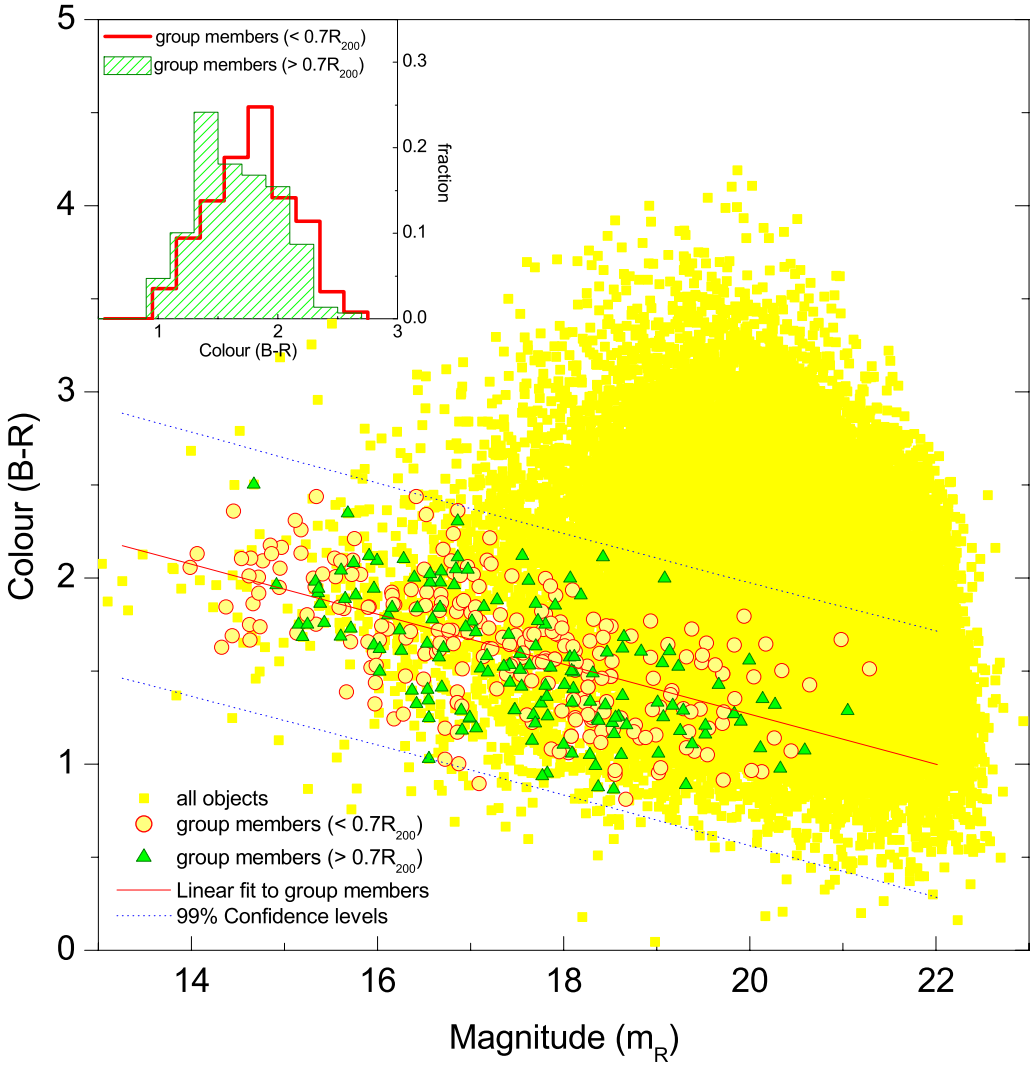

Figure 5.19: The colour-magnitude diagram for all objects within the observed field of views (*yellow data points*). Overlaid are the same for spectroscopically confirmed group members. Galaxy members outside group $0.7R_{200}$ are shown with *green triangles* while *red circles* represent those members which are within group $0.7R_{200}$. The *red line* is a linear fit to all group galaxy members while the *blue dotted-lines* correspond to upper and lower 99% confidence levels. The inset shows the normalised histograms of the $B-R$ colour distribution of group galaxy members inside (*red histogram*) and outside (*green shaded histogram*) group $0.7R_{200}$.

gions.

The [normalised]average luminosity function for all groups and backgrounds are determined separately as illustrated in the Fig. 5.21. This plot shows clearly that the projected density of galaxies within the area of each group is more than those determined from the backgrounds. The plot shows clearly that with the current observation, we can not distinguish between the field objects and group members for objects fainter than $M_R \simeq 20$ mag.

For each group, the final luminosity function was determined by subtracting the normalised background luminosity function from the one extracted for the same group in the R-band. The group R-band luminosity distributions found in this way are shown in Fig. 5.22 for individual groups. On the same plot lines are fitted to the data according to the Schechter function (Schechter 1976)

$$\Phi(M) = (0.4 \ln 10)\Phi^* 10^{0.4(M^*-M)(1+\alpha)} \times \exp\left(-10^{0.4(M^*-M)}\right), \tag{5.10}$$

where Φ^*, M^*, and α are Schechter fitting parameters. Obviously an individual Schechter fit does not necessarily give a reliable information on the nature of these groups as these are relatively poor systems. Therefore, the differential R-band luminosity function of all groups are illustrated in the *right panel* of Fig. 5.23.

Groups are then re-plotted into two categories of high ($\sigma_v \lesssim 250$ km/s) and low ($\sigma_v \gtrsim 250$ km/s) velocity dispersion as is shown in Fig. 5.23 (*middle* and *left* panels respectively). A single Schechter function of the form of Eq. 5.10, yielding best fitting values in R-band as are given in Table. 5.7.4. The *red dashed histograms* in Fig. 5.23 show the R-band luminosity distribution of all spectroscopically confirmed galaxy members within group $0.7R_{200}$. These histograms show clearly that the spectroscopic membership is completed up to for $M_R \lesssim -20.0$, and the spectroscopic information is currently incomplete at fainter magnitudes. The full spectroscopic data have not yet been reduced.

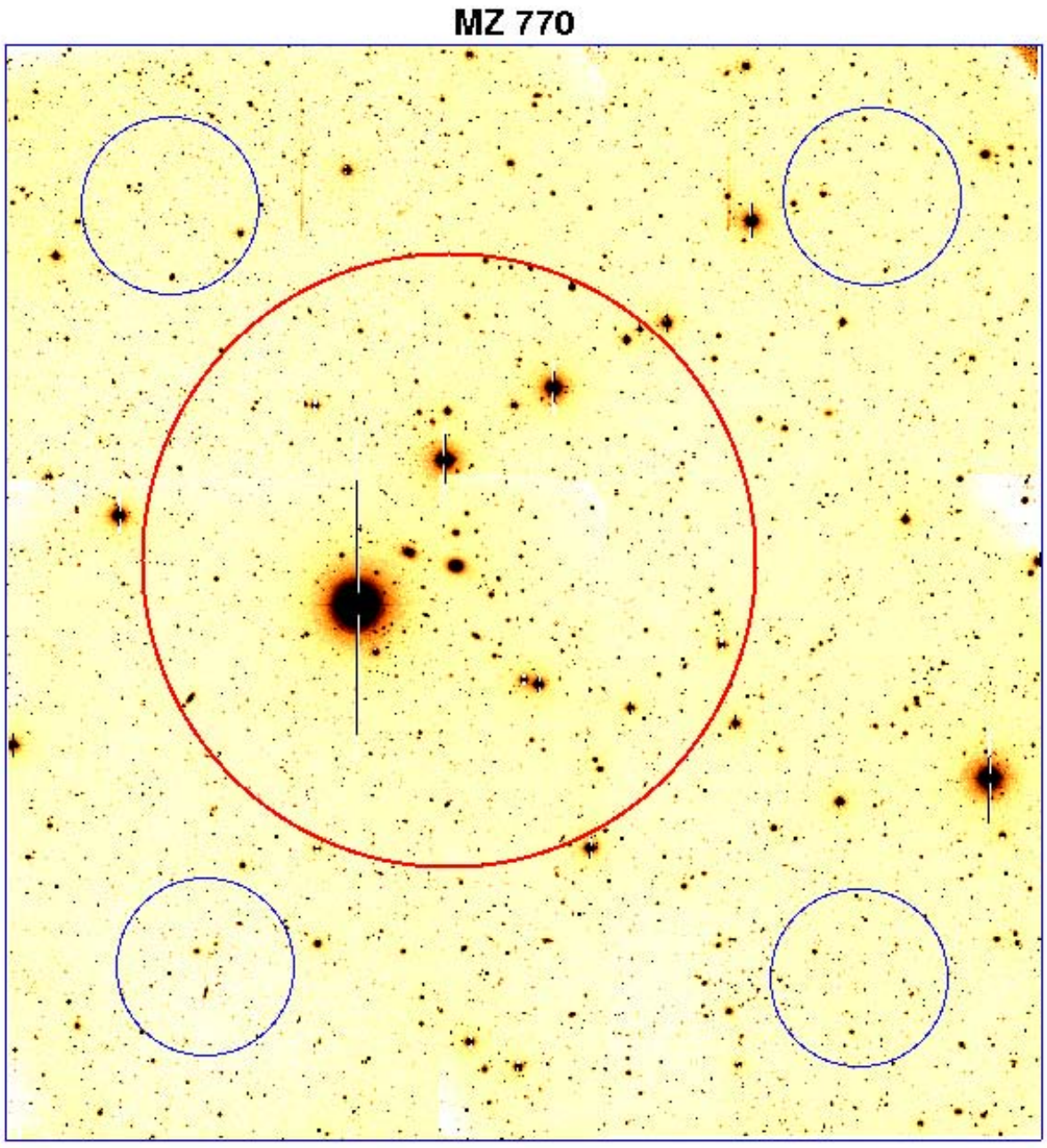

Figure 5.20: The observed mosaic image of MZ 770. The dimension of the image is $\sim 30 \times 30$ arcmin. Four regions (*blue circles*) each ~ 5 arcmin in diameter are selected at the corners of the group in order to perform a statistical background subtraction. The *bold red circle* shows the estimated $0.7R_{200}$ from our study, from which the luminosity function is estimated.

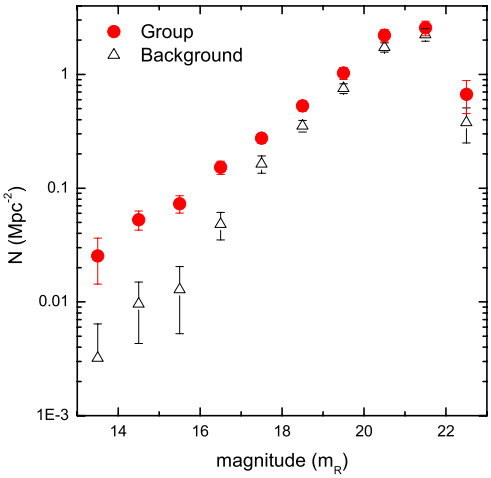

Figure 5.21: The average, normalised luminosity function for all groups (*red circles*) and backgrounds (*triangles*). This plot shows that the projected density of galaxies within the area of each group is more than those determined from the backgrounds, we can not distinguish between the field objects and group members for objects fainter than $M_R \simeq 20$ mag.

5.8 Conclusion

We present the optical properties of a sample of statistically unbiased and redshift selected poor groups as a part of the XMM-IMACS (XI) project. We have performed optical observations in R and B filters using WFCCD camera on the 2.2 m du Pont telescope. The main purpose of imaging of these groups was to perform precise astrometry for the spectroscopic observations with the IMACS multi-slit spectrograph. The estimated offsets in either RA or DEC are $\lesssim$

Table 5.2: Best fitting values of the Schechter function (Eq. 5.10) on the observed group differential luminosity functions in R-band.

Group	M^*	α
all	-22.8 ± 0.7	-1.3 ± 0.1
$\sigma_v \lesssim 250$ km/s	-22.1 ± 0.4	-1.3 ± 0.1
$\sigma_v \gtrsim 250$ km/s	-22.9 ± 0.8	-1.3 ± 0.1

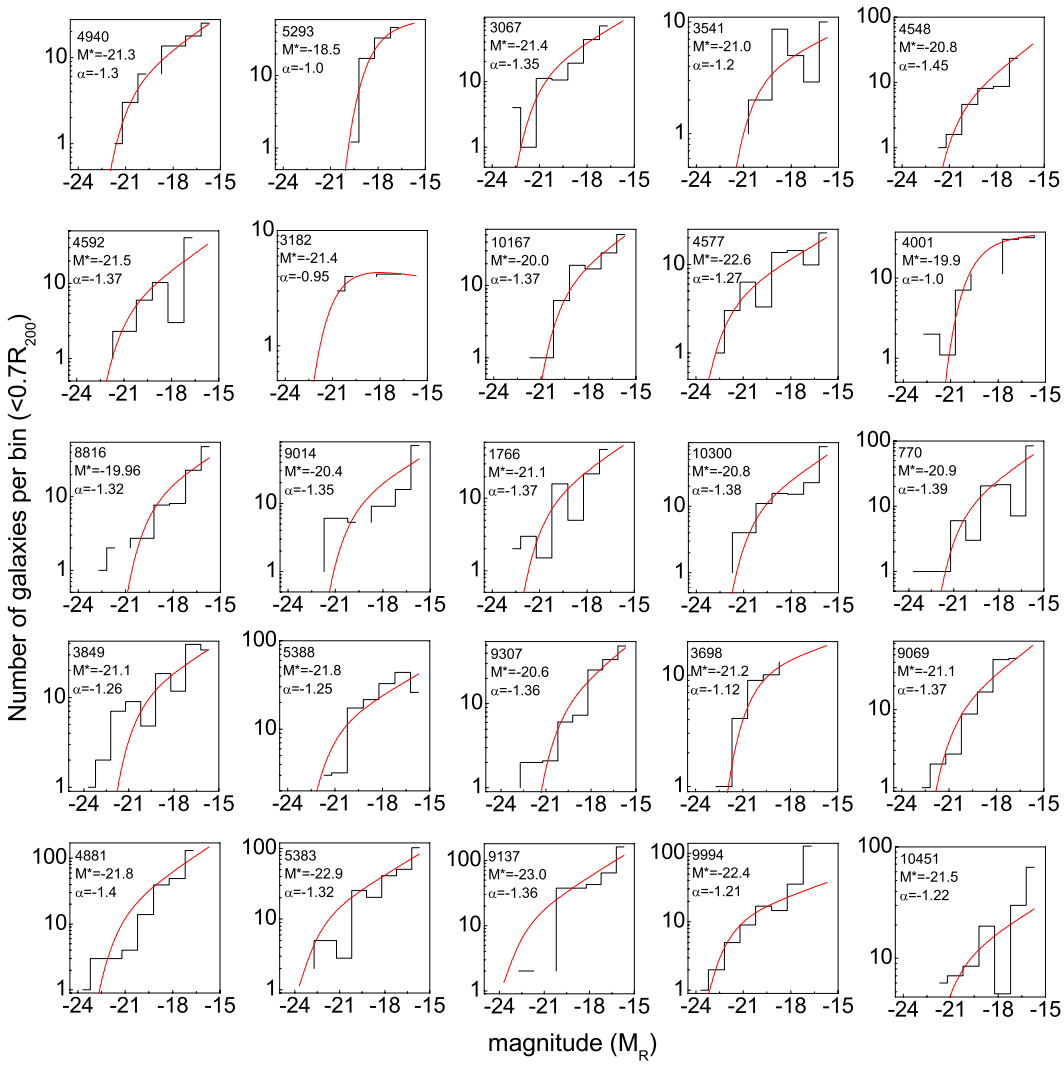

Figure 5.22: The differential group R-band luminosity histograms estimated for individual groups after applying the colour-cut according to Eq. 5.9 and statistical background subtraction. Overlaid on each histogram, is the best Schechter fit according to Eq. 5.10. Groups are ordered by ascending group velocity dispersion σ_v from left to right and top to bottom.

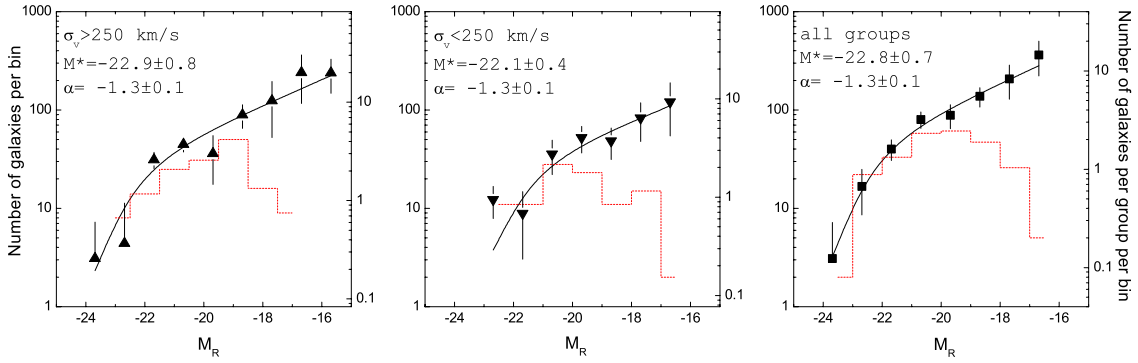

Figure 5.23: Differential R-band luminosity function of all groups (*Right panel*), low-velocity dispersion groups with $\sigma_v \lesssim 250$ km/s (*Middle panel*), and high-velocity dispersion groups with $\sigma_v \gtrsim 250$ km/s (*Left panel*). The parameters for the best Schechter fits *black lines* are given in Table. 5.7.4. The *red dashed histograms* show the R-band luminosity distribution of all spectroscopically confirmed galaxy members within group $0.7R_{200}$.

1.5 arcsec in comparison to those from the USNOA2.0 catalogue. For each group, individual images were combined to make the final mosaic image of the group with a field of view of 30×30 arcmin^2. These images are presented (for one filter) in the Appendix for all the XI groups. Magnitudes were then extracted in both filters following the data reduction of all group images using IRAF and SEXTRACTOR.

Based on the determined group velocity dispersion and the membership, we calculated new positions and virial radii for the group sample. While the former was calculated using the R-band luminosity of the spectroscopic confirmed group galaxies, the latter was determined from the analysis of the Millennium data and the semi-analytic catalogue.

The composite luminosity function of these groups based on their spectroscopic confirmed members suffers from the incompleteness in the spectroscopic observations of these groups though further spectroscopic analysis are underway. We therefore decided to determine the group luminosity function by using the photometric information.

The estimated $B - R$ colour of group members show a positive slope toward the brighter

magnitudes. Such a slope has been observed in clusters (e.g. Gladders et al. 1998). However, unlike clusters the observed slope in our groups is steeper. Here are a few explanations for the existence of such a slope:

1. As group members become brighter, they tend to be redder and hence more massive. We already showed that those galaxies which are in the inner parts of group potential are redder than those which are outside ($\Delta(B-R) \simeq 1.6$). This is because that more massive group galaxies are more evolved than smaller group galaxies.

2. Since structure forms hierarchically, most of the bright galaxies in clusters have been already evolved to some degree in a group-like environment before they fall into the cluster gravitational potential. Therefore though galaxies in clusters form the red sequence, their colour should not be much different from one another. This is not the case in groups where the chance that the infalling galaxies belong to the field is more that those that fall into clusters.

3. Preliminary results of Rasmussen et al. (2006) show that the current sample of groups are possibly a mix of X-ray marginally luminous groups as well as groups which are collapsing for the first time. Such a mix is apparent in the colour-magnitude diagram since the group galaxy population is a mix of highly evolved, massive and red galaxies with a population of intermediate size, or satellite galaxies belonging to non-virialized, collapsing groups.

To quantify different scenarios, more spectroscopic and X-ray information of groups are necessary. For example we have to see whether such an observed slope in colour-magnitude relation changes if we split the sample into X-ray detected and non-detected groups, or even classify the galaxies according to their morphology.

The determined composite luminosity function of XI-groups is similar to the results given by Zabludoff & Mulchaey (2000) who found $M_R^* = -21.6 \pm 0.4 + 5\log h$ and $\alpha = -1.3 \pm 0.1$

for a sample of six poor groups (all spectroscopically observed) out of which five were X-ray detected. Also Trentham & Tully (2002) and Mahdavi, Trentham, & Tully (2005) found similar results to what we have presented. It is interesting since unlike these studies, our groups are optically selected groups though so far X-ray emission has been detected in three out of nine XI-groups.

Bibliography

Bertin, E. & Arnouts, S., 1996, A&AS, 117, 393

Bower, R.G., Benson, A.J., Malbon, R., Helly, J.C., Frenk, C.S., Baugh, C.M., Cole, S., Lacey, C.G., 2006, MNRAS, 370, 645

Gladders, M.D., Lopez-Cruz, O., Yee, H.K.C.,Kodama, T., 1998, ApJ, 501, 571

Sengupta, C., Raychaudhury, S., Mulchaey, J.S., Dariush, A., Dwarakanath, K.S., Ponman, T.J., 2009 (in preparation)

Haynes, M.P. & Giovanelli, R., 1984, AJ, 89, 758

Huchra, J.P. & Geller, M.J., 1982, ApJ, 257, 423

Lupton, R. & Ivezic, Z., ASPC, 338, 151

Mahdavi, A., Trentham, N., Tully, R.B., 2005, AJ, 130, 1502

Mateo, M., 1998, ARA&A, 36, 435

Mercha'n, M. & Zandivarez, A., 2002, MNRAS, 335, 216

Osmond, J.P.F. & Ponman, T.J., 2004, MNRAS, 350, 1511

Rasmussen, J., Ponman, T.J., Mulchaey, J.S., Miles, T.A., Raychaudhury, S., 2006, MNRAS, 373, 653

Roberts, M.S. & Haynes, M.P., 1994, ARA&A, 32, 115

Schechter, P.L., 1976, ApJ, 203, 297

Schlegel, D.J., Finkbeiner, D.P., Davis, M., M., 1998, ApJ, 500, 525

Springel, V., White, S.D.M., Jenkins, A., Frenk, C.S. et al., 2005, Natur, 435, 629

Stetson, P.B., 2000, PASP, 112, 925

Sung, H., Bessell, M. S., 2000, PASA, 17, 244

Trentham, N. & Tully, R.B., 2002, MNRAS, 335, 712

Zabludoff, A.I. & Mulchaey, J.S., 2000, ApJ, 539, 136

Chapter 6

Conclusions and future work

6.1 Summary of results

The motivation of the current research and the work presented in this thesis is to study the formation of old galaxy systems and its connection to observable properties of galaxy groups. It has being implied by several authors (e.g. Ponman & Bertram 1993; Ponman et al. 1994; Jones et al. 2003) that old groups can be characterized from their X-ray luminosities as well as the luminosity gap between the first and the second ranked galaxies in the R-band within half the projected virial radius of the group centre.

Following this, Jones et al. (2003) suggested that such old groups, i.e. *fossil galaxy groups* could be identified based on two criteria: (i) $\Delta m_{12} \geq 2$, and (ii) $L_{\rm X,bol} \geq 0.25 \times 10^{42} h^{-2}$erg s^{-1}. To test this hypothesis, and to find the limitations of the use of fossil galaxy systems in current cosmological analyses, we studied the evolution of present-day fossil galaxy groups (groups with $\Delta m_{12} \geq 2$ and $L_{\rm X,bol} \geq 0.25 \times 10^{42} h^{-2}$erg s^{-1}) in the Millennium Simulation (Springel et al. 2005), and its various associated catalogues which provide useful sources of data for our purpose. The large simulated volume and number of particles of the Millennium Simulation enable us to study thousands of halos within the mass range of galaxy groups.

Using the corresponding Millennium gas simulation and semi-analytic galaxy catalogues (Croton et al. 2006), we selected fossil groups at redshift zero according to the conventional observational criteria, and traced the halos corresponding to these groups backwards in time, extracting the associated dark matter, gas and galaxy properties. The space density of the fossils from our study is remarkably close to the observed estimates (e.g. Jones et al. 2003) and various interpretations for the remaining discrepancies are discussed.

In Chapter 2 we find that the fraction of X-ray bright systems which are fossils appears to be in reasonable agreement with observation, and the simulations predict that fossil systems will be found in significant numbers (3-4% of the population) even in quite rich clusters. Furthermore, it was found that fossils assemble a higher fraction of their mass at high redshift, compared to non-fossil groups, with the ratio of the currently assembled halo mass to final mass, at any epoch, being about 10 to 20% higher for fossil than for non-fossil groups. This supports the paradigm whereby fossils mostly represent undisturbed, early-forming systems in which large galaxies have merged to form a single dominant elliptical.

Though our initial results were in agreement with observational studies of fossil galaxy groups, further investigations into these issues were necessary since (i) The mass assembly history of halos were traced back up to $z \sim 0.55$ and for a sample of $\sim$400 groups, and (ii) the semi-analytic model used was based on the simulated dark matter halos at z=0 which did not let us follow the evolution of the magnitude gap at different redshifts.

Therefore, the mass assembly of groups and clusters of galaxies, in particular the development of the magnitude gap between their two brightest galaxies, was studied in Chapter 3 using the Millennium dark matter simulation and the associated Millennium gas simulations, and semi-analytic catalogues of galaxies of Bower et al. (2006) which was found to better agree with observations than Croton et al. (2006).

We selected $\sim 2 \times 10^4$ galaxy groups at redshift z=1 with dark matter halo mass $M(R_{200}) \geq 10^{13}\, h^{-1}\, \mathrm{M}_{\odot}$, and traced their properties until the present time (z=0). We found that the con-

ventional definition of fossil galaxy groups based on the magnitude gap $\Delta m_{12} \geq 2$ (within R_{200} or $0.5\,R_{200}$) does not fulfil the requirement for a group or cluster to be a genuine old system with an early mass assembly. Furthermore, the selection of fossil groups based on $\Delta m_{12} \geq 2$ does not guarantee that the system remains in a [fossil phase] for a long time. In other words, the fossil phase (where the optical criterion for fossil identification is $\Delta m_{12} \geq 2$) is a temporary phase in the life of groups, and most groups would pass through such a phase in their lifetime.

In addition, our results reveal a weak correlation between the magnitude gap among bright group galaxies and group mass assembly history. We attempt to revise the current optical definition of fossil groups by studying the evolution and history of various physical parameters associated with galaxy groups and clusters, to establish a more meaningful connection with the evolutionary state of the group. However, our results from Chapter 3 show that the identification of old groups, on the basis of their large magnitude gap among their brightest galaxies, does not necessarily separate genuine old galaxy systems from younger ones. In other words, an early-formed group does not necessarily have a large magnitude gap.

Finally we presented the results from imaging of the XI (XMM/IMACS) Groups Project, a study targeting, for the first time, an optically selected, statistically unbiased sample of 25 poor galaxy groups (Rasmussen et al. 2006) at the same redshift. The project aims to advance the understanding of how the properties and dynamics of group galaxies relate to global group properties via a combination of radio observations of cold gas, X-ray observations, and optical imaging and spectroscopy of the galaxy population. Observations and precise astrometry was done for IMACS follow-up spectroscopic observations in order to find group galaxy members and their redshifts. From the extracted group members the centroids plus size of groups was estimated. Though at the time of writing this thesis, the spectroscopy (as well as X-ray observations) of these groups have not been completed, however our initial results show that (i) group galaxy members follow a red sequence on colour magnitude diagram with a slope greater than those observed in clusters, and (ii) the estimated group luminosity function can be fitted with

a single Schechter function (Schechter 1976) with best Schechter fitted parameters similar to those observed in normal and poor groups.

6.2 Future work

6.2.1 Formation and evolution of galaxy groups

One reason that makes cosmological N-body simulations an important tool is that one can study the evolution of astronomical objects at different redshifts. In addition, using different types of simulations such as dark matter simulations together with those from semi-analytic models (of formation and evolution of galaxies), enables us to investigate and correlate the observables with dark matter halo properties. The semi-analytic models are under development as they do not yet take into account all physical processes that exist in the real world. For example, there has been a recent attempt to develop simple analytic models that describe the gas stripping of the hot gaseous halos of galaxies as they fall into massive groups and clusters (McCarthy et al. 2008). Such modification make the predictions from semi-analytic models more reliable in studying the formation of galaxy groups and clusters.

Using the Millennium simulation, the evolution of groups was carried out by studying their halo mass assembly in time while groups were classified according to their semi-analytic optical properties. Such a study could be optimised if the dark matter density profile of group halos were taken into account. In other words, from the shape of the density of group halos and their deviations from NFW profile of Navarro, Frenk, & White (1996), groups could be classified into early and late formed in a more efficient way. In this way, the group semi-analytic optical properties in comparison with the observed properties of fossil groups, can be used to tune the parameters used in such semi-analytic models.

In addition the cosmo-dynamical evolution of groups can be investigated using the Millennium simulation and be compared with the theoretical models. Theoretical studies of Mamon

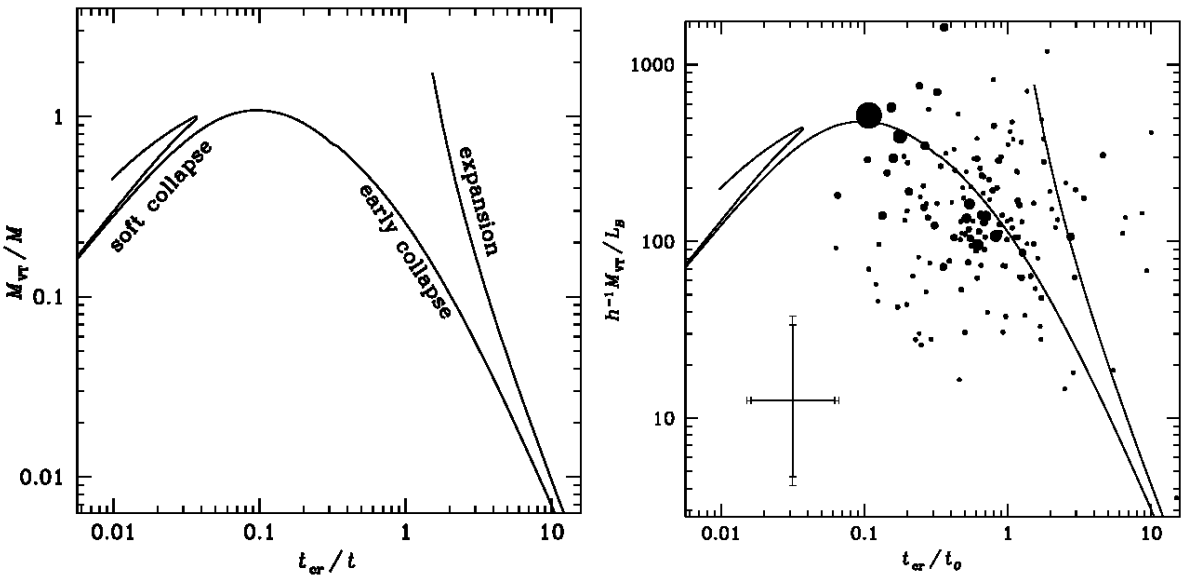

Figure 6.1: Cosmo-dynamical evolution of galaxy systems. The *left panel* shows the theoretical evolution of an isolated binary system of two extended subgroups of very different masses, with no specific angular momentum. The *right panel* shows observed groups (Fouqué et al. 1992; Gourgoulhon et al. 1992), with increasingly larger symbols for richer groups. The largest symbol is the Virgo cluster (Credit: Mamon 2006).

(2006) predict that the members of group follow a track during its dynamical evolution as is shown in Fig. 6.1. Since from the dark matter simulations, we have the dynamical information for the particles, we would like to classify the Millennium groups in our sample into various stages of formation, and find which observable properties can be used to characterise them.

6.2.2 Scaling relation in groups: Is the scatter due to epoch of formation?

Khosroshahi, Ponman, & Jones (2007) presented various X-ray scaling relations in fossil groups with high-resolution X-ray data from Chandra observations and argued that the deviations in the observed scaling relation in fossils in comparison to those of normal groups, indicate that these systems are indeed early formed groups. Taking into account the observed scatter in studies of this kind, it is very difficult to compare the observed scaling relations with those extracted from the simulations. This is clear from Fig. 6.2 where it shows the simulated $L_X - T$ scaling

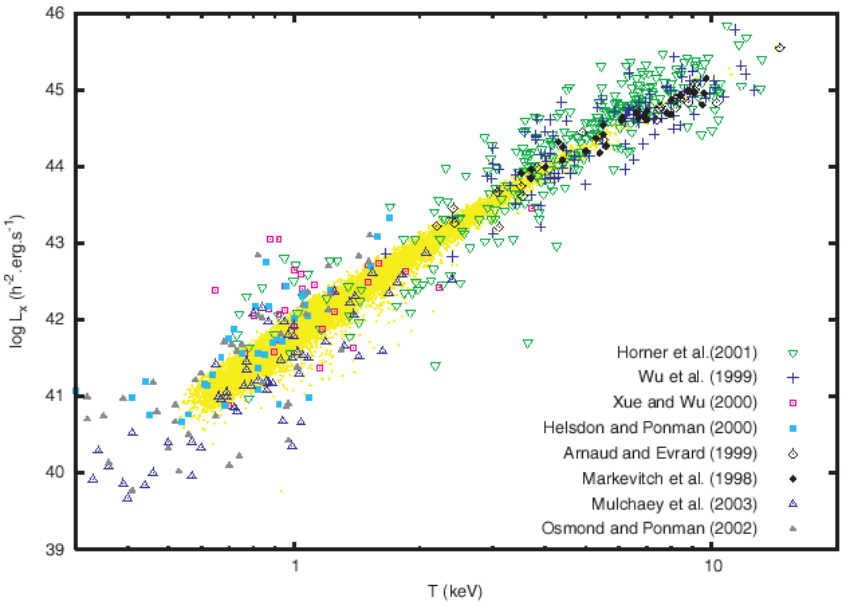

Figure 6.2: Compilation of low redshift observed group and cluster X-ray luminosities within r_{500}, compared to their emission-weighted temperature. The small points are the simulated groups and clusters from the hydrodynamical simulation of the gas particles based on the Millennium dark mater run (Credit: Hartley et al. 2008).

relation from the Millennium gas catalogue in comparison to several other studies from the observations (Hartley et al. 2008). However, we can study various scaling relations for early-formed, late-formed systems using the Millennium simulations and make a detailed comparison between them and find whether the epoch of formation is related to the origin of the scatter in these relations. The results of such comparison is interesting but it needs a careful analysis in selecting the early-formed, late-formed groups from the simulated data.

Group Scaling relations from the Millennium catalogues

Values of the overdensity radius R_{200} were computed for a sample of over 50,000 group-sized halos, in Chapter 4, and a simple relation was found between them and the velocity dispersion of the halos. This relation was used to define the regions over which the luminosity function of the XI groups were determined in Chapter 5.

In principle, such relations can be found by merging the Millennium DM catalogues, and

the corresponding gas catalogues and the semi-analytic galaxy catalogues (as used in Chapters 2 and 3), over a wider range of mass (for groups and clusters), keeping in mind the limitations of each catalogue. These will be useful for the general community. We plan to determine such relations between velocity dispersion and r_{200}, obtained from the DM catalogues, and gas parameters like X-ray luminosity and temperature (also see Hartley et al. 2008), as well optical parameters like luminosity profiles (NFW parameters) and blue galaxy fraction in a later paper (Dariush et al. 2009, in preparation). We will relate these to the observed properties in various samples, including the XI groups sample.

6.2.3 XI groups-future work

Currently the spectroscopic analysis of XI-groups, which is based on the optical imaging presented in the current thesis is not finished yet, even though all the spectroscopic observations using the IMACS instrument on the Badde/Magellan telescope have been completed. As was explained in Chapter 5, further analyses have to be done with the photometric data as soon as the spectroscopic analysis is completed.

Group size and position

As groups in the XI sample are essentially poor groups, it is very important to find the correct centre for each group before study their luminosity functions. We found new group centres from the observed R-band luminosity of spectroscopic confirmed group members by finding their *luminosity weighted mean position*. However, the estimated position for 5 groups (e.g. MZ 3698, MZ 4001, MZ 4548, MZ 4881, and MZ 5388) was based upon the members found using the NASA/IPAC Extragalactic Database (NED), though for the rest 20 groups, group memberships were still incomplete at the time of writing this thesis.

Also we have imaging and photometric information in both B and R which enable us to do weighting the central position of groups according to their stellar mass rather than simply

from their R-band luminosities (see for example Table.1 in Bell & de Jong 2001). Therefore, we need to re-calculate both centres and virial radii as well as group member colour and the luminosity functions when the final spectroscopic information is available.

Cold gas in groups

The surface density (or deficiency) of neutral hydrogen in disk galaxies, and in the inter-galactic medium in groups, is indicative of the level of stripping due to tidal effects of galaxies as well as ram pressure of the IGM, and thus provides information about the nature of the state of evolution of a group. It has be shown (e.g. Sengupta & Balasubramanyam 2006; Sengupta, Balasubramanyam, & Dwarakanath 2007) that galaxies in X-ray bright groups are in general more HI-deficient than in X-ray faint groups, though no significant correlation is found between the diffuse X-ray luminosity of groups (L_X) and the HI deficiency of their galaxies. So the HI deficiency may be indicative of the the state of evolution the group is in, rather than any one of the detailed physical processes that lead to stripping. We would like to investigate this with the XI groups. We have already observed 3 XI groups at 1420 MHz with GMRT, where high levels of HI deficiency are being found (Sengupta et al. 2009, in preparation). I have been measuring the D_{25} values from the R-band images for the XI groups, since from these the HI deficiency values are calculated, and my colleagues are conducting the 21-cm observations. This project will be extended further with the VLA, and I will provide the optical input to this project.

Morphological studies of group members

An important ingredient in studying the dynamical status of groups is to investigate the diversity in the physical shape of group galaxy members. From the current study, we already know that galaxies in the inner parts of the groups are redder than those in the outer parts the others but how does the morphology of these galaxies change with radial distance from the group centres?

Another point of investigation is whether the fundamental plane parameters (e.g. Sérsic

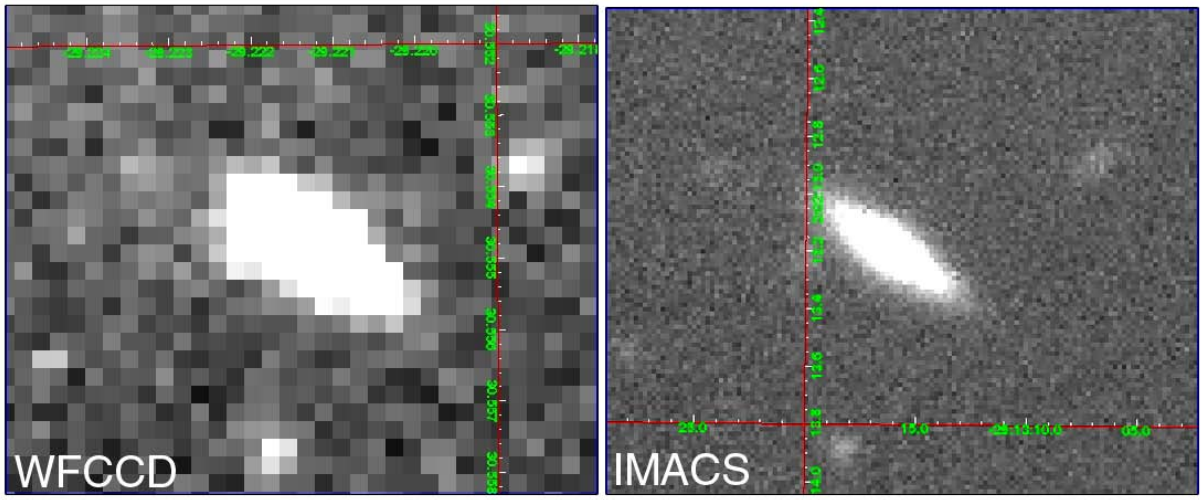

Figure 6.3: A comparison between two images taken from the same galaxy in MZ 9994 with the du Pont WFCCD camera with plate scale ~ 0.8 arcsec/pixel (*left panel*) and IMACS wide-field imager with ~ 0.2 arcsec/pixel (*right panel*).

index) of galaxies vary according to their position in groups, or the kind of group they are in (e.g. Khosroshahi et al. 2004). This is why we had originally planned to perform a detailed morphological analysis of each galaxy-by fitting two dimensional model (Sérsic+exponential) to each of the galaxy images in our sample.

Unfortunately the optical resolution of the currently reduced du Pont images does not let us to do a proper morphological analysis of group members. The plate scale of du Pont WFCCD is ~ 0.8 arcsec/pixel while the same is ~ 0.2 arcsec/pixel for the IMACS wide-field imager (calibrated with a 8192 x 8192 CCD array with 27×27 arcmin FOV) installed on the Magellan/Baade telescope. We now have direct IMACS images of all of our groups taken at the time of the spectroscopic observations.

Fig. 6.3 shows a comparison between two images taken from the same galaxy with the du Pont WFCCD camera with plate scale ~ 0.8 arcsec/pixel (*left panel*) and IMACS wide-field imager with ~ 0.2 arcsec/pixel (*right panel*). Note that this galaxy is a typical medium size galaxy and our groups have many smaller galaxies than the one shown in Fig. 6.3.

To investigate to what extent such difference in pixel size might affect our results of group

members, we analyse the morphology on a few different galaxy sizes using images from both instruments and compare the estimated parameters in each case. Figs. 6.4 and 6.5 illustrates the morphology study of two of our group members using the galaxy/point source fitting algorithm (GALFIT; Peng et al. 2002). In each figure, the *left-top panel* represents an image taken with du Pont WFCCD while *left-bottom panel* shows the image of the same galaxy, taken with IMACS imager. Also in each figure and from left to right, the panels correspond to the **original**, **model**, and **residual** images of the same galaxy. The radial profile of model galaxies in each figure is based on the Sérsic profile with the following functional form:

$$\Sigma(r) = \Sigma_e \exp\left[-k\left(\left(\frac{r}{r_e}\right)^{1/n} - 1\right)\right], \tag{6.1}$$

where Σ_e is the pixel surface brightness at the effective radius r_e, and parameter n refers to as the *concentration parameter* or the Sérsic index. The estimated concentration parameters for the galaxy in Fig. 6.4 are $n = 1.06$ (WFCCD) and $n = 1.05$ (IMACS) respectively. These two numbers are not very different as the galaxy is relatively large but in case of the smaller galaxy shown in Fig. 6.5, the calculated concentration parameters are very different with $n = 1.80$ (WFCCD) and $n = 1.34$ (IMACS).

Therefore the morphological parameters change significantly if the galaxy is small and the signal-to-noise per pixel is not good, or if there are not enough pixels in the image. We also tried to apply the PSF corrections to the low-resolution WFCCD images. However, the results do not change noticeably as the PSF of the du Pont images are very large (~ 1.9)arcsec. Since most of the group members are small galaxies, similar to the one shown in Fig. 6.5, it is better to use IMACS images for morphological classification of galaxies in our group sample. The IMACS observations have been completed for all groups. Further reduction, image processing and data analysis will be in the future.

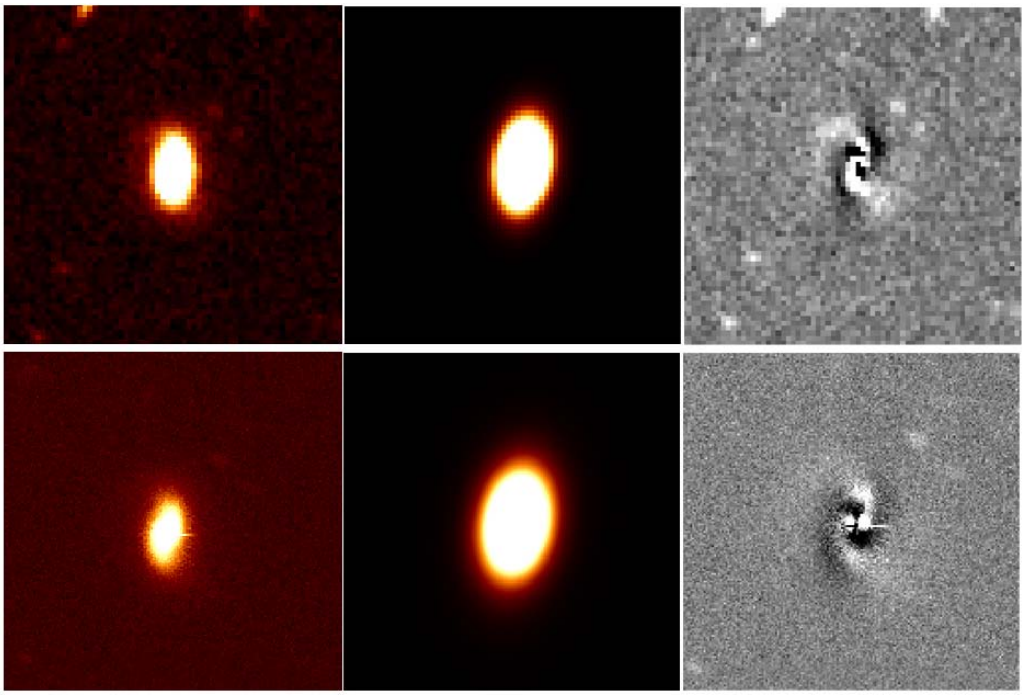

Figure 6.4: Morphological study of a galaxy member belongs to MZ 9014. The *left-top panel* represents an image taken with du Pont WFCCD while the *left-bottom panel* shows the image of the same galaxy, taken with IMACS imager. From left to right, the panels correspond to the **original**, **model**, and **residual** images of the same galaxy. The radial profile of model galaxies (*middle panels*) is based on the Sérsic profile (e.g. Eq. 6.1) with the concentration parameters $n = 1.06$ (WFCCD) and $n = 1.05$ (IMACS) respectively.

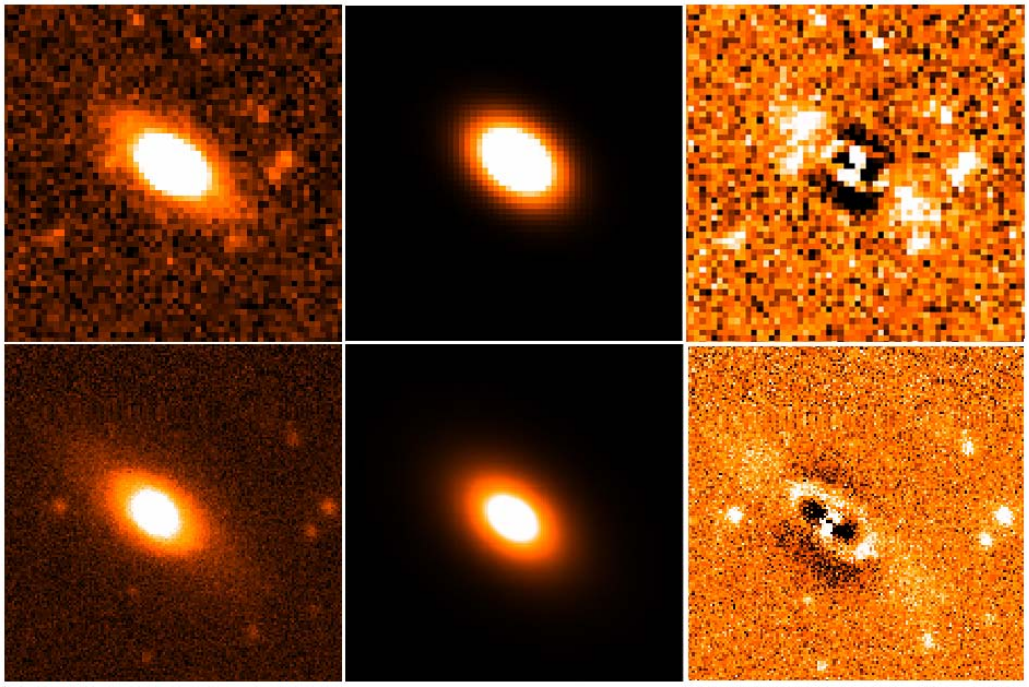

Figure 6.5: The same as in Fig. 6.4 but for a galaxy member belongs to MZ 770. The calculated concentration parameters are $n = 1.80$ (WFCCD) and $n = 1.34$ (IMACS).

6.2.4 GEMS groups

The GEMS catalogue of Osmond & Ponman (2004) consists of s subset of 60 galaxy groups with measured X-ray fluxes from ROSAT PSPC pointed observations. From optical and infrared studies of these group (e.g. Miles et al. 2004 and Miles, Raychaudhury, & Russell 2006) it has been found that the luminosity function of galaxy groups with X-ray luminosity $L_X \lesssim 10^{41.7}$ erg s^{-1} is bimodal. They interpreted this bimodality in the observed luminosity function as a result of enhanced dynamical friction between galaxies in X-ray dim groups (low velocity dispersion), thus resulting in rapid major mergers. This causes galaxies with intermediate luminosity to merge with each other and the brightest group galaxies.

Further questions arise such as: (i) Can a study of morphology of galaxies in these groups support this scenario? and (ii) Is the evolutionary history of X-ray bright groups ($L_X \gtrsim 10^{41.7}$ erg s^{-1}) similar to that of clusters, as the similarity in the form of their luminosity functions

seems to indicate? Therefore, following the work of (Miles, Raychaudhury, & Russell 2006) we intended to study a X-ray selected sample of groups ($L_X \gtrsim 10^{41.7}$ erg s^{-1}) using ESO 2.2m/WFI photometry. On an observing run during March 2006, I observed six X-ray bright GEMS groups (e.g. HCG042, HCG048, NGC3557, NGC3923, NGC4697, HCG062, HCG067) on 5 nights at the the 2.2-m MPG/ESO telescope using The Wide Field Imager (WFI). We however did not have the time to analyse the data fully to include in this thesis.

The newly observed groups together with the previously compiled sample would help us address the following issues:

- Computes luminosity functions of the sample to see whether X-ray bright groups (i.e. groups with high velocity dispersion) have luminosity functions characterised by a single Schechter function as clusters do,
- Morphology of galaxies in rich groups,
- Global Photometric Properties and the Scaling Relations, and
- Dynamical properties of groups.

We have obtained 6dF redshifts for about 20 galaxies per group for all our groups as well as optical wide-field CCD data for the rich groups in the GEMS sample. Thus we have velocity dispersion profiles as another ingredient in our investigation to probe the link between the dynamical history of the group and its evolution. The observations were completed in March 2006 and preliminary reduction for this sample has been done. But our attention was diverted to work on the Millennium groups, and to the XI sample, and thus work is yet to be completed.

Bibliography

Bell, E.F. & de Jong, R.S., 2001, ApJ, 550, 212

Bower, R.G., Benson, A.J., Malbon, R., Helly, J.C., Frenk, C.S., Baugh, C.M., Cole, S., Lacey, C.G., 2006, MNRAS, 370, 645

Dariush, A., Darakanath, K.S., Ponman, T.J., 2009 (in preparation)

Gourgoulhon, E., Chamaraux, P., Fouqué, P., 1992, A&A, 255, 69

Jones, L.R, Ponman, T.J., Horton, A., Babul, A., Ebeling, H. and Burke, D.J., and Forbes, D.A., 2003, MNRAS, 343, 627

Croton, D.J., Springel, V., White, S.D.M., De Lucia, G., Frenk, C.S., Gao, L., Jenkins, A., Kauffmann, G., Navarro, J.F., Yoshida, N., 2006, MNRAS, 365, 11

Fouqué, P., Gourgoulhon, E.,Chamaraux, P., Paturel, G., 1992, A&AS, 93, 211

Hartley, W.G., Gazzola, L., Pearce, F.R., Kay, S.T., Thomas, P.A., 2008, MNRAS, 386, 2015

Khosroshahi, H.G., Raychaudhury, S., Ponman, T.J., Miles, T.A., Forbes, D.A., 2004, MNRAS, 349, 527

Khosroshahi, H.G., Ponman, T.J., Jones, L.R., 2007, MNRAS, 377, 595

Mamon G.A., 2006, arXiv[astro-ph]:0607482v2

McCarthy, I.G., Frenk, C.S., Font, A.S., Lacey, C.G., Bower, R.G., Mitchell, N.L., Balogh,

M.L., Theuns, T., 2008, MNRAS, 383, 593

Miles, T.A., Raychaudhury, S., Forbes, D.A., Goudfrooij, P., Ponman, T.J., Kozhurina-Platais, V. et al., 2004, MNRAS, 355, 785

Miles, T.A., Raychaudhury, S., Russell, P.A., 2006, MNRAS, 373, 1461

Navarro, J.F., Frenk, C.S., White, S.D.M., 1996, ApJ, 462, 563

Osmond, J.P.F. & Ponman, T.J., 2004, MNRAS, 350, 1511

Peng, C.Y., Ho, L.C., Impey, C.D., Rix, H-W, 2002, AJ, 124, 266

Rasmussen, J., Ponman, T.J., Mulchaey, J.S., Miles, T.A., Raychaudhury, S., 2006(b), MNRAS, 373, 653

Schechter, P.L., 1976, ApJ, 203, 297

Sengupta, C. & Balasubramanyam, R., 2006, MNRAS, 369, 360

Sengupta, C., Balasubramanyam, R., Dwarakanath, K.S., 2007, MNRAS, 378, 137

Sengupta, C., Raychaudhury, S., Mulchaey, J.S., Dariush, A., Dwarakanath, K.S., Ponman, T.J., 2009 (in preparation)

Springel, V., White, S.D.M., Jenkins, A., Frenk, C.S. et al., 2005, Natur, 435, 629

Appendix A

In the appendix, we present the R-band images (mosaiced from 2×2 pointings), using the WFCCD camera on the 2.5-meter (100-inch) Irénée du Pont telescope, operating at Las Campanas Observatory. Data obtained in in August/September 2006, December 2007, and April/May 2008. Details of data reduction are presented in Chapter 5, and a summary of the properties of the groups are given by Table 4.1 of Chapter 4 and Table 5.2 of Chapter 5. Each image is $\sim 30 \times 30$ arcmin^2.

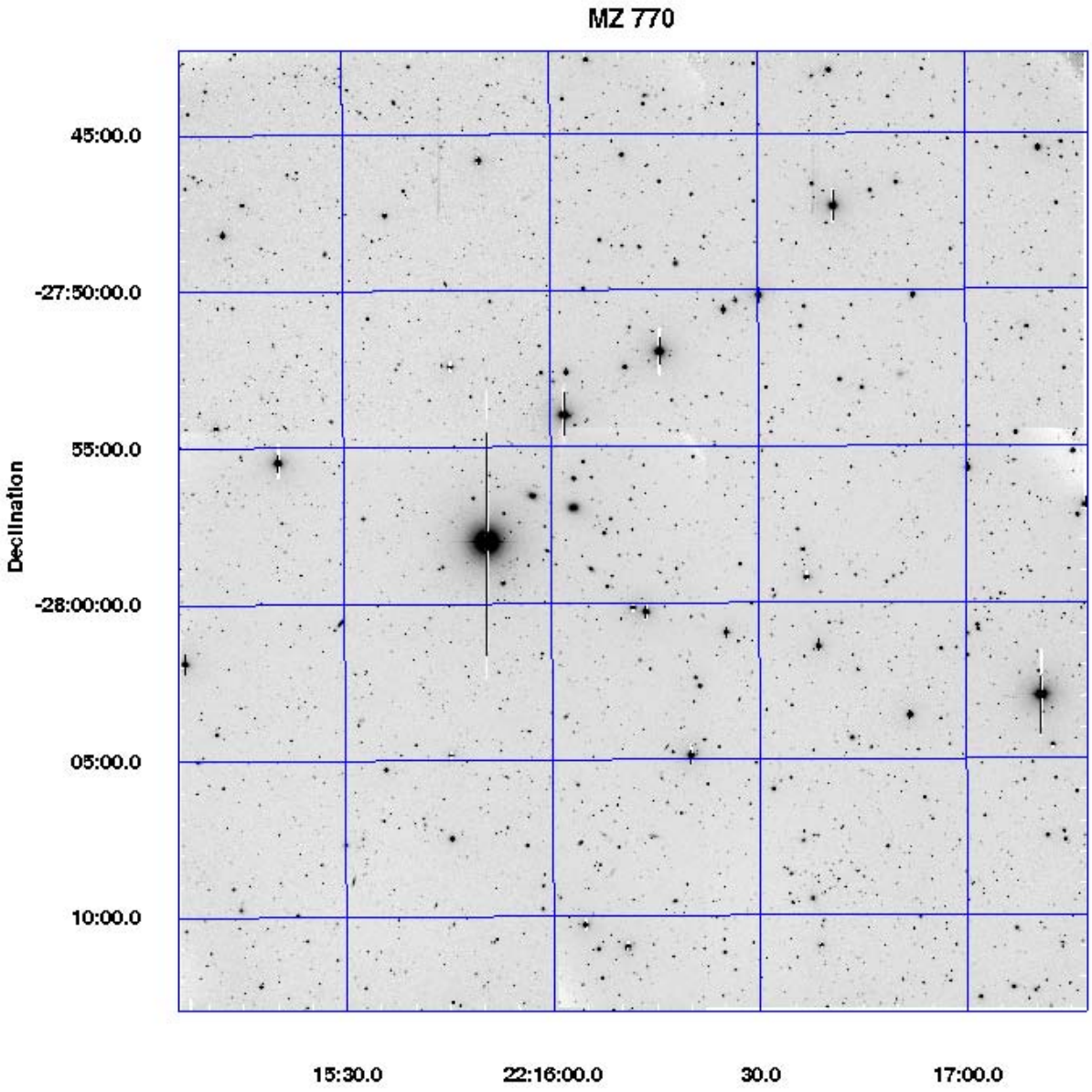

Figure A.1: MZ 770

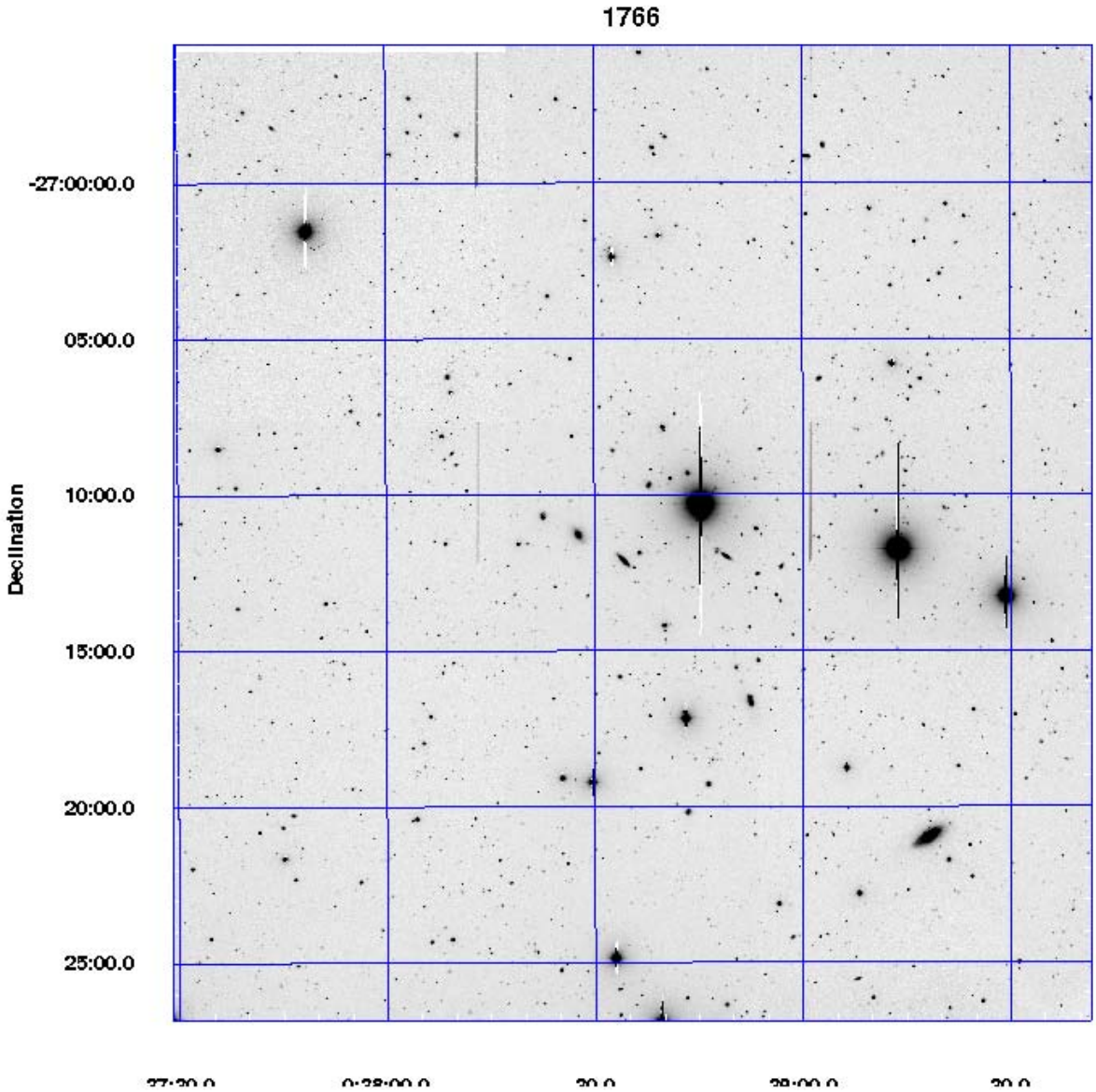

Figure A.2: MZ 1766

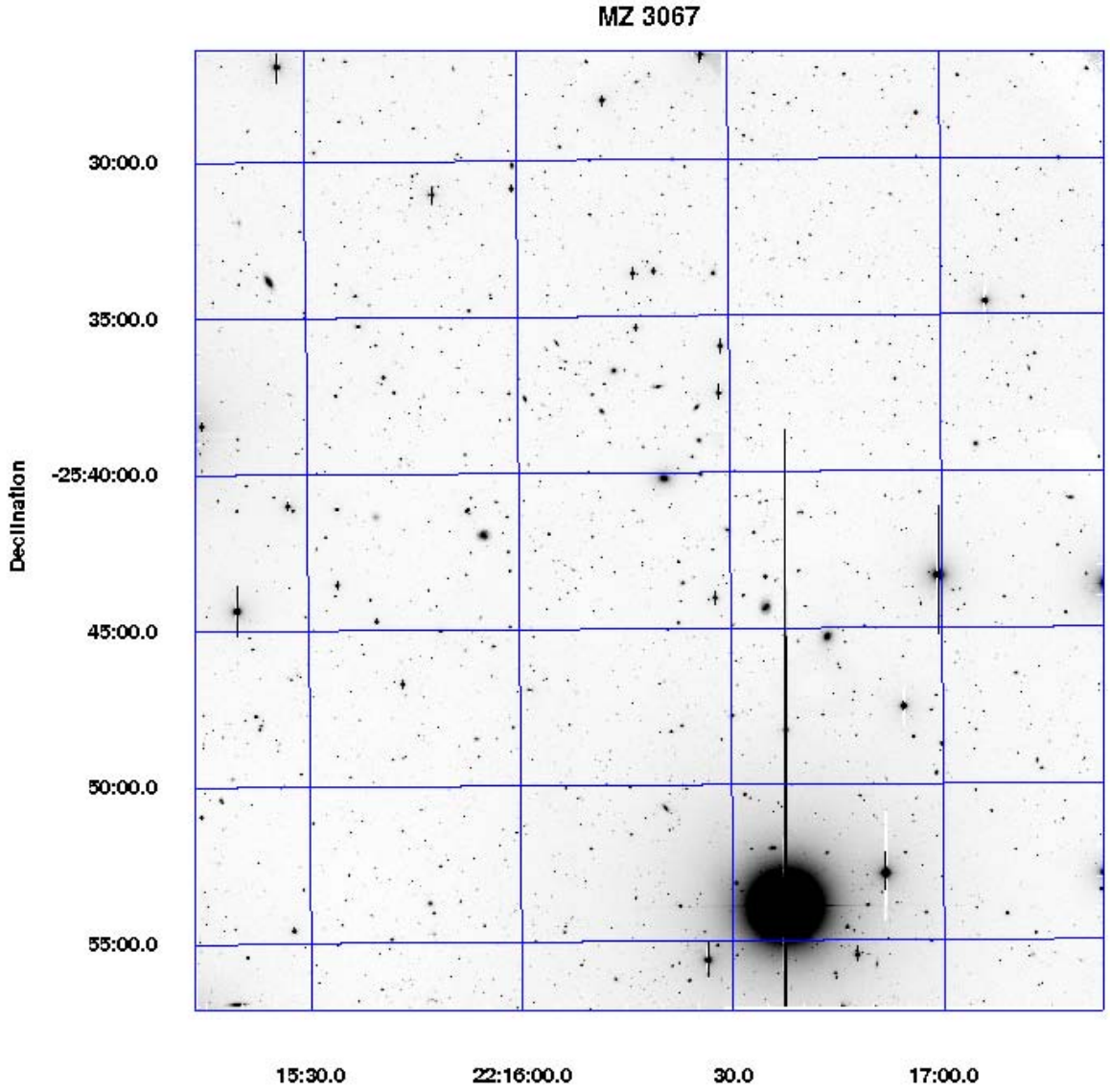

Figure A.3: MZ 3067

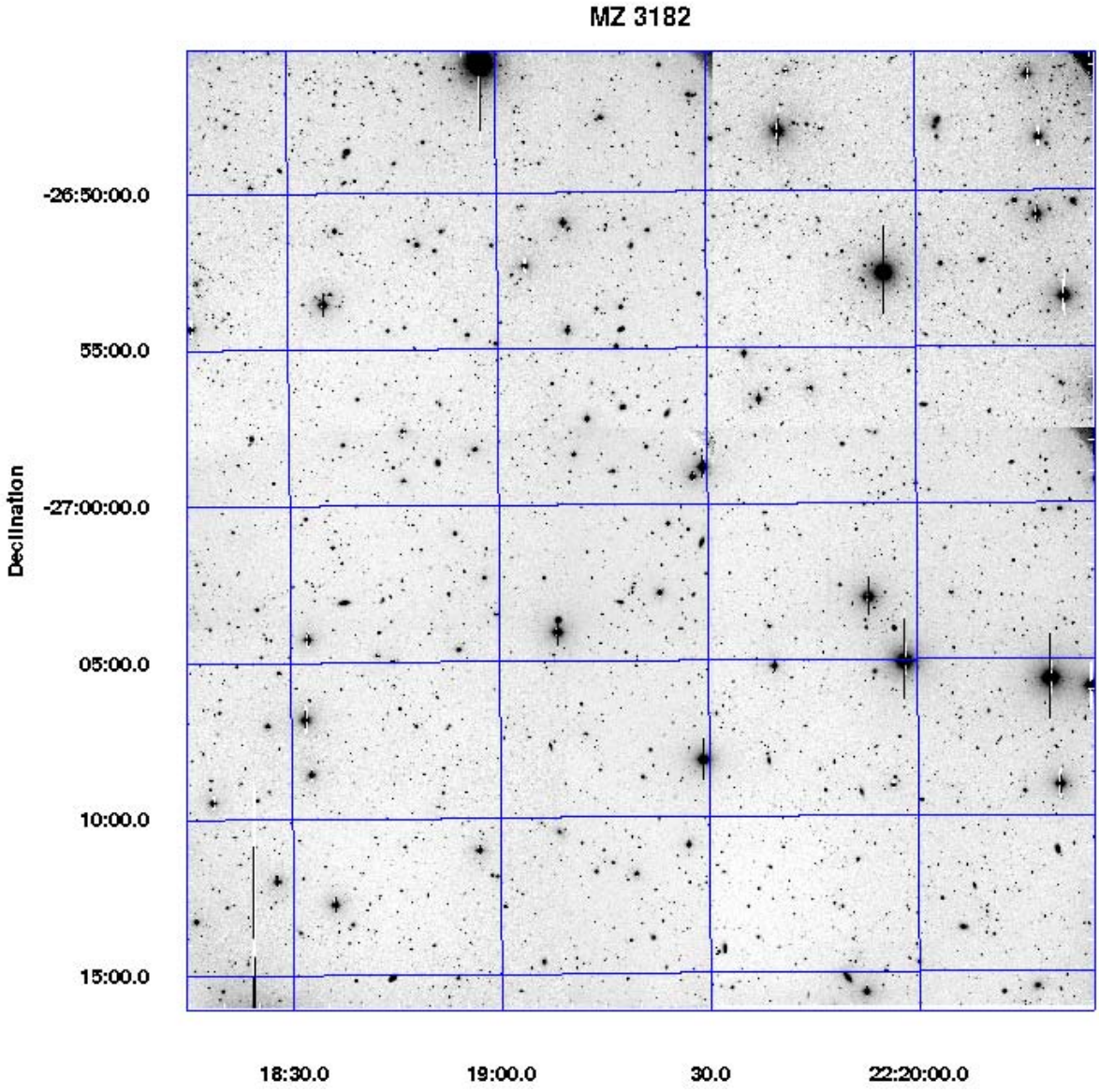

Figure A.4: MZ 3182

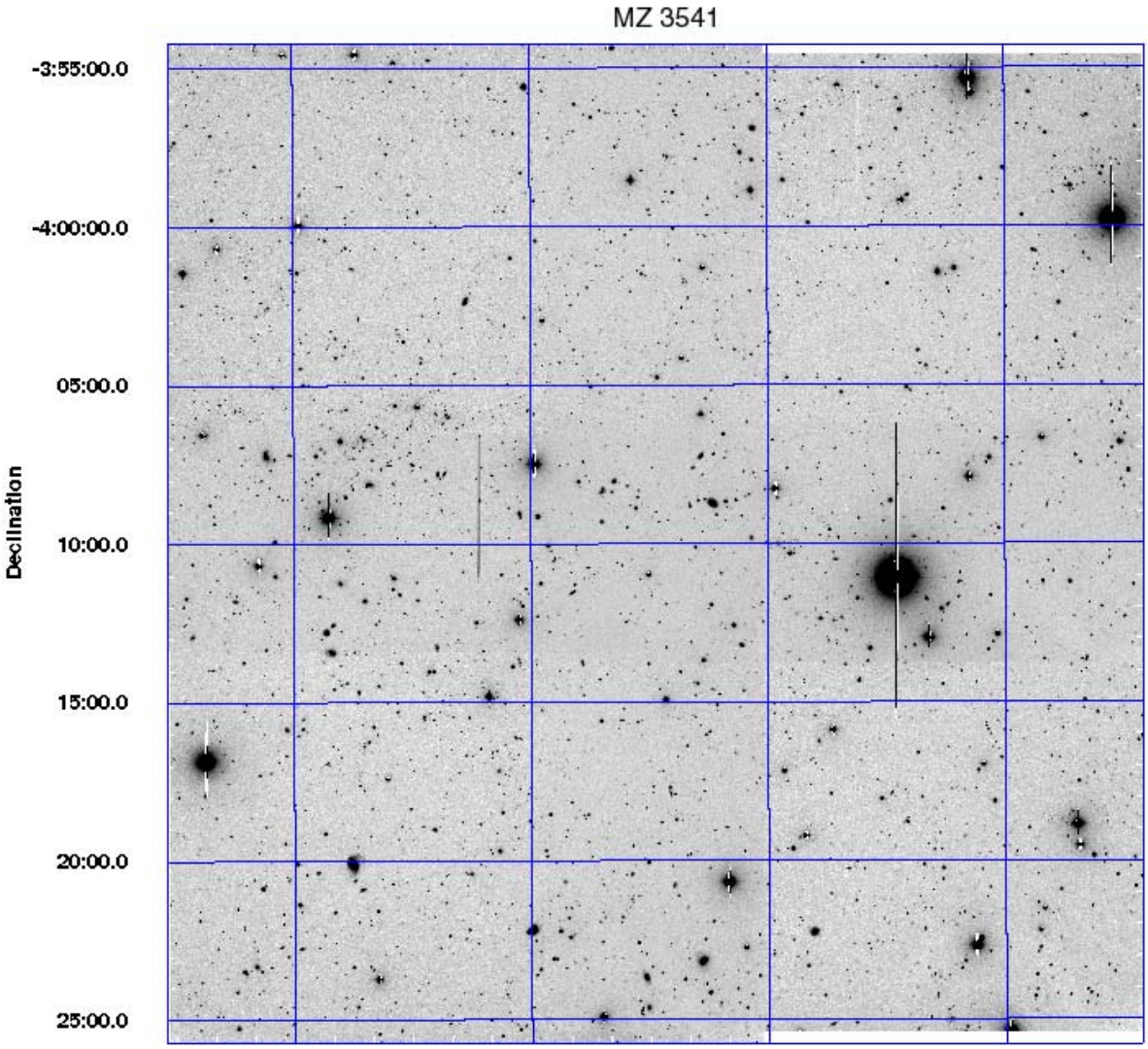

Figure A.5: MZ 3541

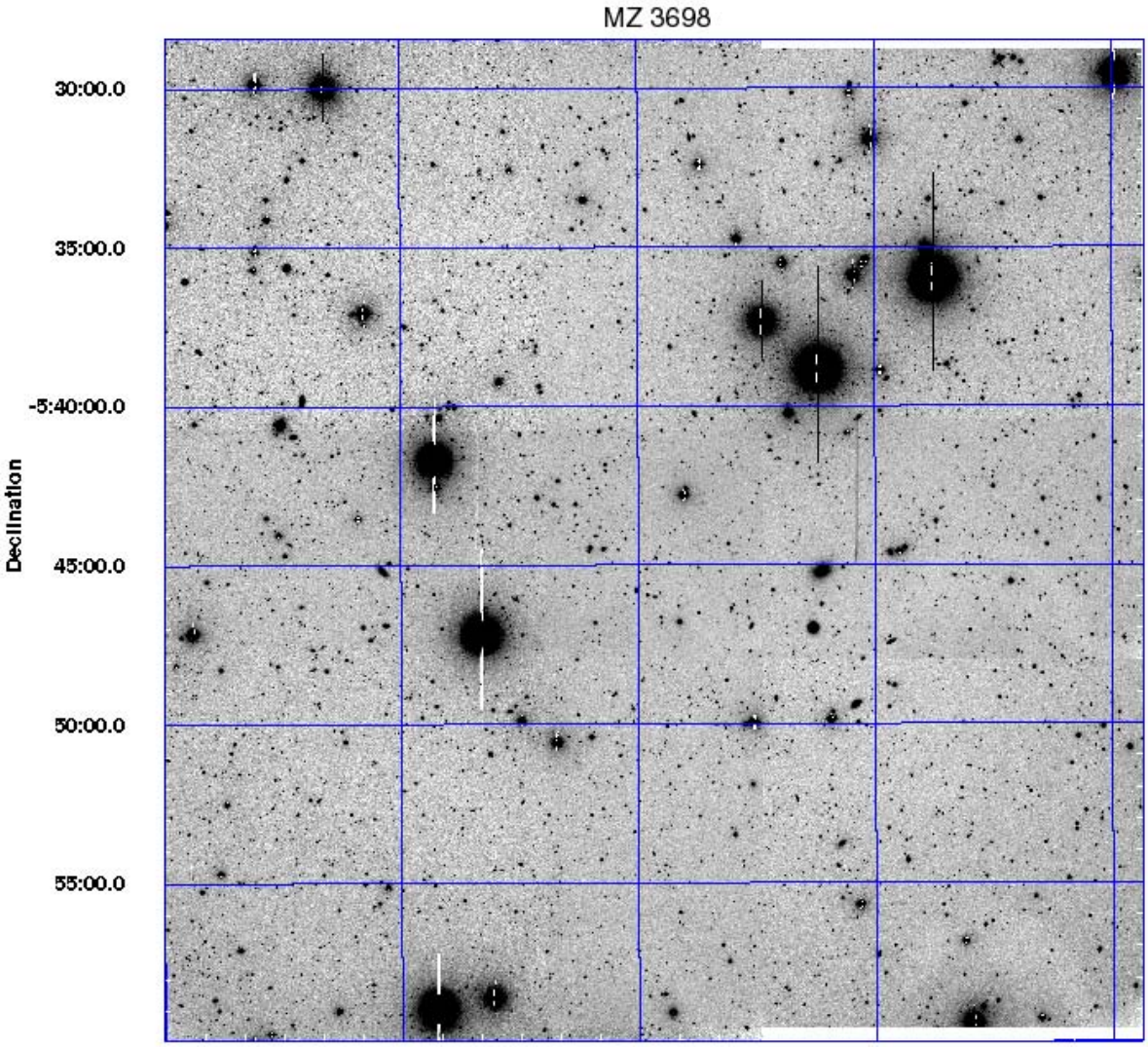

Figure A.6: MZ 3698

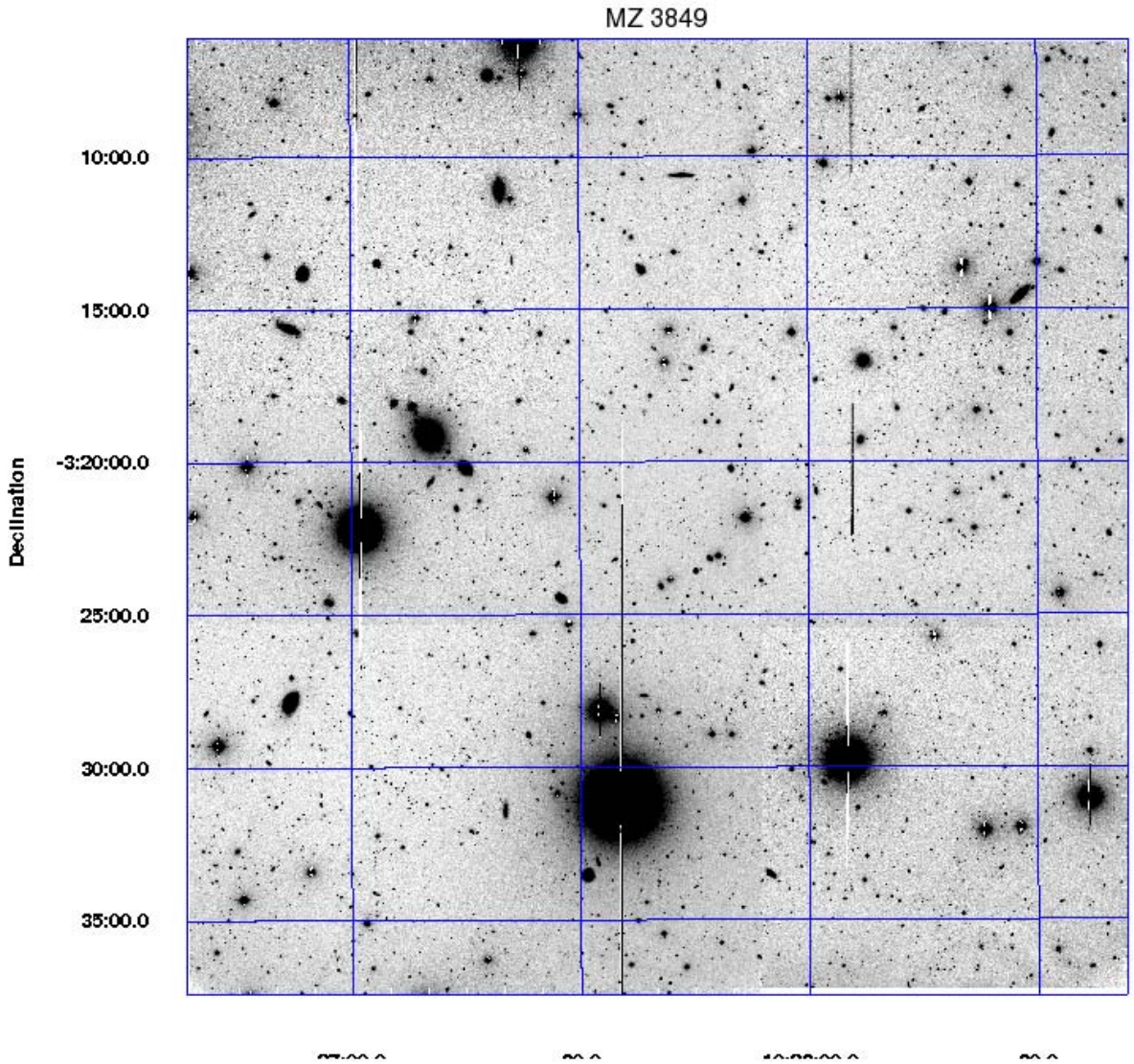

Figure A.7: MZ 3849

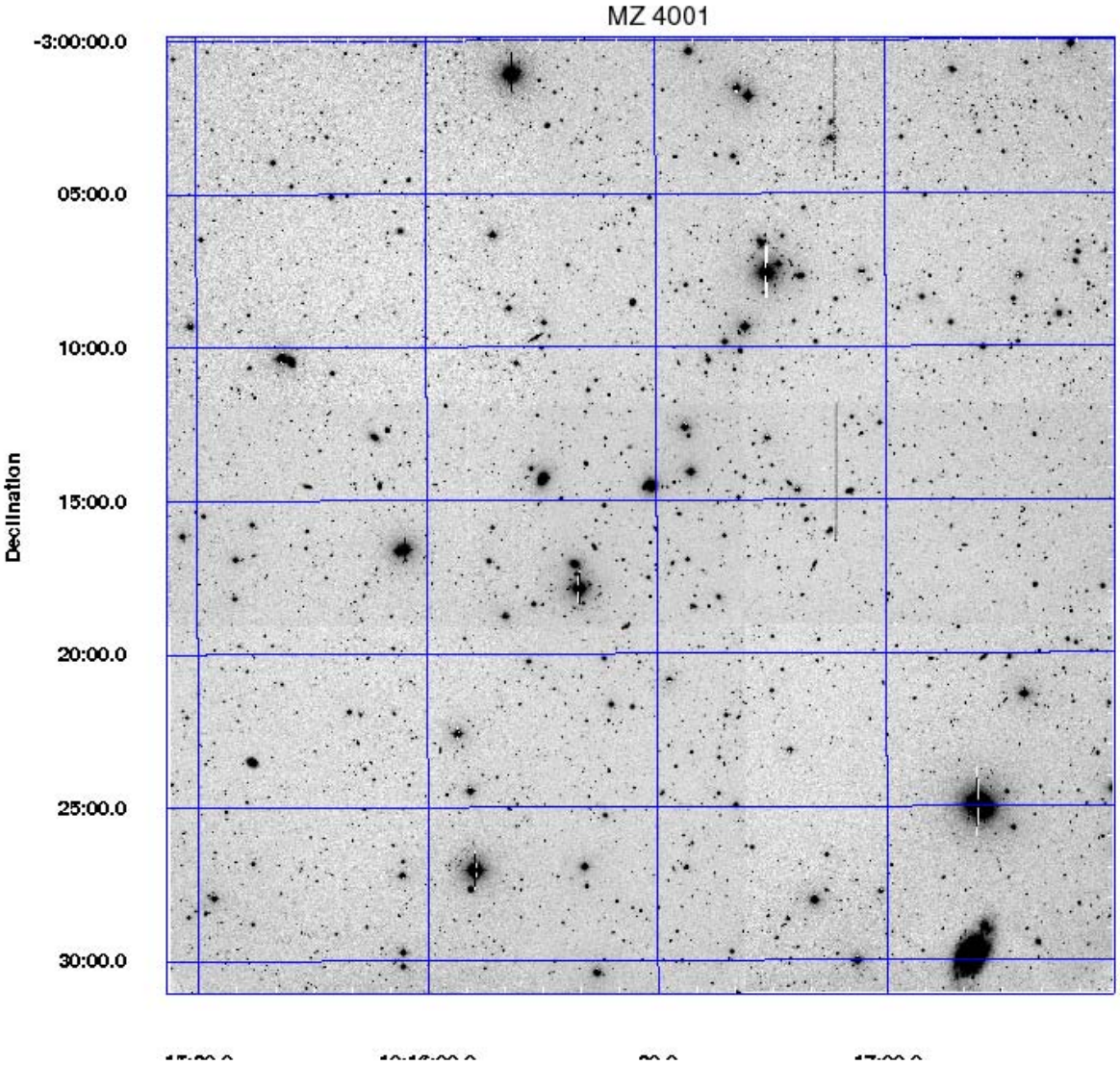

Figure A.8: MZ 4001

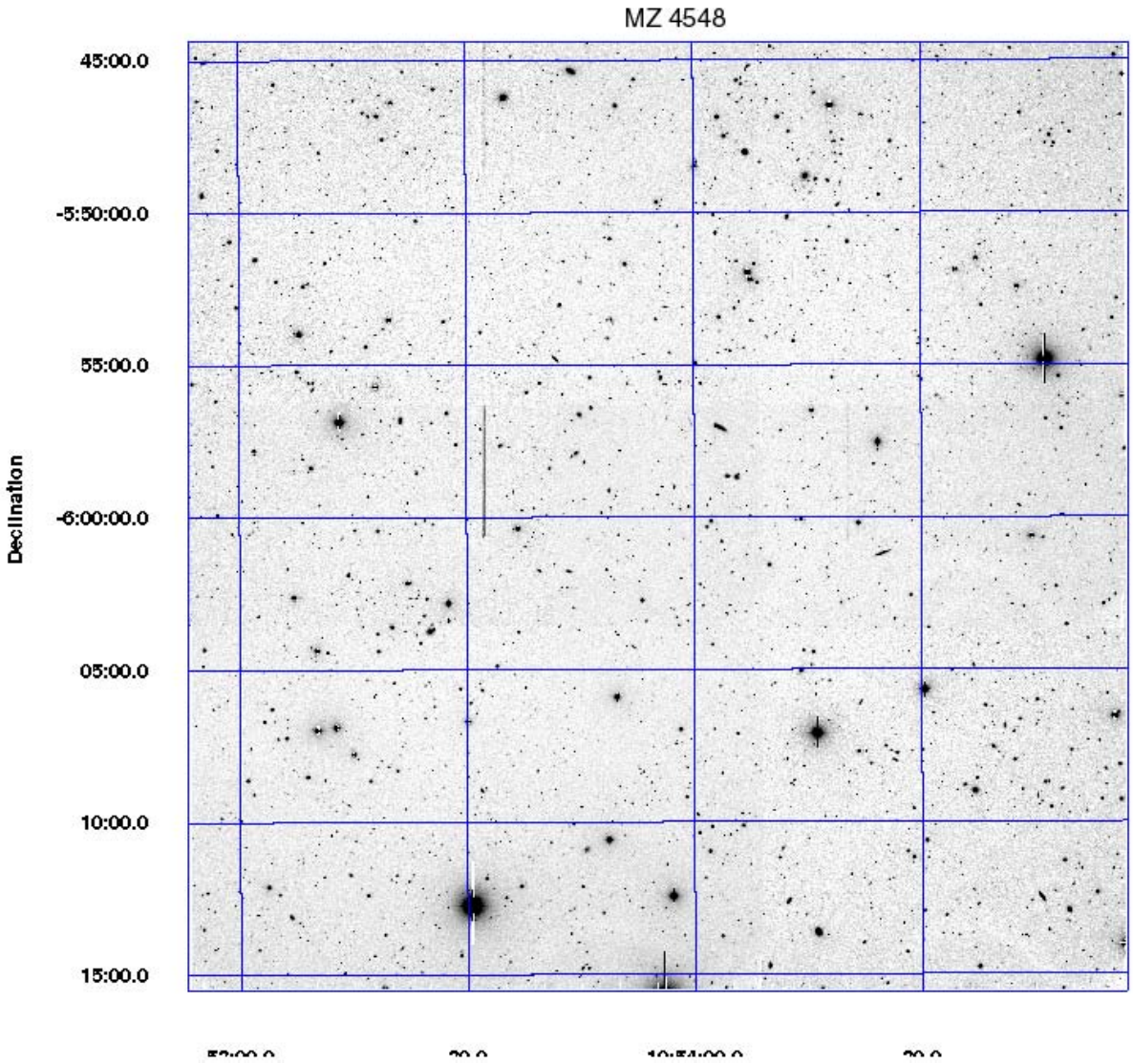

Figure A.9: MZ 4548

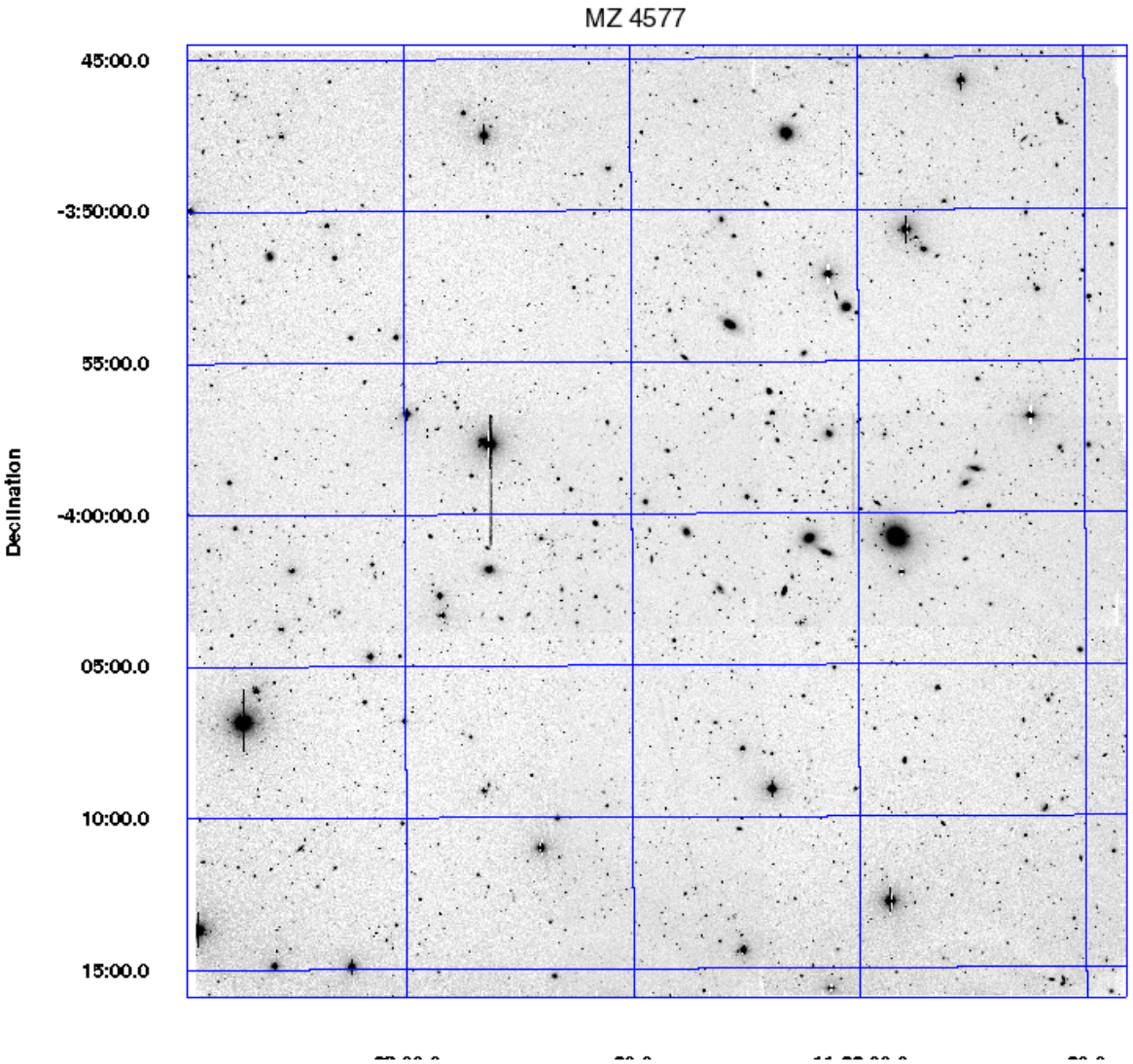

Figure A.10: MZ 4577

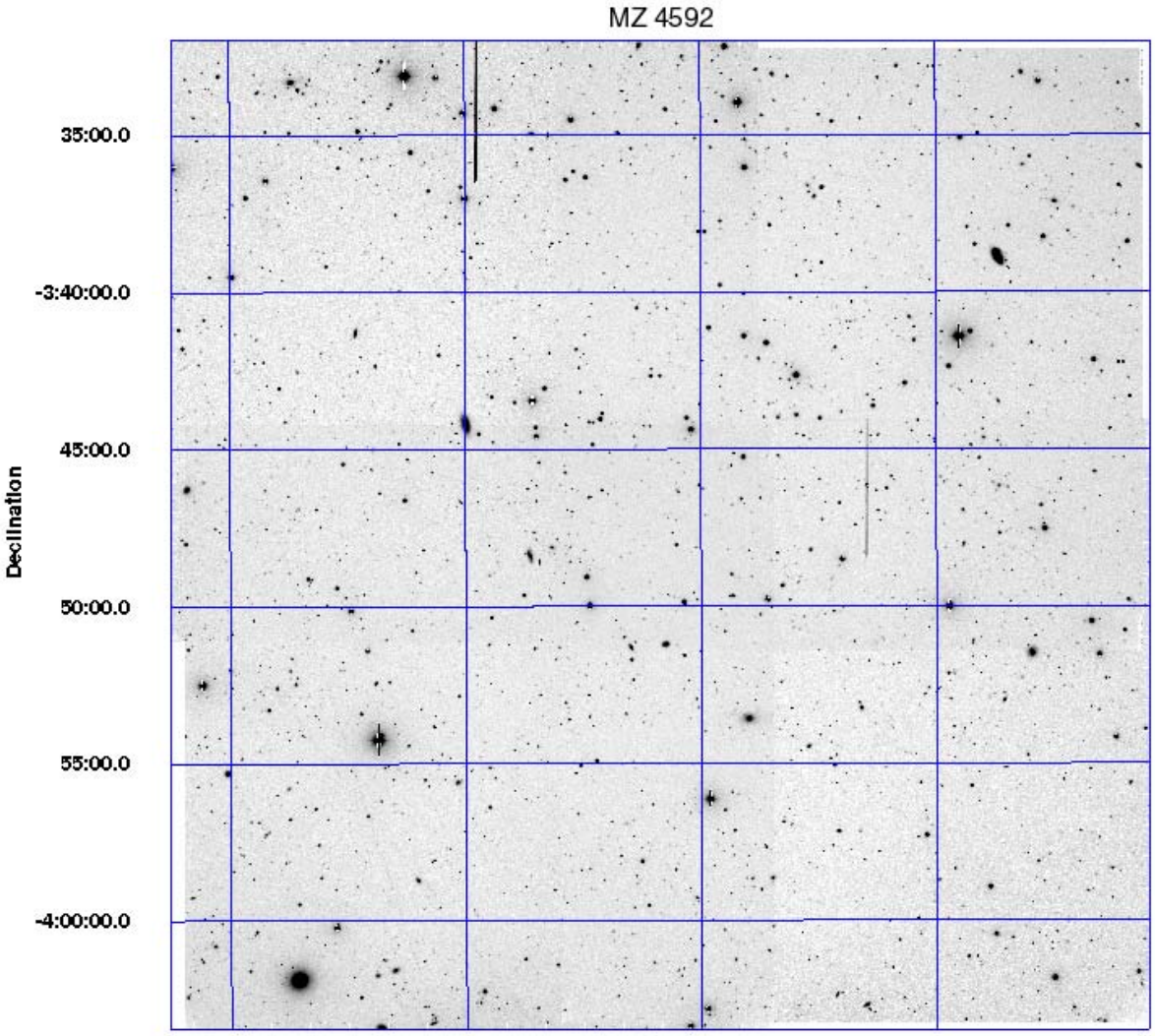

Figure A.11: MZ 4592

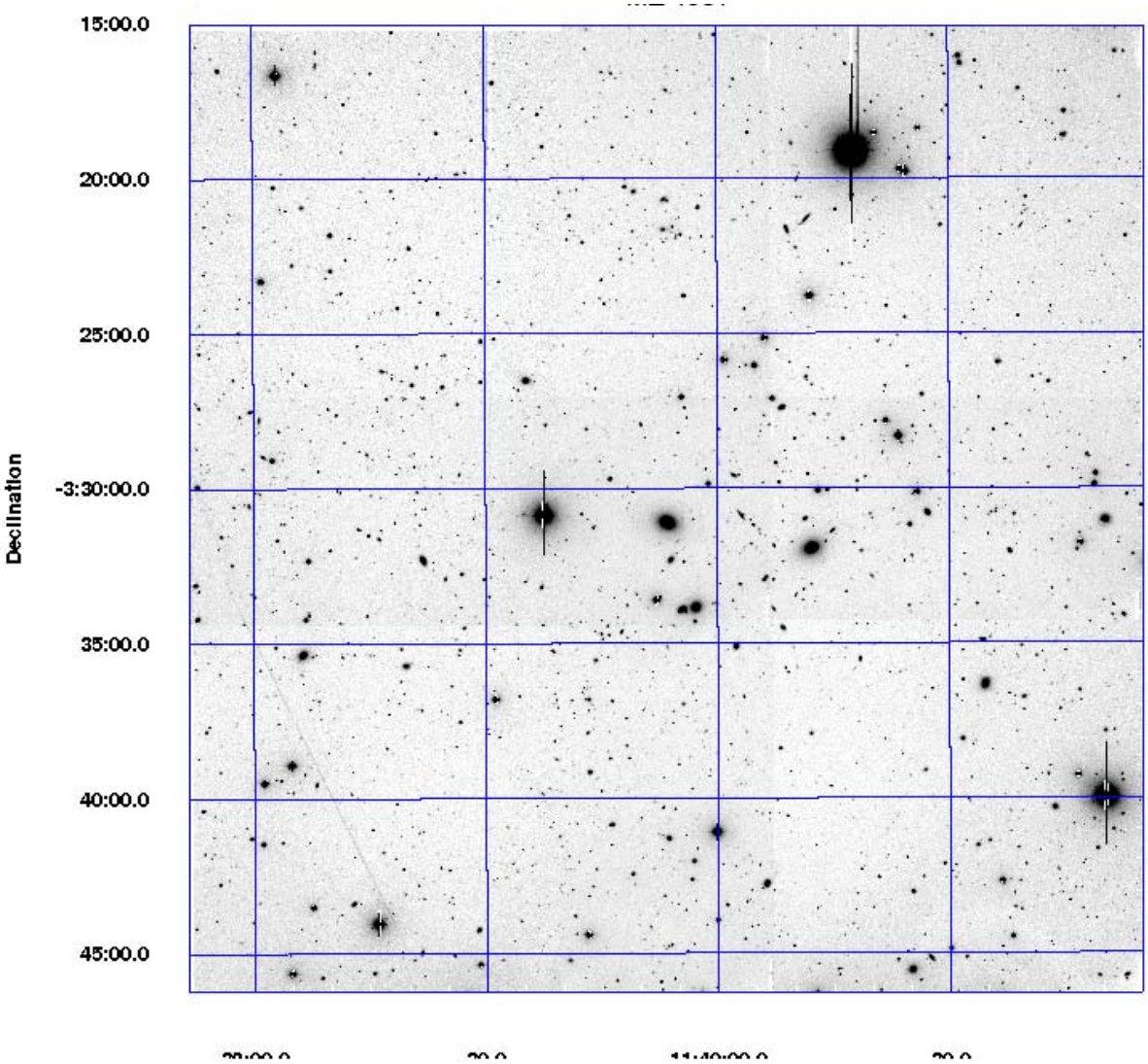

Figure A.12: MZ 4881

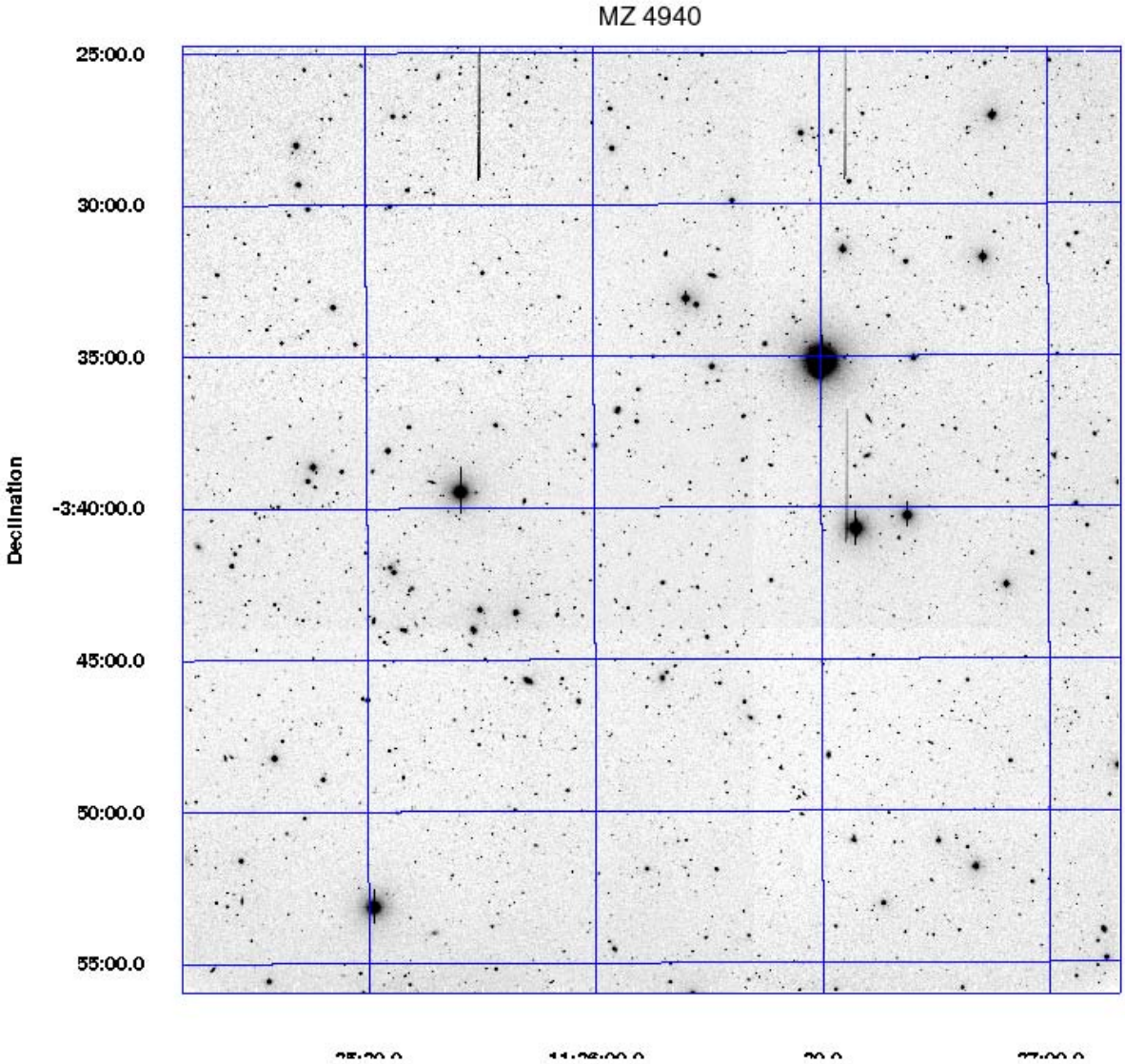

Figure A.13: MZ 4940

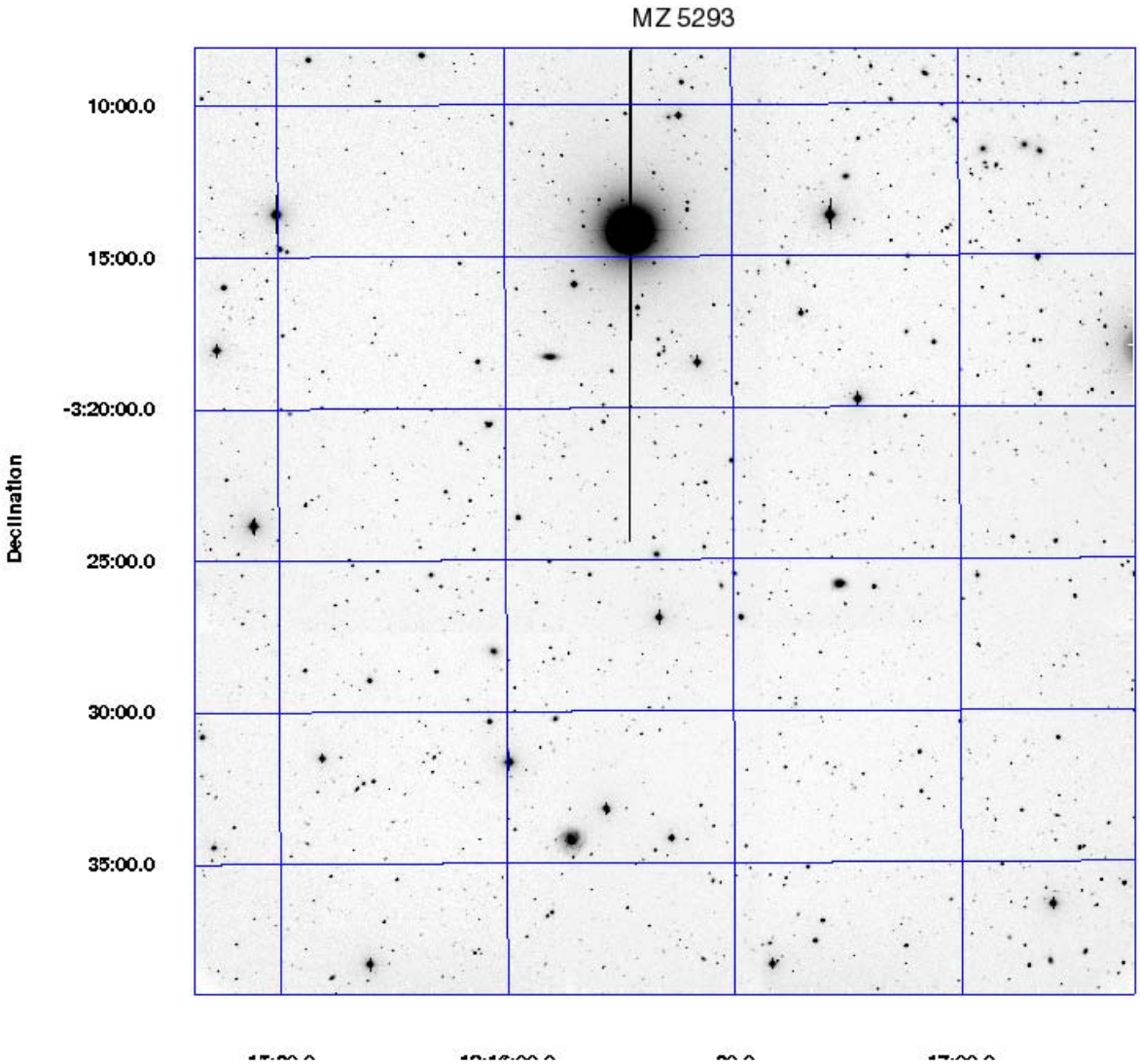

Figure A.14: MZ 5293

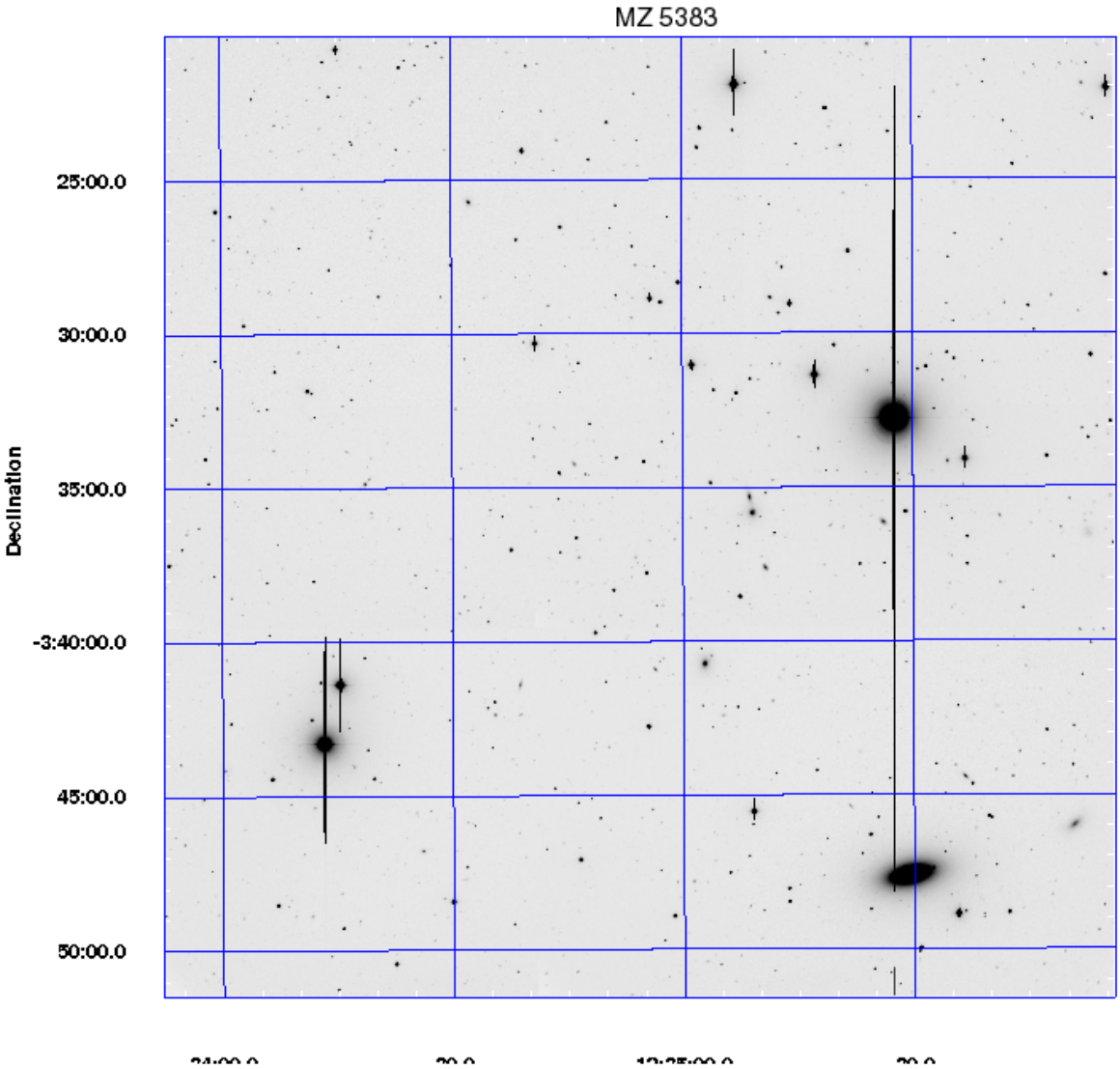

Figure A.15: MZ 5383

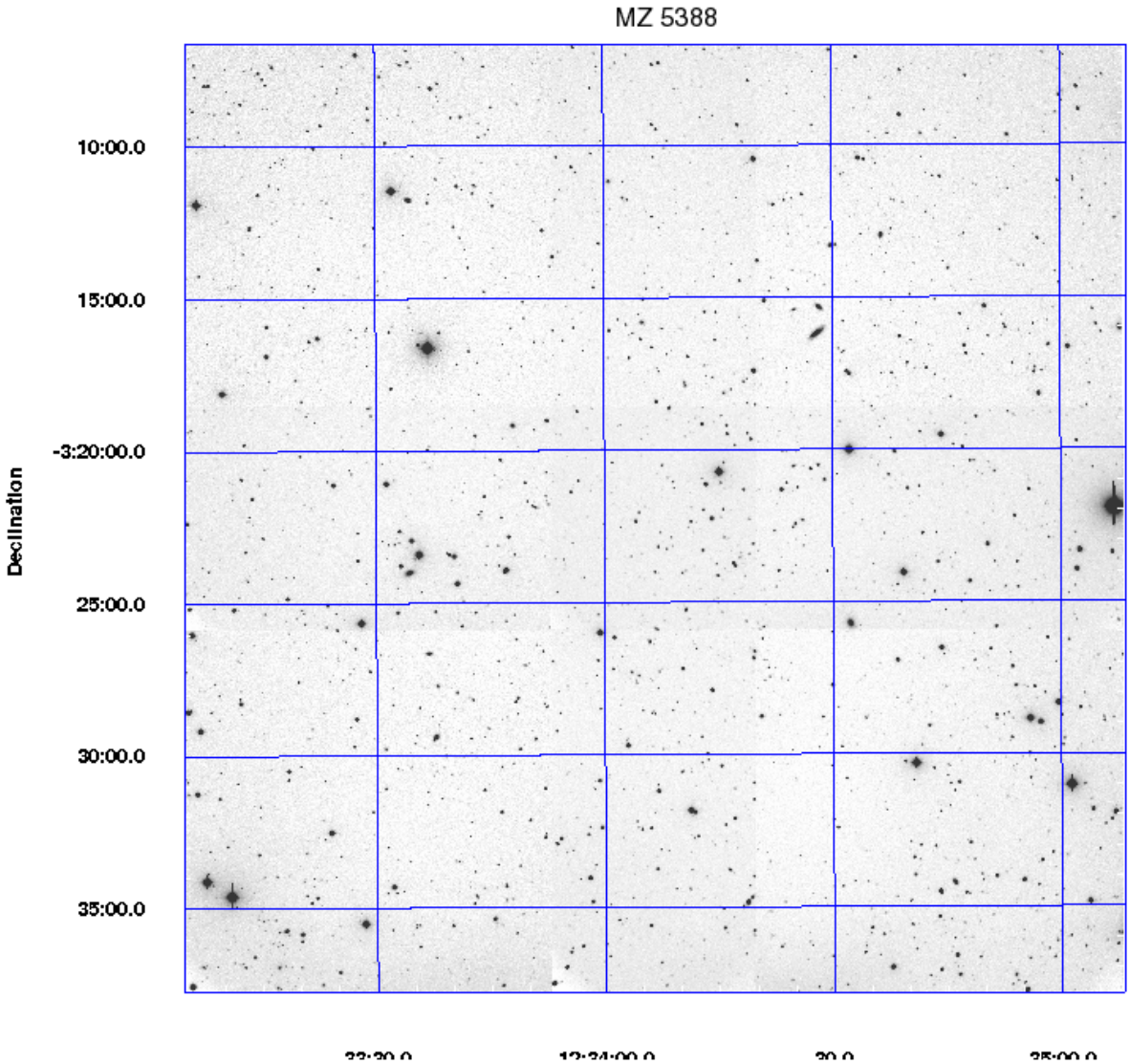

Figure A.16: MZ 5388

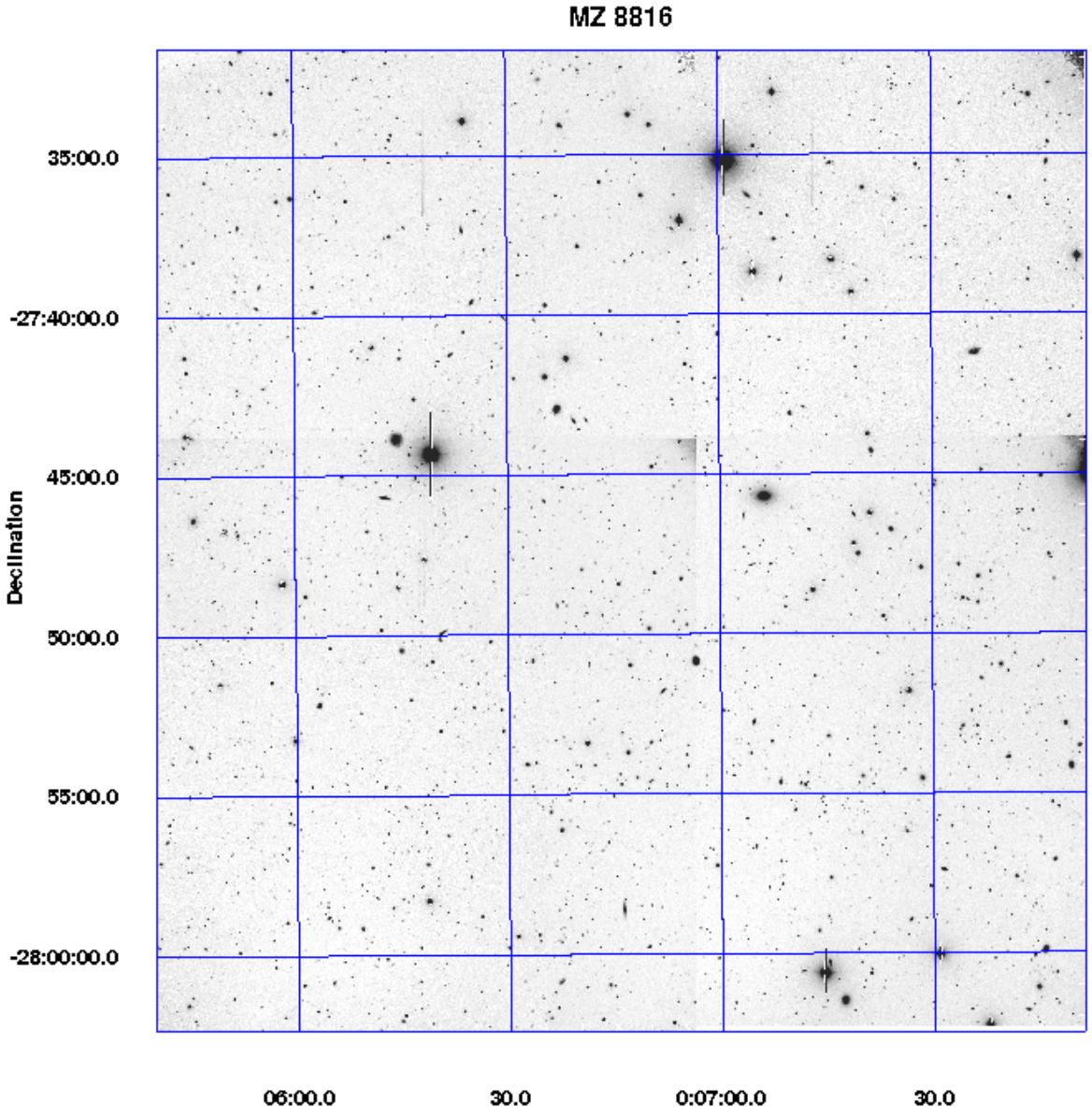

Figure A.17: MZ 8816

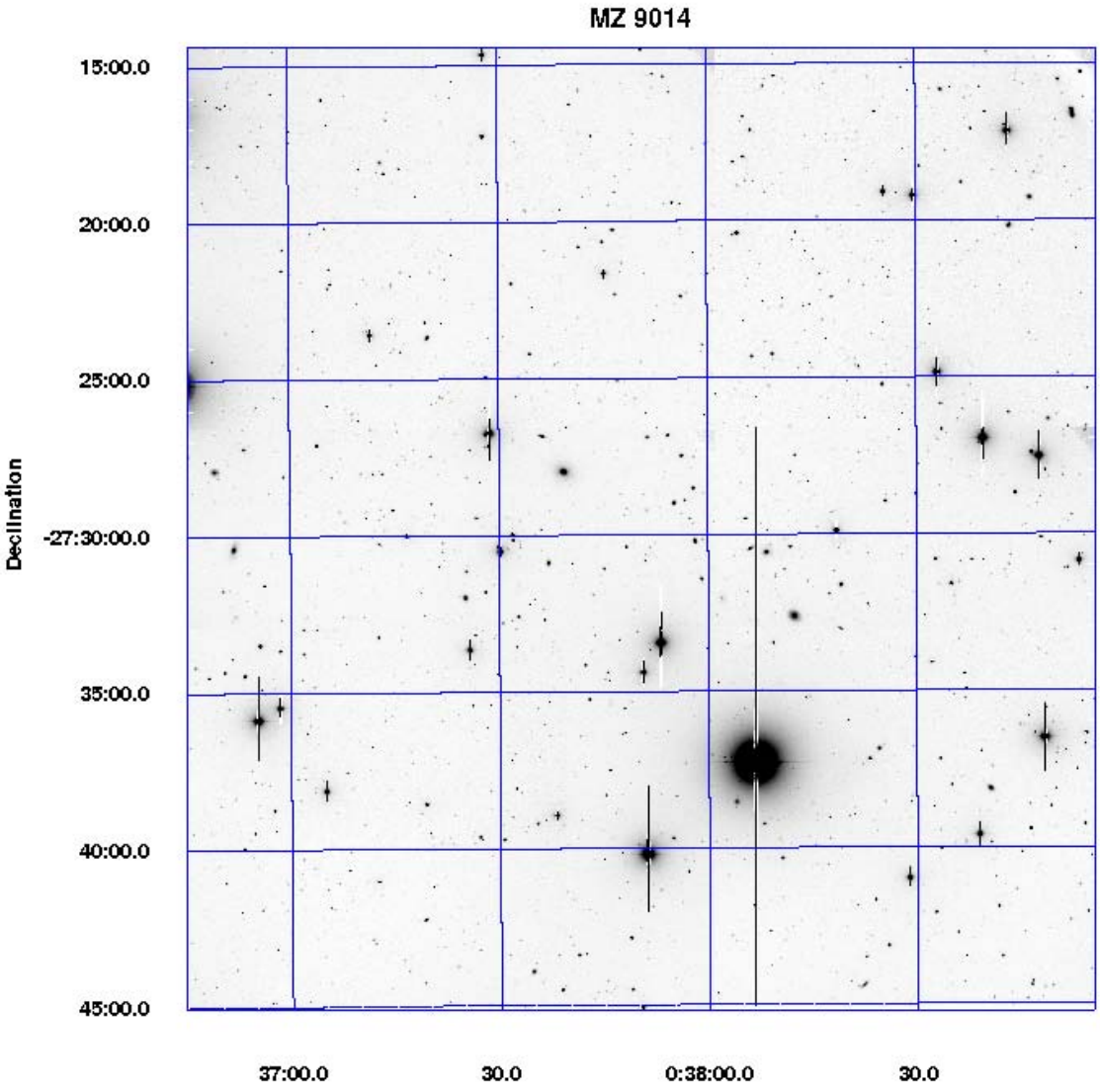

Figure A.18: MZ 9014

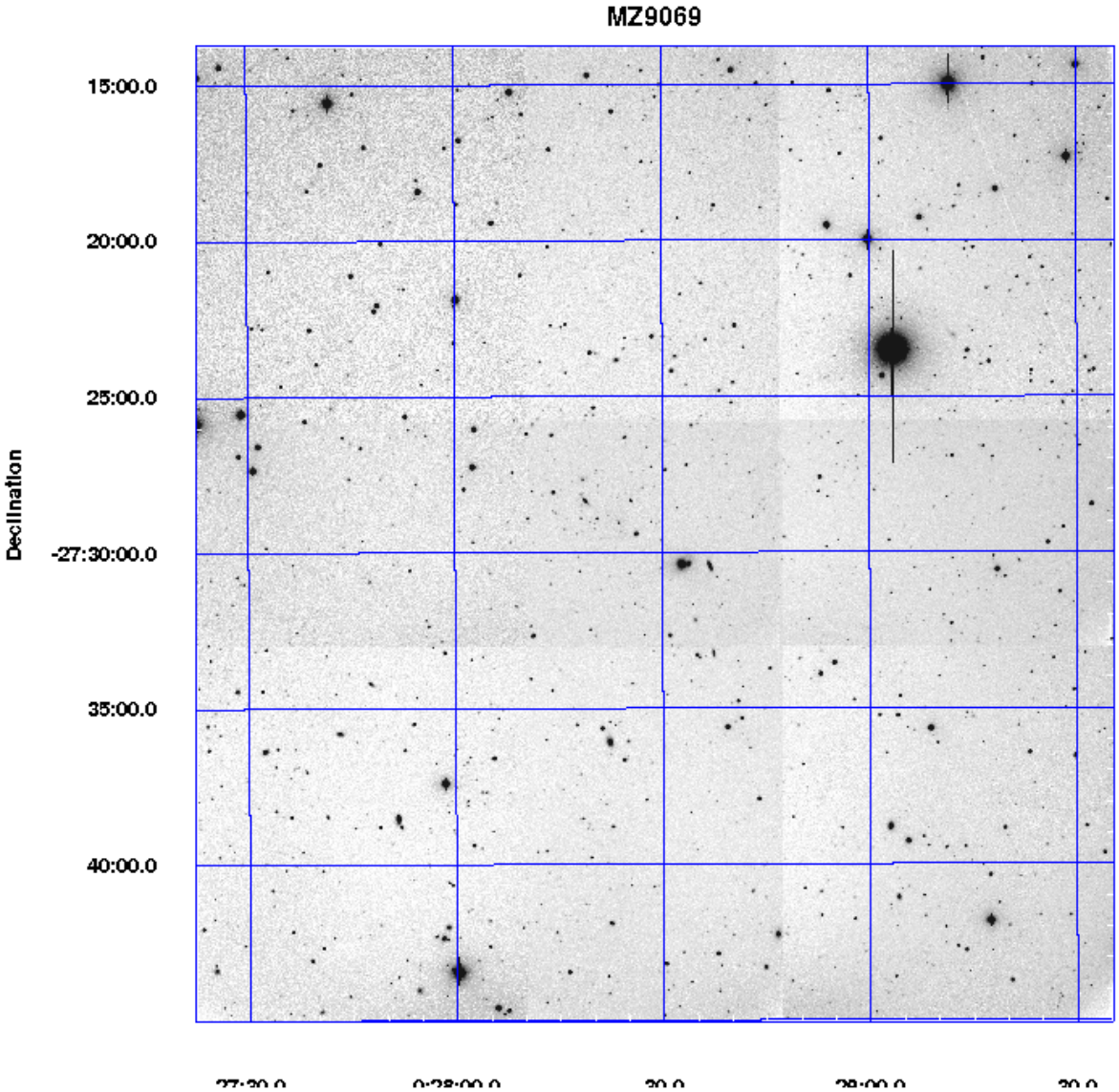

Figure A.19: MZ 9069

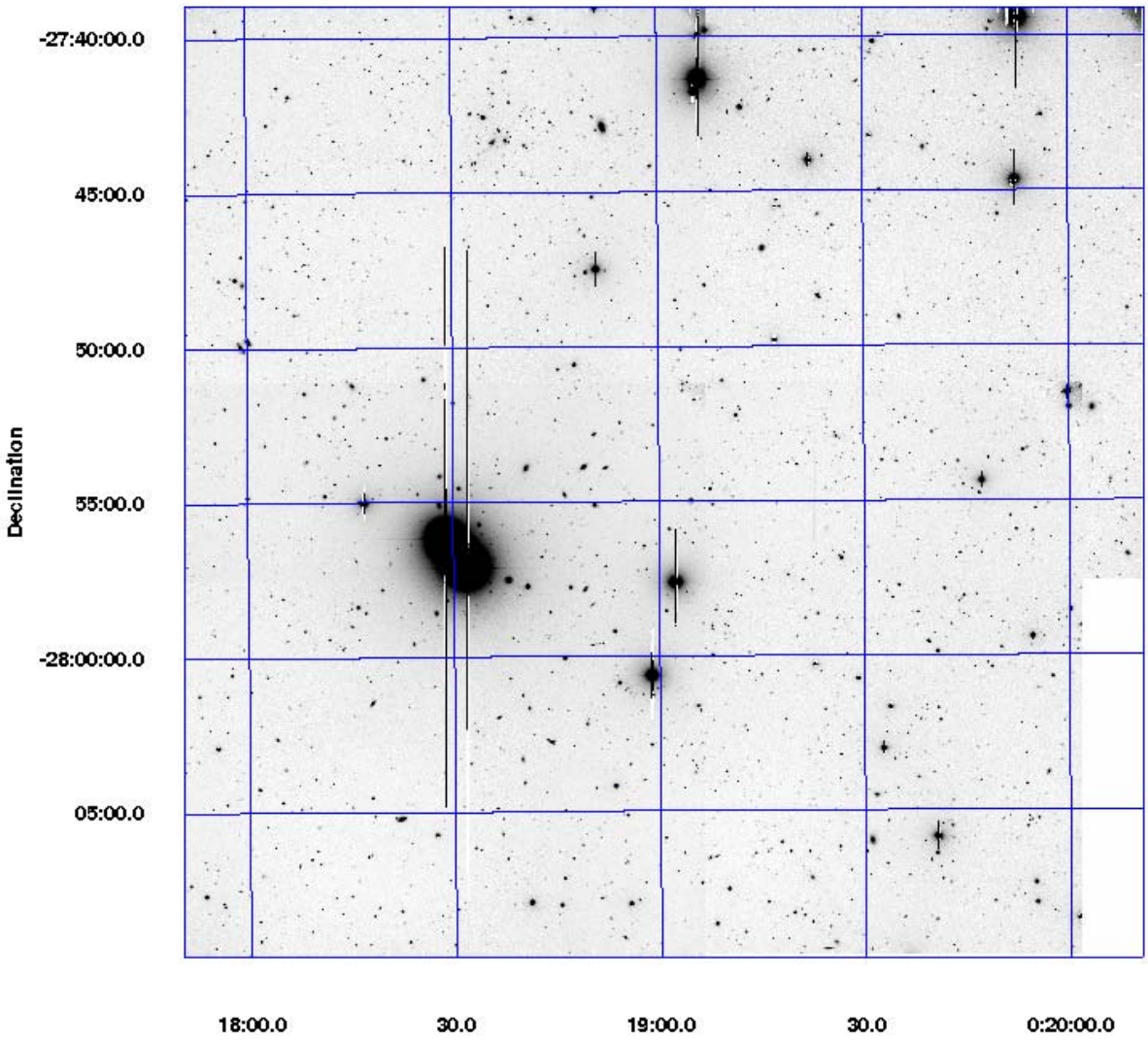

Figure A.20: MZ 9137

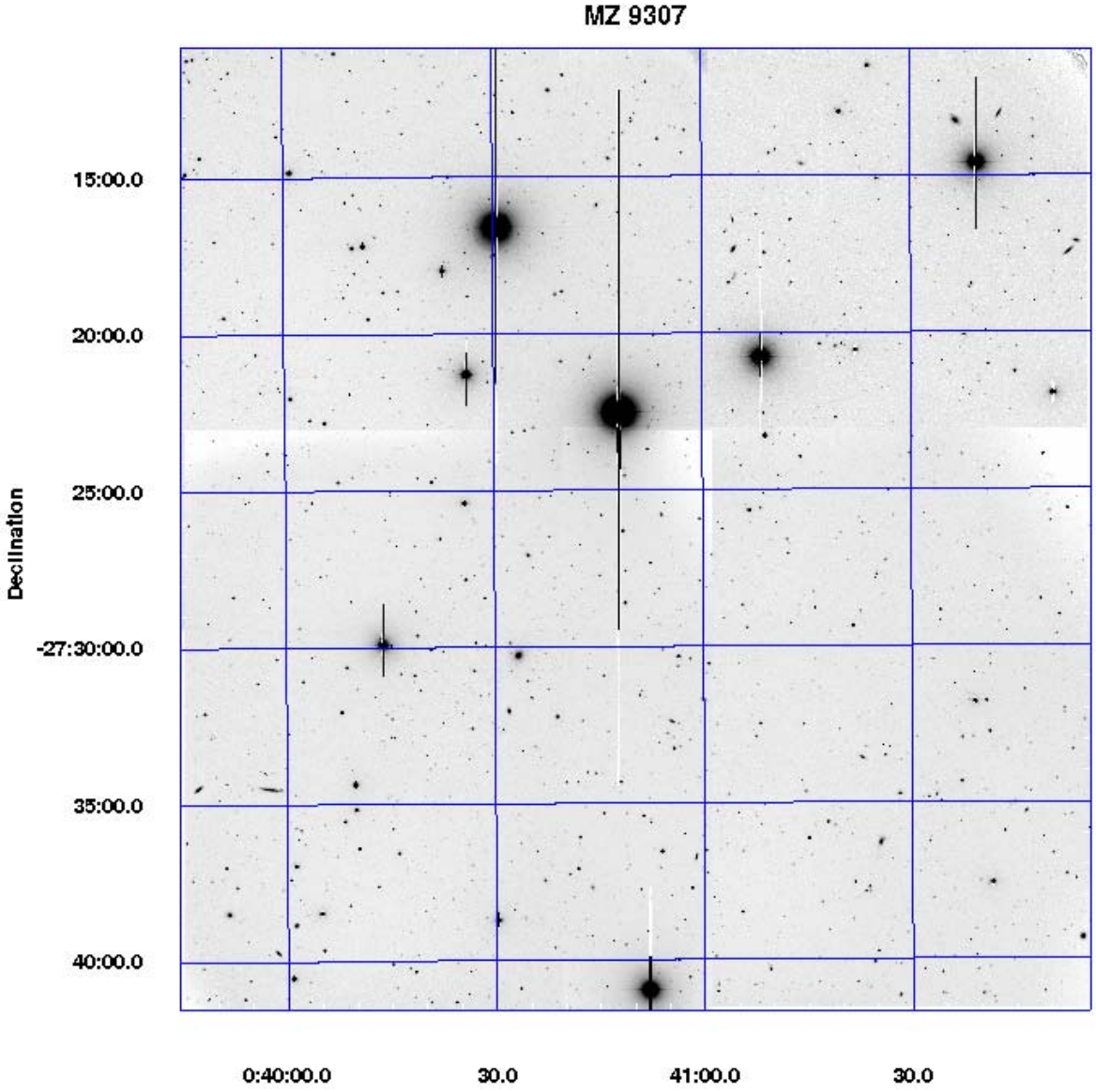

Figure A.21: MZ 9307

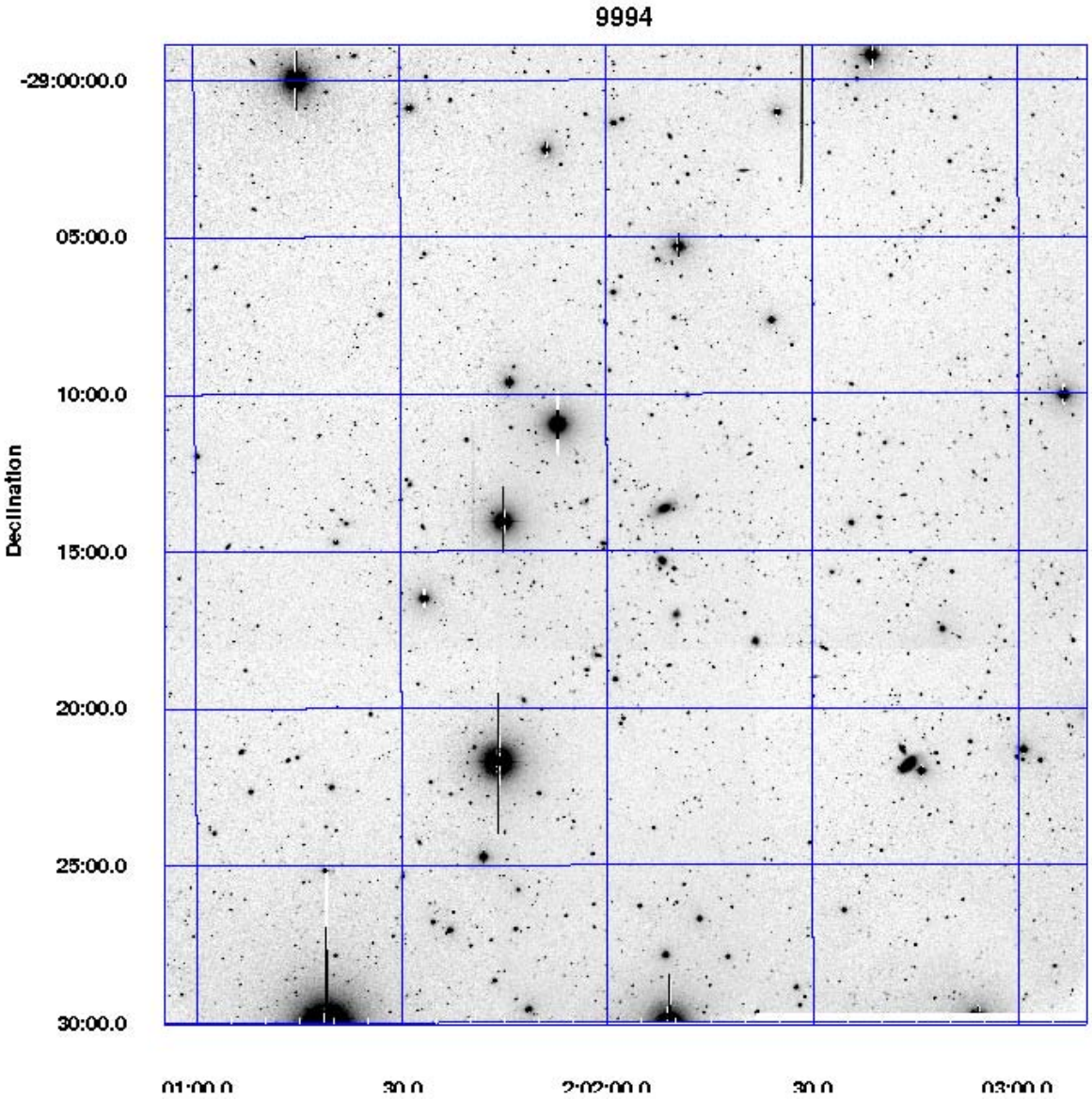

Figure A.22: MZ 9994

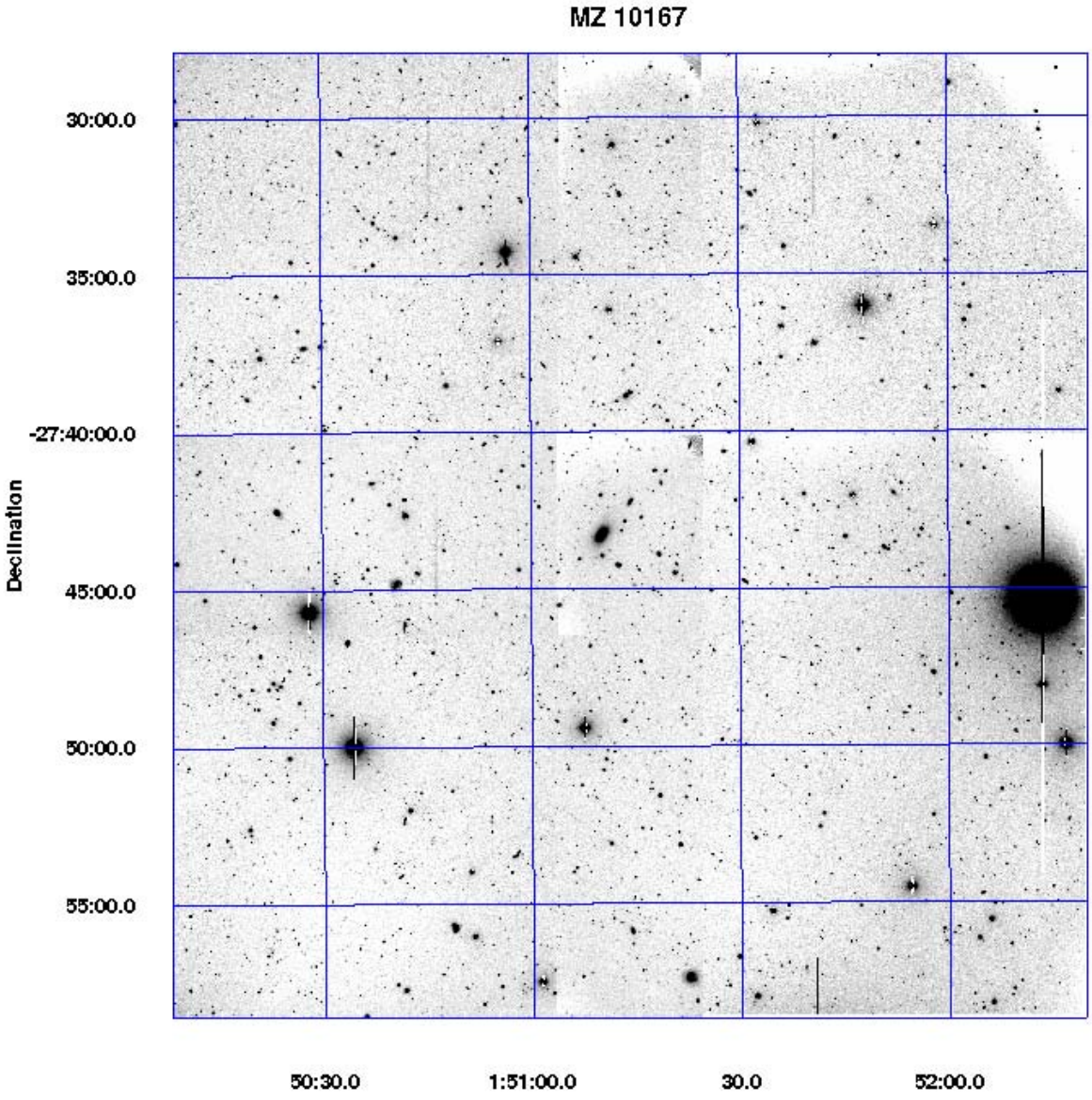

Figure A.23: MZ 10167

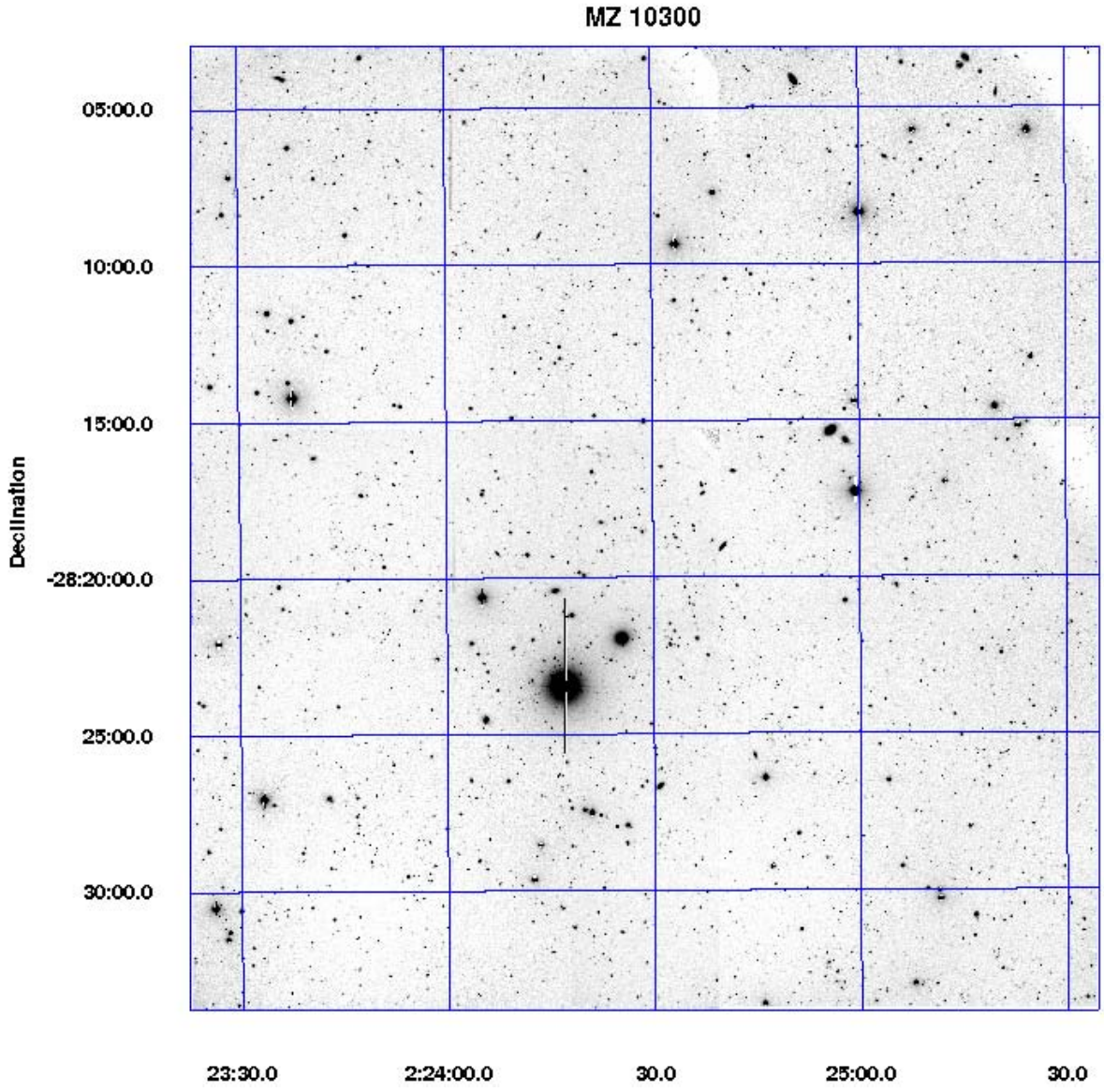

Figure A.24: MZ 10300

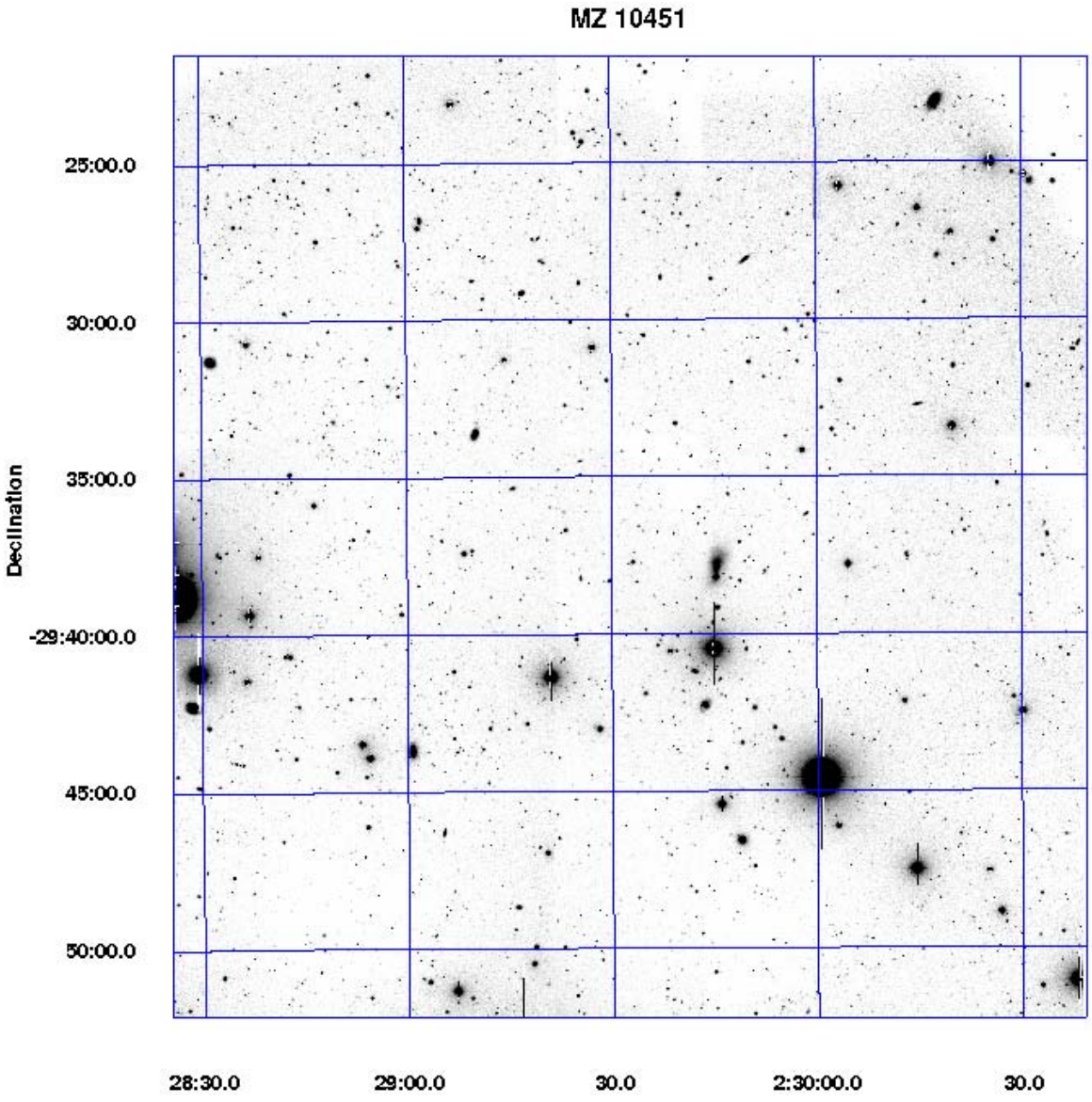

Figure A.25: MZ 10451